UNIVERSIDADE FEDERAL DE SÃO CARLOS
CENTRO DE CIÊNCIAS EXATAS E DE TECNOLOGIA
PROGRAMA DE PÓS-GRADUAÇÃO EM FÍSICA

RENAN DA SILVA SOUZA

ULTRACOLD BOSONS IN RANDOM LATTICE POTENTIALS

SÃO CARLOS, BRAZIL
2023

UNIVERSIDADE FEDERAL DE SÃO CARLOS
CENTRO DE CIÊNCIAS EXATAS E DE TECNOLOGIA
PROGRAMA DE PÓS-GRADUAÇÃO EM FÍSICA

RENAN DA SILVA SOUZA

ULTRACOLD BOSONS IN RANDOM LATTICE POTENTIALS

Tese apresentada ao Programa de Pós-Graduação em Física da Universidade Federal de São Carlos como parte dos requisitos exigidos para a obtenção do título de Doutor em Ciências.

Área de Concentração: Física Básica

Orientador: Prof. Dr. Francisco Ednilson Alves dos Santos

SÃO CARLOS, BRAZIL
2023

UNIVERSIDADE FEDERAL DE SÃO CARLOS

Centro de Ciências Exatas e de Tecnologia
Programa de Pós-Graduação em Física

Folha de Aprovação

Defesa de Tese de Doutorado do candidato Renan da Silva Souza, realizada em 06/04/2023.

Comissão Julgadora:

Prof. Dr. Francisco Ednilson Alves dos Santos (UFSCar)

Prof. Dr. Emanuel Fernandes de Lima (UFSCar)

Profa. Dra. Mônica Adrioli Caracanhas Santarelli (IFSC/USP)

Prof. Dr. Arnaldo Gammal (IFUSP)

Prof. Dr. Axel Pelster (RPTU)

Renan da Silva Souza

O Relatório de Defesa assinado pelos membros da Comissão Julgadora encontra-se arquivado junto ao Programa de Pós-Graduação em Física.

À todos os Professores e Professoras que direta ou indiretamente partciparam e contribuíram para a minha formação. Em especial, às professoras Joana d'Arc de História, Patrícia Scarpa de Física, Regiane e Regina Varderlei de Literatura e Língua Portuguesa e Sônia Noriko de Matemática da Escola Estadual Professor Licínio Carpinelli em Guarulhos.

Agradecimentos

Gostaria de iniciar agradecendo ao meu orientador, Prof. Dr. Francisco Ednilson Alves dos Santos, do Departamento de Física (DF) da Universidade Federal de São Carlos (UFSCar). Lembro-me quando, depois de ter feito uma pergunta sobre teoria quântica de campos numa aula de Física Matemática, fui convidado a fazer uma iniciação científica sem nem mesmo precisar mostrar meu histórico. Obrigado por ter me apresentado o tema do presente trabalho e por todo o conhecimento compartilhado durante esse período.

Meus agradecimentos a todos os professores, professoras, funcionários e funcionárias do DF e do Programa de Pós-Graduação em Física da UFSCar.

Agradeço também o Priv.-Doz. Dr. Axel Pelster da Technische Universität Kaiserslautern. A oportunidade de trabalhar com pesquisa acadêmica em Kaiserslautern certamente me fez crescer cientificamente.

Um agradecimento especial vai para os meus amigos e amigas do grupo P.R.I.M.O.S. no Telegram. Obrigado por todos os momentos de felicidade compartilhados durante esse período.

Expresso minha profunda gratidão aos meus pais, Fátima e Pedro, às minhas irmãs Rosada e Renata e ao meu irmão Rodrigo. Desde quando cheguei a São Carlos e durante todo o período em que estive longe, nunca esqueci das minhas origens e de tudo o que vivemos juntos. Ter chegado até aqui é, com certeza, uma conquista coletiva. Do fundo do meu coração, meu mais sincero obrigado. Agradeço também às minhas sobrinhas Isadora, Iris e Milena por trazerem felicidade à nossa família. Não há motivação maior do que vê-las sorrindo.

O presente trabalho foi realizado com apoio da Coordenação de Aperfeiçoamento de Pessoal de Nível Superior – Brasil (CAPES) – Código de Financiamento 001. A pesquisa contou também com o apoio da CAPES e do Deutscher Akademischer Austauschdienst (DAAD) no âmbito do programa binacional conjunto PROBRAL Nº 88887.627948/2021-00.

"Se o barato é louco e o processo é lento
No momento, deixa eu caminhar contra o vento"

Racionais MC's
Jesus chorou

Resumo

O modelo de Bose-Hubbard descreve bosons sem spin que interagem a curta distância numa rede aleatória. Este modelo é realizado em sistemas de átomos ultra-frios, onde se podem observar transições de fase quânticas. À medida que a profundidade do potencial da rede é aumentada, tal sistema sofre uma transição de fase quântica de um superfluido para uma fase isolante de Mott. Na presença de um potencial externo aleatório, regiões raras de condensado podem surgir dentro de um fundo isolante, formando um estado de vidro de Bose. Apesar das características bem compreendidas do modelo de Bose-Hubbard, uma investigação analítica precisa dos efeitos da desordem no espectro de energia ainda não está disponível, e uma caracterização concreta do espectro de energia do vidro de Bose, bem como da sua fronteira de fase com a fase de Mott, está em falta. Neste trabalho, investigamos como a desordem afeta as excitações elementares do modelo de Bose-Hubbard no limite de interação forte e estudamos a transição de fase quântica de Mott-para-vidro de Bose para temperatura zero e temperaturas finitas. Desenvolvemos um método de perturbação com o formalismo de integrais funcionais para obter uma expansão de acoplamento forte para a função de Green em termos da energia de tunelamento. Aplicando o método de soma parcial, calculamos a influência de um subconjunto infinito de termos em tal expansão na função espectral. Usando o método de Poincaré-Lindstedt, calculamos a expressão renormalizada para a densidade local de estados. Demonstramos que o espectro é composto por excitações estáveis-deslocalizadas em baixas energias e excitações localizadas-amortecidas em energias ligeiramente mais altas. Quando a desordem se torna da ordem das interações, as excitações estáveis-deslocalizadas perdem a sua dispersão devido ao aumento da sua massa efetiva. Neste caso, o tempo de vida das excitações localizadas-amortecidas aumenta, e elas dominam toda a banda de energia. Argumentamos que tais excitações localizadas-amortecidas correspondem aos estados excitados de baixa energia da fase de vidro de Bose. Além disso, analisando a densidade local de estados, mostramos que tais informações espectrais servem como um parâmetro confiável para distinguir sem ambiguidade as fases de Mott e de vidro de Bose, tanto a temperaturas zero como a temperaturas finitas. Os nossos resultados vão além das previsões da teoria de campo médio para a caracterização desses estados fundamentais. Finalmente, sugerimos uma abordagem de ação efetiva e uma expansão de desordem fraca para a análise do espectro de excitações na fase superfluida.

Palavras-chave: Hamiltoniano de Bose-Hubbard. Transições de fase quâticas. Desordem. Superfluido. Isolante de Mott. Vidro de Bose. Função de Green. Função espectral.

Abstract

The Bose-Hubbard model describes short-range interacting spinless bosons on a random lattice. This model is realized in ultracold atomic systems where quantum phase transitions can be observed. When loaded into a deep potential depth perfect lattice, a cloud of cold bosonic atoms undergoes a quantum phase transition from a superfluid to a gapped Mott insulating phase. In the presence of additional random external potential, rare condensate regions can emerge inside an insulating background, forming a gapless Bose-glass state. Despite the well-understood characteristics of the Bose-Hubbard model, a precise analytic investigation of the effects of disorder on the energy spectrum remains unavailable, and a concrete characterization of the Bose-glass energy spectra, as well as its phase boundary with the Mott phase, is lacking. Here, we investigate how disorder affects the elementary excitations of the Bose-Hubbard model in the strongly interacting limit, and study the Mott-to-Bose glass quantum phase transition for zero and finite temperatures. We develop a perturbation method in the functional integral formalism to obtain a strong-coupling expansion for the single-particle Green's function in terms of the tunneling energy. By applying the partial summation method, we calculate the influence of an infinite subset of terms in such an expansion to the spectral function. Using the Poincaré-Lindstedt method, we compute the renormalized expression to the local density of states. We demonstrate that the spectrum is composed of stable-delocalized excitations at low energies and damped-localized excitations at slightly higher energies. When disorder becomes of the order of interactions, the stable-delocalized excitations become dispersionless due to their increased effective mass. In such a limit, the lifetime of the damped-localized excitations increases, and they dominate the whole energy band. We argue that such damped-localized excitations correspond to the low-energy excited states of the Bose-glass phase. Furthermore, by analyzing the local density of states, we show that this spectral information serves as a reliable parameter to unambiguously distinguish the Mott from the Bose-glass states both at zero and finite temperatures. Our results go beyond the mean-field theory predictions for the characterization of these ground states. Finally, we suggest an effective-action approach and a weak disorder expansion for the analysis of the superfluid excitation spectra.

Key-words: Bose-Hubbard Hamiltonian. Quantum phase transitions. Disorder. Superfluid. Mott insulator. Bose glass. Green's function. Spectral function.

List of publications

- R. S. Souza, A Pelster, and F. E. A. dos Santos, "Green's function approach to the Bose-Hubbard model with disorder", *New Journal of Physics*, vol. 23, no. 8, p. 083007, 2021.
- R. S. Souza, A Pelster, and F. E. A. dos Santos, "Emergence of damped-localized excitations of the Mott state due to disorder", *arXiv:2209.02435*, 2022.

List of Figures

1.1 Energy shifts induced on the atomic energy levels due to the electric field. On the left-hand side are energy shifts of the ground and excited states. On the right-hand side we see a qualitative picture of how those energy shifts can be understood as a trapping potential. 16

1.2 Optical dipole traps with far detuned radiation field. For red detuning (left) atoms are trapped in the maxima of light intensity. For blue detuning (blue) atoms move towards minima of light intensity. 17

1.3 Optical lattices. On the left we see how the laser fronts can be superimposed to form two-dimensional (upper) and three-dimensional (lower) lattice potentials. The right image shows the mirror device to produce such crystals of light. 18

1.4 Speckle laser production. a) A laser beam is scattered by a diffusive plate producing a speckle pattern. b) Typical intensity distribution of the speckle pattern. 19

1.5 Band structure of a single particle in a periodic potential for different values of potential depth V_0. As V_0 is increased the difference in energy between the energy bands becomes larger. 21

1.6 Bose-Hubbard Hamiltonian. The lattice is represented by the oscillating green line while the quantum particles are represented by the red dots. The parameters are defined as: V_0 corresponds to the lattice depth, J is the tunneling energy, U represents the on-site interaction, ϵ_i corresponds to the local shift caused by the trapping potential. 23

1.7 Different states for two particles in a double well potential. The upper row corresponds to a symmetric potential while the lower row corresponds to an asymmetric potential. The potential is represented by the green lines and the particles are represented by the red dots. 27

1.8 Superfluid ground state. Particles are delocalized (blue region) through the whole lattice volume (black line). 28

1.9 Mott insulating ground state. An integer number of particles (red dots) gets localized (wave functions in blue) at each lattice site (the lattice is represented by the black line). 29

1.10 Bose glass ground state. On the left side we can see how the particle density (upper row) is accumulated around the minimum of the random potential (lower row) for free particles. In middle we can observe how the particle density gets distributed over the random potential minima in the presence of interactions. On the right side, we show such rare regions of condensed bosons (blue) in an insulating background (pink). 30

1.11 Experimental setup for TOF imaging. On the left side we can see an example of the time sequence for the measurement. On the right side we observe the optical setup for both the random potential and the imaging beam. 32

1.12 Multiple matter wave interference patterns obtained in TOF measurements for different lattice potential depths V_0. (a) 0E_R; (b) 3E_R;(c) 7E_R; (d) 10E_R; (e) 13E_R; (f) 14E_R; (g) 16E_R; and (h) 20E_R. 33

1.13 Density profile of superfluid and Bose glass phases. The white ellipses correspond to the fitted (Thomas-Fermi) radius of the atomic cloud where the fitted profile was subtracted in the right images. The superfluid state presents a smooth density profile while the Bose glass manifests vortex defects indicated by the red arrows. 33

2.1 Low energy eigenvalues of the Hamiltonian $\hat{H}(\mathrm{g})$. On the left side we see the the level actually crossing. On the right side the more general avoided level crossing is shown. 36

2.2 Landau effective potential in the order parameter space for $a_2 > 0$ (left) and $a_2 < 0$ (right). On the left panel, the effective potential has a single minimum at the point where the order parameter vanishes. As the order parameter becomes finite, we observe on the right panel that the effective potential transforms into a Mexican-hat potential characterizing the symmetry-broken phase. 38

2.3 Phase diagram of the Bose-Hubbard Model in the clean case for three dimensions at zero temperature. The phase boundary between superfluid (SF) and Mott insulator (MI) presents a Mott-lobe structure. 40

2.4 Phase transitions for the $n = 1$ Mott lobe. The critical exponents for the generic transitions, which occur off the tip of the Mott lobe, differ from the transition exactly at the tip. The lines of constant density are indicated in gray, while the phase boundary is depicted in blue. 41

2.5 Qualitative phase diagram of the disordered Bose-Hubbard model. The Mott insulator (MI) is shown in blue, the Bose glass (BG) in pink, and the superfluid (SF) in white. The BG intervenes between the MI and SF for finite disorder and dominates the insulating part of the phase diagram if the disorder energy scale is greater than the interaction energy. 43

2.6 Phase diagram of the disordered Bose-Hubbard model obtained with Monte-Carlo simulations. The left graph corresponds to the two-dimensional case and the right graph corresponds to the three-dimensional case. The superfluid, the Mott insilator, and the Bose glass ground states are represented by SF, MI, BG, respectively. Both diagrams show that, for finite disorder strength, no direct SF to MI transition is possible. 44

3.1 Usual experimental procedure. The system is in equilibrium at first (left), an excitation enters the system at time $t_0 = 0$ (middle) and after it has propagated, the excitation lives the system at a later time t when it is measured (right). 50

3.2 Cyclic color function plot over $\arg \overline{g_i(\omega)}$ for a continuous disorder distribution. The upper row represents the case where $n_0 = 0$, that is only the quasiparticle branch is present, while the lower row corresponds to the case $n_0 = 1$ where the quasihole branch appears as well. In the limit of zero disorder (left) the singularities correspond to simple poles. When disorder is finite (middle and right) the simple poles transform into branch cuts. 68

3.3 Time dependence of the absolute square of $\overline{G^R(\mathbf{k},\mathbf{k}';t)}$. For the clean case, $\Delta \to 0$, the amplitude is constant, while it decays rapidly for finite disorder strength $\Delta = 0.1\mu$. 70

3.4 Sketch of a two beam Bragg spectroscopy. A laser beam with wavevector $\mathbf{k}_A$ and frequency ω_A intersects at an angle 2θ with a second laser beam with wavevector $\mathbf{k}_B$ and frequency ω_B (red arrows) creating a lattice grid which is superimposed in the atomic cloud (blue). 71

3.5 Experimental procedure and measurement of the spectral function. (a) A near-resonant speckle laser with detuning Δ_L is applied to create either an attractive (red detuned, $\Delta_L < 0$) or repulsive (blue detuned, $\Delta_L > 0$) random external field which is sensible only to atoms in state $|2\rangle$. In (b) and (c) a radio-frequency (rf) field is applied in the condensed atoms to induce the transition $|1\rangle \to |2\rangle$ where $\mathcal{E}_\delta$ is the energy of the final state which depends on the detuning of the rf-field from the bare transition. The spectral function is then proportional to the transfer rate measured via fluorescence imaging. The resulting measurement of $\overline{A(\mathbf{k}=\mathbf{0},\hbar\delta)}$ for a repulsive disordered potential is shown in (d) and (e) for different disorder strengths Δ. The blue dots correspond to experimental points while the red line represents numerical results of a time-propagation algorithm. 73

5.1 Qualitative sketch of the spectral function $\overline{A(\mathbf{k},\omega)}$ for fixed $a|\mathbf{k}| \ll 1$ in the quasiparticle branch of the spectrum. The sharp dashed-black peak at $\omega_0^+(\mathbf{k})$ corresponds to stable excitations of the clean case. Disorder shifts this peak to $\omega^+(\mathbf{k})$ (red) towards lower energies while it also creates damped states with dispersion $\omega_r(\mathbf{k})$, which appear as a broad peak (blue) of finite width $\Gamma(\mathbf{k})$. These qualitative aspects are analogous for the quasihole branch. . . . 86

5.2 Clean case spectral function (5.5) at $\mathbf{k} = \mathbf{0}$ in the first Mott lobe $n_0 = 1$ for $d = 3$. We have given a finite width to the δ-peaks in order to represent them graphically. The right plot, where the tunneling energy is fixed at $J = 0.0002U$, shows that the quasihole and quasiparticle peaks, which occur at negative and positive frequencies, respectively, appear well separated. When the hopping energy is increased to $J = 0.026U$ in the left plot, the energy gap decreases and the excitation peaks appear close to each other. We have chosen the chemical potential to be $\mu = 0.5U$ on the right plot and $\mu = 0.41U$ on the left plot such that the peaks appear symmetric. 87

5.3 Time evolution of the absolute square values of the retarded Green's function (5.12) for $d = 1$ and $n_0 = 0$. Feature scaling was applied to the curves of finite t. The amplitude spreads through space over time. The tunneling energy and the chemical potential are fixed at $J = 0.035U$ and $\mu = 0.3U$, respectively. Despite the fact that the interactions do not play a role in this case, we select U as the energy scale with the aim of locating the equilibrium points in the $J \times \mu$ phase diagram. 89

5.4 Band structure for the Mott lobe $n_0 = 0$. (a), (d) and (g) correspond to the spectral function (5.32). (b), (e) and (h) represent the dispersion relations (5.24), (5.26) and (5.28). (c), (f) and (i) show the density of states (5.33). The shaded-lightblue region and the dotted-red lines in (b), (e) and (h) correspond to the band of damped states of width Δ and the jumps of the dispersion relations, respectively. Although interactions are not important in this case, we chose U as the energy scale in order to specify the points in the $J \times \mu$ phase diagram. 95

5.5 Effective mass (5.28) (a) and lifetime (5.29) at $\mathbf{k} = \mathbf{0}$ (b). Both plots include the cases of $d = 1$, $d = 2$ and $d = 3$ which are represented respectively by the dotted, the dot-dashed and the continuous red and blue lines. The dashed-black line in (a) represents the effective mass in the clean case (5.27). The dashed-green line in (b) correspond to time scale associated with the inverse of the disorder strength $1/\Delta$. We use the same value of the tunneling energy as the one used in Fig. 5.4. 96

5.6 Band structure for the Mott lobe $n_0 = 1$ in the case of $d = 1$. The upper row depicts to the quasiparticle branch with $\mu = 0.8U$ and the lower row corresponds to the quasihole branch with $\mu = 0.2U$. (a) and (d) represent the spectral function (5.21). (b) and (e) follow from the dispersion relations (5.41). (c) and (f) result from the density of states (5.33). The shaded-lightblue region and the dotted-red lines in (b) and (e) correspond to the band of damped states of width Δ and the jumps of the dispersion relations, respectively. In all plots we have chosen $J = 0.025U$ and $\Delta = 0.2U$. 99

5.7 (a) Effective mass (5.16). (b) Lifetime at $\mathbf{k} = \mathbf{0}$ (5.20). In both plots the dotted and continuous red and blue lines correspond to the quasihole and quasiparticle branches, respectively. The dashed and dot-dashed black lines in (a) correspond respectively clean-case quasiparticle and quasihole effective masses. The dashed-green line in (b) corresponds to the time scale associated with the inverse of the energy scale of disorder, i.e. $1/\Delta$. In both plots we chose $J = 0.025U$. 99

5.8 Time evolution of the absolute square value of the Green's function for $d = 1$ and $n_0 = 0$. (a) correspond to the total Green's function $|\overline{G_{ij}(t)}|^2$, where we have used feature scaling to better illustrate the behavior of the amplitude at long time scales. (b) Contribution $|\overline{G^+_{ij}(t)}|^2$ of the stable states. (c) Contribution $|\overline{G^r_{ij}(t)}|^2$ of the damped states. In all plots we chose $J = 0.035U$, $\Delta = 0.2U$ and $\mu = -0.3U$. 102

6.1 Superfluid phase boundary obtained from (6.4) for the finite temperature $k_B T/U = 0.01$, with $z = 6$, and for different values of the disorder parameter. The disorder energy scales is set at $\Delta/U = 0.5$ in (a) and at $\Delta/U = 1$ in (b). 105

6.2 Density plot of the local density of states obtained from (6.5) for a uniform disorder distribution with $k_B T/U = 0.01$ and $z = 6$. The black regions correspond to the Mott-insulator phase, where $\overline{\rho_i(0)} = 0$, and the grey region corresponds to the Bose-glass phase, where $\overline{\rho_i(0)} \neq 0$. The red line indicates the result (6.4) for the phase boundary to the superfluid phase as shown in Fig. 6.1, which corresponds to the white region of the figures. The disorder strength is fixed with $\Delta/U = 0.5$ in (a) and $\Delta/U = 1$ in (b). 106

6.3 Phase boundaries for the case of $k_B T/U = 0.01$, $z = 6$, and $\Delta/U = 0.5$. The continuous red line corresponds to (6.4), while the dashed-black lines indicate (6.12) for $n = 1,2,3$, i.e., the phase boundary between Mott insulator and Bose glass obtained from the result for the local density of states. The green dots represent the critical points where the three phases coexist. . . . 108

6.4 Comparison between theoretical and numerical results for the first Mott lobe in the disordered case for two and three dimensions at both zero and finite temperatures. The continuous-red line corresponds to (6.4) and (6.12), i.e., the results of our Green's function approach, while the blue dots indicate the numerical predictions of [1] for the $d = 2$ case and [2, 3] for the $d = 3$ cases. Figures (a) and (b) show the $d = 2$ and $d = 3$ zero-temperature phase boundary with $\Delta/U = 0.6$ and $z = 4$ and $z = 6$, respectively. Figure (c) presents the finite temperature $3d$ phase boundary with $\Delta/U = 0.5$, $z = 6$, and $k_B T/U = 0.03$. 110

7.1 Dispersion relation of the excitations in the superfluid phase for a cubic lattice with $k_B T/U = 0.033$, $\mu = 0.4$ and different values of the tunneling energy. For the left, middle, and right images the values are $Jz = 0.18U$, $Jz = 0.20$, and $Jz = 0.22U$, respectively. 122

Contents

Dedicatoŕia ii

Agradecimentos iii

Epígrafe iv

Resumo v

Abstract vi

List of publications vii

List of figures viii

Introduction 1

I Theoretical background 13

1 Cold atoms in random optical lattices 14
- 1.1 AC-Stark effect 14
- 1.2 Optical lattices 17
- 1.3 Speckle laser disorder 19
- 1.4 Bose-Hubbard model 20
  - 1.4.1 Single-particle band structure 20
  - 1.4.2 Bose-Hubbard Hamiltonian 22
  - 1.4.3 Hamiltonian parameters 24
  - 1.4.4 Ground states of the Bose-Hubbard model 25
- 1.5 Detection 31
  - 1.5.1 Time-of-flight imaging 31
  - 1.5.2 Experimental characteristics of the ground states 32

2 Superfluid to insulator phase transition 35
2.1 Quantum phase transitions 35
2.2 Landau Theory 37
2.3 Zero-temperature phase diagram for the clean system 39
2.4 Zero-temperature phase diagram for the disordered system 42

II Methods 48

3 Single-particle Green's functions 49
3.1 Linear response 49
3.2 Källén-Lehmann representation 52
3.3 Spectral function 55
3.4 Imaginary time and Matsubara formalism 58
3.5 General properties in disordered systems 60
3.6 Physical interpretation: elementary excitations 61
3.7 Bose-Hubbard model in the limit of strong interactions 64
3.8 Measurements in disordered systems 70
3.8.1 Bragg spectroscopy 71
3.8.2 Radio-frequency transfer 72

4 Perturbation Theory 75
4.1 Hopping expansion 75
4.2 Partial summation 78
4.3 Poincaré-Lindstedt method 80

III Results 84

5 Excitations of the disordered Bose-Hubbard model 85
5.1 Spectral function 86
5.1.1 Clean case 86
5.1.2 Disordered case 89
5.2 Uniform disorder distribution 92
5.2.1 Mott lobe $n_0 = 0$ 92
5.2.2 Mott lobe $n_0 = 1$ 97
5.2.3 Green's function in space time 100
5.3 Summary of results 102

6 Phase diagram at finite temperatures 103
6.1 Superfluid phase boundary 103
6.2 Local density of states 105

6.3 Mott insulator to Bose glass phase boundary 107
6.4 Comparison with numerical results 109
6.5 Summary of results 111

IV Preliminary calculations 112

7 Superfluid elementary excitations 113
7.1 Effective-action approach 113
7.2 Excitation spectra in the Mott-insulator phase 119
7.3 Excitation spectra in the superfluid phase 121
7.4 Bose-glass spectra 123

8 Free lattice bosons with weak disorder 124
8.1 Disorder expansion 124
8.2 Single-site approximation 129

V Final remarks 131

9 Summary and conclusions 132

References 149

Appendices 151

A Functional-integral formalism 151
A.1 Lattice occupation number representation and Fock space 151
A.2 Coherent states 152
A.3 Imaginary-time path integral and the partition function 154

B Sum rule for the case of $n_0 = 0$ 158

C Limit of large space separations 160

Introduction

Exploring how structure emerges in nature is perhaps one of the most profound and interesting questions in science. One intriguing example comes from atomic theory. At first glance, in the length scales we usually encounter, most things seem to be made of nothing but continuous ordinary matter to the naked eye. However, over the last century, it has been consistently proven that matter is in fact comprised of extremely small and differentiated constituents that interact in such a way as to create emergent structures. These small pieces of matter are called atoms, and their size is usually smaller than one nanometer. In order to properly describe the behavior of such small pieces of matter, one has to rely on the laws of quantum mechanics. It is already challenging enough to understand the nature of one atom or even how a few atoms interact under this framework. To some extent, the task of physicists, since the advent of the quantum description of matter in the first half of the last century, has been to understand that the behavior of large aggregates of such particles cannot be directly derived from a simple extrapolation of the properties of one of their single constituents. This problem was elegantly pointed out by P. W. Anderson in his essay "More Is Different" [4], when analyzing the emergent phenomena that appear in large and complex aggregates of elementary particles. The careful investigation of the quantum origin of emergent phenomena in the field of quantum many-body physics has provided many fundamental discoveries in this regard, including novel states of matter, the experimental observation of previously unseen quantum phase transitions, and new macroscopic quantum phenomena that emerge when the laws of quantum mechanics become important beyond the atomic and subatomic scales, thus determining the collective behavior of macroscopic systems [5].

A simple picture of emergent phenomena in many-body systems may be drawn from their elementary excitations. Given the degrees of freedom of a system composed of a large aggregate of quantum particles, one must use statistical mechanics to describe its thermodynamic properties. The characterization of a closed quantum system, that does not interact with its surroundings, depends on its energy levels as well as on its temperature. The microscopic description of such thermodynamic properties can be derived from the Boltzmann distribution, $p_i \propto \mathrm{e}^{-E_i/k_B T}$, which gives the probability p_i that a macroscopic subpart of the original system will occupy a particular energy state E_i, based on the equilibrium temperature T, where k_B represents the Boltzmann constant. According to this distribution, low energy states have a higher probability of being occupied. At sufficiently low temperatures, the important energy levels correspond to the low-energy excited states. These excited energy levels of the many-body system are often referred to as elementary excitations. This comes from the assumption that any energy level can be acquired from the sum of a finite number of these excitations [6]. In many cases, such excitations behave extremely similar to an individual free particle with a definite energy and velocity. In fact, the only differences may arise from their mass and lifetime. As a result of internal interactions in the system and the coupling to an external potential, these excitations acquire what is called an effective mass. It is as if the mass of the bare particles gets dressed by such interactions [7]. Consequently, such excitations may also be unstable, presenting a finite lifetime. That is, they resemble a real particle only during the time when the conservation of energy and momentum occurs, and decay due to damping afterwards. Thus, another form of referring to these excitations is the term "quasiparticle". It is important to point out that such elementary excitations emerge as a consequence of the collective behavior of a large aggregate of quantum particles. This implies that they pertain to the system as a whole and not to its individual constituents. A great deal of emergent phenomena in quantum many-body systems can be explained by characterizing the energy spectra of quasiparticles.

The fact that identical quantum particles are indistinguishable plays an important role in describing how such particles interact to form macroscopic phenomena. Any permutation of the internal constituents of an ensemble of quantum particles has no relevant consequences for physical observables. One intrinsic property that is relevant in the statistics of large aggregates of quantum particles is their spin angular momentum. This property is associated with internal degrees of freedom that arise only in the quantum description of matter, leading to the spin-statistics theorem of Pauli, which points out the fundamental distinction between two different kinds of quantum particles: fermions with half-integer spin and bosons with integer spin. A simpler picture for this distinction, in the case of atoms, is based on their even smaller constituents: electrons, protons, and neutrons. If the number of constituents is even, these atoms are called bosons, if it is odd, we call them fermions. Many interesting phenomena emerge from this distinction. While identical fermions are not allowed to occupy the same quantum state, as explained by the Pauli exclusion principle, identical bosons are allowed to pile up in the same state. In this thesis, we are particularly interested in the emergent phenomena of large aggregates of neutral bosonic atoms in low-density gas states at low temperatures, where the fact that identical bosons are allowed to occupy the same quantum state is of central importance.

In ordinary atomic gases, particles move randomly in all directions following what is usually called thermal motion. In the quantum description of matter, these atoms are represented as wave-like objects with an extent given by the thermal de Broglie wavelength, λ_{dB}, which scales with the inverse square root of the equilibrium temperature, i.e., $\lambda_{\mathrm{dB}} = (2\pi\hbar^2/k_B mT)^{-1/2}$, where $\hbar$ is Planck's constant. If the equilibrium temperature is sufficiently high, λ_{dB} becomes small and the system can be treated as if each atom were a billiard ball. By cooling the atomic cloud to a certain critical temperature, one can reach a state where the de Broglie wavelength becomes larger than the average distance between the atoms, and the wave functions of the atoms start to overlap. In this state, for bosonic atoms, the individual identity of the particles begins to break down, and they start to behave collectively. This collective behavior originates from the macroscopic aggregation of atoms in the same quantum state, which generates a coherent matter wave. Such an emergent phenomenon was predicted by A. Einstein in 1924 and 1925 [8, 9], based on previous work by S. Bose [10], and characterizes a quantum phase transition to the so-called Bose-Einstein condensate. This phase transition occurs at a critical temperature, where the thermal de Broglie wavelength is of the same order as the average particle distance, which is determined by the inverse cubic root of the particle density. Below this critical temperature, a correlation emerges between the bosonic quantum particles, such that it becomes energetically favorable for the system to respond only as a whole to the action of external forces. A macroscopic number of particles behaves as one quantum wave.

Even though the prediction of the macroscopic condensation of bosons into the same quantum state was made early in the development of quantum theory, its experimental realization in atomic quantum gases was only possible in 1995 [11, 12]. The experiments were carried out by cooling dilute gases of alkali atoms such as Rubidium and Sodium, in which only two-body collisions play a role. It was realized that for very dilute gases at low temperatures, a metastable equilibrium state is possible, but the pathway to liquefaction and solidification is dynamically suppressed.

The first experiments that realized atomic Bose-Einstein condensates were based on two techniques for cooling down the atoms. The first is known as laser cooling, which involves using counterpropagating laser beams to reduce the temperature of the atomic cloud. If the laser light is detuned below atomic resonance, an atom in thermal motion moving towards the laser front may absorb a photon due to the Doppler effect. The atom will eventually decay from its excited state due to spontaneous emission, emitting a photon in a random direction. The result of this process is that the atom loses kinetic energy. By repeating this procedure, it is possible to cool the atomic cloud to the order of microkelvin. The laser-cooling technique was developed in the 1980s [13] and culminated in the 1997 Physics Nobel Prize awarded to S. Chu, C. Cohen-Tannoudji, and W. D. Phillips. The second experimental technique used to cool the atomic gases even further consists of carefully applying a radio frequency field that couples the most energetic atoms to states outside of the trap by creating a repulsive force that expels the atoms. This technique is called evaporative cooling and makes it possible to reach temperatures of the order of nanokelvin in experiments. The Bose-Einstein condensation of ultracold atomic gases was then verified by reaching such extremely low temperatures and releasing the cloud from its trap, allowing it to expand freely for a few milliseconds of time-of-flight. In this free expansion, the most energetic atoms escape rapidly while the condensed atoms remain near the region that corresponds to the center of the now-absent trapping potential. The measurement consists of taking absorption pictures of the expanded cloud, which indicates a large aggregation of atoms in low momentum states corresponding to condensation. The experimental realization of the condensation of atoms in cold gases of neutral atoms led to the achievement by C. Wieman, E. A. Cornell, and W. Ketterle of receiving the Nobel Prize in Physics in 2001. Since the experimental verification of Bose-Einstein condensation in ultracold atomic gases, these systems have become one of the most exciting research areas in modern physics due to their potential to explore fundamental concepts concerning the quantum origin of macroscopic emergent phenomena in quantum many-particle systems. The ever-growing development of experimental techniques in the control and manipulation of these systems has made them promising candidates for realizing R. Feynman's quantum simulator idea [14], in which ultracold atomic gases in different external potentials are used to mimic the physics of other quantum systems of many particles.

One of the most interesting aspects of ultracold atoms is their ability to realize the interplay between superfluidity and localization. This question can be addressed in different ways, one of which is particularly important to the present work: the study of the properties of cold bosonic atoms submitted to a lattice potential. Such a lattice structure consists of artificial crystals of light, known as optical lattices [15]. They are created by generating a standing light wave using counter-propagating laser beams. The coupling between the atoms and the radiation field is mediated by the AC-Stark effect, which induces an atomic dipole moment. The atomic energy levels are then modified, and the energy shift serves as a trapping potential for the condensed atoms. Such an energy shift is proportional to the square of the radiation-field amplitude and hence its intensity. By aligning different pairs of counter-propagating laser beams at distinct angles with respect to each other, one can create optical lattices in one [16, 17], two [18, 19], or three dimensions [19].

When a condensate is loaded into an optical lattice, the modulation of the lattice parameters can drive the system into a strongly correlated regime. If the intensity of the radiation field is small, the coupling of the laser beam with the condensed atoms is weak, and the system can still be described as a coherent matter wave. In this situation, the atoms are delocalized and can flow without friction through the lattice volume, corresponding to a superfluid ground state. In the opposite case, if the intensity of the radiation field is sufficiently large, its coupling with the atoms becomes strong, driving the system into a phase transition such that it can no longer be described by a matter wave. Rather, the frictionless flow of particles gets destroyed, and a finite number of them become localized in each potential well. The strong intensity of the radiation field is directly related to a deep lattice regime where the contact interactions between atoms at the same lattice site become large compared to their kinetic energy. This phenomenon is known as Mott localization, resulting in a Mott insulating ground state. Such a Mott state corresponds to a gapped insulating phase. In contrast to regular band insulators, where the energy gap emerges due to destructive interference between the atomic orbitals, the Mott-insulator energy gap occurs due to the strong repulsion between the quantum particles [20].

The superfluid to Mott insulator phase transition occurs due to the competition between the different energy scales of the system and can take place even at the limit of zero temperature, characterizing it as a quantum phase transition [21]. This phase transition was first predicted in the seminal paper of Fisher et al. [22] and experimentally verified by Greiner et al. [23] based on a proposal by Jaksch et al. [24]. The experiment consisted of measuring the multiple matter wave interference pattern of the atomic cloud by taking absorption pictures after a few milliseconds of free time-of-flight expansion. For shallow lattices, sharp peaks were found in the interference pattern, representing the phase coherence present in the superfluid phase. For deep lattice depths, such a phase coherence pattern gave place to a diffuse background indicating Mott localization.

Another way to address the question of localization is by studying how robust the bosonic matter-wave coherence is in the presence of disorder. This research field is commonly referred to as the dirty boson problem. Such a problem was first investigated in the context of the transport properties of superfluid helium in porous media [25]. In this case, disorder is considered static, meaning that the time scales of thermal and quantum fluctuations are much smaller than the time scale of variation in the disorder. In the field of atomic condensates, the investigation of this problem first arose due to the inevitable presence of imperfections in the trapping potential [26]. However, disorder is believed to be intrinsic to real systems, making the investigation of its effects indispensable to understanding real-world problems. Nowadays, disorder can be realized in different ways, such as the generation of speckle laser fronts, which are highly tunable [27, 28], the use of micromirror devices to produce random potential landscapes [29], or even the presence of impurity atoms at random locations in the system fixed by optical dipole traps [30, 31]. The phenomenon of localization due to disorder was first studied by P. W. Anderson [32] when analyzing a system of non-interacting particles in the presence of a random lattice potential. Anderson verified that if the degree of randomness is sufficiently strong, no diffusion can occur, and the particles become localized. This originates from the interference of particles that have experienced multiple scattering events by the random potential. This phenomenon is usually referred to as Anderson localization, and it was further verified to be a general property for the propagation of waves in a disordered medium [33]. Despite its early development in 1958, the phenomenon of Anderson localization still attracts attention in academic research.

In the case of Bose-Einstein condensates, Anderson localization was only verified by reaching a regime where interactions are negligible. In Ref. [34], localization was verified by reducing the density of the atomic cloud while letting it expand out of the trap through a one-dimensional waveguide. During such an expansion, the interaction energy is converted into kinetic energy, and the condensed atoms diffuse, becoming almost non-interacting. The condensate was then exposed to a random speckle potential. For sufficiently large intensities of this potential, the expansion of the condensate stops, and its density distribution was found to decay exponentially, which is one of the signatures of Anderson localization. On the other hand, Ref. [35] reported the localization of a non-interacting condensate in a one-dimensional quasiperiodic lattice. Such a quasiperiodic lattice potential was generated by superimposing two incommensurate standing waves generated by different pairs of counter-propagating laser beams. Interactions were then tuned to be negligible compared to the kinetic energy of the particles via Feshbach resonance. This technique consists of altering the scattering length, which controls the short-range interactions between the particles by applying an external magnetic field [5]. Similarly to the previous experiments, the atoms were then allowed to diffuse in the quasiperiodic lattice for different strengths of the disorder energy scale. For sufficiently strong disorder, no diffusion was observed, indicating that the system reached an Anderson localized state. One question that remains open, however, is how localization is affected by strong interactions between the particles that compose a many-body system.

Assuming a short correlation length for the disorder distribution of the random potential, one can estimate the probability of having a large region where the potential is at its minimum. Such probability is found to decrease exponentially according to the size of the region, however, it remains finite [36]. If a cloud of non-interacting condensed bosons is put in the presence of such a disordered potential, a macroscopic number of particles would concentrate around the large enough region where the potential is at a minimum. Due to the high density of bosons in such a region, the ground state of the system becomes unstable to the presence of internal interactions between the particles. Thus, in this scenario, even in the weakly interacting regime, the particles would be pushed into other local minima of the disorder potential, producing a localized ground state composed of droplets of condensed particles with no transport between them. This characterizes an insulating phase with local coherence emerging as a direct consequence of the presence of disorder: the Bose-glass phase. The emergence of such a phase in the superfluid to Mott insulator phase transition due to disorder was first predicted in the groundbreaking contributions of Ref. [22] in 1989. Its direct experimental verification was achieved later in 2016 by C. Meldgin et al. [37]. The experiment was done by preparing a Bose-Einstein condensate inside a three-dimensional optical lattice potential with an additional disordered potential produced with laser speckles. The time-of-flight technique was then applied after having prepared the random potential at different disorder strengths. For strong disorder, due to the presence of local puddles of condensed particles, the density profile measured in that experiment after free expansion was found to present modulations, which originated from vortex excitations generated by the interference of local condensates. This characterized a direct probe of the Bose-glass phase. While some features of the Bose-glass phase are comprehended to a certain degree, numerous intriguing inquiries regarding its characterization remain unresolved.

The fundamental problem regarding the interplay between disorder, Mott localization, and superfluidity is brought together by the Bose-Hubbard model. This model describes spinless bosons with short-range interactions within a disorder lattice and is experimentally realized in the lowest Bloch band limit of systems of ultracold bosons in random lattice potentials. The model is characterized by three competing energy scales: the hopping energy, associated with the tunneling of particles from a site to one of its first neighbors; the interaction energy, which accounts for the on-site repulsion between particles at the same lattice site; and an energy shift caused by disorder at each lattice site. If the hopping energy is large compared to the other energy scales, particles can flow without friction, and the ground state is a superfluid. If interactions dominate over disorder and tunneling energies, a finite number of particles become localized in each lattice site, and the ground state becomes a Mott insulator. However, in the case of strong disorder, local puddles of condensed particles emerge in an insulating background, giving rise to a Bose-glass state. These qualitative aspects of the phase diagram corresponding to the disordered Bose-Hubbard model were first investigated in [22]. Since this pioneering contribution, much information about the details of the phase transitions between these phases has been obtained. The superfluid phase is distinguished from the insulating phases by the presence of a macroscopically occupied coherent state, which leads to finite correlations even at the limit of large space separations in the system. This phenomenon is called off-diagonal long-range order. Another key distinction comes from the energy spectrum of elementary excitations in the superfluid phase. Such an energy spectrum is gapless, with low-energy excitations corresponding to the Nambu-Goldstone modes, and the additional presence of a gapped amplitude mode usually referred to as the Higgs mode. The presence of a gapless mode in such a phase is a direct consequence of the breaking of the continuous phase invariance, which follows from the Nambu-Goldstone theorem. In the lattice system, superfluidity occurs when linked to fluctuations in the average number of particles per site, which lead to a finite compressibility. Unlike the superfluid state, both Mott insulator and Bose glass present no long-range order. In the Mott phase, fluctuations in the average on-site particle density are suppressed by the strong interactions, and an integer number of particles become localized at each site. At zero temperature, this leads to a vanishing compressibility. However, for finite temperatures, the Mott phase acquires a residual finite compressibility [38]. The energy spectrum of the Mott phase is identified by its gap for quasiparticle and quasihole excitations. For a perfect lattice, these excitations are stable and delocalized, meaning that they can propagate without damping through the whole system. It has been demonstrated that, in the absence of disorder, the Mott gap closes when the phase boundary to the superfluid phase is crossed, such that the dispersion of the quasiparticles and quasiholes transforms continuously into the Nambu-Goldstone and Higgs amplitude modes [39]. In contrast, the Bose-glass phase, which emerges due to the presence of disorder, corresponds to a gapless insulating phase. The gapless excitations in this phase emerge due to the presence of local condensates, which also lead to a finite compressibility [22].

The analytic expression of the eigenstates and eigenenergies of the Bose-Hubbard model cannot be computed in general. Thus, many methods have been applied to investigate the system. Some of these methods include local [1] and stochastic mean-field techniques [2, 3] and Monte Carlo calculations [40, 41, 42, 43, 44, 45, 46, 47, 48, 49]. However, the analytic investigation of the effects of disorder has been mainly restricted to mean-field theory [38, 50, 51]. Although many aspects of the excitations of the Mott phase have been investigated in the clean case, a precise investigation of the effects of disorder on their energy spectrum remains unavailable. Moreover, a rigorous characterization of the low-energy excitations of the Bose glass phase is still lacking. Another problem that remains unsolved concerns the precise phase boundary between the Mott and the Bose-glass phases. Due to the residual fluctuation in the average particle density inside the Mott phase at finite temperatures, the compressibility becomes an unreliable parameter for such distinction. Based on the different nature of the energy spectrum of these insulating phases, it has been proposed that the local density of states could serve as a parameter to identify them [22, 38]. However, it is important to investigate whether one can use such a quantity to calculate the analytic expression of the phase boundary between the Mott insulator and the Bose glass at finite temperatures, at least for small values of the tunneling energy. With the aim of understanding the microscopic derivations that explain the answer to these questions, this thesis is dedicated to constructing an analytical method to investigate the fundamental details concerning the effects of disorder in the strongly interacting regime of the Bose-Hubbard model.

Our analysis is based on the single-particle Green's function. This function appears as a measure of the linear response of the system to an external perturbation. However, it provides an even deeper physical insight into the behavior of the elementary excitations of the disordered Bose-Hubbard model as well as on the phase boundaries between each of its ground states. The singularities of the Green's function in frequency-momentum space can be related to the eigenstates of the underlying Hamiltonian. We interpret these eigenstates as the elementary excitations of the system. This information is encoded in the so-called single-particle spectral function which presents a peak on the exact location of the singularities of the Green's function. By calculating the location of these peaks, one can obtain the dispersion relation of the excitations in the first Brillouin zone. In the presence of disorder, translational invariance is broken due to the local imperfections of the random lattice. However, if one is interested only in the global effects of disorder and not in some local properties of a specific realization of the random potential, one can average over all possible realizations. This process of disorder ensemble average guarantees that translational invariance is recovered on average. Thus, the same concepts concerning the singularities of the Green's function in frequency-momentum space as well as the peaks of the spectral function for the classification of the excitations can be applied in this case. One can extract from the Green's function the condition which leads to the divergence of long-wavelength correlations and thus obtain the phase boundary to the superfluid phase. Furthermore, one can calculate the local density of states from the local Green's function in space. Such a local density of states is predicted to vanish at zero energy in the Mott phase due to the existence of the energy gap. In contrast, the gapless spectrum of the Bose glass phase leads to a finite local density of states at zero energy. Therefore, the computation of the Green's function gives us access not only to the energy spectrum for elementary excitations in the presence of disorder but also to the phase boundary between different ground states.

We construct a perturbation theory that consists of using the functional integral formalism to determine a strong-coupling hopping expansion to the single-particle Green's function based on the methods of Refs. [52, 53, 54, 55]. This perturbation treatment relies on field theoretical considerations. Within this hopping expansion, we generate an expression for the Green's function that allows us to investigate the disordered Bose-Hubbard model in the strongly interacting regime. By performing a partial summation of an infinite subset of terms in the hopping expansion, we obtain an analytical expression for the disordered-averaged spectral function. With this function, we analyze the nature of the elementary excitations in the disordered case. Considering the first non-vanishing contribution in the hopping expansion to the local Green's function, we apply the Poincaré-Lindstedt method to obtain a renormalized expression for the local density of state, which generalizes the result obtained in Ref. [38] for the case of finite tunneling energy.

We find that, similarly to the clean case, the Mott phase in the presence of disorder still exhibits a gap for stable excitations. However, as the region corresponding to the Mott states in the phase diagram shrinks for finite disorder, the gap for these stable excitations decreases, leading to a shift of their dispersion towards lower energies. We find that the effective mass of these stable excitations increases with the disorder strength, which implies that they become less dispersive. In addition, as a new feature caused by disorder, we find that damped states emerge for slightly higher energies at the center of the band structure. We demonstrate that the lifetime of excitations in that energy range increases with the disorder strength. By analyzing the propagation of these in real space and time, we demonstrate that excitations created in the energy range of the stable states are delocalized and dominate the propagation at long time scales. In contrast, excitations produced in the energy range of the damped states are localized and dominate the propagation at short time scales. When the disorder becomes of the same order as the interactions, the stable-delocalized excitations become dispersionless. In such a limit, the lifetime of the damped-localized excitations increases, and they dominate the whole energy band. Therefore, we argue that such damped-localized excitations correspond to the low-energy excited states of the Bose-glass phase.

By analyzing the renormalized expression for the local density of states, we confirm that such a quantity, which holds information on the available states for excitations at each lattice site, is a reliable parameter to unambiguously identify both the Mott and the Bose-glass phases for zero and finite temperatures and slightly positive values of the tunneling energy. By investigating the energy intervals where such a quantity is finite, we compute an analytic expression for the Mott-to-Bose-glass phase boundary. We then compare our results with numerical calculations from the literature and confirm that our theory goes beyond the standard mean-field theory for the prediction of the phase boundary.

To provide an alternative beyond our current methods for analyzing the system and to extend the calculations to the spectrum of excitations of the superfluid phase, we introduce an effective-action approach and a diagrammatic expansion for weak disorder. These methods can be applied separately or together, and their application appears promising for analytically characterizing the full phase diagram.

Outline of the thesis

This thesis is divided into five parts. The first part, comprising Chapters 1 and 2, is devoted to the theoretical background of the Bose-Hubbard model. The second part, containing Chapters 3 and 4, concerns the theoretical methods that we have applied to study the system. The third part is constituted by Chapters 5 and 6, which presents the main contributions from this work. In the fourth part, corresponding to Chapters 7 and 8, we present some preliminary calculations that could be used to extend the results of the present thesis as well as to produce new and insightful results for the problem examined here. Finally, in the fifth part, we summarize the contribution of this work, presenting the concluding remarks.

In Chapter 1, we start by introducing the coupling between atoms and the radiation field via the optical dipole force. We then demonstrate how one can use counter-propagating laser beams to generate the periodic structure of optical lattices. We also discuss how a random external potential can be created using laser speckles. Next, we introduce the Bose-Hubbard model, first considering the single-particle picture and then deriving the Hamiltonian within the formalism of second quantization. To connect the lattice modulation with the competitions between the parameters of the Bose-Hubbard Hamiltonian, we show how such parameters scale with the lattice potential depth up to the first approximation. We then describe the ground state of the system, as well as the techniques used to experimentally probe them.

Chapter 2 comprises a review of the important aspects of phase transitions between the ground states of the Bose-Hubbard model. Firstly, we present the definition of quantum phase transitions and important aspects concerning the scaling behavior near criticality. Then, we discuss the Landau theory as a method for investigating the symmetry-breaking mechanism that occurs in continuous phase transitions. These critical properties of quantum phase transitions are discussed in the context of the Mott-superfluid phase transition in the clean case. Next, we work how the presence of disorder affects the phase diagram, specifically how the Bose-glass state intervenes.

We present the principal characteristics of the single-particle Green's functions in Chapter 3. First, we discuss how these quantities emerge from linear response theory. Then, we present the general form of the Källén-Lemann representation of Green's functions and derive the spectral function, which incorporates the singularities of the Green's functions. To set the stage for our perturbation treatment, we introduce the Matsubara formalism. Next, we discuss some general properties of Green's functions in disordered systems. We then consider the physical interpretation of Green's functions in the context of elementary excitations and apply these ideas to the disordered Bose-Hubbard model in the limit of strong interactions. To close this chapter, we briefly report the techniques of Bragg spectroscopy and the radio-frequency transfer method, which can be applied in experiments to measure Green's and spectral functions.

In Chapter 4, we develop the perturbation method used to obtain the main results of this thesis. The method relies on a hopping expansion constructed in the functional integral formalism. We first demonstrate how to calculate corrections to the Matsubara Green's function in terms of the tunneling energy at a tree-level approximation. After that, we combine an infinite subset of terms in the hopping expansion of the Green's function by applying the technique of partial summation. This allows us to obtain a result that takes into account the corrections to the path of an excitation which hops through the lattice and undergoes infinitely many scattering events against the disordered potential at each site. By considering the first relevant correction to the local Green's function in the hopping expansion, we then use the Poincaré-Lindstedt method to obtain a renormalized expression for the local density of states.

Chapter 5 is devoted to the analysis of the effect of disorder on the excitation spectrum of the Bose-Hubbard model in the limit of strong interactions. To this end, we derive the spectral function that follows from the partial summation result of the Green's function. First, we present the details of the spectral function in the clean case. Then, we discuss the changes that occur in the disordered case by presenting the results for a bounded uniform disorder distribution. We then analyze the propagation of excitations by observing the spatiotemporal profile of the retarded Green's function.

The results for the phase diagram in the disordered case at finite temperatures and for small values of the tunneling energy are presented in Chapter 6. Firstly, we derive the superfluid phase boundary from the partial summation result of the Green's function. Secondly, by analyzing the renormalized local density of states obtained with the Poincaré-Lindstedt method, we obtain an analytical expression for the phase boundary of the Mott-Bose glass phase transition. Then, we present the phase diagram for a uniform disorder distribution. Finally, we compare our results with numerical calculations from the literature.

In Chapter 7, we present some preliminary calculations that serve as the starting point for investigating the effects of disorder on the excitation spectra of the superfluid phase. These calculations follow from the application of the effective-action approach. We first show how to derive the effective-action functional to recover the results for the excitation spectrum obtained in Chapter 5. By considering first-order fluctuations around its equilibrium value, we discuss how one could obtain the energy spectra for the superfluid excitations within this approach. We then present a possible order parameter that can be used to investigate the excitations in the Bose-glass phase.

Chapter 8 contains the development of a disorder expansion perturbation theory. In this chapter, we consider free lattice bosons in the presence of weak disorder and construct a diagrammatic expansion for the Green's function within the functional integral formalism. By considering a single-site approximation, it is possible to obtain a result for the singularities of the Green's function, which is similar to the one obtained with the partial summation method. We then discuss how to investigate the interacting system by considering the hopping and disorder expansion together, where the fluctuations of each perturbation method could be treated separately.

Finally, Chapter 9 comprises a summary and concluding remarks that contextualize the contributions of the present work. There, we also discuss some prospects and insights that could be topics for future research.

Appendices A, B, and C contain the derivations of the functional integral formulation of the Bose-Hubbard model, the sum rule of the spectral function, and the asymptotic behavior of the Green's function, respectively.

Part I

Theoretical background

Chapter 1

Cold atoms in random optical lattices

The interaction of atomic systems with radiation leads not only to atomic-state transitions but it also modifies the internal structure of the atomic levels. The coupling between radiation field and induced atomic dipole moment causes an energy shift in the atomic spectrum. One can explore this so-called AC-Stark effect to create optical lattices in order to realize the Bose-Hubbard model. In this chapter, we focus on discussing the basic physics of such a model and the distinct characteristics of its ground states. Furthermore, we describe how disorder can be introduced and how the different phases can be experimentally verified.

1.1 AC-Stark effect

One of the main ingredients for trapping and manipulating cold atoms with optical potentials is the optical dipole force, which relies on the AC-Stark effect. Such an effect describes how an external oscillating electric field interacts with a neutral atom, inducing a separation between its positively charged nucleus and its negatively charged electronic cloud. In the limit where the atomic wave function is extended over distances much smaller than the electric field wavelength, this separation is measured in terms of an induced electric dipole moment [56]. The resulting interaction is given by

$$\hat{H}' = -\hat{\mathbf{d}} \cdot \boldsymbol{\mathcal{E}}, \tag{1.1}$$

where $\boldsymbol{\mathcal{E}}$ represents the electric vector field and the $\hat{\mathbf{d}}$ dipole operator for a single atom. The dipole operator is defined as the electron elementary charge e multiplied by the sum of the position operators corresponding to each electron in the atom

$$\hat{\mathbf{d}} = -e \sum_j \hat{\mathbf{r}}_j \tag{1.2}$$

Generally, only the electrons composing the outer shell are important. Alkali atoms have only one outer shell electron [5].

For an oscillating electric field of the form

$$\boldsymbol{\mathcal{E}}(\mathbf{x},t) = \tilde{\boldsymbol{\mathcal{E}}}(\mathbf{x})\mathrm{e}^{i\omega t} + c.c., \tag{1.3}$$

in the limit where the its spatial variation can be considered negligible inside the atom, we can apply standard time-dependent perturbation for the atom-light interaction (1.1). If we consider the atom to be initially in its ground state, which is assumed to be an eigenstate of the parity operator with even parity, the first-order correction vanishes. Up to second order approximation the energy shift is given by [57, 58]

$$\Delta E(\mathbf{r}) = -\frac{1}{2}\mathrm{Re}\{\alpha(\omega)\}\langle \boldsymbol{\mathcal{E}}(\mathbf{x},t)^2\rangle_t, \tag{1.4}$$

where $\langle\cdots\rangle_t$ corresponds to the time average and $\alpha(\omega)$ is the complex polarizability which characterizes the atomic response to external fields. The energy shift in (1.4) is called AC-Stark shift. This result points to the fact that the polarization of the atom oscillates with the same frequency as the external electric field and thus the energy shift works as an effective trapping potential to the atom.

In order to give a simple estimate for the polarizability, we consider the problem of a static radiation field $\boldsymbol{\mathcal{E}} = \mathscr{E}_0\boldsymbol{\varepsilon}$. Using standard perturbation theory we find the second-order approximation to the energy shift to be

$$\Delta E = -\sum_e \frac{|\langle e|\hat{\mathbf{d}}\cdot\boldsymbol{\varepsilon}|g\rangle|^2}{E_e - E_g}\mathscr{E}_0^2 = -\frac{1}{2}\alpha\mathscr{E}_0^2, \tag{1.5}$$

where $|g\rangle$ and $\{|e\rangle\}$ represent the unperturbed ground state and the set of excited states of the atom with energies E_g and E_e, respectively. We have additionally introduced $\boldsymbol{\varepsilon}$ which is the unity vector defining the direction of the electric field. From (1.5) we can see that the polarizability in this case is given by

$$\alpha = 2\sum_e \frac{|\langle e|\hat{\mathbf{d}}\cdot\boldsymbol{\varepsilon}|g\rangle|^2}{E_e - E_g}. \tag{1.6}$$

Considering the simple case of a two-level atom, equation (1.5) reduces to

$$\Delta E = \pm\frac{|\langle e|\hat{\mathbf{d}}\cdot\boldsymbol{\varepsilon}|g\rangle|^2}{E_e - E_g}\mathscr{E}_0^2. \tag{1.7}$$

Such energy shifts correspond to the coupling between the atom and the radiation field producing a dipole potential. This process is depicted in Fig. 1.1.

A more complete derivation of the atomic polarizability could be done by consider-

Figure 1.1 – Energy shifts induced on the atomic energy levels due to the electric field. On the left-hand side are energy shifts of the ground and excited states. On the right-hand side we see a qualitative picture of how those energy shifts can be understood as a trapping potential.

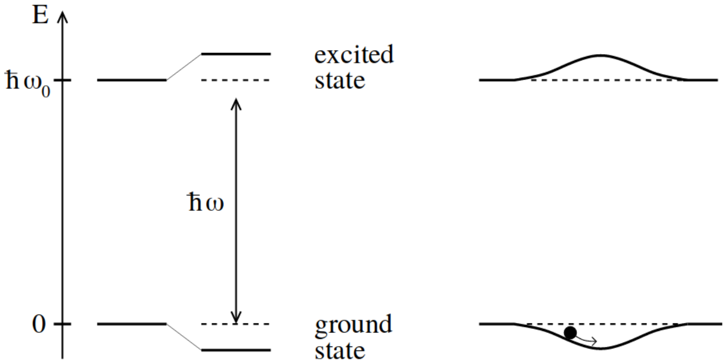

Source: Figure from Ref. [59].

ing the temporal oscillation of the radiation field as well as the finite lifetime of the atomic excited states which decay by spontaneous emission [60]. Taking into account that the energy difference between the ground state and an excited state is nearly resonant with the frequency of the external field, one can rely on a two-level description. Altogether, these considerations along with the rotating wave approximation lead to an atomic polarizability of the form

$$\alpha(\omega) \approx \frac{|\langle e|\hat{\mathbf{d}}\cdot\boldsymbol{\varepsilon}|g\rangle|^2(E_e - E_g - \hbar\omega)}{(E_e - E_g - \hbar\omega)^2 + (\hbar\Gamma_e/2)^2} + i\frac{|\langle e|\hat{\mathbf{d}}\cdot\boldsymbol{\varepsilon}|g\rangle|^2\hbar\Gamma_e/2}{(E_e - E_g - \hbar\omega)^2 + (\hbar\Gamma_e/2)^2}. \tag{1.8}$$

This approximation is valid whenever the detuning

$$\delta = \omega - \frac{E_e - E_g}{\hbar} \tag{1.9}$$

is small. A detailed derivation of these results can be found, for instance, in Ref. [57].

By defining the Rabi frequency for the cycle absorption and spontaneous emission as

$$\Omega_R = \frac{1}{\hbar}|\langle e|\hat{\mathbf{d}}\cdot\tilde{\boldsymbol{\mathcal{E}}}(\mathbf{x})|g\rangle|, \tag{1.10}$$

the conservative potential that traps the atoms can be written as

$$V = \frac{\hbar\Omega_R^2\delta}{\delta^2 + (\hbar\Gamma_e/2)^2}. \tag{1.11}$$

In general, in experiments the resulting mechanical effect comes from the potential of (1.11). Note that the sign of V depends on the detuning δ. For a red detuned trap regime of negative δ the potential becomes attractive and atoms move towards higher-intensity regions. In the case of a blue detuned trap of positive δ the maxima of light intensity correspond to

Figure 1.2 – Optical dipole traps with far detuned radiation field. For red detuning (left) atoms are trapped in the maxima of light intensity. For blue detuning (blue) atoms move towards minima of light intensity.

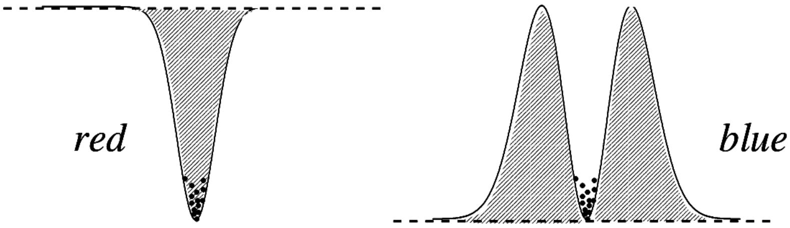

Source: Figure from Ref. [59].

potential maxima and atoms are trapped in lower-intensity regions. An illustration of both cases is shown in Fig. 1.2.

1.2 Optical lattices

Optical lattices are formed by creating a standing light wave which oscillates in time but keeps its peak amplitude stationary in space. This is done by either using a mirror to reflect the radiation field or by aligning a pair of counter-propagating laser beams (see Fig. 1.3). By combining laser beams with different frequencies one can construct optical lattices in one [16, 17], two [18, 19], and three dimensions [19].

In the classical limit, the laser field is well described by a monochromatic wave of the form of (1.3) with the spatial part given by $\tilde{\boldsymbol{\mathcal{E}}}(\mathbf{x}) = \mathcal{E}_0 \boldsymbol{\varepsilon} \cos(\mathbf{k}_L \cdot \mathbf{x})$. Here, the absolute value of the lattice wavevector $k_L = |\mathbf{k}_L|$ relates to the lattice wavelength by $\lambda_L = 2\pi/k_L$.

Assuming that the lasers are well aligned such that the beam width takes the minimal value w_0 of the corresponding beam waist, the intensity of a Gaussian laser beam is given by

$$I(\mathbf{x}) = I_0 \mathrm{e}^{-2r^2/w_0^2} \cos^2(k_{L_z} z), \tag{1.12}$$

where the intensity amplitude I_0 is proportional to the square of the electric field amplitudes and r is the radial distance from the central from the center axis of the beam. We have assumed propagation in the z direction. As a consequence of the AC-Stark effect atoms fill a conservative potential proportional to such amplitudes and are attracted by either the intensity maxima or minima [59]. The resulting potential in $3D$ is given by

$$V(\mathbf{x}) = V_{\text{trap}}(\mathbf{x}) + V_{\text{OL}}(\mathbf{x}) \tag{1.13}$$

Figure 1.3 – Optical lattices. On the left we see how the laser fronts can be superimposed to form two-dimensional (upper) and three-dimensional (lower) lattice potentials. The right image shows the mirror device to produce such crystals of light.

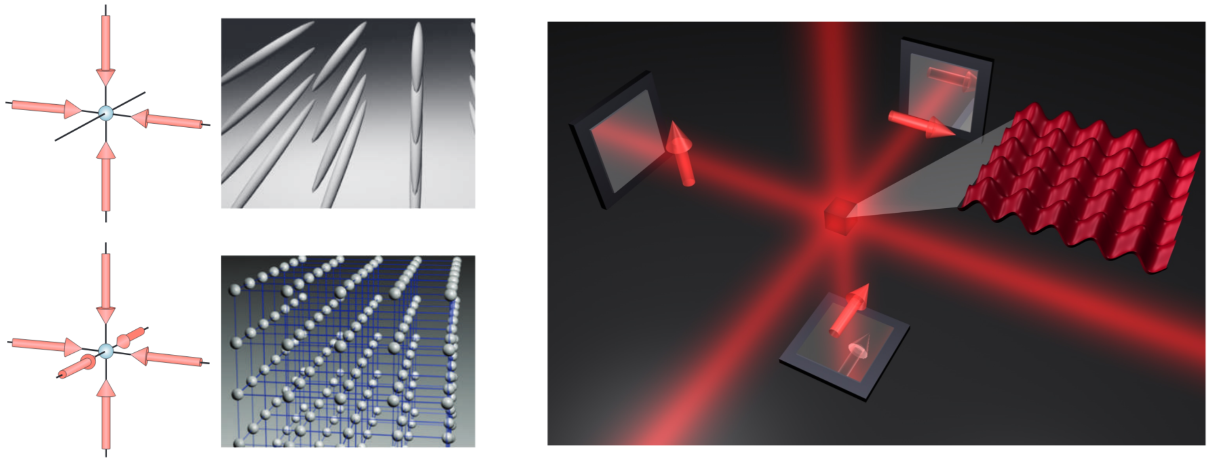

Source: Figures from Refs. [15, 61].

where the trapping potential is

$$V_{\text{trap}}(\mathbf{x}) = -V_0\left(\mathrm{e}^{-2\frac{y^2+z^2}{w_0^2}} + \mathrm{e}^{-2\frac{x^2+z^2}{w_0^2}} + \mathrm{e}^{-2\frac{x^2+y^2}{w_0^2}}\right), \tag{1.14}$$

and the optical lattice potential reads

$$V_{\text{OL}}(\mathbf{x}) = V_0\left(\mathrm{e}^{-2\frac{y^2+z^2}{w_0^2}}\sin^2 k_{L_x}x + \mathrm{e}^{-2\frac{x^2+z^2}{w_0^2}}\sin^2 k_{L_y}y + \mathrm{e}^{-2\frac{x^2+y^2}{w_0^2}}\sin^2 k_{L_z}z\right). \tag{1.15}$$

If the atoms are confined near the trap center one can take the limit $|\mathbf{x}| \ll w_0$. Within this limit the full potential becomes

$$V(\mathbf{x}) \approx -3V_0 + V_{\text{OL}}(\mathbf{x}), \tag{1.16}$$

where the approximation to the optical lattice potential reads

$$V_{\text{OL}}(\mathbf{x}) \approx V_0\left(\sin^2 k_{L_x}x + \sin^2 k_{L_y}y + \sin^2 k_{L_z}z\right). \tag{1.17}$$

Note that the characteristic lattice spacing is given by $a_i = \lambda_{L_i}/2 = \pi/k_{L_i}$ with $i = x, yz$.

It is possible to fine-tune the lattice parameters, such as the lattice spacing, lattice depth, and the orientation of the lattice, in order to create a wide variety of lattice structures with different properties and capabilities. By controlling the interference angle between the laser fronts, one can change the lattice spacing in order to produce different geometries such as triangular [62] and Kagomè [63]. In order to understand how to investigate the effects of disorder in such structures, we review some of the most common experimental

Figure 1.4 – Speckle laser production. a) A laser beam is scattered by a diffusive plate producing a speckle pattern. b) Typical intensity distribution of the speckle pattern.

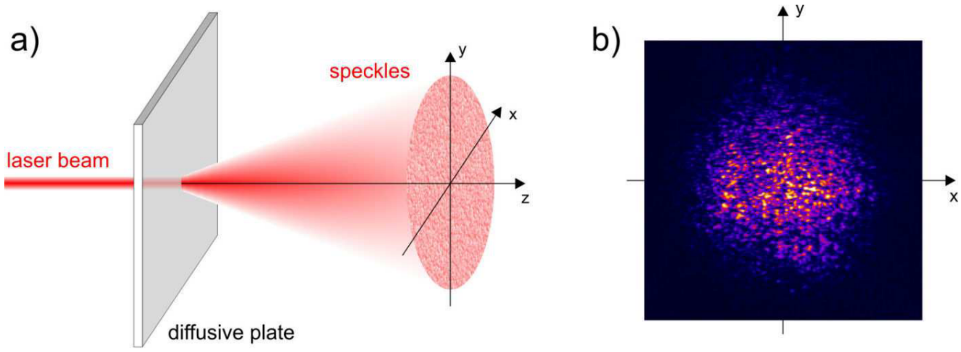

Source: Figures from Ref. [64].

techniques to generate random potential landscapes.

1.3 Speckle laser disorder

The fact that optical lattices are highly controllable and almost free of defects make them an excellent playground to investigate emergent phenomena in many-body physics. It is often pointed out that they represent one of the best possibilities for realizing Feynman's quantum simulator [14]. However, in nature it is unlikely to find a physical system that presents perfect order. In fact, as we shall see, many interesting phenomena can emerge from the presence of impurity defects and the breaking of translational symmetry. Here we review the experimental techniques usually applied to generate random potential landscapes, in particular we focus on the disorder created by laser speckles [27, 28].

When laser light is scattered from a rough surface, partial waves with a random phase coming from different scattering sites interfere. If the rough surface is composed of many scatters, one can assume that no direct transmission occurs. The resulting signal consists of a sum of multiple randomly phased components forming randomly distributed grains of light known as speckle pattern. In experiments, the role of the rough surface is played by a diffusive plate. The production of the speckle as well as an example of the landscape on intensity distributions are shown in Fig 1.4.

The probability density function for the speckle intensity is usually assumed to follow an exponential law

$$\mathscr{P}(I) = \frac{1}{\langle I \rangle} \mathrm{e}^{-I/\langle I \rangle}. \tag{1.18}$$

It is worth metioning that the average speckle intensity is proportional to the disorder strength energy scale. Here we denote such energy scale as Δ, thus the relation reads $\langle I \rangle \propto \Delta$. However, it was shown that one can customize the speckle pattern using a spatial light modulator in order to form uniform, linearly increasing, and bimodal distributions [65].

The size of the grains of light intensity with random magnitudes that characterizes the speckle pattern can be inferred from the width of the intensity autocorrelation function. That is the correlation between the intensity of the random pattern at different space points. The grain size σ_s is typically connected to three length scales: the wavelength λ_s of the lase beam which is shone into the diffusive plate, the aperture size D_s through which light passes, and the distance l_s of the diffuser from the focal plane. Its expression is given by $\sigma_s = \lambda_s l_s / D_s$ [27, 66]. We remark that the inverse of such a quantity defines the maximum value for the spatial frequencies of the random potential if it is decomposed as a sum of many Fourier components.

One can also create disorder by using micromirror devices to engineer light fields [29]. Such devices have millions of tiny mirrors which can be tilted by either $+12^o$ or -12^o with respect to the surface normal. The high reflectivity and broad spectral response of such devices make it possible to produce a large range of potential landscapes with low optical aberrations [67]. Furthermore, disorder can be realized by introducing a gas of atoms in a different internal state or even atoms of another species that are trapped in random nodes of the optical lattice [30, 31].

1.4 Bose-Hubbard model

We have so far discussed the relevant aspect of the realization of optical lattices and disordered external potentials. Now, we turn out attention to the description of interacting spinless bosons loaded into a lattice. The physics of such a system is captured by one of the central focus of this work: the Bose-Hubbard model.

1.4.1 Single-particle band structure

In the absence of any external potential, the properties of a single atom are well described by a plane wave $\mathrm{e}^{i\mathbf{k}\cdot\mathbf{x}}/\sqrt{\mathcal{V}}$, where for a given wavevector $\mathbf{k}$ its energy is given by the free dispersion $E_{\mathbf{k}} = \hbar^2\mathbf{k}^2/2m$. As we shall see, in the presence of a periodic potential the energy dispersion acquires a band structure.

The Schrödinger equation for the wave function in a one-dimensional periodic potential reads

$$\left(-\frac{\hbar^2}{2m}\frac{\partial^2}{\partial x^2} + V_0 \sin^2 k_L x\right)\psi_q^{(b)}(x) = E_q^{(b)}\psi_q^{(b)}(x). \tag{1.19}$$

The periodicity of the potential is characterized by the spacing $a = \pi/k_L$. Solutions of the above equation are given by Bloch's theorem [68, 69, 70] and consist of the product of a

Figure 1.5 – Band structure of a single particle in a periodic potential for different values of potential depth V_0. As V_0 is increased the difference in energy between the energy bands becomes larger.

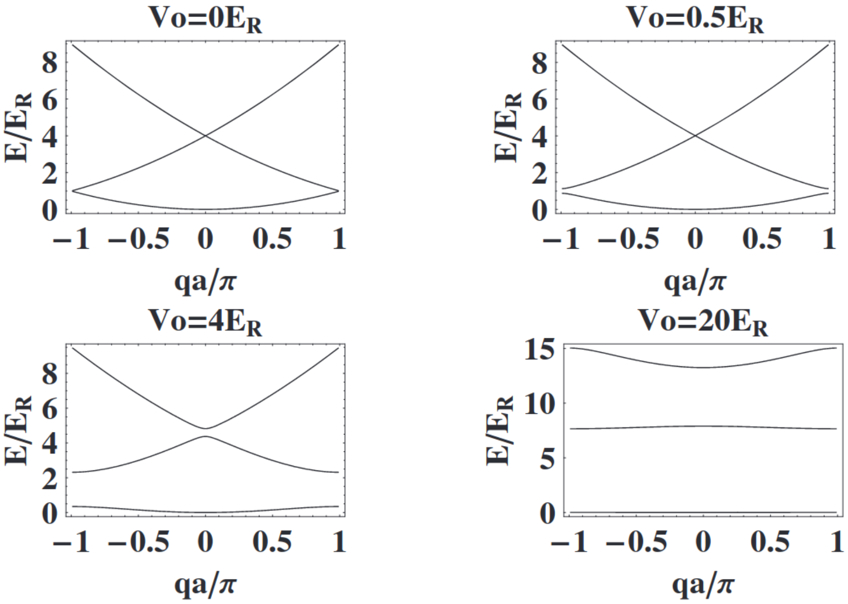

Source: Figure from Ref. [71].

plane wave with a periodically modulated function

$$\psi_q^{(b)}(x) = \mathrm{e}^{iqx} u_q^{(b)}(x), \tag{1.20}$$

where $u_q^{(b)}(x+a) = u_q^{(b)}(x)$, i.e. this function has the same period as the potential. Such solutions of (1.19) are usually called Bloch waves and introduce two additional parameters. The quantity q, called quasimomentum or crystal momentum, can be interpreted as the quantum number representing the translational symmetry of the periodic potential. We can see that values of q differing by $2\pi m/a$ with $m \in \mathbb{Z}$ are equivalent and thus one can restrict the analysis to the first Brillouin zone $-\pi/a < q \leq \pi/a$. For a given q, equation (1.19) becomes a set of eigenvalue problems on the fixed interval $0 < x < a$. Thus, one can find many solutions of the Schrödinger equation with a discretely spaced spectrum of modes. These correspond to the energy bands characterized by the band index b. For a large lattice, the energy levels of the periodic potential vary continuously with the quasimomentum q for a fixed band index b. The description of such energy levels by means of the continuous functions $E_q^{(b)}$ is usually referred to as band structure [71].

It is convenient to rewrite (1.19) in the form

$$\left(-\frac{\partial^2}{\partial \tilde{x}^2} + \frac{V_0}{4E_R}(2-2\cos 2\tilde{x})\right)\psi_q^{(b)}(\tilde{x}) = \frac{E_q^{(b)}}{E_R}\psi_q^{(b)}(\tilde{x}), \tag{1.21}$$

where we have introduced the atomic recoil energy $E_R = \hbar^2 k_L^2/2m$ and the transformation $\tilde{x} = k_L x$. Note that (1.21) has the form of Mathieu's differential equation. Solutions to such equation are generally expressed in the Floquet form of (1.20) [71]. The energy dispersion of such solutions is shown in Fig. 1.5 for different values of the potential depth V_0. There one can observe that the separation between the energy bands increases by increasing V_0. For reasonably deep lattices, it is then justified to assume that transitions between energy bands are suppressed. In this situation a cold bosonic gas would be confined to the lowest band. This approximation will be better explored in what follows.

1.4.2 Bose-Hubbard Hamiltonian

We have so far discussed the effects of a radiation field and of a periodic external potential on a single atom. We want now to extend the analysis to describe a system composed of many interacting atoms in a lattice potential. A convenient way to describe such a many-particle quantum system is the formalism of second quantization [72, 6, 73]. In such a formalism, the states of the system of N interacting particles are accommodated in the Fock space composed of a direct sum of n-particle Hilbert spaces

$$\mathcal{F} = \bigoplus_{N=0}^{\infty} \mathscr{H}^N, \tag{1.22}$$

where $\mathscr{H}^0$ represents the Hilbert space whose element is the state with no particles present, and so on and so forth. The general form of operators in the formalism of second quantization is given in terms of creation and annihilation operators [74]. In order to construct the many-body Hamiltonian, it is particularly helpful to use the coordinate basis in real space. The real space representation is usually described in terms of the quantum field operators $\hat{\Psi}(\mathbf{x})$ and $\hat{\Psi}^\dagger(\mathbf{x})$, which respectively remove or add a boson to the system at position $\mathbf{x}$.

In the non-relativistic limit, a system composed of many interacting bosons in the presence of an external potential $V(\mathbf{x})$, which includes the lattice potential as well as the trapping potential defined in (1.13), is well described by the Hamiltonian [72, 74, 75, 6, 73]

$$\begin{aligned}\hat{H} &= \int d^3x \hat{\Psi}^\dagger(\mathbf{x})\left(-\frac{\hbar^2}{2m}\nabla^2 + V(\mathbf{x}) - \mu\right)\hat{\Psi}(\mathbf{x}) \\ &+ \frac{1}{2}\int d^3x \int d^3x' \hat{\Psi}^\dagger(\mathbf{x})\hat{\Psi}^\dagger(\mathbf{x}')U_{int}(\mathbf{x},\mathbf{x}')\hat{\Psi}(\mathbf{x})\hat{\Psi}(\mathbf{x}').\end{aligned} \tag{1.23}$$

Here μ denotes the grand-canonical chemical potential while the interaction between two particles is represented by $U_{int}(\mathbf{x},\mathbf{x}')$. At low energies one can assume that interactions are dominated by s-wave scattering [24, 76] which amounts to a contact interaction of the form

$$U_{int}(\mathbf{x},\mathbf{x}') = g\delta(\mathbf{x}-\mathbf{x}'), \tag{1.24}$$

where $g = 4\pi a_s\hbar^2/m$ and a_s is the s-wave scattering length. The field operators satisfy the

Figure 1.6 – Bose-Hubbard Hamiltonian. The lattice is represented by the oscillating green line while the quantum particles are represented by the red dots. The parameters are defined as: V_0 corresponds to the lattice depth, J is the tunneling energy, U represents the on-site interaction, ϵ_i corresponds to the local shift caused by the trapping potential.

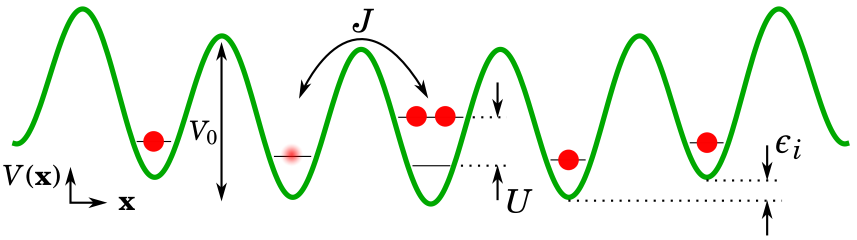

Source: Prepared by the author.

commutation relations

$$[\hat{\Psi}(\mathbf{x}),\hat{\Psi}^\dagger(\mathbf{x}')]=\delta(\mathbf{x}-\mathbf{x}') \quad \text{and} \quad [\hat{\Psi}(\mathbf{x}),\hat{\Psi}(\mathbf{x}')]=[\hat{\Psi}^\dagger(\mathbf{x}),\hat{\Psi}^\dagger(\mathbf{x}')]=0. \tag{1.25}$$

For low energies and sufficiently deep optical lattices, it is justified to assume that all atoms are confined to the lowest Bloch band. In this way, the states are given by Bloch's theorem in the same form of (1.20). Such states can be superposed into a complete set of the Wannier functions $w(\mathbf{x})$ which are localized

$$w(\mathbf{x}-\mathbf{x}_i)=\left(\frac{a}{2\pi}\right)^3\int_{\mathrm{BZ}} d^3q\,\mathrm{e}^{-\mathrm{i}\mathbf{q}\cdot\mathbf{x}_i}\psi_{\mathbf{q}}(\mathbf{x}), \tag{1.26}$$

where the integration in $\mathbf{q}$ runs over the first Brillouin zone. Such functions obey the orthonormality condition [75]

$$\int d^3x\; w^*(\mathbf{x}-\mathbf{x}_i)w(\mathbf{x}-\mathbf{x}_j)=\delta_{ij}, \tag{1.27}$$

where $\mathbf{x}_i$ represents the position of the lattice site i. In terms of such localized Wannier functions, the field operators can be decomposed as

$$\begin{aligned}\hat{\Psi}(\mathbf{x}) &= \sum_i \hat{a}_i w(\mathbf{x}-\mathbf{x}_i),\\ \hat{\Psi}^\dagger(\mathbf{x}) &= \sum_i \hat{a}_i^\dagger w^*(\mathbf{x}-\mathbf{x}_i),\end{aligned} \tag{1.28}$$

where $\hat{a}_i$ and $\hat{a}_i^\dagger$ correspond to the annihilation and creator operators of a particle at the lattice site i. The orthonormality condition satisfied by the Wannier functions leads to the following bosonic commutations relations

$$[\hat{a}_i,\hat{a}_j^\dagger]=\delta_{ij} \quad \text{and} \quad [\hat{a}_i,\hat{a}_j]=[\hat{a}_i^\dagger,\hat{a}_j^\dagger]=0. \tag{1.29}$$

By introducing the decomposition of the fields (1.26) into (1.23), we obtain Bose-

Hubbard Hamiltonian

$$\hat{H} = -\sum_{\langle ij\rangle} J_{ij}\hat{a}_i^\dagger \hat{a}_j + \frac{U}{2}\sum_i \hat{a}_i^\dagger \hat{a}_i^\dagger \hat{a}_i \hat{a}_i + \sum_i (\epsilon_i - \mu)\hat{a}_i^\dagger \hat{a}_i. \tag{1.30}$$

where the parameters are defined as

$$\begin{aligned} J_{ij} &= -\int d^3x\, w^*(\mathbf{x}-\mathbf{x}_i)\left(-\frac{\hbar^2}{2m}\nabla^2 + V(\mathbf{x})\right)w(\mathbf{x}-\mathbf{x}_j), && (1.31)\\ U &= \int d^3x\, g|w(\mathbf{x})|^4, && (1.32)\\ \epsilon_i &= \int d^3x\, w^*(\mathbf{x}-\mathbf{x}_i)\left(-\frac{\hbar^2}{2m}\nabla^2 + V(\mathbf{x})\right)w(\mathbf{x}-\mathbf{x}_i). && (1.33) \end{aligned}$$

Using the commutation relations of the creation and annihilation operators $\hat{a}_i^\dagger$ and $\hat{a}_i$, one can rewrite the Hamiltonian (1.30) as

$$\hat{H} = -\sum_{\langle ij\rangle} J_{ij}\hat{a}_i^\dagger \hat{a}_j + \frac{U}{2}\sum_i \hat{n}_i(\hat{n}_i - 1) + \sum_i (\epsilon_i - \mu)\hat{n}_i, \tag{1.34}$$

where $\hat{n}_i = \hat{a}_i^\dagger \hat{a}_i$ is the number operator. It can be shown that for reasonably deep lattices, i.e. for a Wannier function localized at a given site, contributions due to the overlap between sites further than the first neighbors can be neglected [75], therefore, the sum $\langle ij\rangle$ is restricted to the nearest neighboring sites. The first term in (1.34) defines the hopping energy J_{ij} which is associated with the tunneling of an atom from one lattice site to one of its neighbors, where we define the J_{ij} as being equal to J if i and j are first neighbors and vanishes otherwise. The on-site energy U is associated with the interaction between two particles at the same site. The local potential ϵ_i represents the local energy shift caused by the trapping potential at each lattice site (see Fig. 1.6). One can study the effects of disorder by considering that just these local energy shifts become random. We will discuss this case in more detail at a later stage.

1.4.3 Hamiltonian parameters

In order to estimate the dependency of the Bose-Hubbard Hamiltonian parameters on the external potential, one can assume that the lattice is sufficiently deep so that a harmonic approximation to the minimum of the potential at each site is justified [77]. Within such an approximation the Wannier functions become a product of harmonic oscillator states. Therefore, we focus on the one-dimensional Schrödinger equation given by

$$\left(-\frac{\hbar^2}{2m}\frac{\partial^2}{\partial x^2} + V_0 k_L^2 x^2\right)w(x) = Ew(x), \tag{1.35}$$

where the ground state solution for each lattice potential in dimensionless units well reads

$$w(x) = \left(\frac{\pi}{a^2}\sqrt{\frac{V_0}{E_R}}\right)^{1/4} \exp\left[-\frac{\pi}{2}\sqrt{\frac{V_0}{E_R}}\left(\frac{x}{a}\right)^2\right]. \tag{1.36}$$

By using the explicit form of the parameters expressed in (1.31)-(1.33) one can integrate the solution (1.36) which yields [24, 78, 79]

$$\frac{J}{E_R} = \frac{4}{\sqrt{\pi}}\left(\frac{V_0}{E_R}\right)^{3/4} \exp\left(-2\sqrt{\frac{V_0}{E_R}}\right) \tag{1.37}$$

$$\frac{U}{E_R} = \frac{a_s\sqrt{8\pi}}{a}\left(\sqrt{\frac{V_0}{E_R}}\right)^{3/4} \tag{1.38}$$

$$\frac{\epsilon_i}{E_R} = 3\sqrt{\frac{V_0}{E_R}}. \tag{1.39}$$

Even though the results were obtained within a harmonic approximation to each potential well, one can explicitly see that by varying the lattice potential depth V_0 one can tune the interplay between the Hamiltonian parameters. As we will discuss in what follows, depending on which energy scale dominates, the system will reach equilibrium in a different ground states. Thus, by increasing the lattice potential depth one can drive the system into a phase transition. These details will be further explored in the following sections.

1.4.4 Ground states of the Bose-Hubbard model

The competition between the parameters of the Bose-Hubbard Hamiltonian leads to different ground states. In order to give an intuitive picture about such ground states, we follow the path of Ref. [80] and analyze first the case of two bosonic neutral atoms in a double well potential.

Two particles in a double well

Consider first a single particle in a symmetric double well potential in one dimension. If the potential obeys reflection symmetry, i.e. it is symmetric under the transformation $x \to -x$, the Hamiltonian commutes with the parity operator. Hence the eigenfunctions of the Hamiltonian have definite parity. Due to the fact that the odd eigenfunction has necessarily a node at $x = 0$ regardless of the height of the barrier, its eigenenergy is higher than the one of the even eigenfunction [81]. By representing the even and odd eigenfunctions as $\phi(x)$

and $\tilde{\phi}(x)$, respectively, we can form the liner combinations

$$\langle x|L\rangle = \frac{1}{\sqrt{2}}\big(\phi(x)+\tilde{\phi}(x)\big), \tag{1.40}$$

$$\langle x|R\rangle = \frac{1}{\sqrt{2}}\big(\phi(x)-\tilde{\phi}(x)\big), \tag{1.41}$$

where $|L\rangle$ ($|R\rangle$) corresponds to the state in which the particle is located on the left (right) potential well. Conversely, we note that the even and odd eigenfunctions can be written as

$$\phi(x) = \frac{1}{\sqrt{2}}(\langle x|L\rangle + \langle x|R\rangle), \tag{1.42}$$

$$\tilde{\phi}(x) = \frac{1}{\sqrt{2}}(\langle x|L\rangle - \langle x|R\rangle). \tag{1.43}$$

Thus, the ground state of the system, which corresponds to the even eigenfunction, consists of a symmetric combination of the particles being either on the left or on the right well, while the first excited state corresponds to an anti-symmetric superposition of these two possibilities. We define the difference between these two energy levels to be J. This energy scale depends on the barrier height separating the two wells and characterizes the tunneling between them [80].

If we introduce an additional particle, the quantum state of the two-particle system can be described in Fock space by the basis state $|n_L,n_R\rangle$, where n_L and n_R are non-negative integers that count the number of particles in the left and right wells, respectively. Restricting the analysis to the non-interacting case, the state with the lowest energy is the one where each atom occupies the symmetric state (1.42). This state corresponds to the superposition of the states where two atoms are on the left well $|2,0\rangle$ with the state where they are both on the right well $|0,2\rangle$ and the state where each particles is in one well $|1,1\rangle$. Such states are coupled via first-order tunneling. The average number of particles per site is always one, however there is a non-vanishing probability of finding either zero, one, or two atoms at the same site. Such fluctuations in the atom number occur due to the delocalized single-particle states. Therefore, one can make a connection between the above described state and the superfluid state of the many-body system.

By adding the possibility of a contact interaction between the two particles, the total energy of the symmetric state will increase as an effect of having contributions from states where the two atoms are located at the same potential well [81]. We define such interaction cost to be U. The presence of such an interaction creates an interplay between the different energy scales of the system. Whenever the interaction cost U is larger than the energy difference between the symmetric and anti-symmetric states J, each atom will be in a superposition of these states. In the Fock basis, this results in a suppression of transitions from the state $|1,1\rangle$ to either $|2,0\rangle$ or $|0,2\rangle$. Thus, the state of the full system will be described by $|1,1\rangle$, where there is exactly one particle per lattice potential well. Such state

Figure 1.7 – Different states for two particles in a double well potential. The upper row corresponds to a symmetric potential while the lower row corresponds to an asymmetric potential. The potential is represented by the green lines and the particles are represented by the red dots.

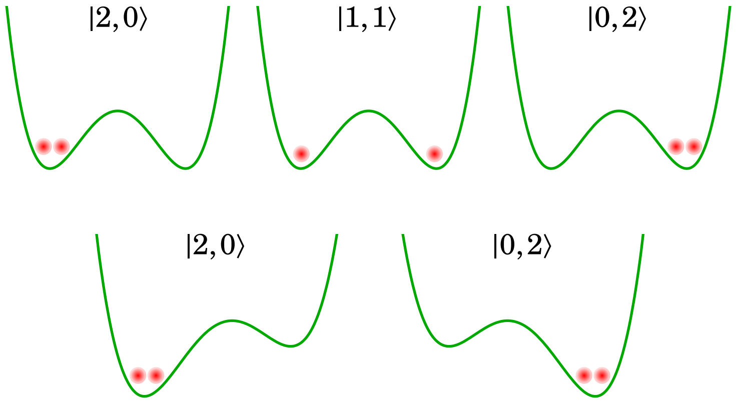

Source: Prepared by the author.

resembles a Mott insulating phase, where the atoms are localized due to the interaction cost.

For a symmetric double well the value of the potential at the minimum of each well is exactly the same. Thus, the state where the two particles are on the left well, i.e. $|2,0\rangle$, has the same energy as the state where the two particles are on right well, i.e. $|0,2\rangle$. By making the double well asymmetric, that is, by introducing an energy difference Δ between the two potential minima, one can bias the two-particle system into choosing either the state $|2,0\rangle$ or the state $|0,2\rangle$. If interactions are weak, both particles can occupy the ground state of the biased well. One can make the analogy between this state and the Bose-glass state of the many-body system where particles can condense around the local minima of the potential, but tunneling is suppressed.

A schematic drawing of the different states of the double well can be observed in Fig. 1.7. Note that by adiabatically tuning the barrier height of the double well potential or the difference between the two potential minima, one can imagine that the system would eventually transition from the delocalized state to either a localized state where each particles is in one well or both are localized in the same well.

We must remark that we have chosen to make a rather simple discussion about the problem of a two interacting particles in a symmetric or asymmetric double well potential with the aim of illustrating the qualitative aspects of the different ground states of the Bose-Hubbard model. However, this problem can in fact be extremely complicated. Thus, for a more complete quantitative analysis of such a problem, we refer the reader to look for more details, for instance, in Refs. [82, 83, 84].

Figure 1.8 – Superfluid ground state. Particles are delocalized (blue region) through the whole lattice volume (black line).

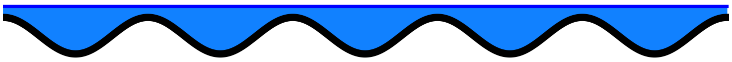

Source: Prepared by the author.

Superfluid ground state

We now turn back to the problem of many atoms loaded on an optical lattice described by the Bose-Hubbard Hamiltonian. We consider first the case where the tunneling J is much larger than the interaction energy U and the local shift ϵ_i. By extending the qualitative aspects of the analysis made previously, one can conclude that in the ground state the single-atom wave functions are delocalized over the entire lattice volume. In this situation, the ground state of a system composed of N bosons on top of a lattice with L sites can be approximated as a product of identical Bloch states

$$|\Psi_{SF}\rangle \propto \left(\sum_{i=1}^{L} \hat{a}_i\right)^N |0\rangle \quad \text{in the limit} \quad \frac{U}{J} \to 0, \tag{1.44}$$

where $|0\rangle$ corresponds to the single-particle state with no particles present.

As the atomic states are delocalized one can associate the full system with a matter wave field where many atoms would start to accumulate in the same quantum sate. In this situation, the many-body wave function at a single site can be described by a superposition of basis states with a different number of atoms which is equivalent to a coherent state $|\Phi_i\rangle$. This process is characterized by the emergence of the non-vanishing expectation value $\psi_i = \langle\Phi_i|\hat{a}_i|\Phi_i\rangle$ which can be written as $\psi_i = \sqrt{n_i}\mathrm{e}^{i\varphi_i}$, where n_i is the expected number of bosons at site i. The system is then best described by a macroscopic wave function where the real part of the expectation value of the hopping energy in the Bose-Hubbard Hamiltonian is given in this basis as

$$\mathrm{Re}\{\langle -J\hat{a}_i^\dagger \hat{a}_j\rangle\} = -J\sqrt{n_i n_j}\cos\left(\varphi_j - \varphi_i\right), \tag{1.45}$$

which can be related to the Josephson tunneling energy where $\varphi_j - \varphi_i$ is the macroscopic phase difference between the neighboring sites i and j. In a macroscopically occupied coherent state the phase becomes a well defined quantity and thus the system is able to reduce its energy by an amount J for each Josephson junction. The emergence of such a well defined phase is linked to the mechanism of spontaneous symmetry breaking that takes place when this phase emerges, as we shall discuss later.

The superfluid ground state is therefore associated with a macroscopic wave function where momentum flows without dissipation and each atom is delocalized through the lattice (see Fig. 1.8).

Figure 1.9 – Mott insulating ground state. An integer number of particles (red dots) gets localized (wave functions in blue) at each lattice site (the lattice is represented by the black line).

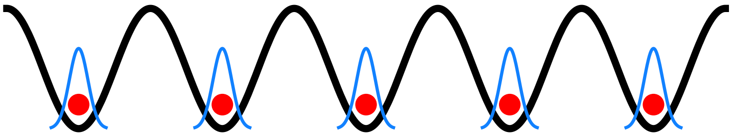

Source: Prepared by the author.

Mott Insulating ground state

If interactions are strong and dominate over the hopping and local shift terms of the Bose-Hubbard Hamiltonian, the expectation value for the matter wave field vanishes, i.e., $\psi_i = 0$. Consequently, fluctuations in average number of particles at each lattice site get suppressed. Each atomic state can be well described by localized Wannier functions that minimize the interaction energy. In this limit, the ground state of the full system becomes a product of local states in Fock space with a commensurate filling n of atoms for every lattice site

$$|\Psi_{MI}(n)\rangle \propto \prod_{i=1}^{L}(\hat{a}_i^{\dagger})^n |0\rangle \quad \text{as} \quad \frac{J}{U} \to 0. \tag{1.46}$$

This state describes a Mott insulator.

If we compare the expectation value of the interaction energy for the coherent states $Un_i^2/2$ with the same quantity in the Fock state of the Mott regime $Un_i(n_i-1)/2$ with average atom density n_i, we notice that the system is now able to reduce its energy by an amount of $U/2n_i$ if the later localized state is formed in place of the coherent superfluid ground state.

The system becomes localized with a fixed integer number of particles per site (see Fig. 1.9). Because fluctuations in the atom number become negligible such a state is incompressible in the limit of zero temperature. In order to create a delocalized excitation, one has to give an energy at least of the same order of the interactions. This characterizes the energy gap of the Mott insulator ground state.

Disorder and the Bose glass ground state

The study of disorder in many-body systems is important for understanding the properties of real-world materials. Disorder can lead to different kinds of phenomena such as new phases of matter and new types of excitations. Since the seminal paper of Anderson [32], a fundamental question in this regard concerns how localization manifests itself in the quantum realm. In the classical limit, a particle with kinetic energy larger than the typical strength of the disordered potential would follow a ballistic motion above the random potential landscape. In the opposite case, if the particle energy is smaller than the disorder barrier, localization takes place and the transport over long distances is suppressed. A quantum particle however can tunnel through potential hills larger than its kinetic energy as

Figure 1.10 – Bose glass ground state. On the left side we can see how the particle density (upper row) is accumulated around the minimum of the random potential (lower row) for free particles. In middle we can observe how the particle density gets distributed over the random potential minima in the presence of interactions. On the right side, we show such rare regions of condensed bosons (blue) in an insulating background (pink).

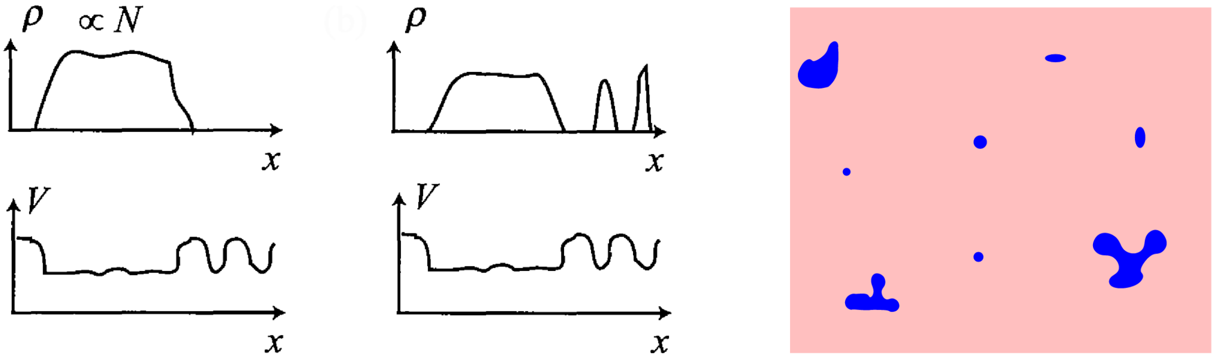

Source: Figures from Refs. [36, 85].

well as be reflected by small potential fluctuations. The motion of such a quantum particle after many scattering events against the random potential would resemble a random walk. This changes drastically the scenario compared to the classical case. Here we discus how disorder is introduced in the Bose-Hubbard Hamiltonian.

Assuming that the trapping potential $V_{\text{trap}}(\mathbf{x})$ varies slowly compared to the lattice potential and that its characteristic length extends over to distances much larger than the spatial extent of the Wannier functions, we can approximate the local energy shift in the Bose-Hubbard Hamiltonian as [24]

$$\epsilon_i \approx V_{\text{trap}}(\mathbf{x}_i). \tag{1.47}$$

Disorder is usually addressed by considering that this local term varies randomly through the lattice according to some probability distribution $\mathscr{P}(\epsilon_i)$. In experiments this corresponds of superimposing, for instance, a laser speckle field to the lattice potential and studying its influence in the system by the random local shifts ϵ_i. In the case we are interested, the disordered potential time scale can be considered much greater than the thermodynamic times scale of the system. This amounts to a disorder which is effectively frozen in time, the so-called quenched diagonal disorder.

In order to provide a simple picture about the effects of disorder in the Bose-Hubbard model, let us follow the arguments Ref. [36]. We define the strength of the disordered potential to be controlled by the energy scale Δ. If the disorder dominates the Bose-Hubbard Hamiltonian, the bosons can be regarded as free particles. In the absence of interactions the presence of disorder can lead to the localization of the bosons in a finite but large enough region of space, namely where the disorder is around its minimum $-\Delta$. When confined to such a region, bosons end up lowering their kinetic energy while the potential energy is increased by $-\Delta$. If the size of the region where the bosons aggregate is large, it becomes favorable for a macroscopic amount of particles to condense in such a minimun. The probability of such a region to occur is exponentially small but it still is finite. As the density of bosons condensed in such a region is extremely large the ground state becomes unstable. If interactions are made finite, the particles would be pushed into other local minima of the random potential landscape. This phase, which consists of local droplets of condensates with a Mott insulating background, is a new ground state steaming from the presence of disorder (see Fig. 1.10), the so called Bose glass [22, 85]. Such a phase has properties from both superfluid and Mott insulator ground states. Even though it is characterized by the absence of macroscopic phase coherence, it is an insulating phase with a gappless spectrum and a finite compressibility at zero temperature. The questions about what are the main characteristics of the excitations in such a phase are still open. This work aims of contributing to a more fundamental understanding in this direction. We now discuss the characteristics of the phase transitions between the different Bose-Hubbard Hamiltonian ground states.

1.5 Detection

The experimental detection of each ground state of the Bose-Hubbard model was realized with the use of the time-of-flight imaging. Here, we give an introduction to such a technique and how it was applied to distinguish the different ground states.

1.5.1 Time-of-flight imaging

Time-of-flight (TOF) imaging is one of the most successful experimental techniques to probe cold atoms in external potentials. The experimental procedure consists of suddenly turning off the external potential that was keeping the atomic gas in order to let the cloud expand freely [86, 87, 88, 89]. After a few milliseconds, the most energetic atoms escape over large distances compared to the size of the initial cloud, while the less energetic ones remain near the center of the now absent external potential. Due to the decrease in the density during the expansion, the interactions become negligible. The measurement is then performed by either taking absorption pictures of a resonant laser beam through the dilute gas or by measuring the fluorescence of the falling atomic cloud over a resonant probe beam. Such a procedure provides the real space density profile which can be directly related to the integrated velocity and momentum distribution at the time of the release.

In Fig. 1.11 we show the experimental sequence as well as the optical setup for a TOF measurement. On the left image we note that the turning on of the lattice (red) and random (green) potential is an adiabatic process. Subsequently, both potentials are kept constant and then switched off. The gas then expands freely after the absorption pictures

Figure 1.11 – Experimental setup for TOF imaging. On the left side we can see an example of the time sequence for the measurement. On the right side we observe the optical setup for both the random potential and the imaging beam.

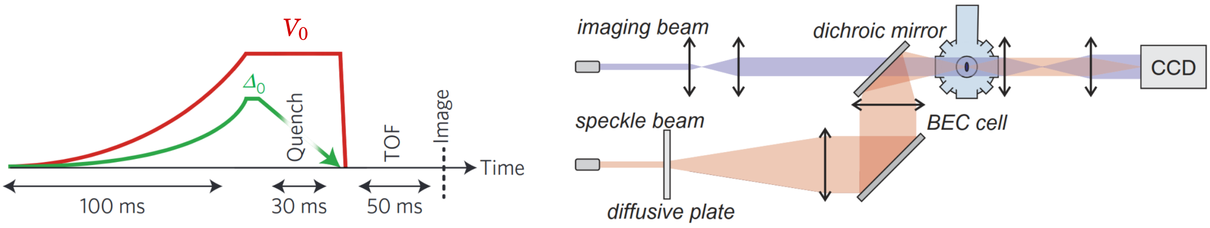

Source: Figures from Refs. [90, 37].

are taken. On the right side, we note the schematic generation of the random potential with the use of a diffusive plate and the imaging beam. Both are then shone on the cell which keeps the ultracold gas. The imaging is realized with a charge coupled device (CCD) camera.

In what follows we show how the experimental evidence coming from TOF measurements was used to identify each ground state of the Bose-Hubbard Hamiltonian.

1.5.2 Experimental characteristics of the ground states

It turns out that the ground states of the Bose-Hubbard Hamiltonian can be distinguished by their profile measured in TOF experiments. In the absence of disorder, one can use the momentum distribution which comes from the TOF imaging to distinguish the superfluid and Mott insulating phases. As the gas is let to expand after the trapping potentials are turned off, the atomic wave packets which are located at each lattice site start to spread until eventually they begin to overlap and interfere with each other. As we have discussed, deep in the superfluid phase for a shallow lattice, the system can be associated with a matter wave field with a single-site many-body wave function described by a coherent state. The result of the release of these coherent states from each lattice site is a multiple matter wave interference pattern. The momentum distribution of the superfluid state reveals narrow peaks which occur due to the constant macroscopic phase over the lattice sites. The position of these narrow peaks brings to light the periodicity of the reciprocal lattice structure (Fig. 1.11b-c). As the lattice depth is increased, the interference peaks start getting destroyed by the localization of the wave packets caused by interactions. For deep lattice potentials, the matter wave field gives place to an incoherent background in the momentum distribution, signaling that no superfluid fraction remains in the sample (Fig. 1.11g-h). This pattern is associated to the Mott insulating state. The characteristics of this ground state was first tested in the clean case by M. Greiner et al. [23]. In Fig. 1.12 we show a picture of the measured interference patterns identifying each phase.

In the presence of disorder, as the Bose-glass phase is characterized by the ab-

Figure 1.12 – Multiple matter wave interference patterns obtained in TOF measurements for different lattice potential depths V_0. (a) $0E_R$; (b) $3E_R$;(c) $7E_R$; (d) $10E_R$; (e) $13E_R$; (f) $14E_R$; (g) $16E_R$; and (h) $20E_R$.

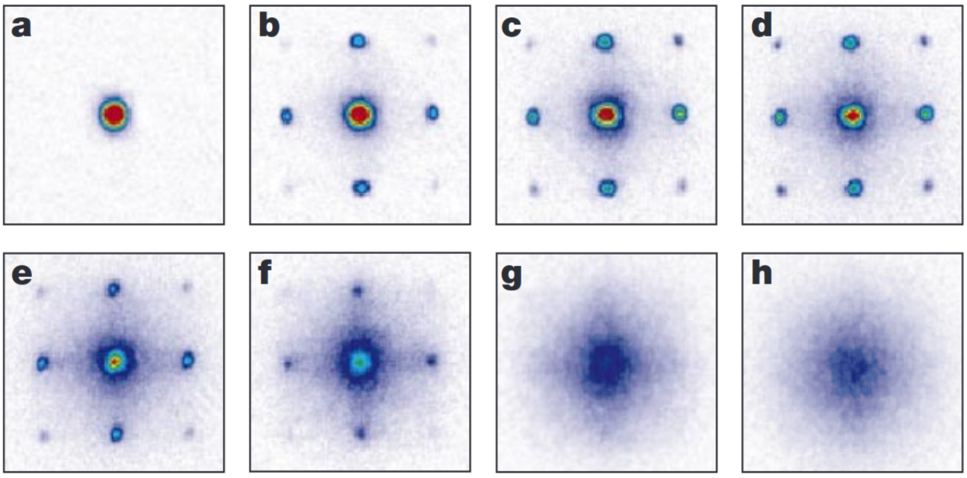

Source: Figure from Ref. [23].

Figure 1.13 – Density profile of superfluid and Bose glass phases. The white ellipses correspond to the fitted (Thomas-Fermi) radius of the atomic cloud where the fitted profile was subtracted in the right images. The superfluid state presents a smooth density profile while the Bose glass manifests vortex defects indicated by the red arrows.

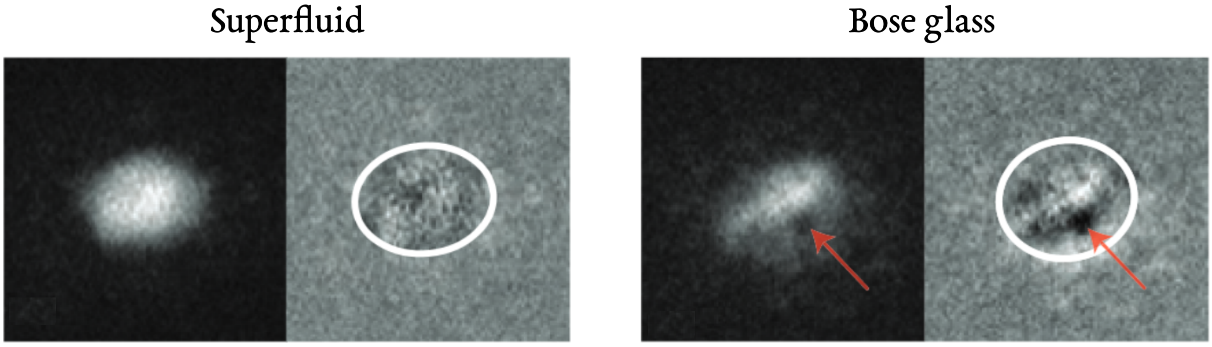

Source: Figures from Ref. [37].

sence of a macroscopic phase coherence, in principle, it would be difficult to distinguish it from the Mott phase by looking at the momentum distribution. In fact, most of the contributions of the present work are related to the key aspects of distinction between both insulating phases. From the experimental side, a more prominent option was to distinguish the Bose glass from the superfluid phase. The characterization of such a ground state was indirectly tested with transport and coherence measurements in one dimension in random [31], a quasi-periodic [91, 92], and in three dimensions in a random lattice [93]. Here, we focus on the experiments realized by C. Meldgin et al. [37] where a direct measurement was dynamically made using quantum quenches of disorder. Since the Bose glass is composed of rare regions of local condensates, it produces excitations when released from the trap in TOF experiments. Due to the different phases resulting from the scattering against the random potential, vortex excitations are created when the local condensates are allowed to expand and interfere. Such excitations are associated with modulations of the density profile and the measured optical depth. The Bose-glass phase was then identified by the presence of such vortices in the density profile coming from the interference of the independent phases corresponding to different local condensates. This density profile is shown in Fig. 1.13. In the case of the superfluid phase, due to the macroscopic phase, the density profile shows nothing but a continuous background.

Even though some of the characteristics of these ground states are well understood, many interesting questions are still open. For instance, a clear distinction between Mott and Bose glass is yet to be experimentally realized. In the following chapter we present the study of the quantum phase transitions between the ground states of the Bose-Hubbard Hamiltonian.

Chapter 2

Superfluid to insulator phase transition

The competition between the parameters of the Bose-Hubbard Hamiltonian leads to different ground states. By tuning the lattice potential depth as well as the intensity of the disordered potential, one can drive the system into a phase transition from one ground state to another. In this chapter, we review the concepts of quantum phase transitions and its relation to symmetry breaking. We also discuss the details of the phase diagram of the Bose-Hubbard model both for clean and disordered cases.

2.1 Quantum phase transitions

The fact that matter can change its properties under variations of the external conditions is the subject of the study of phase transitions. Everyday examples include when water vaporizes while boiling or when it freezes to ice under a reduction of its temperature. However, even the condensation of a gas of bosons below the critical temperature can be understood in terms of phase transitions. Phase transitions are classified according to whether the thermodynamic potential, which represents the equilibrium state of the system, varies continuously or not at the transition point [94]. In the case of freezing water to ice for instance, the water molecules have no particular order, but at the transition point they acquire order to become ice. This abrupt change in the internal arrangement of the molecules is associated with a discontinuity of the thermodynamic potential and characterizes the so-called first-order phase transitions. In contrast, in the condensation of bosons, the thermodynamic potential varies continuously when the macroscopic wave function emerges. Such transitions are usually called second order or continuous phase transitions. Here we shall be concerned with continuous phase transitions.

Continuous phase transitions may be driven not only by changes in temperature, where the macroscopic order is destroyed by thermal fluctuations, but also by variations of non-thermal external parameter such as pressure or magnetic field. In fact, there is a special kind of phase transitions where quantum fluctuations play a large role, which can occur

Figure 2.1 – Low energy eigenvalues of the Hamiltonian $\hat{H}(g)$. On the left side we see the the level actually crossing. On the right side the more general avoided level crossing is shown.

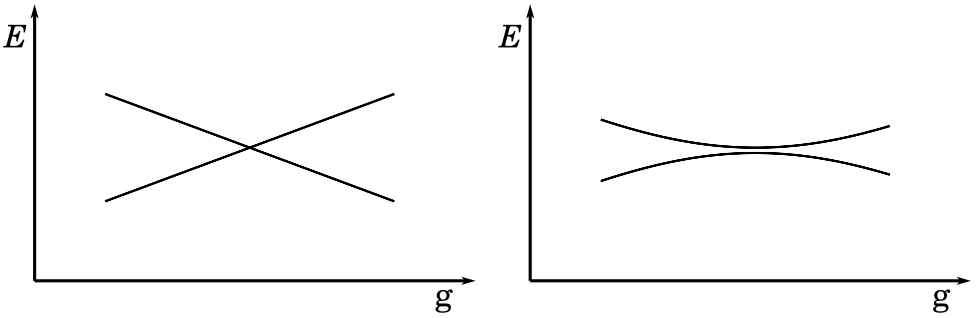

Source: Figure adapted from Ref. [21].

even at the zero-temperature limit. Those are the so-called quantum phase transitions. The effect of quantum fluctuations emerging from the competition of Hamiltonian control parameters can be incorporated as non-analycities in the energy function of the ground sate of a given system [21]. Consider, for instance, that the degrees of freedom of a lattice are embodied on a Hamiltonian $\hat{H}(g)$ which varies according to the dimensionless coupling g. In the situation where we can write the Hamiltonian as

$$\hat{H}(g) = \hat{H}_0 + g\hat{H}_1, \tag{2.1}$$

where $\hat{H}_0$ and $\hat{H}_1$ commute, i.e. the parameter g couples to a conserved quantity and the two parts of the Hamiltonian can be simultaneously diagonalized, a level-crossing where an excited state becomes a ground state may occur at critical point $\mathrm{g} = \mathrm{g}_c$. This corresponds to a non-analytic point in the ground state energy. Any point where the ground sate energy of a sufficiently large system is non-analytic can be identify to a quantum phase transition. Thus, such a phase transition corresponds to a level crossing of an excited state which becomes a ground state. More generally, an avoided level crossing becomes sharper in the limit of an infinite lattice (see Fig. 2.1).

The fundamental aspects of a quantum phase transition can be studied by investigating its scaling behavior at the transition point [95]. In these transitions the characteristic energy scale of the fluctuations ΔE vanishes when the crossing point $\mathrm{g} = \mathrm{g}_\mathrm{c}$ is approached. The energy difference between the ground state and the lowest excited state is assumed to behave asymptotically as

$$\Delta E \sim \mathscr{J}|\mathrm{g} - \mathrm{g}_\mathrm{c}|^{z\nu} \quad \text{as} \quad \mathrm{g} \to \mathrm{g}_\mathrm{c}, \tag{2.2}$$

where $\mathscr{J}$ is the energy scale of the microscopic coupling and $z\nu$ are so-called critical exponents. Additionally, quantum phase transitions are accompanied by the divergence of a characteristic length scale ξ, which could be related, for instance, with the exponential decay of the relevant equal-time correlation functions in the ground state. The asymptotic behavior of this length scale is usually described as

$$\xi^{-1} \sim \Lambda |g - g_c|^{\nu} \quad \text{as} \quad g \to g_c, \tag{2.3}$$

where Λ is defined as the inverse length scale of the same order as the inverse of the lattice spacing. A simple comparison between the asymptotic behavior of both the energy gap ΔE and the length scale ξ leads to

$$\Delta E \sim \frac{\mathscr{J}}{\Lambda^{z}} \xi^{-z} \quad \text{as} \quad g \to g_c. \tag{2.4}$$

From this expression one can read that the energy gap closes as the characteristic length diverges. In this limit, near the critical point where the quantum phase transition takes place, the system is said to acquire a scale-invariant behavior, where all observables depend on the dimensionless coupling via power law. The critical exponents associated with these scaling behavior of the system near the critical point characterizes the universality class of the quantum phase transition [95].

Another important aspect of quantum phase transition is that in most cases they can be associated with the spontaneous breaking of a symmetry. In the next section, we discuss the phenomenological Landau theory of phase transitions, where the symmetry breaking mechanism plays a large role.

2.2 Landau Theory

One important aspect in the study of phase transitions is the concept of symmetry. This concept refers to the properties of a system that remain unchanged under a certain transformation. At the vicinity of a phase transition, the symmetry present in one of the phases is reduced when the transition point is crossed. This concept of a broken symmetry was introduced by L. Landau [96, 97, 98] to describe continuous phase transitions. In order to characterize the symmetry breaking during the transition, Landau proposed a unique variable called order parameter. Here we represent the order parameter by ψ. Such a quantity represents a measure of the degree of order across the phase boundary increasing from zero in the symmetric phase to a finite valued in the phase where the symmetry was reduced.

The main idea of Landau's theory is that in the vicinity of the phase boundary the order parameter is small enough such that the effective thermodynamic potential $\mathscr{F}$ can be expanded in terms of a such quantity. We assume an underlying Hamiltonian with global U(1) symmetry. This implies that the effective potential must be invariant under phase

Figure 2.2 – Landau effective potential in the order parameter space for $a_2 > 0$ (left) and $a_2 < 0$ (right). On the left panel, the effective potential has a single minimum at the point where the order parameter vanishes. As the order parameter becomes finite, we observe on the right panel that the effective potential transforms into a Mexican-hat potential characterizing the symmetry-broken phase.

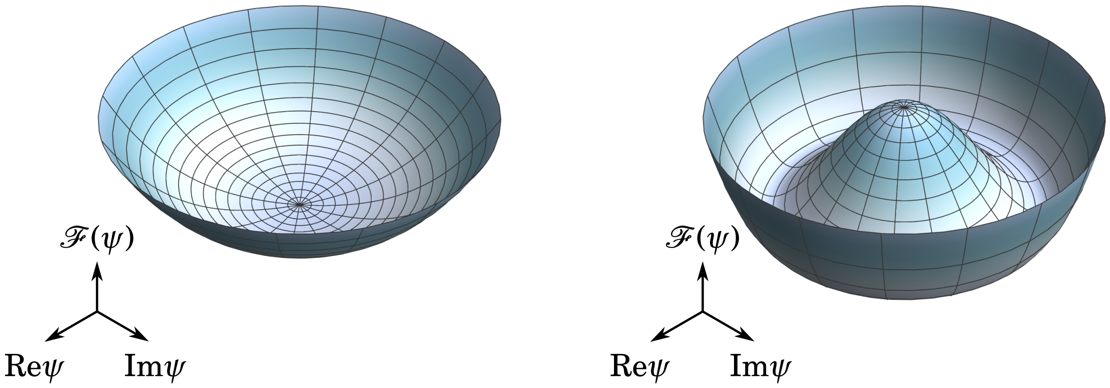

Source: Prepared by the author.

rotations of the order parameter ψ. Thus, we can express the expansion as

$$\mathscr{F}(\psi) = a_0 + \frac{a_2}{2}|\psi|^2 + \frac{a_4}{4}|\psi|^4 + \cdots. \tag{2.5}$$

The stability of an equilibrium state of the system requires that such state occupies a minimum of this effective potential in the space of the order parameter

$$\frac{\partial \mathscr{F}(\psi)}{\partial \psi} = 0, \quad \frac{\partial \mathscr{F}(\psi)}{\partial \psi^*} = 0. \tag{2.6}$$

The minimization condition up to forth order reads

$$|\psi|^2 = -\frac{a_2}{a_4}. \tag{2.7}$$

Note that for the absolute value of the order parameter to be real, the ratio between the coefficients of the free energy must be negative. Assuming that a_4 is always a finite, positive and real, two situations of the free energy can be distinguished by whether a_2 is positive or negative (see Fig. 2.2).

For positive values of the coefficient of the second-order term in (2.5), i.e. $a_2 > 0$, the only real solution for (2.7) is that the order parameter vanishes, i.e. $\psi = 0$. This situation characterizes the symmetric phase where the effective potential has only one minimum. In contrast, in the opposite case, where the a_2 is negative, the effective potential acquires infinitely many minima associated with different phases φ for finite absolute values of the order parameter in the complex plane. This situation represents the symmetry-broken phase.

As a consequence, the points where a_2 vanishes define the phase boundary which separates the symmetric from the symmetry-reduced phase. It is important to mention, that such coefficient is proportional to the inverse of the so-called single particle Green's function and thus the quantum phase transition can be investigated by studying the divergences of such a quantity. This relation will become important to the analyzes developed in Chapters 5 and 7 where it is discussed in more detail.

We have described in Section 1.4 that the superfluid state of the Bose-Hubbard model is connected to the emergence of a finite expectation value of the single-site annihilation operator with respect to the emerging coherent-state many-body wave function at a single site, that is $\psi_i = \langle \hat{a}_i \rangle = \sqrt{n_i} e^{i\varphi_i}$. Therefore, this is the appropriate order parameter to characterize the quantum phase transition to the superfluid phase. For a homogeneous system, the site dependency of such an order parameter may be dropped out and the phase transition follows the same symmetry breaking mechanism just described with the Landau theory. Each possible value of the phase φ is associated with a set of microscopic configurations of the system which lead to the same equilibrium energy [54, 55]. This corresponds the U(1)-global symmetry of the Bose-Hubbard Hamiltonian. It follows from the ergodic hypothesis the assumption that, as time progresses, the trajectory of the system in phase space runs through all microscopic configurations compatible with the total equilibrium energy. For a large system with many particles, the number of configurations approached infinity, and so does the time necessary to access the whole set of configurations in phase space. Consequently, in practice the system becomes confined in a subspace of the microscopic arrangements and it pics up a definite direction φ. This dynamical manifestation of ergodicity breaking is at the origin of the spontaneous symmetry breaking which takes place at the transition to the superfluid phase.

In the next section, we introduce the phase diagram for the clean case phase transition between Mott insulator and superfluid.

2.3 Zero-temperature phase diagram for the clean system

The phase diagram of the Mott-superfluid transition is usually constructed in the $\mu \times J$ plane. Such a phase diagram was first predicted in the seminal paper of Fisher et al. [22] and has since been the subject of a substantial amount of research. We consider first the clean case, where there is no disorder, following the derivation of Ref. [22]. In order to get an intuitive picture of the phase diagram we consider first the so-called hard-core limit, where interactions are strong and the bosons are not allowed to tunnel to neighboring sites, i.e. the limit $J = 0$ of the Bose-Hubbard Hamiltonian (1.34). As we discussed in Section 1.4, in this case the ground state is Mott insulator. The eigenvalues of the Bose-Hubbard

Figure 2.3 – Phase diagram of the Bose-Hubbard Model in the clean case for three dimensions at zero temperature. The phase boundary between superfluid (SF) and Mott insulator (MI) presents a Mott-lobe structure.

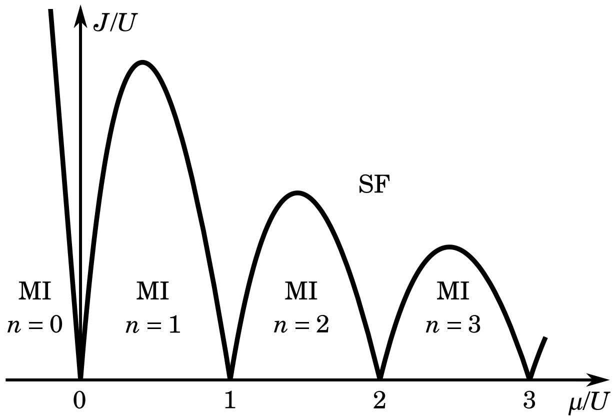

Source: Figure adapted from Ref. [22].

Hamiltonian can be described by the single site energies

$$E(n) = \frac{U}{2}n(n-1) - \mu n, \tag{2.8}$$

where n is the integer number of particles that minimizes the energy. For positive values of the the chemical potential on the interval $n-1 < \mu/U < n$, there are exactly n particles per site. For negative μ, we have the vacuum state where $n = 0$.

Consider the situation where μ is fixed inside the region where $n \geq 1$. If we allow J to be finite but still smaller than the interaction energy U the system will not be able to overcome potential energy cost by creating an excitation which can hop around the lattice. The conclusion from this argument is that, because of the gap in the Mott phase, there should be a finite region in the phase diagram where the average number of particles at each site is fixed by the integer number n. These regions are usually called Mott lobes, and their structure can be observed in Fig. 2.3. As the average number of particles is fixed, this phases are incompressible at zero temperature. However, it turns out that for finite temperatures thermal fluctuations lead to a finite compressibility in this phase [38].

One of the main properties of the Mott lobes is the characteristic energy gap for quasiparticle or quasihole excitations. We use the prefix quasi to point out that the mass of these excited atoms gets dressed by the many-body interactions and the lattice structure. This will be discussed in more details in Chapter 3. For a fixed tunneling energy J the energy gap for creating a quasiparticle (hole) is just the distance in the direction of the chemical potential to the right (left) phase boundary. Hence, the creation of a quasiparticle plus a quasi hole excitation conserves the number of particles in the system. Note that for integer numbers of the ratio μ/U the superfluid phase extends all over the phase diagram reaching the $J = 0$ line. For those values of the chemical potential, the energy for occupying

Figure 2.4 – Phase transitions for the $n = 1$ Mott lobe. The critical exponents for the generic transitions, which occur off the tip of the Mott lobe, differ from the transition exactly at the tip. The lines of constant density are indicated in gray, while the phase boundary is depicted in blue.

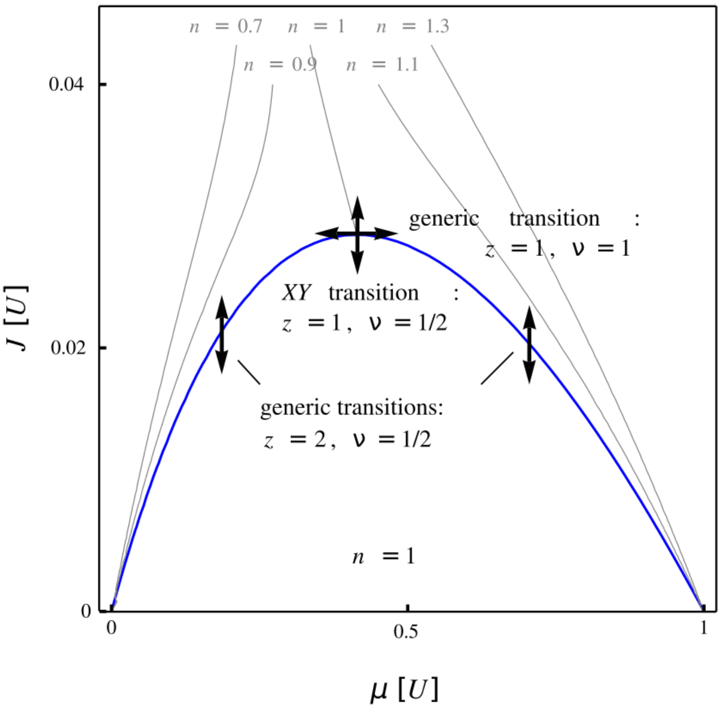

Source: Figure from Refs. [54, 39].

a lattice site with n particles becomes the same as the energy of occupying a site with $n+1$ particles. Thus, for each site there are two degenerate states exactly for those values of the chemical potential which represents a degeneracy of two to the power of the number of lattice site for the whole system [21]. Therefore, there is no energy cost for creating excitations at those points, and superfluidity occurs for any arbitrarily small values of the tunneling energy J which lifts the degeneracy [22].

By increasing μ for a fixed J one eventually gets to the situation where the kinetic energy of creating an excitation will balance the potential energy cost caused by interactions. In this scenario, the average density of particle starts to fluctuate creating a finite number of excitations which are allowed to hop freely through the lattice. These excitations will condense into a superfluid state and thus one gets the phase boundary. The transition which occurs due to fluctuations in the average number of particles per site is called generic transition. At the tip of the Mott lobes, however, there exists a multi-critical point. The transition at that point is dominated by phase fluctuations rather than density fluctuations. For the generic transition, the product of the dynamical and the correlation length critical exponents is found to be $z\nu = 1$, while for the transition at the tip of the Mote lobes this product turns out to be $z\nu = 1/2$, which is associated with the universality class of the $(d+1)$-dimensional XY-model [22, 21, 39]. A phase diagram for the Mott lobe of $n = 1$ where each transition is specified can be observed in Fig. 2.4. In the present work, we shall be concerned with the generic transition.

The clean case phase diagram has been investigated in a numerous amount of scientific research papers. Here, we reference some that are of particular importance for the analysis of the present work [52, 53, 54, 39, 99]. In what follows, we discuss what changes in the phase diagram when disorder is introduced.

2.4 Zero-temperature phase diagram for the disordered system

As we have already discussed in Section 1.4, in the presence of disorder, a Bose glass state can emerge in the Bose-Hubbard model. In order to investigate such a problem, we assume the local energy shifts ϵ_i to be randomly distributed within the interval $[-\Delta/2, \Delta/2]$. Furthermore, we assume the disorder distribution to be uniform, meaning that any value of the local shifts within that interval has the same probability to occur. Following again the same path of Ref. [22], we begin by considering the $J = 0$ case. In such a case, from (1.34), the local single site energies are given by

$$E(n_i) = \frac{U}{2} n_i(n_i - 1) - \mu n_i + \epsilon_i n_i. \tag{2.9}$$

The condition for the minimization of this energy leads a separation of the chemical potential line in interval of size exactly given by $U - \Delta$. In the case where the disorder strength is smaller then the interaction energy, i.e. $\Delta < U$, values of the chemical potential within these intervals are allowed to minimize the single site energy by fixing the average particle density at integer values $n \in \{1, 2, 3, \ldots\}$. Such interval are defined by

$$U(n-1) + \frac{\Delta}{2} \leq \mu \leq Un - \frac{\Delta}{2}. \tag{2.10}$$

This is analogous to the clean case situation, where the intervals defined the extension of the Mott lobes. However, in the disordered case, theses intervals become smaller. Thus, one can conclude that the presence of weak disorder leads to the shrinking of the Mott lobes. In between the intervals (2.10), where the average number of particles is fixed, there emerge gaps of width given by Δ, which can be defined as

$$Un - \frac{\Delta}{2} < \mu < Un + \frac{\Delta}{2}. \tag{2.11}$$

For values of the chemical potential inside these gaps, the average occupation at the ith site, n_i, is either $n + 1$ or n depending if the realization of the random shift ϵ_i at that site is less or greater then $Un + \mu$. This argument follows from the minimization of the single site energies (2.9). These fluctuations of the average occupation number at each site even at

Figure 2.5 – Qualitative phase diagram of the disordered Bose-Hubbard model. The Mott insulator (MI) is shown in blue, the Bose glass (BG) in pink, and the superfluid (SF) in white. The BG intervenes between the MI and SF for finite disorder and dominates the insulating part of the phase diagram if the disorder energy scale is greater than the interaction energy.

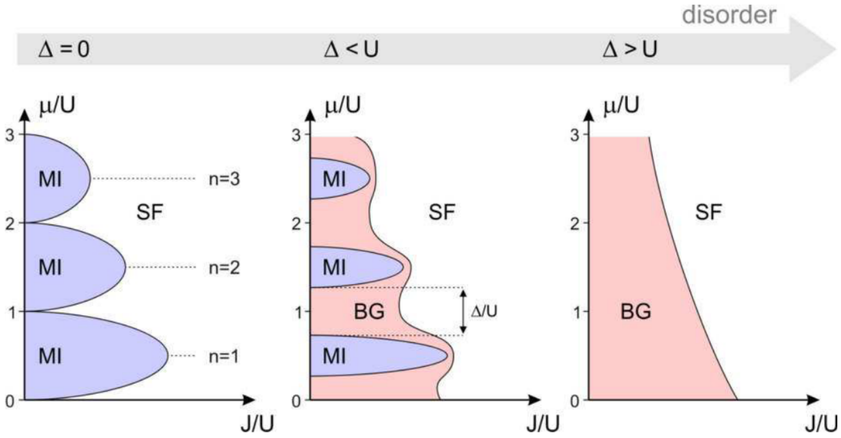

Source: Figure from Ref. [64].

zero tunneling energy is already a manifestation of the Bose-glass state. We point out that for $\mu < -\Delta/2$ the average particle density is strictly zero, i.e. $n_i = 0$.

For weak disorder, inside the intervals (2.10) there are exactly n particles per site in the decoupled limit of zero tunneling. If J is made slightly positive, but still insufficient to overcome the energy cost imposed by the repulsive on-site interaction U, no extra particles can be added to occupied sites and the Mott lobe structure of the clean case can still exist. However, as it was argued in [22], the Bose-glass phase always intervenes between the Mott and the superfluid state and it dominates the insulating part of the phase diagram for strong disorder, i.e., disorder of the same order or greater than the interaction energy, $\Delta \geq U$. In this limit, the average particles density never sticks to an integer value, making it impossible for the formation of a Mott insulating state. A qualitative picture of the phase diagram in the disordered case can be observed in Fig. 2.5.

One can observe, from middle graph at Fig. 2.5, the lack of a direct Mott to superfluid phase transition in the weak disordered limit. The argument that justifies this qualitative picture, which follows from [22], is based on the nature of the lowest lying available states to create excitations at the vicinity of the Mott-lobe phase boundaries. Due to the presence of disorder, it is expected that these correspond to localized states which prevent the small density of excitations created just outside the Mott insulator phase boundaries to immediately produce superfluidity. In Chapter 5 of the present work, we investigate further these argument by characterizing the physical aspects of these low-lying excited states.

In agreement with the above described predictions, numerical simulations have obtained phase diagrams which confirm the absence of a direct Mott-superfluid phase transition in the presence of diagonal disorder [43, 44, 46]. Such phase diagrams are shown

Figure 2.6 – Phase diagram of the disordered Bose-Hubbard model obtained with Monte-Carlo simulations. The left graph corresponds to the two-dimensional case and the right graph corresponds to the three-dimensional case. The superfluid, the Mott insilator, and the Bose glass ground states are represented by SF, MI, BG, respectively. Both diagrams show that, for finite disorder strength, no direct SF to MI transition is possible.

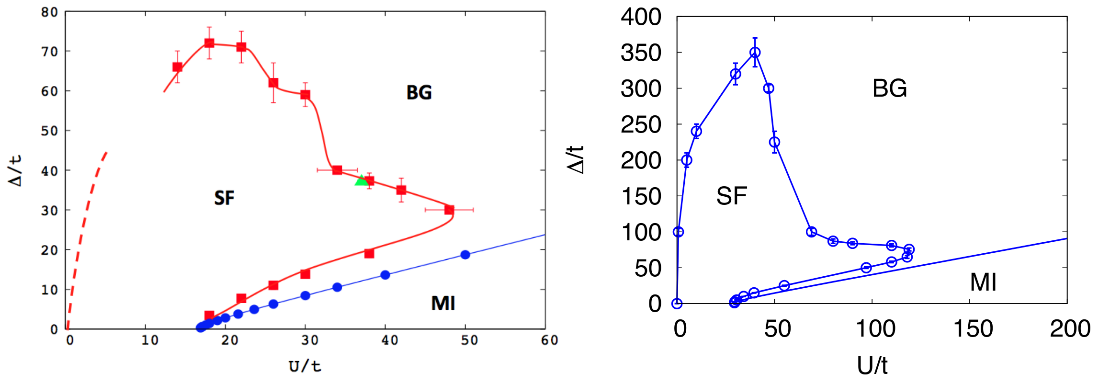

Source: Figure from Refs. [43, 44, 46].

in Fig. 2.6. These studies have applied the path-integral Monte Carlo simulations with the worm algorithm to investigate the effects of uniform diagonal disorder to the Bose-Hubbard model in two and three dimensions. The distinction between the different ground states was made by calculating the superfluid stiffness together with the isothermal compressibility. The superfluid stiffness measures the phase rigidity of the macroscopic wave function thus identifying the superfuild phase. It is important to point out that this quantity does not respect the self-averaging property in the Bose-glass phase. This implies its average over the disordered ensemble does not converge even for larger systems. The compressibility measures variations on the average particle density per site as a function of the chemical potential. Since such a density if fixed in the Mott regime, the compressibility vanishes in that region of the phase diagram, which differs from the Bose-glass phase where such a quantity is finite due to density fluctuations. However, thermal fluctuations lead to a residual finite compressibility inside the Mott phase [38], making it a non-reliable parameter to identify the Mott-Bose glass phase transition at finite temperatures. Therefore, even though these Monte-Carlo simulations lead to an incredibly accurate result for the phase boundaries, the fundamental characteristics of the Bose-glass phase cannot be directly extracted from them. We shall demonstrate, in Chapter 6, that a more reliable quantity to distinguish the Mott state from the Bose glass states at zero and finite temperatures is the local density of states, which takes the energy spectrum structure of theses states into account.

Another argument which in favors the qualitative picture of Fig. 2.5, comes from the so-called Harris' criterion for the stability of the clean case critical point against the presence of disorder [21, 100, 101, 102]. The derivation of such a criterion follows a similar path to the scaling arguments developed in Section 2.1. In the clean case, by considering g as the general dimensionless parameter of the Hamiltonian, the divergence of the correlation length near the critical point g_c, where the phase transition takes place, is described by (2.3). One can analyze the phase transition by dividing the system into regions of linear size given by ξ. Due to the presence of disorder, one can attribute to each one of these regions denoted by i a local critical point $g_c(i)$, which may be differ from region to region. The basic idea developed by Harris was to compare the variations of the local critical points for different regions Δg_c with the distance $g - g_c$ of the global phase transition [100]. In the case that Δg_c is less than $g - g_c$ all blocks may be assumed to be in the same side of the phase transition. In contrast, in the opposite case, if Δg_c is greater than $g - g_c$, the regions may be in different phases which makes a uniform phase transition unlikely. The values of the local critical points $g_c(i)$ can be estimated by considering the average over a large number of random variables within each region. From the central limit theorem, the standard deviations of these local values are proportional to the inverse of the square root of the volume of each region

$$\Delta g_c \propto \xi^{-d/2}. \tag{2.12}$$

In the situation where all such regions are in the same side of the phase transition, i.e. $\Delta g_c < g - g_c$, as the phase transition is approached a comparison between (2.3) and (2.12) leads to the following relation

$$\xi^{-d/2} < \xi^{-1/\nu}, \tag{2.13}$$

which implies the condition

$$d\nu > 2. \tag{2.14}$$

The above condition constitutes the Harris criterion for the robustness of the clean case scaling behavior to the presence of disorder. As a consequence, if the condition (2.14) is satisfied, the ratio $\Delta g_c/(g - g_c)$ goes to zero at the critical point, which implies that the random fluctuation of the local critical values $g_c(i)$ cased by disorder have become smooth and do not influence the critical behavior of the clean case phase transition. In the oposite case, if the criterion (2.14) is not fulfilled, the ratio $\Delta g_c/(g - g_c)$ becomes larger as the phase transition is approached. This implies that while some regions of the system are in one side of the phase boundary, another blocks are on the other side. This arguments ware generalized to quantum phase transitions in [103].

From the discussion of the last section, one can observe that neither the generic nor the multi-critical phase transitions from the Mott insulator to the superfluid phase of the Bose-Hubbard model in the clean case satisfy the condition (2.14). Even though there is no precise argument to what happens when such a criterion is violated, one possibility is that the clean case phase transition is replaced by another continuous phase transition with a different scaling behavior near criticality. That is, in the presence of disorder the system features a new universality class with a different correlation length exponent which satisfies the inequality (2.14) [100]. In the case of the disorder Bose-Hubbard model, this is characterized by the emergence of the Bose-glass phase. However, we must remark that the precise characterization of the university class of the Mott insulator to Bose glass as well as the Bose glass to superfluid phase transitions is still lacking in literature.

The transition from Mott to the Bose glass phase is predicted to be dominated by rare regions of the random potential where the gap for creating excitations vanishes locally. The theorem of inclusions was used by Refs. [104, 43] to prove that such a transition is of Griffiths type. Such a theorem states that for a generic phase transition in the presence of bounded disorder, there are large regions of competing phases across the phase boundary. For the superfluid to insulator quantum phase transition, this theorem immediately implies that no direct Mott-superfluid transition can exist in the presence of continuous disorder. The Mott insulating phase can only be destroyed if the gap present in its excitation spectrum vanishes. In the presence of disorder, this means that the phase boundary out of the Mott states depends only on the value of the bound of the disorder distribution Δ, which is the energy scale that controls the disorder strength. Hence, if Δ is larger then the energy gap, no Mott phase can exist. As we have discussed in Section 1.4, there always exists the possibility that large enough regions where the disordered potential is minimum will occur. At those regions, the fluctuations of the disorder potential mimic a homogeneous chemical potential shift. If the minimum value of the disorder potential is of the same order as the interaction energy, the energy gap of the Mott phase vanishes locally and droplets of condensed bosons can emerge. This constitutes the local emergence of phase coherence in an insulating background. The phase transition which is associated with the emergence of rare regions where local order is present is called Griffiths phase transition, in analogy to the predictions which followed from the work of R. Griffiths when analyzing the random Ising ferromagnet [105].

The Bose glass to superfluid phase transition is predicted to follow the universality character of percolation class. This prediction comes from assuming that the local puddles of condensed bosons in the Bose glass phase represent clusters that percolate due to the competition between the tunneling and the disorder energy scales to form superfluidity. From the arguments already presented, near the phase boundary to the Mott phase, the Bose glass is characterized by rare regions where the coherence is restored locally. One can therefore argue that, by increasing disorder the incoherent background in between these regions would be filled in, favoring a coherent superflow of atoms through the whole system's volume. This superflow would then lead to a finite superfluid fraction. A similar picture is expected if instead of increasing disorder, one increases the tunneling energy. In this situation, the tunneling would connect the condensate puddles forming a global superflow. This percolation picture has been confirmed in Ref. [106], where the dynamical and the correlation length critical exponents were calculated using quantum Monte Carlos simulations.

Even though many features the these phase transitions in the presence of disorder are well established, the complete characterization of the phase diagram from an analytical point of view is still lacking. As it was discussed in this chapter, the nature of the low energy excited states near the phase boundary plays an important role not only in understanding the universal aspects of the quantum phase transition, but also on identifying the fundamental properties the ground states. The purpose of the present work is fill in these gap by deriving from analytical methods the effects of disorder on the excitations of the Bose-Hubbard model. Furthermore, we aim on demonstrating the energy spectrum information can be used to unambiguously distinguish the Mott from the Bose-glass state even for finite temperatures and small values of the tunneling energy. On the next part of this work, we introduce the essential quantities which underlie our theoretical methods.

Part II

Methods

Chapter 3

Single-particle Green's functions

The Green's function formalism provides a powerful framework for investigating quantum many-body systems. These functions can be used to calculate different properties of the system, such as the spectral function, the density of states and the correlation functions. Here, we give an overview of how the elementary excitations of the system can be studied with the use of Green's functions. We do not wish to cover all the content of applications of Green's functions, but rather to present the properties which are relevant to the present work.

3.1 Linear response

In experiments the usual situation can be described as follows. The system in equilibrium is exposed to an external field at some arbitrary time. The field perturbs the system creating excitations. One then measures the response of the system to the perturbation, e.g. one measures the energy $\hbar\omega$ and wavevector $\mathbf{k}$ of the emitted particles at a latter time. This situation is demonstrated in Fig. 3.1. We follow here the derivation of Ref. [107]. The typical situation is that such a perturbation will cause some macroscopic observable quantity to change in experiments. Thus it becomes necessary to define the notion of the expectation value of a function of the dynamical variables. In quantum mechanics, we represent such an observable quantity by the macroscopic operator $\hat{O}$ and its expectation value is defined as

$$\langle \hat{O} \rangle = \mathrm{tr}\, \hat{\rho}\hat{O}. \tag{3.1}$$

The operator $\hat{\rho}$ is usually referred to as the density matrix and it describes the quantum state of the system in the general case where temperature fluctuations are present. The question is then how to describe the time evolution of the average value of this observable quantity due to the presence of the external field or force. It is completely equivalent to consider that the observable quantity changes in time for a given quantum state or that the observable remains unchanged while the quantum state evolves in time as a consequence

Figure 3.1 – Usual experimental procedure. The system is in equilibrium at first (left), an excitation enters the system at time $t_0 = 0$ (middle) and after it has propagated, the excitation lives the system at a later time t when it is measured (right).

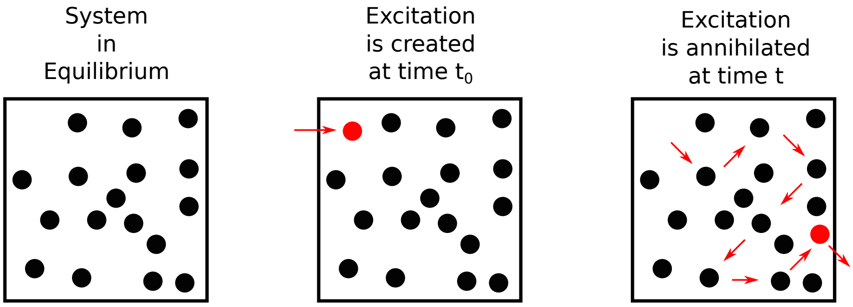

Source: Prepared by the author.

of the perturbation. This occurs because the Heisenberg and Schrödinger representations are equivalent up to a unitary transformation. In the former representation, one can understand the time evolution of the quantum state by applying the so-called von Neumann equation for the density matrix

$$\mathrm{i}\hbar\frac{\partial\hat{\rho}}{\partial t} = [\hat{H}, \hat{\rho}], \tag{3.2}$$

where the Hamiltonian $\hat{H}$ is the operator whose eigenvalues coincide with the energy spectrum of the system. In order to investigate the response of the macroscopic system to the external perturbation, one must solve the above equation.

We are particularly interested in the case where $\hat{H}(t)$ is composed of the sum of a time-independent unperturbed part $\hat{H}_0$ plus a perturbation part $\hat{H}_1(t)$ representing the external field

$$\hat{H}(t) = \hat{H}_0 + \hat{H}_1(t), \tag{3.3}$$

where the perturbation has the form

$$\hat{H}_1(t) = \hat{B}F(t). \tag{3.4}$$

The function $F(t)$ can be interpreted as a generalized force and $\hat{B}$ as the operator pertaining to the system to which this force couples. We assume that the system is in thermal equilibrium at temperature T in the grand-canonical ensemble before the perturbation acts. In such a limit, the expected value of any physical quantities is specified with respect to the unperturbed density matrix [108, 94]

$$\hat{\rho}_0 = \frac{\mathrm{e}^{-\beta\hat{H}_0}}{Z}, \tag{3.5}$$

where the partition function reads

$$Z = \mathrm{tr}\,\mathrm{e}^{-\beta\hat{\mathrm{H}}_0}, \tag{3.6}$$

and the inverse temperature is defined as

$$\beta = \frac{1}{k_B T}, \tag{3.7}$$

with k_B denoting the Boltzmann constant. Note that this definition leads to the normalization condition for the density matrix

$$\mathrm{tr}\,\hat{\rho}_0 = 1. \tag{3.8}$$

Equation (3.5) is a solution of (3.2) in the absence of the perturbation $\hat{H}_1$ provided that the unperturbed Hamiltonian commutes with the number operator $\hat{N}$, i.e. it conserves the total number of particles. To solve the original problem, we can apply the transformation to the Dirac interaction picture

$$\hat{\sigma}(t) = \hat{U}(t)\hat{\rho}(t)\hat{U}^{\dagger}(t), \tag{3.9}$$

where $\hat{U}(t) = \mathrm{e}^{\mathrm{i}\hat{H}_0 t/\hbar}$. Equation (3.2) can be rewritten as

$$\mathrm{i}\hbar\frac{\partial\hat{\sigma}}{\partial t} = \left[\hat{H}_1(t), \hat{\sigma}\right]. \tag{3.10}$$

where $\hat{H}_1(t) = \hat{U}(t)\hat{H}_1\hat{U}^{\dagger}(t)$. Assuming that the initial condition at $t = 0$ is satisfied

$$\hat{\sigma}(0) = \hat{U}(0)\hat{\rho}(0)\hat{U}^{\dagger}(0) = \hat{\rho}_0, \tag{3.11}$$

we find, by iteration, that the first order correction in $\hat{H}_1$ reads

$$\hat{\sigma}(t) = \hat{\rho}_0 - \frac{\mathrm{i}}{\hbar}\int_0^t dt'[\hat{H}_1(t'), \hat{\rho}_0] + \cdots, \tag{3.12}$$

which in the Schrödinger picture becomes

$$\hat{\rho}(t) = \hat{\rho}_0 - \frac{\mathrm{i}}{\hbar}\hat{U}^{\dagger}(t)\int_0^t dt'[\hat{H}_1(t'), \hat{\rho}_0]\hat{U}(t) + \cdots. \tag{3.13}$$

The above expression characterizes what changes in the density matrix up to first order as the perturbation $\hat{H}_1$ is switched on.

The question is then how the observable quantum and thermal average compares with an experiment at a given time t. Turning back to (3.1), with the result (3.13) we obtain

$$\langle\hat{O}\rangle = \mathrm{tr}\,\hat{\rho}_0\hat{O} - \frac{\mathrm{i}}{\hbar}\mathrm{tr}\left(\hat{O}\hat{U}^{\dagger}(t)\int_0^t dt'[\hat{H}_1(t'), \hat{\rho}_0]\hat{U}(t)\right) + \cdots. \tag{3.14}$$

We recognize that the first term is just the average over the equilibrium ensemble of $\hat{H}_0$, which we can represent by $\langle\hat{O}\rangle_0$. The second term consists of fluctuations around this equilibrium average value of the observable due to the external field, which we can denote by $\delta\langle\hat{O}\rangle(t)$. The time dependence is only explicit in such fluctuations. Equation (3.14) can then be rewritten as

$$\langle \hat{O} \rangle = \langle \hat{O} \rangle_0 + \delta \langle \hat{O} \rangle (t) + \cdots . \tag{3.15}$$

One can then apply the cyclic property of the trace of products between operators to write such fluctuation term as

$$\delta \langle \hat{O} \rangle (t) = \frac{\mathrm{i}}{\hbar} \int_0^t dt' \, \mathrm{tr}\big(\hat{\rho}_0 [\hat{H}_1(t'), \hat{O}(t)]\big), \tag{3.16}$$

where $\hat{O}(t)$ corresponds to the interaction picture representation of the observable. This result consists of the linear response of the system to an external perturbation and it is often referred to as Kubo's formula after its first derivation by R. Kubo in 1957 [109].

Inserting the form (3.4) of the perturbation in (3.14) we get

$$\delta \langle \hat{O} \rangle (t) = \int_0^\infty dt' G^R(t,t') F(t'), \tag{3.17}$$

where we have introduced the quantity

$$G^R(t,t') = -\frac{\mathrm{i}}{\hbar} \Theta(t-t') \, \mathrm{tr}\big(\hat{\rho}_0 [\hat{O}(t), \hat{B}(t')]\big). \tag{3.18}$$

The above equation defines the so-called Green's function, which characterizes the linear response of the system to an external perturbation. In this definition, in particular, the Heaviside step function Θ ensures a causal relation such that the Green's function appears as a measure of the retarded response of the system after the external field is switched on. We use this derivation as to motivate the use of such functions. However, as we shall discuss, one can extract a plethora of important information on many-body systems from the Green's functions.

3.2 Källén-Lehmann representation

In Section 1.4, while deriving the Bose-Hubbard Hamiltonian , we have introduced the formalism of second quantization. There we defined the field operator $\hat{\Psi}^\dagger(\mathbf{x})$ and its adjoint $\hat{\Psi}(\mathbf{x})$ which, when acting on the state of the system, respectively add or remove a particle from the point $\mathbf{x}$. Any operator in this formalism can be described by products of such field operators. Therefore it makes sense to define the Green's function with the use of such operators. However, instead of the retarded Green's function that we derived in the last section, it is often useful to define the so-called time-ordered Green's function

$$G(\mathbf{x}t, \mathbf{x}'t') \equiv -\frac{\mathrm{i}}{\hbar} \langle \mathcal{T} \hat{\Psi}(\mathbf{x}t) \hat{\Psi}^\dagger(\mathbf{x}'t') \rangle , \tag{3.19}$$

where we use the Heisenberg representation

$$\hat{\Psi}(\mathbf{x}t) = \mathrm{e}^{\mathrm{i}\hat{H}t/\hbar}\hat{\Psi}(\mathbf{x})\mathrm{e}^{-\mathrm{i}\hat{H}t/\hbar}. \tag{3.20}$$

In the definition (3.19), $\mathscr{T}$ is usually called the time-ordering operator which acts in the product of the bosonic field operators such that they obey the following relation

$$\mathscr{T}\hat{\Psi}(\mathbf{x}t)\hat{\Psi}^{\dagger}(\mathbf{x}'t') = \begin{cases} \hat{\Psi}(\mathbf{x}t)\hat{\Psi}^{\dagger}(\mathbf{x}'t') & \text{if} \quad t > t', \\ \hat{\Psi}^{\dagger}(\mathbf{x}'t')\hat{\Psi}(\mathbf{x}t) & \text{if} \quad t < t'. \end{cases} \tag{3.21}$$

This definition motivates the interpretation of the Green's function in many-body theory as the amplitude of propagation of an excitation created at space-time point $\mathbf{x}'t'$ and follows a path to be annihilated at space-time point $\mathbf{x}t$. From now on, we shall assume that $\hbar = 1$ such that energy is measured in terms of frequencies. We follow here the derivations of Refs. [110, 73].

As it is the case for the Bose-Hubbard Hamiltonian, we assume no explicit time dependence for $\hat{H}$. This assumption implies that time translation invariance is respected and the that Green's function depends only on the difference $t - t'$. Furthermore, we shall assume that the system is homogeneous such that it respects translational symmetry. In this case, the Green's function reduces to

$$G(\mathbf{x}t, \mathbf{x}'t') = G(\mathbf{x} - \mathbf{x}', t - t'). \tag{3.22}$$

We will discus latter the more complicated case when disorder is present.

With the use of the time ordering (3.21) we can define the correlation functions

$$G^{>}(\mathbf{x}, t) = -\mathrm{i}\langle\hat{\Psi}(\mathbf{x}t)\hat{\Psi}^{\dagger}(0)\rangle \quad \text{for} \quad t > 0, \tag{3.23}$$

$$G^{<}(\mathbf{x}, t) = -\mathrm{i}\langle\hat{\Psi}^{\dagger}(0)\hat{\Psi}(\mathbf{x}t)\rangle \quad \text{for} \quad t < 0. \tag{3.24}$$

These functions are called the greater and lesser correlation functions. Under the present consideration of a homogeneous system, the momentum operator $\hat{\mathbf{p}}$, which is the generator of translations in space [111], commutes with the Hamiltonian. It can therefore be proved by using a plane-wave basis [73] that the Heisenberg form of the field operators can be written as

$$\hat{\Psi}(\mathbf{x}t) = \mathrm{e}^{-\mathrm{i}\hat{\mathbf{p}}\cdot\mathbf{x}}\mathrm{e}^{\mathrm{i}\hat{H}t}\hat{\Psi}(0)\mathrm{e}^{-\mathrm{i}\hat{H}t}\mathrm{e}^{\mathrm{i}\hat{\mathbf{p}}\cdot\mathbf{x}}. \tag{3.25}$$

Consequently, one can choose to evaluate traces corresponding to the averages in (3.23) and (3.24) in terms of the set of exact eigenstates of the Hamiltonian $\hat{H}$ and the momentum operator $\hat{\mathbf{p}}$

$$\hat{H}\,|\phi_m\rangle = E_m\,|\phi_m\rangle\,, \tag{3.26}$$

$$\hat{\mathbf{p}}\,|\phi_m\rangle = \mathbf{p}_m\,|\phi_m\rangle\,. \tag{3.27}$$

Thus, we obtain the following expressions

$$G^{>}(\mathbf{x},t) = -\frac{\mathrm{i}}{Z}\sum_{mn}|\langle\phi_m|\hat{\Psi}(0)|\phi_n\rangle|^2 \mathrm{e}^{-\beta E_m+\mathrm{i}(\mathbf{p}_n-\mathbf{p}_m)\cdot\mathbf{x}-\mathrm{i}(E_n-E_m)t} \quad \text{for} \quad t>0, \tag{3.28}$$

$$G^{<}(\mathbf{x},t) = -\frac{\mathrm{i}}{Z}\sum_{mn}|\langle\phi_m|\hat{\Psi}(0)|\phi_n\rangle|^2 \mathrm{e}^{-\beta E_n+\mathrm{i}(\mathbf{p}_n-\mathbf{p}_m)\cdot\mathbf{x}-\mathrm{i}(E_n-E_m)t} \quad \text{for} \quad t<0, \tag{3.29}$$

where we have applied the completeness relation of the basis states. The sums over the set of states in the above equation come from the assumption that the system has a discrete energy spectrum, however, one could generalize this to an integration in case of a continuum energy spectrum.

With the use of the Heaviside step functions, one can write the time-ordered Green's function as

$$G(\mathbf{x},t) = \Theta(t)G^{>}(\mathbf{x},t)+\Theta(-t)G^{<}(\mathbf{x},t). \tag{3.30}$$

Up to this point we have not specified any constraint for the space variable apart from homogeneity. We can therefore make a Fourier transform to momentum space. Moreover, one can introduce a Fourier transform from time to frequency space. Altogether, these transformations read

$$G(\mathbf{k},\omega) = \int_{\mathbb{R}^d} d^dx \int_{-\infty}^{\infty} dt G(\mathbf{x},t)\mathrm{e}^{-\mathrm{i}\mathbf{k}\cdot\mathbf{x}}\mathrm{e}^{\mathrm{i}\omega t}. \tag{3.31}$$

Such a transformation becomes subtle when evaluating the integrals in time as the exponentials oscillate rapidly in the limit of $t\to-\infty$ in the case of $G^{<}(\mathbf{x},t)$ and in the limit of $t\to\infty$ in the case of $G^{>}(\mathbf{x},t)$. One can sort out this problem by introducing the technique of analytic continuation in order to extend the domain of the Fourier transformed Green's function over frequencies defined in the complex plane. In our present analysis, for $t>0$, for instance, this consists of introducing an imaginary part to the frequency with the transfomation $\omega\to\omega+\mathrm{i}0^{+}$ and then considering the limit that such a part tends to zero from above. The situation is analogous for $t<0$, however one has to use the complex conjugation of the former transformation $\omega\to\omega-\mathrm{i}0^{+}$. Consequently, the transformation results in the following expression

$$\begin{aligned} G(\mathbf{k},\omega) = {} & \frac{(2\pi)^3}{Z}\sum_{mn}|\langle\phi_m|\hat{\Psi}(0)|\phi_n\rangle|^2\delta[\mathbf{k}-(\mathbf{p}_n-\mathbf{p}_m)] \\ & \times\left[\frac{\mathrm{e}^{-\beta E_m}}{\omega-(E_n-E_m)+\mathrm{i}0^{+}}-\frac{\mathrm{e}^{-\beta E_n}}{\omega-(E_n-E_m)-\mathrm{i}0^{+}}\right]. \end{aligned} \tag{3.32}$$

Note that the analytic continuation results in shifting the poles of the Green's function either to the lower or the upper half of the complex plane.

The result (3.32) corresponds to the so-called Källén-Lehmann representation in the non-relativistic limit. It was derived independently by G. Källén and H. Lehmann while studying the general features of renormalization constants in quantum field theory [112, 111, 113, 114]. A crucial detail concerning such a general result is that it implies that the Green's function in Fourier space is a meromorphic function of the frequencies. This means that it is complex-differentiable in a neighborhood of each point defined in a domain of the complex plane except for a set of isolated points where singularities occur. These singularities consist of simple poles located exactly at the excitation energies corresponding to wave vector $\mathbf{k}$ with residue proportional to $|\langle\phi_m|\hat{\Psi}(0)|\phi_n\rangle|^2$. It is essential to notice that if one obtains as result of some perturbation theory, for instance, terms of the Green's function where higher order poles appear, it becomes necessary to renormalize such singularities so that the simple pole structure is recovered. Although, this result was derived in the continuum limit, the implications are true even in the lattice case.

3.3 Spectral function

As we have shown in Section 3.1, in many cases it is convenient to work with the retarded Green's function. In the case of the field operators such a function is defined as

$$G^R(\mathbf{x}t,\mathbf{x}'t') \equiv -\mathrm{i}\Theta(t-t')\langle[\hat{\Psi}(\mathbf{x}t),\hat{\Psi}^\dagger(\mathbf{x}'t')]\rangle\,. \tag{3.33}$$

Assuming time and space translational symmetries, we can follow the same path presented in the last section to obtain the Källén-Lehmann representation

$$G^R(\mathbf{k},\omega) = \frac{(2\pi)^3}{Z}\sum_{mn}\mathrm{e}^{-\beta E_m}|\langle\phi_m|\hat{\Psi}(0)|\phi_n\rangle|^2\delta[\mathbf{k}-(\mathbf{p}_n-\mathbf{p}_m)]\frac{1-\mathrm{e}^{-\beta(E_n-E_m)}}{\omega-(E_n-E_m)+\mathrm{i}0^+}. \tag{3.34}$$

The analytic continuation can be further explored by separating the real and imaginary parts. To this end, we consider the symbolic identity

$$\frac{1}{\omega\pm\mathrm{i}0^+} = \mathrm{p.v.}\frac{1}{\omega}\mp\mathrm{i}\pi\delta(\omega), \tag{3.35}$$

which is only valid for $\omega\in\mathbb{R}$. Here, $\mathrm{p.v.}$ denotes the principal value of that function. This identity is to be understood in a distribution sense, i.e. it is only well defined mathematically when considered over an integral. With this identity, equation (3.34) becomes

$$\begin{aligned}G^R(\mathbf{k},\omega) &= \frac{(2\pi)^3}{Z}\sum_{mn}\mathrm{e}^{-\beta E_m}|\langle\phi_m|\hat{\Psi}(0)|\phi_n\rangle|^2\delta[\mathbf{k}-(\mathbf{p}_n-\mathbf{p}_m)]\\ &\times\left(1-\mathrm{e}^{-\beta(E_n-E_m)}\right)\left\{\mathrm{p.v.}\frac{1}{\omega-(E_n-E_m)}-\mathrm{i}\pi\delta[\omega-(E_n-E_m)]\right\}.\end{aligned} \tag{3.36}$$

From the imaginary part of the above expression, we define the so-called spectral function

$$A(\mathbf{k},\omega) = -\frac{1}{\pi}\,\mathrm{Im}\,G^R(\mathbf{k},\omega), \tag{3.37}$$

which in the present case turns out to be

$$A(\mathbf{k},\omega) = \frac{(2\pi)^3}{Z}\sum_{mn} \mathrm{e}^{-\beta E_m}\,|\,\langle\phi_m|\hat{\Psi}(0)|\phi_n\rangle\,|^2\delta[\mathbf{k}-(\mathbf{p}_n-\mathbf{p}_m)]\left(1-\mathrm{e}^{-\beta\omega}\right)\delta[\omega-(E_n-E_m)]. \tag{3.38}$$

Note that in this case, such a function is represented by an energy-dependent Dirac delta distribution which is directly related to the simple pole singularity of the Källén-Lehmann representation for the Green's function.

An important characteristics of the spectral function is that one can recover the full Green's function by integrating it over the frequency domain. For the retarded Green's function (3.34) this representation reads

$$G^R(\mathbf{k},\omega) = \int_{-\infty}^{\infty} d\omega' \frac{A(\mathbf{k},\omega')}{\omega-\omega'+\mathrm{i}0^+}, \tag{3.39}$$

while for the time-ordered Green's function the integration is given by

$$G(\mathbf{k},\omega) = \int_{-\infty}^{\infty} d\omega' A(\mathbf{k},\omega')\left[\mathrm{p.v.}\frac{1}{\omega-\omega'} - \mathrm{i}\pi\frac{\delta(\omega-\omega')}{\tanh\left(\beta\omega/2\right)}\right]. \tag{3.40}$$

Expressions (3.39) and (3.40) are commonly referred to as the spectral representation of the Green's functions. The spectral function becomes then a central character as it can be used to obtain the Källén-Lehmann representation of the important Green's functions.

One can prove an important property of the spectral function by considering the inverse Fourier transform integral

$$G^R(\mathbf{k},t) = \int_{-\infty}^{\infty} \frac{d\omega}{2\pi} G^R(\mathbf{k},\omega)\mathrm{e}^{-\mathrm{i}\omega t}. \tag{3.41}$$

Using the spectral representation (3.39) we get

$$\begin{aligned} G^R(\mathbf{k},t) &= \int_{-\infty}^{\infty}\frac{d\omega}{2\pi}\int_{-\infty}^{\infty} d\omega' \frac{A(\mathbf{k},\omega')}{\omega-\omega'+\mathrm{i}0^+}\mathrm{e}^{-\mathrm{i}\omega t} \\ &= \int_{-\infty}^{\infty} d\omega' A(\mathbf{k},\omega')\int_{-\infty}^{\infty}\frac{d\omega}{2\pi}\frac{\mathrm{e}^{-\mathrm{i}\omega t}}{\omega-\omega'+\mathrm{i}0^+} \\ &= -\mathrm{i}\Theta(t)\int_{-\infty}^{\infty} d\omega' A(\mathbf{k},\omega')\mathrm{e}^{-\mathrm{i}\omega' t}. \end{aligned} \tag{3.42}$$

There the last line was obtained by recognizing that the ω integral is the Fourier representation of the Heaviside step function. The above equation is important as it shows that one can obtain the retarded Green's function in time by integrating the spectral function over the frequency domain. On the other hand, we can solve the integral (3.41) by introducing the Fourier representation (3.31) along with the definition (3.33)

$$\begin{aligned} G^R(\mathbf{k},t) &= \int_{\mathbb{R}^d} d^dx G^R(\mathbf{x},t)\mathrm{e}^{-\mathrm{i}\mathbf{k}\cdot\mathbf{x}} \\ &= -\mathrm{i}\Theta(t)\int_{\mathbb{R}^d} d^dx \, \langle[\hat{\Psi}(\mathbf{x}t),\hat{\Psi}^\dagger(0)]\rangle \ \mathrm{e}^{-\mathrm{i}\mathbf{k}\cdot\mathbf{x}}. \end{aligned} \tag{3.43}$$

Comparing both expressions (3.42) and (3.43) we can see that

$$\int_{-\infty}^{\infty} d\omega A(\mathbf{k},\omega)\mathrm{e}^{-\mathrm{i}\omega' t} = \int_{\mathbb{R}^d} d^dx \, \langle[\hat{\Psi}(\mathbf{x}t),\hat{\Psi}^\dagger(0)]\rangle \ \mathrm{e}^{-\mathrm{i}\mathbf{k}\cdot\mathbf{x}}. \tag{3.44}$$

In the limit of $t \to 0^+$, one can use the commutation relations of the field operators defined in (1.25) to show that the right-rand side of the above equation simplifies to

$$\begin{aligned} \int_{\mathbb{R}^d} d^dx \, \langle[\hat{\Psi}(\mathbf{x}0),\hat{\Psi}^\dagger(0)]\rangle \ \mathrm{e}^{-\mathrm{i}\mathbf{k}\cdot\mathbf{x}} &= \int_{\mathbb{R}^d} d^dx \delta(\mathbf{x})\mathrm{e}^{-\mathrm{i}\mathbf{k}\cdot\mathbf{x}} \\ &= 1. \end{aligned} \tag{3.45}$$

With this, we have derived the so-called sum rule for the spectral function

$$\int_{-\infty}^{\infty} d\omega A(\mathbf{k},\omega) = 1. \tag{3.46}$$

The sum rule is a general property of the spectral function and it turns out to hold even in the case of frozen disorder. Furthermore it plays an important role when defining the properties of convergence of the Green's function as it fixes the asymptotic behavior for large $|\omega|$. By applying equation (3.39), this asymptotic limit reads

$$G^R(\mathbf{k},\omega) \sim \frac{1}{\omega}\int_{-\infty}^{\infty} d\omega' A(\mathbf{k},\omega') \sim \frac{1}{\omega} \quad \text{as} \quad |\omega| \to \infty. \tag{3.47}$$

Moreover, another general property of the spectral function can be derived by noticing for positive frequencies that every term in the summations over the states in (3.38) is positive. The opposite is true for negative frequencies, i.e. each term in the sums is negative. Therefore, the spectral function obeys the following positive-definite property

$$(\mathrm{sgn}\ \omega)\mathrm{A}(\mathbf{k},\omega) \geq 0. \tag{3.48}$$

The sum rule (3.46) turns out to hold even for fermions. However, the positive-definite property is different in that case [73].

As we shall see, the spectral function plays an important role in the description of many-body systems. It incorporates the singularities of the Green's functions and can be used to investigate the excitations of a system. However, we focus next on constructing a formalism which allows one to investigate equilibrium properties of the system.

3.4 Imaginary time and Matsubara formalism

When studying equilibrium properties of interacting quantum many-body systems at finite temperatures it is often the case that exact solutions are not available. Thus, one must rely on perturbation theory. However, in most situations approximations up to lowest orders are insufficient, due to the presence of divergent terms, and one must consider the effect of an infinite amount of terms in the perturbation [115]. For real-time Green's functions, like the ones defined in the last section, which involve correlation functions of the form

$$\langle\hat{\Psi}(\mathbf{x}t)\hat{\Psi}^{\dagger}(0)\rangle = \frac{1}{Z}\mathrm{tr}[\mathrm{e}^{-\beta\hat{H}}\mathrm{e}^{\mathrm{i}\hat{H}t}\hat{\Psi}(\mathbf{x})\mathrm{e}^{-\mathrm{i}\hat{H}t}\hat{\Psi}^{\dagger}(0)], \tag{3.49}$$

a straightforward application of perturbation theory is generally challenging due to the arguments of the exponentials inside the trace. While $-\beta$ is real the exponents $\pm\mathrm{i}t$ are imaginary.

By exploring the similarities between the operators, one can notice that the term $\mathrm{e}^{-\beta\hat{H}}$ can be interpreted as a quantum evolution-operator in imaginary time τ from 0 to β. This motivates introduction of the so-called Wick rotation $\mathrm{i}t \to \tau$ [107, 111]. With such a transformation, perturbation theory becomes applicable. This approach is used since the development of the Euclidean formulation of quantum field theory [116] and it is commonly known as Matsubara formalism [117]. It turns out that such a method yields an important access to equilibrium thermodynamic properties of the many-particle system.

The Matsubara Green's function is therefore defined as

$$\mathscr{G}(\mathbf{x}\tau,\mathbf{x}'\tau') \equiv -\langle\mathscr{T}_{\tau}\hat{\Psi}(\mathbf{x}\tau)\hat{\Psi}^{\dagger}(\mathbf{x}'\tau')\rangle, \tag{3.50}$$

where the Heisenberg picture for the field operators in imaginary time reads

$$\begin{aligned}\hat{\Psi}(\mathbf{x}\tau) &= \mathrm{e}^{\tau\hat{H}}\hat{\Psi}(\mathbf{x})\mathrm{e}^{-\tau\hat{H}}, &(3.51)\\ \hat{\Psi}^{\dagger}(\mathbf{x}\tau) &= \mathrm{e}^{\tau\hat{H}}\hat{\Psi}^{\dagger}(\mathbf{x})\mathrm{e}^{-\tau\hat{H}}, &(3.52)\end{aligned}$$

while the operator $\mathscr{T}_{\tau}$ defines the order in imaginary time of products of field operators analogously to (3.21)

$$\mathscr{T}_{\tau}\hat{\Psi}(\mathbf{x}\tau)\hat{\Psi}^{\dagger}(\mathbf{x}'\tau') = \begin{cases}\hat{\Psi}(\mathbf{x}\tau)\hat{\Psi}^{\dagger}(\mathbf{x}'\tau') & \text{if} \quad \tau > \tau', \\ \hat{\Psi}^{\dagger}(\mathbf{x}'\tau')\hat{\Psi}(\mathbf{x}\tau) & \text{if} \quad \tau < \tau'.\end{cases} \tag{3.53}$$

Assuming imaginary time and space translational symmetry, we follow the path of Section 3.2 to obtain

$$\begin{aligned}\mathscr{G}(\mathbf{x},\tau) &= -\langle\hat{\Psi}(\mathbf{x}\tau)\hat{\Psi}^{\dagger}(0)\rangle\\ &= -\frac{1}{Z}\sum_{mn}|\langle\phi_m|\hat{\Psi}(0)|\phi_n\rangle|^2\mathrm{e}^{-\beta E_m+\mathrm{i}(\mathbf{p}_n-\mathbf{p}_m)\cdot\mathbf{x}-(E_n-E_m)\tau},\end{aligned} \tag{3.54}$$

where we show only the case of $\tau > 0$. As we have mentioned, the imaginary-time variable is defined over the interval $\tau \in [0,\beta]$, so we can define the Fourier transform to frequency space

$$\mathcal{G}(\mathbf{x},\mathrm{i}\omega_l) = \int_0^\beta d\tau \mathcal{G}(\mathbf{x},\tau)\mathrm{e}^{\mathrm{i}\omega_l\tau}. \tag{3.55}$$

The conjugated variable of imaginary time corresponds to a set of discrete complex frequencies $\{\omega_l\}$, the so-called Matsubara frequencies. In the present case of bosonic particles such frequencies are defined as

$$\omega_l = \frac{2\pi l}{\beta}, \tag{3.56}$$

where $l \in \mathbb{Z}$. For future reference, we present the inverse of the Matsubara-Fouries transform

$$\mathcal{G}(\mathbf{x},\tau) = \frac{1}{\beta}\sum_{l=-\infty}^{\infty} \mathcal{G}(\mathbf{x},\mathrm{i}\omega_l)\mathrm{e}^{-\mathrm{i}\omega_l\tau}. \tag{3.57}$$

Applying the transformation (3.55) to (3.54) together with the Fourier transform to momentum space defined in (3.31), we obtain

$$\mathcal{G}(\mathbf{k},\mathrm{i}\omega_l) = \frac{(2\pi)^3}{Z}\sum_{mn} \mathrm{e}^{-\beta E_m} |\langle\phi_m|\hat{\Psi}(0)|\phi_n\rangle|^2 \delta[\mathbf{k}-(\mathbf{p}_n-\mathbf{p}_m)]\frac{1-\mathrm{e}^{-\beta(E_n-E_m)}}{\mathrm{i}\omega_l-(E_n-E_m)}. \tag{3.58}$$

The above equation corresponds to the Källén-Lehmann representation of the Matsubara Green's function.

Using the spectral function of (3.38), one can immediately write the spectral representation of (3.58) as

$$\mathcal{G}(\mathbf{k},\mathrm{i}\omega_l) = \int_{-\infty}^{\infty} d\omega' \frac{A(\mathbf{k},\omega')}{\mathrm{i}\omega_l-\omega'}. \tag{3.59}$$

It is important to note that when calculating the Green's function on the Matsubara-frequency space, one obtains a representation which is valid only over discrete frequency points in the complex plane. In order to obtain a more complete representation in connection, for instance, with the retarded Green's function, one has to perform an analytic continuation to the real frequency domain. In such a case, this analytic continuation turns out to be $\mathrm{i}\omega_l \to \omega + \mathrm{i}0^+$. However, one has to make sure that this analytic continuation leads to a unique representation such that the asymptotic behavior of the Green's function for large $|\omega|$ converges. Since the sum rule fixes such a limit, one can first calculate the spectral function from the Matsubara Green's functions transforming into continuous frequencies and then obtain other types of Green's functions using the spectral representation. Hence, we establish the relation between the Matsubara Green's function and the spectral function

$$A(\mathbf{k},\omega) = \frac{1}{\mathrm{i}}[\mathcal{G}(\mathbf{k},\mathrm{i}\omega_l)|_{\mathrm{i}\omega_l\to\omega-\mathrm{i}0^+} - \mathcal{G}(\mathbf{k},\mathrm{i}\omega_l)|_{\mathrm{i}\omega_l\to\omega+\mathrm{i}0^+}]. \tag{3.60}$$

We have derived the most important aspects of the Green's functions and spectral functions which are relevant to our analysis. However, we have so far only considered the case where space translational invariance is present. It becomes necessary to discuss what changes when this symmetry is broken by disorder. Therefore, we shall focus next on the general properties of Green's function and spectral functions in disordered systems.

3.5 General properties in disordered systems

So far we have discussed the properties of Green's functions in systems that present translational invariance. Here we consider how such a formalism could be applied in disorder systems, where translational symmetry is broken. We focus on the case of frozen disorder, meaning that the time scale of the random potential is much larger than the thermodynamic time scale of the system. In this way, one can consider the thermal average over the equilibrium ensemble of the underlying Hamiltonian considering the random potential to be fixed. Furthermore, we assume a lattice system within the case of diagonal disorder, where the random potential appears as a diagonal term in the Hamiltonian. It turns out that this system already encompasses many interesting phenomena.

In order to account for the stochastic character of disorder, we consider the random potential to be described by local energy shifts ϵ_i which are randomly distributed through the lattice volume. We demand these local shifts to be independent and identically distributed according to a common probability distribution $\mathscr{P}(\epsilon_i)$. As a result, quantities like the Green's function become random variables in their own right. If one is not interested in local properties of an specific landscape of disorder, one can study global effects by looking into averaged quantities in the disorder ensemble. That is, one can consider many realizations of disorder and then average over all them. The disorder-ensemble average is therefore defined as

$$\overline{G} = \prod_i \int_{-\infty}^{\infty} d\epsilon_i \mathscr{P}(\epsilon_i) G(\epsilon_i). \tag{3.61}$$

The result is supposed to converge to the expected value of the Green's function for large enough systems and many realizations of the random potential [118, 107, 119]. This is equivalent to assuming that the probability distribution of the random variables $G(\epsilon_i)$ is sharply peaked around its average value, such that $\overline{G}$ is a representative of the ensemble.

In the case of the Bose-Hubbard model, for instance, the term which represents the random potential reads

$$\sum_i \epsilon_i \hat{a}_i^\dagger \hat{a}_i. \tag{3.62}$$

By decomposing the creation and annihilation operators into the lattice Fourier representation

$$\hat{a}_i = \left(\frac{a}{2\pi}\right)^d \int_{\mathrm{BZ}} d^d k \hat{a}(\mathbf{k}) \mathrm{e}^{\mathrm{i}\mathbf{k}\cdot\mathbf{x}_i}, \tag{3.63}$$

the representation of the disordered potential in reciprocal space becomes

$$\sum_i \epsilon_i \hat{a}_i^\dagger \hat{a}_i = \left(\frac{a}{2\pi}\right)^d \int_{\mathrm{BZ}} d^d k \int_{\mathrm{BZ}} d^d k' \hat{a}^\dagger(\mathbf{k}) \epsilon(\mathbf{k},\mathbf{k}') \hat{a}(\mathbf{k}'), \tag{3.64}$$

where we have defined

$$\epsilon(\mathbf{k},\mathbf{k}') = \left(\frac{a}{2\pi}\right)^d \sum_i \epsilon_i \mathrm{e}^{\mathrm{i}(\mathbf{k}-\mathbf{k}')\cdot \mathbf{x}_i}. \tag{3.65}$$

Note that in contrast the the previous sections, $\mathbf{k}$ represents the crystal momentum and the Fourier integral is defined over the first Brillouin zone. The expression (3.64) shows that the disordered potential couples states with different wavevectors leading to an off-diagonal contribution to the Hamiltonian in reciprocal space. Thus, one can expect that, instead of the delta distribution in $\mathbf{k}$-space shown in (3.32), the Källén-Lehmann representation of the Green's function in the disordered case would involve a superposition of states with different momentum. However, as the disordered average in (3.61) is supposed to converge and therefore it commutes with the trace of the the definition (3.19), the averaged Green's function becomes statistically homogeneous and translational symmetry is recovered. This implies that the terms of $G(\epsilon_i)$ which couple states with different wavevectors average over to zero. As a consequence, the averaged Green's function resembles the clean case in reciprocal space, i.e.

$$\overline{G(\mathbf{k},\mathbf{k}';\omega)} = \delta(\mathbf{k}-\mathbf{k}')\overline{G(\mathbf{k},\omega)}. \tag{3.66}$$

Consequently, the definition of the spectral function and all properties derived in the past sections, such as the sum rule, still hold in the disordered case after having performed the disorder ensemble average.

The singularities of the Green's function however may change due to disorder. In contrast to the delta-like peaks represented in the clean-case spectral function, a broad distribution may emerge. This leads to a different interpretation of their physical character. We shall discuss these implications in the next section.

3.6 Physical interpretation: elementary excitations

In the first section of the present chapter, we have shown that Green's functions provide a way to simplify the description of many-body systems by capturing their response to an external field or force. Up to a linear approximation, they are connected to how the expected value of an observable changes in time due to such a perturbation. This already constitutes an important connection to physical quantities. Another physical interpretation, which is of particular importance for the present work, comes from the singularities of the Green's function in the Källén-Lehmann representation. To see this, we rely on the limit of zero temperature.

In the zero-temperature limit, equation (3.32) becomes

$$\frac{G(\mathbf{k},\omega)}{(2\pi)^3}=\sum_m\left[\frac{\delta_{\mathbf{k},\mathbf{p}_m}\langle\phi_0|\hat{\Psi}(0)|\phi_m\rangle\langle\phi_m|\hat{\Psi}^\dagger(0)|\phi_0\rangle}{\omega-(E_m-E_0)+\mathrm{i}0^+}+\frac{\delta_{\mathbf{k},-\mathbf{p}_m}\langle\phi_0|\hat{\Psi}^\dagger(0)|\phi_m\rangle\langle\phi_m|\hat{\Psi}(0)|\phi_0\rangle}{\omega+(E_m-E_0)-\mathrm{i}0^+}\right], \tag{3.67}$$

where we have set $\hat{\mathbf{p}}\,|\phi_0\rangle=0$. We assume that the ground state of the system has N particles. As the operator field operator $\hat{\Psi}^\dagger$ creates one particle, the intermediate states in sum of the first term on the right hand side of (3.66) must correspond to states with $N+1$ particles. The energy dependency of the Green's functions in Fourier space stems from its denominators. In the first term, we can rewrite the denominator as

$$\omega-[E_m(N+1)-E_0(N)]=\omega-[E_m(N+1)-E_0(N+1)]-[E_0(N+1)-E_0(N)]. \tag{3.68}$$

The difference $E_0(N+1)-E_0(N)$ is associated to the energy gained by the system when an extra particle is added to its ground state while keeping the volume constant. This characterizes the chemical potential. The remaining term $E_m(N+1)-E_0(N+1)$ corresponds to the energy difference between the ground state and the excited state of the $N+1$ particle system. The analysis of the second term is analogous and the denominator can be written as

$$\omega+[E_m(N-1)-E_0(N)]=\omega+[E_m(N-1)-E_0(N-1)]-[E_0(N)-E_0(N-1)]. \tag{3.69}$$

The term $E_0(N)-E_0(N-1)$ represents the chemical potential as well, since in the thermodynamic limit one must have $\mu(N+1)=\mu(N)$ with corretions of order N^{-1} [73], while the term $E_m(N-1)-E_0(N-1)$ is again the energy difference between the ground and the excited states, this time for the $N-1$ particle system.

From the arguments presented above, we can interpret that the Green's function incorporates the information of the creation or removal of a particle from the system. Although they may resemble some features of the physical particles composing the system, it is often the case that some of their properties are changed. For instance, such particles, which are represented by the Green's function, may get dressed by the interaction with the other particles and thus acquire an effective mass which is different from the real mass. Additionally, it could also be the case that these are not stable particles, but rather have a finite lifetime. For this reason, it is usual to call them quasiparticles or quasiholes. It should be pointed out that quasiparticles and quasiholes represent excited energy levels of the many-body system, hence it is also common to refer to them as elementary excitations. Therefore, the key information about the excitations can be obtained from the singularities of the Green's function in frequency space.

Since the singularities of the Green's function are characterized by the spectral function, one can attempt to obtain further information about the excitations from such a quantity.

We consider first the case of positive energies. In the zero-temperature limit, the spectral function of (3.38) reduces to

$$A(\mathbf{k},\omega) = \sum_m \delta_{\mathbf{k},\mathbf{p}_m} |\langle\phi_m|\hat{\Psi}^\dagger(0)|\phi_0\rangle|^2 \delta[\omega - (E_m - E_0)]. \tag{3.70}$$

From the expression above, one can read off that the sum in the spectral function counts the number of states with a well defined wavevector $\mathbf{k}$ associated with an excitation energy ω which are linked to the ground state by the creation of an extra particle [107]. Thus, there is a straightforward relation to the concept of the density of states. The total density of states can be defined as

$$\rho(\omega) = \frac{1}{(2\pi)^d} \int_{\mathbb{R}^d} d^d k A(\mathbf{k},\omega). \tag{3.71}$$

This quantity measures the total number of available quantum states per unit frequency range in a system of definite volume. In systems where translational symmetry is not present, such as disordered systems, another quantity which might be of interest is the local density of states. Such a quantity can be defined from the imaginary part of the Green's function in space

$$\rho(\mathbf{x},\omega) = -\frac{1}{\pi} \mathrm{Im} G^R(\mathbf{x},\mathbf{x};\omega). \tag{3.72}$$

The relation between both densities of states is given by

$$\rho(\omega) = \int_{\mathbb{R}^d} d^d x \rho(\mathbf{x},\omega). \tag{3.73}$$

The result is analogous to the case of negative energies where the spectral function measures the number of states with wavevector $\mathbf{k}$ and corresponding excitation energy ω which are connected to the ground state by the creation of a hole, i.e. the removal of a particle [107]. The total density of states will be further explored when analyzing the nature of the excitations of the Bose-Hubbard model, while the local density of states will be used to construct a phase diagram for finite temperatures.

One would expect that the eigenenergies of the Hamiltonian would depend on the local random potential when disorder is introduced. Therefore, by averaging over all disorder realizations, the sharp Dirac delta distributions in equation (3.70) would transform into a broad distribution. An additional interpretation of the Green's functions concerns the propagation and stability of these excitations in this case. We demonstrate the concepts which connect the Green's functions with the propagation of the excitations in Chapter 5. To best demonstrate the relation to the stability of the states, we treat the strongly interacting limit of the Bose-Hubbard Model in the next section.

3.7 Bose-Hubbard model in the limit of strong interactions

From the definition (1.34) of the Bose-Hubbard Hamiltonian, we note that, in the case of vanishing hopping, such a Hamiltonian becomes diagonal in the number operator basis

$$\hat{H}_0 = \sum_i \hat{H}_{0_i}, \tag{3.74}$$

with

$$\hat{H}_{0_i} = \frac{U}{2}\hat{n}_i(\hat{n}_i - 1) - \mu_i \hat{n}_i, \tag{3.75}$$

where we have introduced the notation $\mu_i = \mu - \epsilon_i$. Such a situation could be achieved in the deep lattice regime, where interactions are strong enough to localize the atoms suppressing fluctuations on the average number of particles per site, i.e. $J/U \to 0$. Additionally, one has to consider that the disorder strength is not of the order of the interactions. This limit sets the stage for the perturbation methods to be introduced in the next chapter. As we shall see, one can construct a perturbation series in terms of the hopping energy in order to investigate the problem of the full Hamiltonian (1.34). Therefore, in this section our aim is to discuss the key aspects of the unperturbed Hamiltonian above. Since our interest is to construct a perturbation expansion in the next section, we apply here the Matsubara formalism.

From the decomposition of the field operators in terms of maximally localized Wannier functions (1.28), one can conclude that a proper definition to the Green's function in the case of lattice consists of

$$\mathscr{G}_{ij}(\tau, \tau') = -\langle \mathscr{T}_\tau \hat{a}_i(\tau)\hat{a}_j^\dagger(\tau')\rangle\,, \tag{3.76}$$

where instead of the full field operators, we have the Heisenberg representation of the bosonic creation and annihilation operators with commutation relations given by (1.29). In the limit of strong interactions, where the system is described by the Hamiltonian (3.74), an excitation created at a given site cannot propagate due to its vanishing tunneling energy. Thus, such an excitation can only create local fluctuations in the average particle density per site. Hence, in this limit, the proper definition to the Green's function is given by

$$g_i(\tau, \tau') = -\langle \mathscr{T}_\tau \hat{a}_i(\tau)\hat{a}_i^\dagger(\tau')\rangle_0\,, \tag{3.77}$$

where the average must be taken over the equilibrium ensemble of (3.74) for fixed ϵ_i. The obvious choice of a basis to take the trace are the eigenstates $|n_i\rangle$ of the number operator

$\hat{n}_i$. The corresponding single-site eigenenergies correspond to

$$\hat{H}_{0_i}|n_i\rangle = E_{n_i}(\mu_i)|n_i\rangle, \tag{3.78}$$

$$E_{n_i}(\mu_i) = \frac{U}{2}n_i(n_i-1)-\mu_i n_i. \tag{3.79}$$

Taking the trace implicit in (3.77) respect to the basis states defined above, we obtain

$$\begin{aligned} g_i(\tau,\tau') = &-\sum_{n=0}^{\infty}\frac{\mathrm{e}^{-\beta E_n(\mu_i)}}{Z_0(\mu_i)} \\ &\times\left\{\Theta(\tau-\tau')(n+1)\mathrm{e}^{(\tau-\tau')[E_n(\mu_i)-E_{n+1}(\mu_i)]}-\Theta(\tau'-\tau)n\mathrm{e}^{(\tau-\tau')[E_{n-1}(\mu_i)-E_n(\mu_i)]}\right\}. \end{aligned} \tag{3.80}$$

Since in this limit the average number of particles in each site is fixed, we have chosen to suppress the site index in the average particle density $n_i \equiv n$. In this case, the partition function is defined as

$$Z_0(\mu_i) = \sum_{n=0}^{\infty}\mathrm{e}^{-\beta E_n(\mu_i)}. \tag{3.81}$$

Note that (3.80) respects imaginary time translational symmetry. Making the substitution $\tau \to \tau+\tau'$ and transforming to the Matsubara frequency space we obtain the following expression

$$g_i(\mathrm{i}\omega_l) = \sum_{n=0}^{\infty}\frac{\mathrm{e}^{-\beta E_n(\mu_i)}}{Z_0(\mu_i)}\left(\frac{n+1}{\mathrm{i}\omega_l+\mu_i-Un}-\frac{n}{\mathrm{i}\omega_l+\mu_i-U(n-1)}\right). \tag{3.82}$$

Therefore, in the limit of strong interactions, the full Matsubara Green's function can be written as

$$\mathscr{G}_{ij}(\mathrm{i}\omega_l) = \delta_{ij}g_i(\mathrm{i}\omega_l) \quad \text{as} \quad \frac{J}{U}\to 0. \tag{3.83}$$

Note that for fixed μ_i the Green's function is characterized by two simple poles, one corresponding to the quasiparticle branch and the other to the quasihole branch. In the case of zero tunneling, such excitations can only be created exactly at chemical potentials where the Mott lobes intersect, $\mu_i/U = n$. In such a point the energy for occupying a site with n particles is the same as the one to occupy a site with $n+1$ particles (see Section 3.2). This leads to local fluctuations in the average number of particles at those points. If μ_i becomes random, for a continuous disorder distribution, this point turns into a continuum set of points defined in the gaps (2.11) of the phase diagram.

To demonstrate this, we investigate the limit of zero temperature. In such a limit, i.e. as $\beta\to\infty$, one would expect that the system goes to its ground state. In the strongly interacting case, the ground state is a Mott insulating state where fluctuations in the average particle density per site are suppressed and each site contains exactly n_0 bosons. Thus, (3.82) simplifies to

$$g_i(\mathrm{i}\omega_l) = \frac{n_0+1}{\mathrm{i}\omega_l+\mu_i-Un_0}-\frac{n_0}{\mathrm{i}\omega_l+\mu_i-U(n_0-1)}. \tag{3.84}$$

This constitutes the so-called atomic limit of the unperturbed Green's function at zero temperature.

We can now consider what happens when the Fourier transform to reciprocal space is taken. In the lattice case, such a Fourier transform and its inverse are defined as

$$\begin{aligned} \mathscr{G}(\mathbf{k},\mathbf{k}';\mathrm{i}\omega_l) &= \sum_{ij}\mathscr{G}_{ij}(\mathrm{i}\omega_l)\mathrm{e}^{-\mathrm{i}(\mathbf{k}\cdot\mathbf{x}_i-\mathbf{k}'\cdot\mathbf{x}_j)}, & (3.85)\\ \mathscr{G}_{ij}(\mathrm{i}\omega_l) &= \left(\frac{a}{2\pi}\right)^{2d}\int_{\mathrm{BZ}}d^dk\int_{\mathrm{BZ}}d^dk'\mathscr{G}(\mathbf{k},\mathbf{k}';\mathrm{i}\omega_l)\mathrm{e}^{\mathrm{i}(\mathbf{k}\cdot\mathbf{x}_i-\mathbf{k}'\cdot\mathbf{x}_j)}, & (3.86) \end{aligned}$$

where the integrals in reciprocal space run over the first Brillouin zone. Inserting (3.83) in (3.85) we obtain

$$\mathscr{G}(\mathbf{k},\mathbf{k}';\mathrm{i}\omega_l)=\sum_i g_i(\mathrm{i}\omega_l)\mathrm{e}^{-\mathrm{i}(\mathbf{k}-\mathbf{k}')\cdot\mathbf{x}_i}. \tag{3.87}$$

One can immediately see that for a homogeneous system, i.e. $\mu_i=\mu$, only the exponential contributes to the sum over all sites, which yields

$$\sum_i \mathrm{e}^{-\mathrm{i}(\mathbf{k}-\mathbf{k}')\cdot\mathbf{x}_i}=\left(\frac{2\pi}{a}\right)^d\delta(\mathbf{k}-\mathbf{k}'). \tag{3.88}$$

This would amount to a system which is invariant under translations. However, the sum becomes non-trivial when disorder is present. To see this, we first consider the first term on the right-hand side of (3.84). Note that by using the explicit form of the local chemical potential $\mu_i=\mu-\epsilon_i$ it can be expressed as a series expansion of the form

$$\frac{1}{\mathrm{i}\omega_l+\mu-\epsilon_i-Un_0}=\sum_{m=0}^{\infty}\frac{\epsilon_i^m}{(\mathrm{i}\omega_l+\mu-Un_0)^{m+1}}. \tag{3.89}$$

Its Fourier transform then becomes

$$\sum_i \mathrm{e}^{-\mathrm{i}(\mathbf{k}-\mathbf{k}')\cdot\mathbf{x}_i}\frac{1}{\mathrm{i}\omega_l+\mu-\epsilon_i-Un_0}=\sum_{m=0}^{\infty}\frac{1}{(\mathrm{i}\omega_l+\mu-Un_0)^{m+1}}\sum_i\epsilon_i^m\mathrm{e}^{-\mathrm{i}(\mathbf{k}-\mathbf{k}')\cdot\mathbf{x}_i}. \tag{3.90}$$

One can clearly see that the first term in the sum, $m=0$, recovers the clean case where the singularity corresponds to a simple pole. For $m=1$ however, we obtain the Fourier transform of the local potential shown in equation (3.65). For any finite m we observe the following situation. The terms which maintain the conservation of translational invariance, namely for $\mathbf{k}=\mathbf{k}'$, lead to the sum

$$\sum_i\epsilon_i^m. \tag{3.91}$$

Since we must take the average over all configurations of the disorder potential, the above summation represents a positive coupling between the moments of order m of the random distribution. Thus, in this case the summation in m of equation (3.90) corresponds to a sum over all moments of the distribution at each site. Note that each moment of order m

contributes to the sum with a pole of order $m+1$. In the opposite case, that is considering the terms in with $\mathbf{k} \neq \mathbf{k}'$, the coupling between the terms of the sum over all sites in (3.90) can be negative or even complex. Consider, for instance, the one-dimensional case. The space variable simplifies to $x_j = aj$ where $j \in \mathbb{Z}$. For the case of $k - k' = \pi/2a$, the exponential clearly becomes $\mathrm{e}^{-\mathrm{i}\pi j/2} = (-\mathrm{i})^j$, which yields either plus or minus the imaginary unit i. In such a case, the sum

$$\sum_j \epsilon_j^m \mathrm{e}^{-\mathrm{i}(k-k')aj}, \tag{3.92}$$

leads to a complex coupling between the moments of the random shifts ϵ_j at each site. Note that we have used j to represent the site index to avoid confusion with the imaginary unit i. The case where $k - k' = \pi/2a$ will play an important role when we analyze the energy spectrum in Chapter 5.

Taking the disorder-ensemble average, we get

$$\begin{aligned} \sum_i \overline{\epsilon_i^m} \mathrm{e}^{-\mathrm{i}(\mathbf{k}-\mathbf{k}')\cdot\mathbf{x}_i} &= \overline{\epsilon_i^m} \sum_i \mathrm{e}^{-\mathrm{i}(\mathbf{k}-\mathbf{k}')\cdot\mathbf{x}_i} \\ &= \left(\frac{2\pi}{a}\right)^d \overline{\epsilon_i^m} \delta(\mathbf{k}-\mathbf{k}'). \end{aligned} \tag{3.93}$$

Hence, the terms where $\mathbf{k} \neq \mathbf{k}'$ average over to zero and translational invariance is restored as it was discussed in Section 3.5. Equation (3.90) reduces to

$$\sum_{m=0}^{\infty} \frac{1}{(\mathrm{i}\omega_l + \mu - Un_0)^{m+1}} \sum_i \overline{\epsilon_i^m} \mathrm{e}^{-\mathrm{i}(\mathbf{k}-\mathbf{k}')\cdot\mathbf{x}_i} = \left(\frac{2\pi}{a}\right)^d \delta(\mathbf{k}-\mathbf{k}') \overline{[\mathrm{i}\omega_l + \mu - \epsilon_i - Un_0]^{-1}}. \tag{3.94}$$

If we take the analytic continuation to the real frequency domain consistent with a retarded response, i.e. $\mathrm{i}\omega_l \to \omega + \mathrm{i}0^+$, the unperturbed retarded Green's function in the disordered case then reads

$$\overline{g_i(\omega)} = \mathrm{Re}\,\overline{g_i(\omega)} + \mathrm{i}\,\mathrm{Im}\,\overline{g_i(\omega)}, \tag{3.95}$$

with

$$\begin{aligned} \mathrm{Re}\,\overline{g_i(\omega)} &= \mathrm{p.v.}\int_{-\infty}^{\infty} d\epsilon_i \mathscr{P}(\epsilon_i) \left(\frac{n_0+1}{\omega + \mu - \epsilon_i - Un_0} - \frac{n_0}{\omega + \mu - \epsilon_i - U(n_0 - 1)} \right), &(3.96) \\ \mathrm{Im}\,\overline{g_i(\omega)} &= \pi \Big(n_0 \mathscr{P}[\omega + \mu - U(n_0 - 1)] - (n_0 + 1) \mathscr{P}[\omega + \mu - Un_0] \Big), &(3.97) \end{aligned}$$

where $\mathrm{p.v.}$ denotes the principal value of the integration in (3.96) and we have chosen to show the explicit form of the local chemical potential $\mu_i = \mu - \epsilon_i$. The full retarded Green's function in reciprocal space reads

$$\overline{G^R(\mathbf{k},\mathbf{k}';\omega)} = \left(\frac{2\pi}{a}\right)^d \delta(\mathbf{k}-\mathbf{k}') \Big\{ \mathrm{Re}\,\overline{g_i(\omega)} + \mathrm{i}\,\mathrm{Im}\,\overline{g_i(\omega)} \Big\} \tag{3.98}$$

We point out that the behavior of the imaginary part of $\overline{g_i(\omega)}$ in (3.97) is determined

Figure 3.2 – Cyclic color function plot over $\arg \overline{g_i(\omega)}$ for a continuous disorder distribution. The upper row represents the case where $n_0 = 0$, that is only the quasiparticle branch is present, while the lower row corresponds to the case $n_0 = 1$ where the quasihole branch appears as well. In the limit of zero disorder (left) the singularities correspond to simple poles. When disorder is finite (middle and right) the simple poles transform into branch cuts.

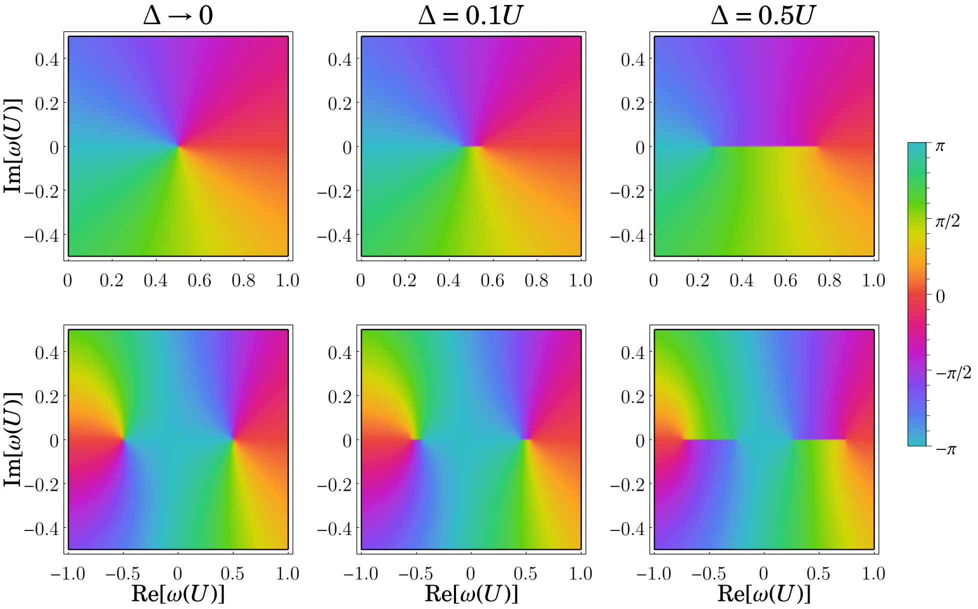

Source: Prepared by the author.

by the disorder distribution $\mathscr{P}(\epsilon_i)$. One can recover the clean case by choosing

$$\mathscr{P}(\epsilon_i) = \delta(\epsilon_i). \tag{3.99}$$

As we have already discussed, the simple poles of the Green's function in the clean case are mapped into Dirac delta distribution peaks of the imaginary part. One can deduce that any discrete probability distribution of the random potential would lead to additional delta distribution like peaks in $\mathrm{Im}\,\overline{g_i(\omega)}$. To see this, take, for instance, the case where disorder is realized by impurity atoms trapped at random sites which can be described by assuming a binary disorder distribution [120]

$$\mathscr{P}(\epsilon_i) = \frac{L - L'}{L}\delta(\epsilon_i) + \frac{L'}{L}\delta(\epsilon_i - U'), \tag{3.100}$$

where L is the number of lattice sites and L' represents the number of impurities. In this case, the energy of each site where an impurity atom is located gets shifted by the impurity interaction U'. Due to the presence of such impurities, additional delta distribution like peaks would emerge in $\mathrm{Im}\,\overline{g_i(\omega)}$. These peaks are therefore related to simple poles of the Green's function. One can imagine that including different energy shifts in a discrete probability distribution for the disorder would increase the number of peaks in the imaginary part of the unperturbed Green's function. However, in the limit of many energy shifts, which are close in energy, the distribution becomes continuous and the simple pole singularities become a branch cut. The emergency of such a branch cut can be observed in Fig. 3.2, where we consider a disorder distribution

$$\mathscr{P}(\epsilon_i) = \frac{1}{\Delta}\left[\Theta\left(\epsilon_i + \frac{\Delta}{2}\right) - \Theta\left(\epsilon_i - \frac{\Delta}{2}\right)\right], \tag{3.101}$$

which is uniformly distributed on the bounded interval $[-\Delta/2, \Delta/2]$.

The transformation of the singularities from simple poles into a branch cut has an influence on the lifetime of these elementary excitations. In order to exemplify this, we consider the spectral function, which is obtained applying the definition (3.37) to equation (3.98)

$$\overline{A(\mathbf{k},\omega)} = (n_0+1)\mathscr{P}[\omega+\mu-Un_0] - n_0\mathscr{P}[\omega+\mu-U(n_0-1)]. \tag{3.102}$$

For simplicity we take the case of $n_0 = 0$

$$\overline{A(\mathbf{k},\omega)} = \mathscr{P}(\omega+\mu). \tag{3.103}$$

In the clean case, where the distribution takes the form (3.99), the time dependence of the retarded Green's function can be recovered by applying (3.42) which yields

$$G^R(\mathbf{k},\mathbf{k}';t) = -\mathrm{i}\Theta(t)\left(\frac{2\pi}{a}\right)^d \delta(\mathbf{k}-\mathbf{k}')\mathrm{e}^{\mathrm{i}\mu t}. \tag{3.104}$$

For $t > 0$ this is clearly an oscillating function where the amplitude of the oscillations is constant. Hence, one can see that a discrete disorder distribution such as (3.100) would only lead to more oscillating terms in the time dependence of the retarded Green's function. In the case of continuously distributed disorder, the distribution $\mathscr{P}(\epsilon_i)$ differs from a Dirac delta distribution and it can acquires a finite width. Suppose, for instance, that such a distribution has a Cauchy-Lorentz form

$$\mathscr{P}(\epsilon_i) = \frac{1}{\pi}\frac{\Delta/2}{\epsilon_i^2 + (\Delta/2)^2}, \tag{3.105}$$

where the full width of half maximum is given by the disorder energy scale Δ. In such a case, the averaged retarded Green's function becomes

$$\overline{G^R(\mathbf{k},\mathbf{k}';t)} = -\mathrm{i}\Theta(t)\left(\frac{2\pi}{a}\right)^d \delta(\mathbf{k}-\mathbf{k}')\mathrm{e}^{\mathrm{i}\mu t-\Delta t/2}. \tag{3.106}$$

For positive t, the above equation has a a decaying exponential $\mathrm{e}^{-\Delta t/2}$. Thus, the finite width of the spectral function in the disordered case leads to a decaying amplitude of $\overline{G^R(\mathbf{k},\mathbf{k}';t)}$ in time. One can conclude that the excitations are damped due to disorder with a lifetime, in this case, given by $2/\Delta$. Another type of distribution, which is of particular interest to

Figure 3.3 – Time dependence of the absolute square of $\overline{G^R(\mathbf{k},\mathbf{k}';t)}$. For the clean case, $\Delta \to 0$, the amplitude is constant, while it decays rapidly for finite disorder strength $\Delta = 0.1\mu$.

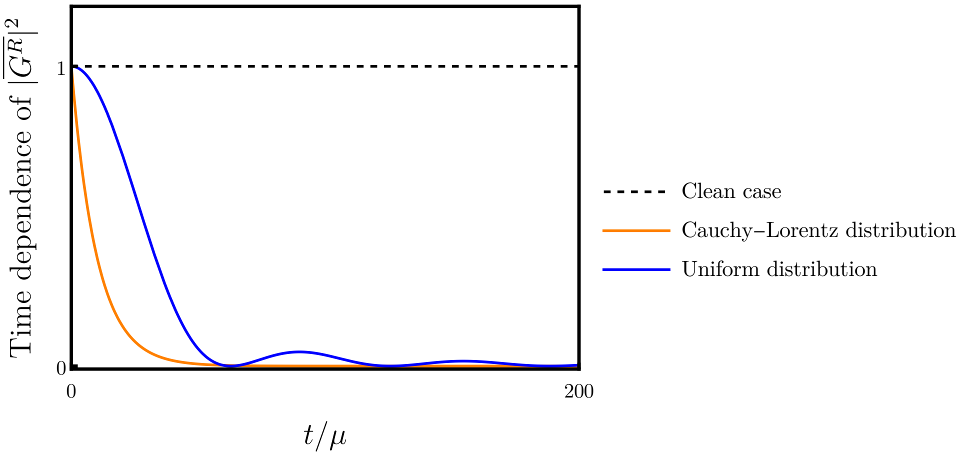

Source: Prepared by the author.

this work, is the uniform disorder distribution (3.101). For such a distribution, the retarded Green's function reads

$$\overline{G^R(\mathbf{k},\mathbf{k}';t)} = -\mathrm{i}\Theta(t)\left(\frac{2\pi}{a}\right)^d \delta(\mathbf{k}-\mathbf{k}')\mathrm{e}^{\mathrm{i}\mu t}\frac{\sin(\Delta t/2)}{\Delta t/2}, \tag{3.107}$$

which decays in time with the rate $2/\Delta$. For each of these cases, we plot the time dependence of $\overline{G^R(\mathbf{k},\mathbf{k}';t)}$ in Figure 3.3.

All things considered, we have shown that in the limit of strong interactions of the Bose-Hubbard model, the stable excitations, which lead to local fluctuations in the average density of particles in the clean case, become damped in the disordered case. This can be understood by remembering that, in the clean case, the excitations are true eigenstates of the Hamiltonian. In the disordered case, however, these excitations resemble a true eigenstate for a finite lifetime after which they decay. One can therefore conclude that disorder dresses up the elementary excitations by producing a damping effect. All this information can be extracted from the Green's functions and from the analysis of the peaks of the spectral function. In Chapter 5, we demonstrate how such effects could be understood in the presence of finite tunneling energy J. In the next section, we explain some measurements which could provide information on the spectral and the Green's functions.

3.8 Measurements in disordered systems

Even though this chapter was reserved to introduce the relevant aspects of Green's functions that serve the purposes of the present work, we recognize that it would be interesting to present here how such a quantity could be experimentally probed. Thus, in

Figure 3.4 – Sketch of a two beam Bragg spectroscopy. A laser beam with wavevector $\mathbf{k}_A$ and frequency ω_A intersects at an angle 2θ with a second laser beam with wavevector $\mathbf{k}_B$ and frequency ω_B (red arrows) creating a lattice grid which is superimposed in the atomic cloud (blue).

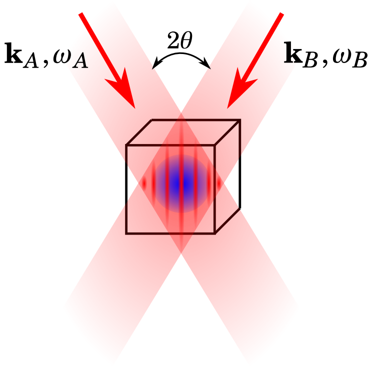

Source: Prepared by the author inspired by Ref. [129].

the following we give a brief introduction to the techniques of Bragg spectroscopy and the radio-frequency transfer method.

3.8.1 Bragg spectroscopy

We have already stated that systems of ultracold atoms serve as a playground to study Hamiltonians such as the Bose-Hubbard model. One of the main experimental techniques used to probe spectral properties of these systems is the so-called Bragg spectroscopy. Such a technique was first demonstrated in Ref. [121], and has since generated many other studies, some of which are Refs. [122, 123, 124, 125, 126, 127, 128, 129].

The experiment is based on exposing the atomic cloud to two collimated laser beams, one with wavevector $\mathbf{k}_A$ and frequency ω_A and the other with wavevector $\mathbf{k}_B$ and frequency ω_B. Such lasers are usually called Bragg beams. The beams intersect at an angle 2θ creating a standing wave. By controlling the angle between the laser beams one can change the periodicity of such standing wave. In the absence of spontaneous emission, the momentum transfer from the radiation field to the atomic cloud stems from the coupling between the induced atomic dipole moment and the gradient of the standing light wave, as we have discussed in Section 1.1. An atom which trades a photon by means of absorption and stimulated emission with the two Bragg beams, gains momentum given by the difference $\mathbf{k}_A-\mathbf{k}_B$ [121]. As a result an induced excitation with frequency given by $\omega_A-\omega_B$ is created. One can adjust such excitation frequency by controlling the detuning between the laser beams. The magnitude of momentum transferred to the atoms is characterized by both the angle θ and the wavelength λ of the laser beams [128]

$$|\mathbf{k}_A-\mathbf{k}_B| = \frac{4\pi}{\lambda}\sin\theta. \tag{3.108}$$

One can then determine the excitation spectrum, for instance, by measuring the resulting heating rate [124, 129] or the absorption spectrum [127]. In both cases the experiments give access to the so-called dynamic structure factor.

The dynamic structure factor measures fluctuations in the density-density correlations of the many-body system. Such a quantity can be related to the response of the system by the fluctuation-dissipation theorem [130, 131] and characterizes the spectra of collective excitations. In contrast to the elementary excitations, collective excitations do not emerge from individual particles dressed by the interactions with its neighbors, but rather involve the wavelike motion of the whole system [7]. These excitations are outside the scope of the analysis carried out in this work, as they involve the so-called two-particle propagator.

Even though the usual quantity measured in Bragg spectroscopy is not the single-particle Green's function, it was shown in Ref. [127] that the excitation scheme of such a technique for inter-band transitions contains important information on the single-particle elementary excitations in the Mott-insulator phase. In particular, it was demonstrated in that study that one can investigate the coherence of quasiparticles and quasiholes from the asymmetry of the spectra in the absorption rate. Furthermore, the study proposed that by counting the population of the excited states with a band mapping technique, such as the one applied in [132], it is possible to measure the single-particle spectral function and thus obtain the spectrum of the elementary excitations.

3.8.2 Radio-frequency transfer

Electromagnetic fields in the range of radio frequencies are widely used in experiments of cold atoms. Some examples are evaporative cooling, where a radio-frequency (rf) field is applied to the atomic cloud in order to couple the most energetic particles to states outside the trap such that they get expelled leaving the sample colder [133], and rf-spectroscopy which can be used to characterize and control magnetic traps and adiabatic potentials [134]. Here, we focus of the experiments reported in [135], where the spectral function of ultracold atoms in a disordered potential was measured with the rf-transfer method.

The experiment was realized with a Bose-Einstein condensate of Rubidium-87 atoms carefully prepared in the initial state $|F=1, m_F=-1\rangle \equiv |1\rangle$ in the presence of a random potential generated by laser speckles. A clever idea was then to use the hyperfine structure of those atoms by tuning the disordered potential in such a way to affect only the state $|F=2, m_F=1\rangle \equiv |2\rangle$. The transition $|1\rangle \to |2\rangle$ was then induced by applying an external rf-field. In such configuration the energy levels of the disorder potential form an effective continuum and for weak rf coupling the transition rate is given by Fermi's golden rule. Such a transition rate is proportional to the overlap between the initial and the final states multiplied by the density of states [136, 56]. As we have already shown, the density of states can

Figure 3.5 – Experimental procedure and measurement of the spectral function. (a) A near-resonant speckle laser with detuning Δ_L is applied to create either an attractive (red detuned, $\Delta_L < 0$) or repulsive (blue detuned, $\Delta_L > 0$) random external field which is sensible only to atoms in state $|2\rangle$. In (b) and (c) a radio-frequency (rf) field is applied in the condensed atoms to induce the transition $|1\rangle \to |2\rangle$ where $\mathcal{E}_\delta$ is the energy of the final state which depends on the detuning of the rf-field from the bare transition. The spectral function is then proportional to the transfer rate measured via fluorescence imaging. The resulting measurement of $\overline{A(\mathbf{k}=\mathbf{0},\hbar\delta)}$ for a repulsive disordered potential is shown in (d) and (e) for different disorder strengths Δ. The blue dots correspond to experimental points while the red line represents numerical results of a time-propagation algorithm.

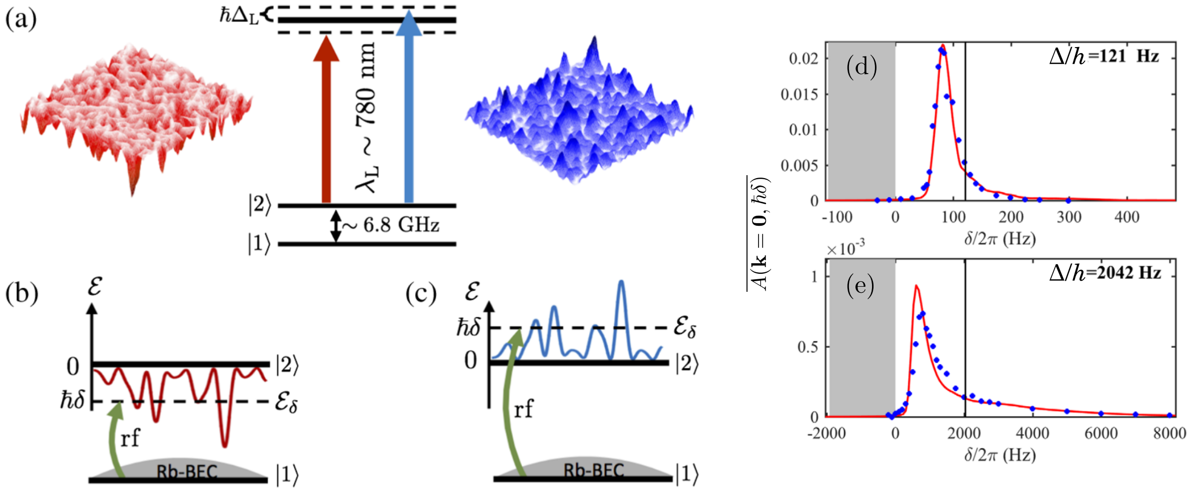
(a)
$\hbar\Delta_L$
$\lambda_L \sim 780$ nm
$|2\rangle$
$|1\rangle$
~ 6.8 GHz
(b)
$\mathcal{E}$
0
$\hbar\delta$
$|2\rangle$
$\mathcal{E}_\delta$
rf
Rb-BEC
$|1\rangle$
(c)
$\mathcal{E}$
$\hbar\delta$
0
$\mathcal{E}_\delta$
$|2\rangle$
rf
Rb-BEC
$|1\rangle$
$\overline{A(\mathbf{k}=\mathbf{0},\hbar\delta)}$
(d)
Δ/h=121 Hz
0.02
0.015
0.01
0.005
0
-100
0
100
200
300
400
$\delta/2\pi$ (Hz)
$\times 10^{-3}$
(e)
Δ/h=2042 Hz
1
0.5
0
-2000
0
2000
4000
6000
8000
$\delta/2\pi$ (Hz)

Source: Figure from Ref. [135].

be written as a momentum integral over the spectral function via (3.71). In the presence of disorder, one has to consider the average of the transition rate over many realizations of the random potential. In the limit that the average of the overlap function and the average of the density of states can be taken separately, the transition rate becomes proportional to the average spectral function. Therefore, by counting the number excited atoms in a given period of time via fluorescence imaging for many realizations of the random potential, one can obtain a direct measurement of the spectral function in disordered systems as was realized in [135]. Such an experimental process is shown in Fig. 3.5 along with some of the measurements. One can clearly see in Fig. 3.5(d) and (e) that the spectral function has a peak which indicates the excitation energies of the disordered potential. This peak has a finite width, which, as we have already discussed, provides a measure of the lifetime of these excitations.

The experiment referenced above seems to be prominent in determining the spectral properties of cold atoms in disordered external potentials. Although the measure was realized only for $\mathbf{k} = \mathbf{0}$, the authors argue that by applying different kinds of transfer methods it is possible to have access to finite values of $\mathbf{k}$. In addition to the information on the lifetime of the excitations, by measuring the spectral function for different values of the wavevector one would obtain the dispersion relation and the band structure of such excitations. Such an information could be used to extract, for instance, the effective mass of these quasiparticles. We remark however, that the experiments mentioned above were carried out without the presence of a lattice in the limit of weak interaction between the atoms.

In conclusion, we have introduced here some basic properties of Green's function and how they can be used to investigate the spectra of elementary excitaions as well as some possibilities for experimental measurements in disordered systems. In what follows we focus on the perturbation theory to construct a broader understanding of the Bose-Hubbard model.

Chapter 4

Perturbation Theory

One of the aims of this work is to study the effects of disorder on the strongly interacting limit of the Bose-Hubbard Hamiltonian for finite values of the tunneling energy. If the disorder energy scale is not strong compared to the interactions, one can expect that there are still some regions of the phase diagram where fluctuations of the particle density at each lattice site are suppressed by the interactions and the ground state is a Mott insulator. In that region, it is then justified to treat the hopping energy as a perturbation which tries to delocalize the particles creating excitations. Such a class of approximations is commonly referred to as strong-coupling expansion, however it could also be understood as an extension of the so-called locator expansion [32, 137, 138] to an interacting system. Rather than using the operator formalism as we have done in Refs. [139, 140], here we choose to demonstrate this perturbation treatment in the functional integral formalism. We apply the same formalism in Chapters 7 and 8 to demonstrate some preliminary calculations which follow from the results presented in this thesis. Therefore, the choice for the functional integral formalism makes the full body of this work uniform. Furthermore, it is often the case that such a functional integral formulation offers an easier path to perturbation treatments than other traditional methods. The basic derivation of such a formalism in imaginary-time is carried out in Appendix A.

4.1 Hopping expansion

The action corresponding to the Bose-Hubbard Hamiltonian is given by

$$\begin{aligned} S[\psi^*,\psi] = &\int_0^\beta d\tau \sum_i \left[\psi_i^*(\tau)\left(\frac{\partial}{\partial\tau} - \mu\right)\psi_i(\tau) + \frac{U}{2}\psi_i^*(\tau)^2\psi_i(\tau)^2\right] \\ &- \int_0^\beta d\tau \sum_{ij} \psi_i^*(\tau) J_{ij} \psi_j(\tau) + \int_0^\beta d\tau \sum_i \psi_i^*(\tau)\epsilon_i\psi_i(\tau), \end{aligned} \tag{4.1}$$

where the fields ψ and ψ^* can be associated to the degrees of freedom of bosonic particles on a lattice. One interesting point is that the steepest decent condition, i.e. the Euler-Lagrange equations to this action correspond to the lattice version of the Gross-Pitaevskii equations

$$\begin{aligned}
\frac{\partial\psi_i(\tau)}{\partial\tau} &= -\sum_j J_{ij}\psi_j(\tau) - \mu\psi_i(\tau) + U|\psi_i(\tau)|^2\psi_i(\tau) + \epsilon_i\psi_i(\tau), &(4.2)\\
-\frac{\partial\psi_i^*(\tau)}{\partial\tau} &= -\sum_j J_{ij}\psi_j^*(\tau) - \mu\psi_i^*(\tau) + U|\psi_i(\tau)|^2\psi_i^*(\tau) + \epsilon_i\psi_i^*(\tau). &(4.3)
\end{aligned}$$

As we want to study the system near the phase transition, we introduce to the action a source term

$$(\mathrm{j}|\psi) + (\psi|\mathrm{j}) = \int_0^\beta d\tau \sum_i \left[\mathrm{j}_i^*(\tau)\psi_i(\tau) + \mathrm{j}_i(\tau)\psi_i^*(\tau)\right], \tag{4.4}$$

where we have introduced the abbreviation

$$(\mathrm{j}|\psi) = \int_0^\beta d\tau \sum_i \mathrm{j}_i^*(\tau)\psi_i(\tau). \tag{4.5}$$

This auxiliary source term can be interpreted as fluctuations that couple to the bosonic fields near the phase transition explicitly breaking the global U(1) symmetry of the Bose-Hubbard Hamiltonian. The introduction of such a term is made based on general quantum field theory considerations [111, 141, 114]. With this source term it is possible to define the unperturbed partition function as

$$\mathcal{Z}_0[\mathrm{j}^*,\mathrm{j}] = \frac{\oint \mathcal{D}\psi^* \oint \mathcal{D}\psi \, \mathrm{e}^{-S_0[\psi^*,\psi] + (\mathrm{j}|\psi) + (\psi|\mathrm{j})}}{\oint \mathcal{D}\psi^* \oint \mathcal{D}\psi \, \mathrm{e}^{-S_0[\psi^*,\psi]}}, \tag{4.6}$$

where the unperturbed action corresponds to (4.1) in the case of a vanishing tunneling term, i.e., $J = 0$. We define the partition function so that it satisfies $\mathcal{Z}_0[0,0] = 1$. The functional integral representation corresponds to the summation over all configurations of the bosonic matter fields with periodic boundary conditions in imaginary time, i.e. $\psi(0) = \psi(\beta)$. We note that (4.6) consists of the average

$$\mathcal{Z}_0[\mathrm{j}^*,\mathrm{j}] = \langle \mathrm{e}^{(\mathrm{j}|\psi) + (\psi|\mathrm{j})} \rangle_0, \tag{4.7}$$

where $\langle \cdots \rangle_0$ denotes the average over the equilibrium ensemble of the unperturbed system for a fixed local potential ϵ_i. The partition function can then be rewritten as

$$\mathcal{Z}_0[\mathrm{j}^*,\mathrm{j}] = \mathrm{e}^{W_0[\mathrm{j}^*,\mathrm{j}]}, \tag{4.8}$$

where the negative free-energy functional is defined as

$$W_0[\mathrm{j}^*,\mathrm{j}] = \log \langle \mathrm{e}^{(\mathrm{j}|\psi)+(\psi|\mathrm{j})} \rangle_0 . \tag{4.9}$$

Note that the source dependent partition function constitutes the generating functional of moments corresponding to the bosonic fields with respect to the unperturbed equilibrium ensemble. Hence, the negative free energy $W_0[\mathrm{j}^*,\mathrm{j}]$ defines the cumulant generating functional.

By considering the tunneling energy as a perturbation parameter, and expanding the exponential with respect to the hopping term, we realize that corrections to the partition function in the hopping expansion can be calculated according to

$$\mathscr{Z}[\mathrm{j}^*,\mathrm{j}] = \exp\left(\sum_{ij} J_{ij} \int_0^\beta d\tau \frac{\delta^2}{\delta \mathrm{j}_i^*(\tau)\delta \mathrm{j}_j(\tau)} \right) \mathscr{Z}_0[\mathrm{j}^*,\mathrm{j}]. \tag{4.10}$$

With this approach, one can study physical quantities by calculating correlation functions up to any order. Here, we restrict the calculation to the two-point Green's function which can be obtained via [141]

$$\mathscr{G}_{ij}(\tau,\tau') = - \left. \frac{\delta^2 \mathscr{Z}[\mathrm{j}^*,\mathrm{j}]}{\delta \mathrm{j}_i^*(\tau)\delta \mathrm{j}_j(\tau)} \right|_{\mathrm{j}^*,\mathrm{j}=0} . \tag{4.11}$$

All single-particle properties of the system can be extracted from the two-point function.

In order to properly calculate the hoping corrections to the Green's function, we must consider the cumulant expansion of the free energy

$$W_0[\mathrm{j}^*,\mathrm{j}] = \int_0^\beta d\tau \int_0^\beta d\tau' \sum_i \mathrm{j}_i^*(\tau) \langle \mathscr{T}_\tau \hat{a}_i(\tau) \hat{a}_i^\dagger(\tau') \rangle_0 \mathrm{j}_i(\tau') + \cdots , \tag{4.12}$$

where we recognize the average in between the sources on the right-hand side as the unperturbed Green's function (3.77) defined in Section 3.7. We choose not to show the subsequent terms in this expansion as they are not relevant to the analysis carried in this thesis. Such terms would be important, for instance, in the effective-action approach developed in [52, 53, 54, 55] where a diagrammatic notation simplifies the calculations. The result of the functional derivatives of (4.10) acting on the cumulant expansion of (4.12) is to generate different terms composed of products of unperturbed contributions joined by the hopping matrix. As a consequence of the linked-cluster theorem, one can describe all the terms by considering only the so-called connected contributions [142, 143, 72, 144, 145].

After applying (4.11) the perturbation series in the reads

$$\begin{aligned}\mathscr{G}_{ij}(\tau,\tau') &= \delta_{ij}g_i(\tau,\tau') + J_{ij}\int_0^\beta d\tau_1 g_i(\tau,\tau_1)g_j(\tau_1,\tau') \\ &+ \sum_l J_{il}J_{lj}\int_0^\beta d\tau_1\int_0^\beta d\tau_2 g_i(\tau,\tau_1)g_l(\tau_1,\tau_2)g_j(\tau_2,\tau') + \cdots .\end{aligned} \tag{4.13}$$

This amounts to a tree-level approximation to the Green's function. Each term in this series can be interpreted as the amplitude of propagation for an excitation which is created at imaginary time τ' at site j and hops along the lattice being annihilated after reaching site i at imaginary time τ. It turns out that such an approximation is already sufficient to study how disorder affects the energy spectrum in the strongly interacting regime as well as to obtain an analytical expression to the phase boundary between Mott and Bose glass states. In what follows we discuss how one can use the above described expansion to construct analytical solutions.

4.2 Partial summation

As it was mentioned in the last chapter, singular points of the Green's functions in the Kälén-Lehmann representation can be directly linked to the eigenstates of the underlying Hamiltonian giving the energy dispersion of the low-energy excitations of the system [119]. However, up to any finite order, the expansion of the Green's function in (4.13) is an analytic power series in terms of the tunneling energy J. Thus, one must sum an infinite amount of terms in such an expansion. This can be done by breaking down sequences of terms into infinite subsets and then combining them in a partial summation to find the final result [7, 115].

In order to proceed with such a summation, we consider only the first-order contribution in (4.13). After taking the disorder average it can be written as

$$\overline{\mathscr{G}_{ij}(\tau,\tau')} = \delta_{ij}\overline{g_i(\tau,\tau')} + J_{ij}\int_0^\beta d\tau_1 \overline{g_i(\tau,\tau_1)}\;\overline{g_j(\tau_1,\tau')} + \cdots . \tag{4.14}$$

Note that the average over the product of the unperturbed Green's function in the first-order correction factorizes as a consequence of the hopping matrix being off-diagonal, i.e. $J_{ii} = 0$. Expression (4.14) can be further simplified by transforming in the Matsubara frequency domain with the definition (3.55)

$$\overline{\mathscr{G}_{ij}(\mathrm{i}\omega_l)} = \delta_{ij}\overline{g_i(\mathrm{i}\omega_l)} + J_{ij}\overline{g_i(\mathrm{i}\omega_l)}\;\overline{g_j(\mathrm{i}\omega_l)} + \cdots , \tag{4.15}$$

where we have used the imaginary-time translational invariance property of the Green's function, namely $\overline{\mathscr{G}_{ij}(\tau,\tau')} = \overline{\mathscr{G}_{ij}(\tau-\tau',0)}$. The inverse of (4.15) can be written as

$$\left[\overline{\mathscr{G}_{ij}(\mathrm{i}\omega_l)}\right]^{-1} = \delta_{ij}\left[\overline{g_i(\mathrm{i}\omega_l)}\right]^{-1} - J_{ij} + \cdots . \tag{4.16}$$

With the disorder-ensemble average the unperturbed Green's function $\overline{g_i(\mathrm{i}\omega_l)}$ becomes homogeneous and space translational invariance broken by the random random potential is recovered [146, 147]. Afterwards, we perform the Fourier transform into momentum space defined as

$$\left[\overline{\mathscr{G}(\mathbf{k},\mathbf{k}';\mathrm{i}\omega_l)}\right]^{-1} = \sum_{ij}\left[\overline{\mathscr{G}_{ij}(\mathrm{i}\omega_l)}\right]^{-1} \mathrm{e}^{-\mathrm{i}(\mathbf{k}\cdot\mathbf{x}_i - \mathbf{k}'\cdot\mathbf{x}_j)}. \tag{4.17}$$

One can invert this expression exactly in the Fourier-Matsubara space to obtain

$$\overline{\mathscr{G}(\mathbf{k},\mathbf{k}';\mathrm{i}\omega_l)} = \left(\frac{2\pi}{a}\right)^d \frac{\delta(\mathbf{k}-\mathbf{k}')}{\left[\overline{g_i(\mathrm{i}\omega_l)}\right]^{-1} - J(\mathbf{k})}. \tag{4.18}$$

We point out that this result is equivalent to the partial summation of simple chain contributions to the Green's function obtained for the clean case in [99] and for the disordered case in [139, 140]. It has the same form as the Dyson equation, where the dispersion for a d-dimensional hypercubic lattice

$$J(\mathbf{k}) = 2J\sum_{p=1}^{d}\cos\left(ak_p\right) \tag{4.19}$$

plays the role of the self-energy. This result consists of considering that the scattering events against the disordered potential between each hopping process are statistically independent such that the average over products of the unperturbed amplitudes of propagation factorizes. In the actual disordered system, the reciprocal space representation of the Green's function must have off-diagonal elements, which couple states with different wavevectors. Such elements vanish after the disorder ensemble average is performed [118]. However, as we shall see latter, their physical effects still remain in the system influencing the transport properties. From (4.18) we define the Green's function obtained by the partial summation method as

$$\overline{\mathscr{G}(\mathbf{k},\mathrm{i}\omega_m)} = \frac{1}{\left[\overline{g_i(\mathrm{i}\omega_l)}\right]^{-1} - J(\mathbf{k})}. \tag{4.20}$$

In the next chapter, we show how one can obtain information on the energy spectrum for single-particle excitations from such a quantity.

4.3 Poincaré-Lindstedt method

The theory developed by Fisher et al. [22] regarding the Bose-glass phase posits that in this well-localized regime, the density of states of low-lying excitations reaches a finite value at zero excitation energy for vanishing tunneling energy. This occurs due to the continuous distribution of the random potential in the system. This case was further analyzed in Ref. [38]. The finite density of states for zero energy is a consequence of the gapless spectrum of the Bose-glass state and it should persist even when the hopping energy is made slightly positive. In order to gain a deeper understanding of this phenomenon, our perturbation theory takes into account the hopping corrections to the local Green's function. In the local case, the first-order contribution in the hopping expansion (4.13) vanishes and the Green's function can be written as

$$\mathscr{G}_i(\tau,\tau') = g_i(\tau,\tau') + \sum_j J_{ij}J_{ji}\int_0^\beta d\tau_1 \int_0^\beta d\tau_2 g_i(\tau,\tau_1) g_l(\tau_1,\tau_2) g_i(\tau_2,\tau') + \cdots . \tag{4.21}$$

Assuming imaginary-time translational invariance, in the Matsubara representation (3.55), the above expression becomes

$$\mathscr{G}_i(\mathrm{i}\omega_l) = g_i(\mathrm{i}\omega_l) + \sum_j J_{ij}J_{ji} g_i(\mathrm{i}\omega_l)^2 g_j(\mathrm{i}\omega_l) + \cdots . \tag{4.22}$$

The second term on the right-hand side of the above expression involves double poles which come from the square of the unperturbed Green's function. Such a term could be interpreted as the cyclic path of an excitation which starts at site i, hops to one of its first neighbors and then hops back to the original site. One can represent such double poles as derivatives of simple poles. This simplifies the analytic continuation $\mathrm{i}\omega_m \to \omega + \mathrm{i}0^+$ from the Matsubara frequencies to the real frequency domain. The imaginary part of the local Green's function $\rho_i(\omega) = -\mathrm{Im}\mathscr{G}_i(\omega + \mathrm{i}0^+)/\pi$ [6, 73, 72] corresponds to the local density of state which reads

$$\begin{aligned}
\rho_i(\omega) = {} & \sum_{n=0}^{\infty} \frac{\mathrm{e}^{-\beta E_n(\mu_i)}}{Z_0(\mu_i)} \Big\{(n+1)\delta[\omega + \mu_i - Un] - n\delta[\omega + \mu_i - U(n-1)]\Big\} \\
& - \sum_j J_{ij}J_{ji} \sum_{n=0}^{\infty} \left((n+1)\frac{\mathrm{e}^{-\beta E_n(\mu_i)}}{Z_0(\mu_i)}\right)^2 \frac{\partial}{\partial \mu_i}\Big\{\delta[\omega + \mu_i - Un] g_j(Un - \mu_i)\Big\} \\
& - \sum_j J_{ij}J_{ji} \sum_{n=0}^{\infty} \left(n\frac{\mathrm{e}^{-\beta E_n(\mu_i)}}{Z_0(\mu_i)}\right)^2 \frac{\partial}{\partial \mu_i}\Big\{\delta[\omega + \mu_i - U(n-1)] g_j(U(n-1) - \mu_i)\Big\} \\
& + \cdots ,
\end{aligned} \tag{4.23}$$

where we have defined the local chemical potential $\mu_i = \mu - \epsilon_i$. Here we show only the terms which will be important to our analyses. By taking the disorder average we obtain

$$\begin{aligned}
\overline{\rho_i(\omega)} &= \sum_{n=0}^{\infty} (n+1) \frac{\mathrm{e}^{-\beta E_n(Un-\omega)}}{Z_0(Un-\omega)} \mathscr{P}[\omega+\mu-Un] \\
&- \sum_{n=0}^{\infty} n \frac{\mathrm{e}^{-\beta E_n(U(n-1)-\omega)}}{Z_0(U(n-1)-\omega)} \mathscr{P}[\omega+\mu-U(n-1)] \\
&+ zJ^2 \overline{g_j(\omega)} \sum_{n=0}^{\infty} \left((n+1) \frac{\mathrm{e}^{-\beta E_n(Un-\omega)}}{Z_0(Un-\omega)} \right)^2 \mathscr{P}'[\omega+\mu-Un] \\
&+ zJ^2 \overline{g_j(\omega)} \sum_{n=0}^{\infty} \left(n \frac{\mathrm{e}^{-\beta E_n(U(n-1)-\omega)}}{Z_0(U(n-1)-\omega)} \right)^2 \mathscr{P}'[\omega+\mu-U(n-1)] \\
&+ \cdots .
\end{aligned} \tag{4.24}$$

Note that, after the disorder average the sum of the hopping matrix over nearest neighbors can be directly evaluated to

$$\sum_j J_{ij} J_{ji} = zJ^2, \tag{4.25}$$

where z is the lattice coordination number. The hopping corrections to the local density of states (4.23) are multiplied by derivatives of the disorder distribution. The derivatives originate from the double poles of the local Matsubara Green's function (4.21) and appear as a result of using the property

$$\int_{-\infty}^{\infty} dx \delta'(x) f(x) = -f'(0) \tag{4.26}$$

of derivatives of the Dirac delta function when taking the disordered average of (4.22). As it was mentioned in the last chapter, in Matsubara space the discrete singularities of the Green's function should only correspond to simple poles [73, 72]. These anomalies, which come from the double poles implicit in (4.21), can be understood in first approximation as a consequence of including correlations between scattering events against the disordered potential at the same lattice site for the cyclic path of an excitation created in system.

In order to deal with the above described problem, one has to renormalize the local density of states. One alternative to do this is to use the Poincaré-Lindstedt method. In a simple picture, this method was first applied in celestial mechanics to renormalize the frequency associated to the orbit of objects in outer space with the aim of eliminating secular non-periodic terms [148, 149]. More recently, this method has been applied to treat nonlinear problems such as the Duffing oscillator [150] or even the dynamics of Bose-Einstein condensates [151, 152]. In the usual Poincaré-Lindstedt method, periodic terms transform into simple poles in frequency space. In contrast, secular terms appear as poles of higher order. We can therefore interpret the Dirac delta functions in (4.22) as the imaginary part of a simple pole and its derivatives as coming from the imaginary part of higher order poles.

In analogy to the Poincaré-Lindstedt method, we propose the use of the following transformations

$$\begin{aligned} \gamma_n^- = \omega + \mu - U(n-1) \quad &\rightarrow \quad \Omega_n^- + \lambda(\gamma_n^- - \Omega_n^-), \\ \gamma_n^+ = \omega + \mu - Un \quad &\rightarrow \quad \Omega_n^+ + \lambda(\gamma_n^+ - \Omega_n^+), \\ J^2 \quad &\rightarrow \quad \lambda J^2. \end{aligned} \tag{4.27}$$

Note that by setting $\lambda = 1$ one recovers the initial situation. Expanding (4.23) up to the first order in λ we obtain

$$\begin{aligned} \overline{\rho_i(\omega)} = & \sum_{n=0}^{\infty} (n+1) \frac{\mathrm{e}^{-\beta E_n(Un-\omega)}}{Z_0(Un-\omega)} \mathscr{P}(\Omega_n^+) \\ & - \sum_{n=0}^{\infty} n \frac{\mathrm{e}^{-\beta E_n(U(n-1)-\omega)}}{Z_0(U(n-1)-\omega)} \mathscr{P}(\Omega_n^-) \\ & + \lambda \sum_{n=0}^{\infty} (n+1) \frac{\mathrm{e}^{-\beta E_n(Un-\omega)}}{Z_0(Un-\omega)} (\gamma_n^+ - \Omega_n^+) \mathscr{P}'(\Omega_n^+) \\ & - \lambda \sum_{n=0}^{\infty} n \frac{\mathrm{e}^{-\beta E_n(U(n-1)-\omega)}}{Z_0(U(n-1)-\omega)} (\gamma_n^- - \Omega_n^-) \mathscr{P}'(\Omega_n^-) \\ & + \lambda z J^2 \overline{g_j(\omega)} \sum_{n=0}^{\infty} \left((n+1) \frac{\mathrm{e}^{-\beta E_n(Un-\omega)}}{Z_0(Un-\omega)} \right)^2 \mathscr{P}'(\Omega_n^+) \\ & + \lambda z J^2 \overline{g_j(\omega)} \sum_{n=0}^{\infty} \left(n \frac{\mathrm{e}^{-\beta E_n(U(n-1)-\omega)}}{Z_0(U(n-1)-\omega)} \right)^2 \mathscr{P}'(\Omega_n^-) \\ & + \cdots \end{aligned} \tag{4.28}$$

The renormalization consists of determining the values of $\Omega_n^\pm$ that cancel the derivatives of the disorder distributions on the above expression. In this case, such values are given by

$$\Omega_n^-(J) = \omega + \mu - U(n-1) + zJ^2 n \frac{\mathrm{e}^{-\beta E_n(U(n-1)-\omega)}}{Z_0(U(n-1)-\omega)} \overline{g_j(\omega)}, \tag{4.29}$$

$$\Omega_n^+(J) = \omega + \mu - Un - zJ^2 (n+1) \frac{\mathrm{e}^{-\beta E_n(Un-\omega)}}{Z_0(Un-\omega)} \overline{g_j(\omega)}. \tag{4.30}$$

With this choice, the disorder average of the local density of states becomes

$$\overline{\rho_i(\omega)} = \sum_{n=0}^{\infty} (n+1) \frac{\mathrm{e}^{-\beta E_n(Un-\omega)}}{Z_0(Un-\omega)} \mathscr{P}[\Omega_n^+(J)] - \sum_{n=0}^{\infty} n \frac{\mathrm{e}^{-\beta E_n(U(n-1)-\omega)}}{Z_0(U(n-1)-\omega)} \mathscr{P}[\Omega_n^-(J)] + \cdots. \tag{4.31}$$

We can therefore interpret the renormalization of the arguments of the disorder distribution in the local density of states as the Poincaré-Lindstedt method in frequency space.

The renormalized expression of the local density of states (4.31) constitutes a resummation of the original expression (4.24), which makes them equivalent up to second order in J. This result generalizes the expression of the density of states computed in Ref. [38] with corrections due to finite tunneling energy. We are now in the position to discuss the implications of such results and how they can be used to explain the effects of disorder in the strongly interacting regime of the Bose-Hubbard model.

Part III

Results

Chapter 5

Excitations of the disordered Bose-Hubbard model

At commensurate fillings, for a sufficiently deep lattice potential depth, the ground state of a cloud of cold bosonic atoms is a Mott insulator. In a perfect lattice, the low-lying excited states above this ground state correspond to gapped quasiparticle and quasihole excitations with a well-defined wavevector $\mathbf{k}$, which are still eigenstates of the Bose-Hubbard Hamiltonian and propagate without decay through the system's volume. The properties of these stable excitations are mapped into Dirac delta distributions of the spectral function, which occur at finite energies. The main characteristics of such low-energy excitations have been the subject of extensive investigation [153, 154, 155, 156, 157, 158, 159]. However, the problem of how disorder affects the energy spectrum in the strong-interacting limit remains unclear so far. Here, we present an extended version of the results partially available in Ref. [140] in the zero-temperature limit. There, we have shown that sharp peaks associated with stable excitations still appear in the spectral function when disorder is present. In contrast to the clean case, however, the gap for creating these excitations becomes smaller due to disorder, and thus the peak for stable states in the spectral function is shifted towards lower energies. In addition, a broad peak of width $\Gamma(\mathbf{k})$ associated with damped states emerges in the spectral function for slightly higher energies. A schematic drawing showing the qualitative aspects of these findings is depicted in Fig. 5.1. The analysis presented in this chapter is obtained from the Green's function derived in Section 4.2 using the partial summation method.

Figure 5.1 – Qualitative sketch of the spectral function $\overline{A(\mathbf{k},\omega)}$ for fixed $a|\mathbf{k}| \ll 1$ in the quasiparticle branch of the spectrum. The sharp dashed-black peak at $\omega_0^+(\mathbf{k})$ corresponds to stable excitations of the clean case. Disorder shifts this peak to $\omega^+(\mathbf{k})$ (red) towards lower energies while it also creates damped states with dispersion $\omega_r(\mathbf{k})$, which appear as a broad peak (blue) of finite width $\Gamma(\mathbf{k})$. These qualitative aspects are analogous for the quasihole branch.

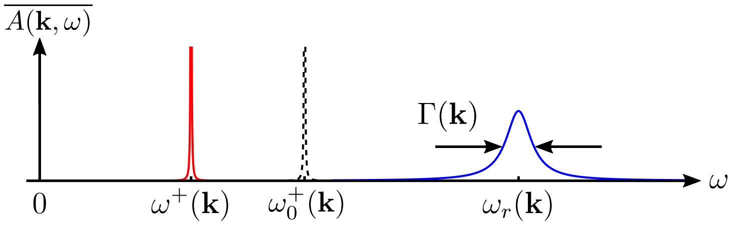

Source: Figure from Ref. [140].

5.1 Spectral function

It has already been pointed out that the spectral function generalizes the concept of a dispersion relation. In this section, we present how such a quantity can be used to investigate the effects of disorder in the strongly interacting limit of the Bose-Hubbard Hamiltonian.

5.1.1 Clean case

In order to give contrast to what changes in the presence of disorder, we begin by discussing the clean case. In this limit, the resummed expression for the Green's function obtained in (4.20) simplifies to

$$\mathscr{G}(\mathbf{k},\mathrm{i}\omega_l) = \frac{1}{[g(\mathrm{i}\omega_l)]^{-1} - J(\mathbf{k})}, \tag{5.1}$$

where $g(\mathrm{i}\omega_l)$ corresponds to the homogeneous version of (3.82), i.e., for $\mu_i = \mu$. Using the zero-temperature limit of (3.84) we can separate the quasiparticle (+) and quasihole (−) contributions and rewrite (5.1) as

$$\mathscr{G}(\mathbf{k},\mathrm{i}\omega_m) = \frac{\Pi_0^+(\mathbf{k})}{\mathrm{i}\omega_m - \omega_0^+(\mathbf{k})} + \frac{\Pi_0^-(\mathbf{k})}{\mathrm{i}\omega_m - \omega_0^-(\mathbf{k})}, \tag{5.2}$$

where we have defined the clean case dispersion relations

$$\omega_0^\pm(\mathbf{k}) = \frac{1}{2}\Big(U(2n-1) - 2\mu - J(\mathbf{k}) \pm \sqrt{J(\mathbf{k})^2 - 2J(\mathbf{k})U(2n+1) + U^2}\Big), \tag{5.3}$$

as well as the weights which characterize the amount of energy stored in each excitation

$$\Pi_0^\pm(\mathbf{k}) = \frac{1}{2}\left(1 \pm \frac{U(2n+1) - J(\mathbf{k})}{\sqrt{J(\mathbf{k})^2 - 2J(\mathbf{k})U(2n+1) + U^2}}\right). \tag{5.4}$$

Figure 5.2 – Clean case spectral function (5.5) at $\mathbf{k} = \mathbf{0}$ in the first Mott lobe $n_0 = 1$ for $d = 3$. We have given a finite width to the δ-peaks in order to represent them graphically. The right plot, where the tunneling energy is fixed at $J = 0.0002U$, shows that the quasihole and quasiparticle peaks, which occur at negative and positive frequencies, respectively, appear well separated. When the hopping energy is increased to $J = 0.026U$ in the left plot, the energy gap decreases and the excitation peaks appear close to each other. We have chosen the chemical potential to be $\mu = 0.5U$ on the right plot and $\mu = 0.41U$ on the left plot such that the peaks appear symmetric.

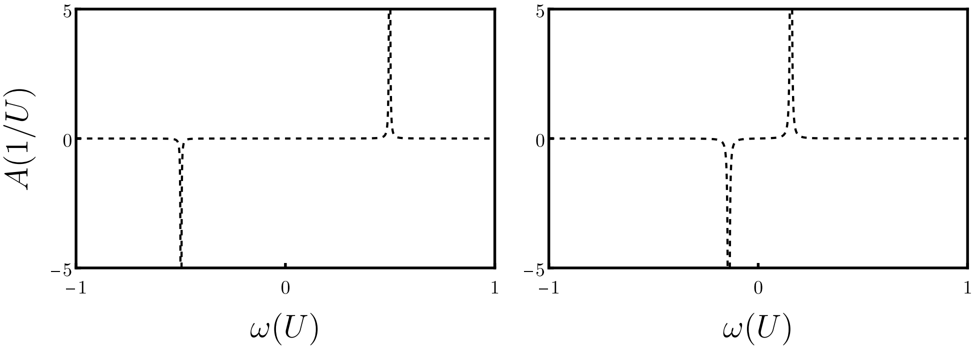

Source: Prepared by the author.

By considering the analytic continuation $\mathrm{i}\omega_m \to \omega + \mathrm{i}0^+$ and applying the definition (3.37) to equation (5.2), we obtain the following expression for the spectral function:

$$A(\mathbf{k},\omega) = \Pi_0^+(\mathbf{k})\delta(\omega - \omega_0^+(\mathbf{k})) + \Pi_0^-(\mathbf{k})\delta(\omega - \omega_0^-(\mathbf{k})). \tag{5.5}$$

One can straightforwardly check that this expression satisfies the sum rule. This result is the same as the one obtained in Ref. [39] with the use of the Schwinger-Keldysh formalism. Notice that the spectral function in this case is represented by Dirac delta distributions peaked exactly at the clean case dispersion relations $\omega_0^\pm(\mathbf{k})$. In Fig. 5.2, we show a plot of the spectral function for the first Mott lobe.

Since the density of states is an integral in reciprocal space of the spectral function via (3.71), we obtain from equation (5.5):

$$\rho(\omega) = \frac{1}{(2\pi)^d}\int_{\mathrm{BZ}} d^d k\,\Pi_0^+(\mathbf{k})\delta[\omega - \omega_0^+(\mathbf{k})] + \frac{1}{(2\pi)^d}\int_{\mathrm{BZ}} d^d k\,\Pi_0^-(\mathbf{k})\delta[\omega - \omega_0^-(\mathbf{k})]. \tag{5.6}$$

To solve the above integrals, one has to sum over all the roots of the arguments of the Dirac delta distributions in the first Brillouin zone. In a d-dimensional reciprocal space, these roots form a $(d-1)$-dimensional surface satisfying $\omega^\pm(\mathbf{k}) = \omega$. The sum over all these roots then leads to an integral over the constant energy surface:

$$\rho(\omega) = \frac{1}{(2\pi)^d}\int\limits_{\omega_0^+(\mathbf{k})=\omega} dS\,\frac{\Pi_0^+(\mathbf{k})}{|\nabla_{\mathbf{k}}\omega_0^+(\mathbf{k})|} + \frac{1}{(2\pi)^d}\int\limits_{\omega_0^-(\mathbf{k})=\omega} dS\,\frac{\Pi_0^-(\mathbf{k})}{|\nabla_{\mathbf{k}}\omega_0^-(\mathbf{k})|}, \tag{5.7}$$

where dS represents an infinitesimal portion of the surface. Note that the gradient of the dispersion relations in the denominators corresponds to the group velocities $\mathbf{v}_g^{\pm} = \nabla_{\mathbf{k}}\omega^{\pm}(\mathbf{k})$. Hence, at stationary points of the dispersion relations, i.e., at the points where the group velocity vanishes, the density of states diverges. Such divergences of $\rho(\omega)$ are commonly referred to as Van Hove singularities [160].

To see that the excitations in the clean case are stable, we can, for instance, consider the inverse Fourier transform of the retarded Green's function, from frequency space to time. In terms of the spectral function, using equation (3.42), it becomes

$$G(\mathbf{k},t) = -\mathrm{i}\Theta(t)\int_{-\infty}^{\infty} d\omega A(\mathbf{k},\omega)\mathrm{e}^{-\mathrm{i}\omega t}, \tag{5.8}$$

where we defined $G^R \equiv G$. Inserting equation (5.5), the integration reduces to

$$G(\mathbf{k},t) = -\mathrm{i}\Theta(t)\Pi_0^+(\mathbf{k})\mathrm{e}^{-\mathrm{i}\omega_0^+(\mathbf{k})t} - \mathrm{i}\Theta(t)\Pi_0^-(\mathbf{k})\mathrm{e}^{-\mathrm{i}\omega_0^-(\mathbf{k})t}. \tag{5.9}$$

Note that the time dependence of the Green's function follows from the complex exponentials. As the energy dispersion relations are real in the clean case, the amplitude just oscillates without any damping. This occurs due to the fact that, in the clean case limit, there is no mechanism trough which an excitation could loose its initial momentum. Therefore, any excitation created in this limit is stable and will not decay. As we have discussed in Section 3.7, this picture changes when disorder is present.

It is possible to study the propagation of these excitations by considering the inverse Fourier transform from reciprocal space to real space defined in (3.86). In the case of $n_0 = 0$, for instance, where only the quasi particle branch exists, the representation of the Greens functions in real space reads

$$G_{ij}(t) = -\mathrm{i}\Theta(t)\Big(\frac{a}{2\pi}\Big)^d \mathrm{e}^{\mathrm{i}\mu t}\int_{\mathrm{BZ}} d^d k \mathrm{e}^{\mathrm{i}[J(\mathbf{k})t + \mathbf{k}\cdot(\mathbf{x}_i - \mathbf{x}_j)]}. \tag{5.10}$$

For each dimension in reciprocal space, with the use of the lattice dispersion (4.19), the integrals simplify to

$$\int_{-\pi/a}^{\pi/a} dk \mathrm{e}^{\mathrm{i}[2Jt\cos(ak) + k(x_i - x_j)]} = \frac{2\pi \mathrm{i}^{|x_{ij}|/a}}{a}\mathscr{J}_{|x_{ij}|/a}(2Jt), \tag{5.11}$$

where $x_{ij} = (x_i - x_j)$ and $\mathscr{J}_{x_{ij}/a}(2Jt)$ corresponds to a Bessel function of first kind. Hence, (5.10) becomes

$$G_{ij}(t) = -\mathrm{i}\Theta(t)\mathrm{e}^{\mathrm{i}\mu t}\prod_{p=1}^{d} \mathrm{i}^{|x_{ij}^{(p)}|/a}\mathscr{J}_{|x_{ij}^{(p)}|/a}(2Jt), \tag{5.12}$$

where $x_{ij}^{(p)}$ corresponds to the p-th component of the vector $\mathbf{x}_i - \mathbf{x}_j$. The amplitude of propagation of the stable quasiparticle excitations in the clean case is therefore given by (5.12). We plot the time evolution of the absolute square value of $G_{ij}(t)$ in Fig. 5.3. Note that

Figure 5.3 – Time evolution of the absolute square values of the retarded Green's function (5.12) for $d = 1$ and $n_0 = 0$. Feature scaling was applied to the curves of finite t. The amplitude spreads through space over time. The tunneling energy and the chemical potential are fixed at $J = 0.035U$ and $\mu = 0.3U$, respectively. Despite the fact that the interactions do not play a role in this case, we select U as the energy scale with the aim of locating the equilibrium points in the $J \times \mu$ phase diagram.

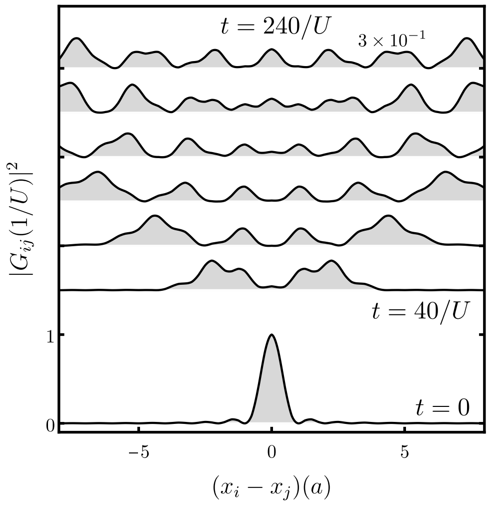

Source: Prepared by the author.

as time increases the amplitude of $G_{ij}(t)$ becomes extended remaining finite even for long distances. This implies that the quasiparticle excitations are extend and as time increases there is a finite probability to find the excitation at a site arbitrarily distant from the lattice site where it was created.

We remark that the properties derived here for the excitations in the clean case are general. This implies that, in the absence of disorder, the elementary excitations above the Mott insulator ground state correspond to stable-extended quasiparticle and quasihole states. In the next section, we discuss how this picture changes when disorder is finite.

5.1.2 Disordered case

The spectral function is defined as the imaginary part of the retarded Green's function (3.37). Using the result (4.20) of the partial summation method obtained in the last chapter, the spectral function can be written as

$$\overline{A(\mathbf{k},\omega)} = -\frac{1}{\pi}\frac{\mathrm{Im}\,\overline{g_i(\omega)}}{[1 - J(\mathbf{k})\mathrm{Re}\,\overline{g_i(\omega)}]^2 + [J(\mathbf{k})\mathrm{Im}\,\overline{g_i(\omega)}]^2}. \tag{5.13}$$

The states of the excitations are then represented by peaks of the spectral function for a fixed wavevector $\mathbf{k}$ in the frequency domain. As we have shown in the last section, $\mathrm{Im}\,\overline{g_i(\omega)}$ is a smooth function of ω controlled by the continuous disorder distribution $\mathscr{P}(\epsilon_i)$. Hence, the peaks of the spectral function correspond to frequencies that make the first term in the denominator on the right-hand side of (5.13) vanish

$$1 - J(\mathbf{k})\mathrm{Re}\overline{g_i(\omega)} = 0. \tag{5.14}$$

The dispersion relation of the excitations can thus be obtained by solving (5.14) for each fixed average particle density per site n_0.

Outside of the energy range where the imaginary part of the unperturbed Green's function is finite, i.e. in the limit of $\mathrm{Im}\overline{g_i(\omega)} \to 0$, the spectral function of (5.13) is strictly zero except when the condition (5.14) is fulfilled where it becomes sharply peaked. In that limit, we can represent the spectral function as

$$\overline{A^{\pm}(\mathbf{k},\omega)} = \pm \frac{\delta[\omega - \omega^{\pm}(\mathbf{k})]}{|J(\mathbf{k})^2 \partial_\omega \mathrm{Re}\overline{g_i[\omega^{\pm}(\mathbf{k})]}|}, \tag{5.15}$$

where $\omega^+(\mathbf{k})$ ($\omega^-(\mathbf{k})$) corresponds to the dispersion of excitations in the quasiparticle (quasi-hole) branch of the spectrum. These strong peaks represented by δ-distributions with vanishing width indicate that stable excitations can still be created in the strong interacting limit of the Bose-Hubbard Hamiltonian. However, as we shall demonstrate in the following section, their dispersion gets altered by the disorder. To ivestigate how the dispersion changes, we can define the effective-mass tensor [69]

$$(m^*)^{-1}_{ij} = \left.\frac{\partial^2 \omega^{\pm}(\mathbf{k})}{\partial k_i \partial k_j}\right|_{\mathbf{k}=\mathbf{0}}, \tag{5.16}$$

where i and j represent components of the wavevector $\mathbf{k}$ in this case. The effective mass gives a measure of how the dispersion of these excitations occurs in the system. Its increase, for instance, reveals that the excitations become less dispersive.

In contrast to the previous limit, in the energy range where $\mathrm{Im}\overline{g_i(\omega)}$ is finite, the spectral function acquires a finite spread. From the discussion of Section 3.7, we concluded that, for a continuous disorder distribution, the singularities of the unperturbed Green's function transform into a branch cut. Over the energy interval where this branch cut is located, the states become degenerate. One can argue from perturbation theory that these states will be coupled with the exact solution being given by linear combinations of the original states with an energy which is spread out by the perturbation [136, 107]. Such an information gets mapped into the finite width of the spectral function in that region. However, resonances appear whenever (5.14) is satisfied. In the neighborhood of the frequencies where the resonances occur, $\omega \approx \omega_r(\mathbf{k})$, we can expand the spectral function as

$$\frac{\mathrm{Im}\overline{g_i(\omega)}}{|1 - J(\mathbf{k})\overline{g_i(\omega)}|^2} \approx \frac{\Pi(\mathbf{k})\Gamma(\mathbf{k})}{[\omega - \omega_r(\mathbf{k})]^2 + \Gamma(\mathbf{k})^2}. \tag{5.17}$$

This corresponds to an approximation of the spectral function by a Caychy-Lorentz distribution in the region where $\mathrm{Im}\overline{g_i(\omega)}$ is finite. Such an approximation yields and estimate to the weight of these excitations

$$\Pi(\mathbf{k}) = |J(\mathbf{k})^2 \partial_\omega \mathrm{Re}\overline{g_i[\omega_r(\mathbf{k})]}|^{-1}, \tag{5.18}$$

also called renormalization factor. This quantity can be interpreted as the proportion of a real particle which enters into the creation of an excitation in the energy range where the resonances occur [161, 119]. Additionally, the width of the distribution is given by

$$\Gamma(\mathbf{k}) = \left| \frac{\mathrm{Im}\overline{g_i[\omega_r(\mathbf{k})]}}{\partial_\omega \mathrm{Re}\overline{g_i[\omega_r(\mathbf{k})]}} \right|. \tag{5.19}$$

Such a quantity is directly linked to the fact that these excitations are not individually invariant under translations, i.e. they are not eigenstates of the crystal momentum [118]. As a consequence, such excitations decay in time with a lifetime given by the inverse of the width of the spectral function [119]

$$\tilde{\tau}(\mathbf{k}) = \frac{1}{\Gamma(\mathbf{k})}. \tag{5.20}$$

Since the energy interval where $\mathrm{Im}\overline{g_i(\omega)}$ is finite is contained within the bounds of the disorder distribution, we conclude that the emergence of these damped states is directly linked to the presence of the random potential. Note that, within this approximation, the resonances correspond to poles of the retarded Green's function $\overline{G(\mathbf{k}, \omega + \mathrm{i}0^+)}$ in the lower half of the complex plane.

As a result, for every Mott lobe with a fixed particle density n_0, the energy band is divided into two distinct regions. The first region is associated with stable states which resemble the excitations of the clean case. On the other hand, the second region arises as a result of disorder and corresponds to damped states that have a finite lifetime, represented by the characteristic time $\tilde{\tau}(\mathbf{k})$. This separation of the spectral function into two distinct regions allows us to differentiate between the stable states and the damped states that are produced by disorder. By doing so, we are able to distinguish the corresponding terms in the spectral function and gain a better understanding of the underlying physical processes. Accordingly, the spectral function can be written as

$$\begin{aligned}
\overline{A(\mathbf{k}, \omega)} = {} & \frac{\delta(\omega - \omega^+(\mathbf{k}))}{|J(\mathbf{k})^2 \partial_\omega \mathrm{Re}\overline{g_i[\omega^+(\mathbf{k})]}|} - \frac{\delta(\omega - \omega^-(\mathbf{k}))}{|J(\mathbf{k})^2 \partial_\omega \mathrm{Re}\overline{g_i[\omega^-(\mathbf{k})]}|} \\
& + \frac{(n_0+1)\mathscr{P}[\omega + \mu - U n_0]}{[1 - J(\mathbf{k})\mathrm{Re}\overline{g_i(\omega)}]^2 + \pi^2 (n_0+1)^2 J(\mathbf{k})^2 \mathscr{P}[\omega + \mu - U n_0]^2} \\
& - \frac{n_0 \mathscr{P}[\omega + \mu - U(n_0 - 1)]}{[1 - J(\mathbf{k})\mathrm{Re}\overline{g_i(\omega)}]^2 + \pi^2 n_0^2 J(\mathbf{k})^2 \mathscr{P}[\omega + \mu - U(n_0-1)]^2}.
\end{aligned} \tag{5.21}$$

So far, our analysis has been carried out without making any assumptions about the specific value of n_0 or the shape of the bounded distribution $\mathscr{P}(\epsilon_i)$. This means that our conclusions are valid for each Mott lobe within the context of our approximations, making them generally applicable. It is worth noting that although our method is designed to work well in high-dimensional systems, it can still be applied to one-dimensional systems ($d = 1$) for small enough values of the tunneling energy J. At this point, we will shift our focus to the case of a uniform distribution, where the distribution $\mathscr{P}(\epsilon_i)$ is evenly spread across the interval $[-\Delta/2, \Delta/2]$.

5.2 Uniform disorder distribution

In order to gain further insight into the new properties contained in the above described results, we investigate the case where the random potential obeys a uniform probability distribution, which we have defined in equation (3.101) of Section 3.7. We remind the reader that such a distribution can be experimentally realized, for instance, in experiments where the speckle-laser intensity is customized [65].

For a uniform disorder distribution, the real part of the unperturbed Green's function of (3.96) can be written as

$$\mathrm{Re}\,\overline{g_i(\omega)} = \frac{n_0+1}{\Delta}\log\left|\frac{\omega+\mu-Un_0-\Delta/2}{\omega+\mu-Un_0+\Delta/2}\right| + \frac{n_0}{\Delta}\log\left|\frac{\omega+\mu-U(n_0-1)+\Delta/2}{\omega+\mu-U(n_0-1)-\Delta/2}\right|. \tag{5.22}$$

Hence, equation (5.14) takes the form

$$\begin{aligned} &\left|\omega+\mu-Un_0-\frac{\Delta}{2}\right|^{n_0+1}\left|\omega+\mu-U(n_0-1)+\frac{\Delta}{2}\right|^{n_0} \\ &-\mathrm{e}^{\Delta/J(\mathbf{k})}\left|\omega+\mu-Un_0+\frac{\Delta}{2}\right|^{n_0+1}\left|\omega+\mu-U(n_0-1)-\frac{\Delta}{2}\right|^{n_0}=0. \end{aligned} \tag{5.23}$$

Even though we have derived the above equation from (5.14), it is important to point out that we expect from the general results discussed on the last section only four solutions of (5.23) to be associated with real excitations for each Mott lobe with $n_0 \geq 1$. For both the quasiparticle and quasihole branches of the energy spectrum, two of such solutions would correspond to the dispersion relation of stable excitations and the remaining two would be associated with the dispersion of damped states. However, one can observe from (5.23) that the solutions for each Mott lobe with integer particle density n_0 must be considered separately.

5.2.1 Mott lobe $n_0 = 0$

We first consider the simpler case where the average density of particles per site in the system is $n_0 = 0$ which occurs for $\mu < -\Delta/2$. In this case, only the quasiparticle branch of the spectrum exists and (5.23) admits two solutions.

The solution associated with the energy dispersion of a stable state is given by

$$\omega^{+}(\mathbf{k}) = -\mu - \frac{\Delta}{2}\coth\left(\frac{\Delta}{2J(\mathbf{k})}\right). \tag{5.24}$$

Applying the definition (5.16) to the above equation, we obtain that the diagonal components of the effective-mass tensor read

$$m^{*} = \frac{8Jd^{2}}{a^{2}\Delta^{2}}\sinh^{2}\left(\frac{\Delta}{4Jd}\right). \tag{5.25}$$

In order to make a comparison, we take the limit $\Delta \to 0$ to recover the clean case results

$$\begin{aligned} \omega_{0}^{+}(\mathbf{k}) &= -\mu - J(\mathbf{k}), & (5.26)\\ m_{0}^{*} &= \frac{1}{2Ja^{2}}. & (5.27) \end{aligned}$$

Therefore, the energy dispersion of the stable excitations in the disordered case maps back into the dispersion relation of the stable-delocalized excitations in the clean case limit.

For the damped state the solution is rather given by

$$\omega_{r}(\mathbf{k}) = -\mu - \frac{\Delta}{2}\tanh\left(\frac{\Delta}{2J(\mathbf{k})}\right), \tag{5.28}$$

where the respective lifetime of these excitation obtained from (5.20) reads

$$\tilde{\tau}(\mathbf{k}) = \frac{4}{\pi\Delta}\cosh^{2}\left(\frac{\Delta}{2J(\mathbf{k})}\right). \tag{5.29}$$

Note that in the clean case limit

$$\lim_{\Delta\to 0}\omega_{r}(\mathbf{k}) = -\mu \tag{5.30}$$

the damped states become dispersionless while their lifetime

$$\lim_{\Delta\to 0}\tilde{\tau}(\mathbf{k}) \to \infty \tag{5.31}$$

diverges. In such a limit, excitations can only be produced for $J = 0$ at integer values of μ/U. One can understand this by observing the clean case phase diagram. The superfluid phase extends all the way down to zero tunneling in the region in between the Mott lobes where the ratio between chemical potential and interaction energy becomes an integer [22]. For vanishing hopping, the integer ratio $\mu/U = n_0$ implies that the energy for an atom to occupy a site with n_0 particles is the same as the energy to occupy a site with $n_0 + 1$. This leads to fluctuations in the average density of particles a thus superfluidity emerges at at arbitrarilly small J. However, as there is no dependence on the wavevector, excitations in this situation are dispersionless and do not propagate in space. Hence, as a consequence of the limits

(5.30) and (5.31), we conclude that the damped state of the disordered case map back to stable localized excitations in the clean case limit.

From (5.20), we obtain that the spectral function for $n_0 = 0$ can be written as

$$\begin{aligned}\overline{A(\mathbf{k},\omega)} &= \frac{\Delta^2}{4J(\mathbf{k})^2}\operatorname{csch}^2\left(\frac{\Delta}{2J(\mathbf{k})}\right)\delta(\omega-\omega^+(\mathbf{k}))\\ &+\frac{\frac{1}{\Delta}[\Theta(\omega+\mu+\frac{\Delta}{2})-\Theta(\omega+\mu-\frac{\Delta}{2})]}{\left[1-\frac{J(\mathbf{k})}{\Delta}\log\left|\frac{\omega+\mu-\Delta/2}{\omega+\mu+\Delta/2}\right|\right]^2+\pi^2J(\mathbf{k})^2/\Delta^2}.\end{aligned} \tag{5.32}$$

In Appendix B one can find the proof that the above expression satisfies the sum rule. From the definition (3.71), by integrating the spectral function over the fist Brillouin zone we obtain the density of states in the disordered case

$$\rho(\omega) = \frac{1}{(2\pi)^d}\int_{\mathrm{BZ}} d^dk\overline{A(\mathbf{k},\omega)}. \tag{5.33}$$

These results allow us to construct the band structures for one, two and three dimensions which are shown in Fig. 5.4. We remark that, even though the expressions (5.24)-(5.28) have no dependence on the on-site interaction U we employ such an energy as a scale for the other relevant energies. By doing this, we can better locate the equilibrium points in the $J\times\mu$ phase diagram. We chose to represent the dispersion relation in two and three dimensions by using the critical points in the Brillouin zone. For $d = 2$ such points are defined as $\Gamma = (0,0)$, $X = (0,\pi)$, $M = (\pi,\pi)$, whereas for $d = 3$ the definition reads $\Gamma = (0,0,0)$, $X = (0,\pi,0)$, $M = (\pi,\pi,0)$, and $R = (\pi,\pi,\pi)$.

The spectral function for $\mathbf{k} = \mathbf{0}$ is plotted in Fig. 5.4(a), (d) and (g). We note that the strong peak of the stable states in the disorder case (red) is shifted towards lower energies in comparison with the clean case stable states (dashed black). For slightly higher energies there emerges a broad distribution which is characteristic of the damped states (blue). Such states appear in the center of the band as can be observed in the light-blue shaded region with width Δ of the dispersion relations. We point out that (5.24) and (5.28) plotted in Fig. 5.4(b), (e) and (h) present jumps which are represented by the dotted-red lines. We can understand such jumps as originating from the scattering effects of the excitations against the random potential. If one decomposes the disordered potential in a sum of infinitely many spatial Fourier components, as the disorder is not spatially correlated, one must consider that none of these components is allowed to have spatial frequency larger then π/a. As a result, an excitation which propagates, for instance, in the k_x direction would interact separately with every component of the random potential thus meeting the condition for Bragg scattering exactly at wavevector $k_x = \pm\pi/2a$. In fact this argument can be extended even to spatially correlated disorder, where the restriction on the spatial frequencies comes from the grain size of the disorder distribution, as it is shown in Ref. [162]. We remark that

Figure 5.4 – Band structure for the Mott lobe $n_0 = 0$. (a), (d) and (g) correspond to the spectral function (5.32). (b), (e) and (h) represent the dispersion relations (5.24), (5.26) and (5.28). (c), (f) and (i) show the density of states (5.33). The shaded-lightblue region and the dotted-red lines in (b), (e) and (h) correspond to the band of damped states of width Δ and the jumps of the dispersion relations, respectively. Although interactions are not important in this case, we chose U as the energy scale in order to specify the points in the $J \times \mu$ phase diagram.

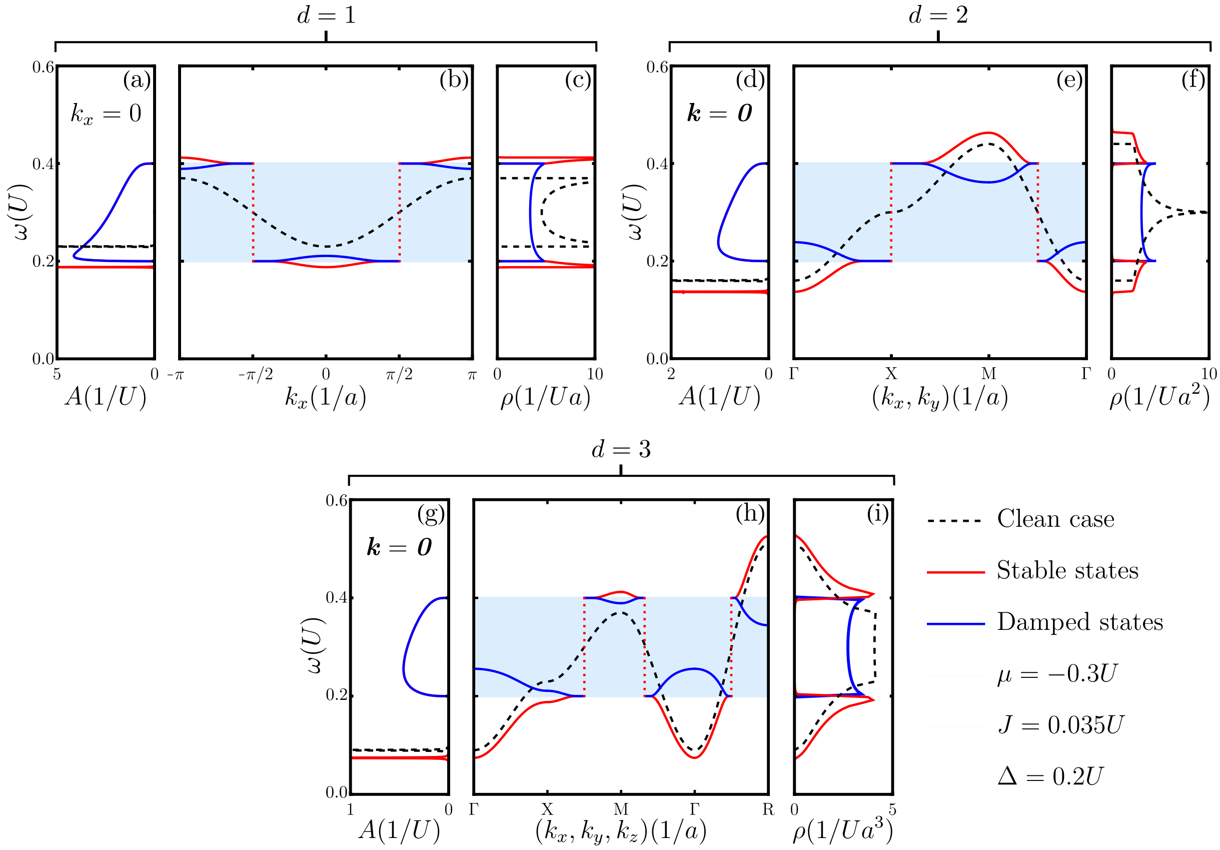

Source: Prepared by the author.

the dispersion relations become flat at those points, implying that the group velocity defined by the gradient $\mathbf{v}_g = \nabla_{\mathbf{k}}\omega(\mathbf{k})$ vanishes and therefore leads to the localization of the wave packets. In agreement with these results, the emergence of sub bands in the disordered Bose-Hubbard model has been reported previously in Ref. [163]. Furthermore, we note that the Van Hove singularities in the density of states are altered by the disorder. The band width is increased to $\Delta\coth(\Delta/4Jd)$. In the $d = 1$ case plotted in Fig. 5.4(c) we can observe that the strong singularities corresponding to the stable states (red) still appear at the band edges, however the damped states dominate the center of the band. This qualitative features are repeated for $d = 2$ and $d = 3$ as can be observed in Fig. 5.4(f) and (i), respectively. Nevertheless, the strong singularity at the center of band in the $d = 2$ case gets divided into two soft peaks located at $\omega = -\mu \pm \Delta/2$ in the disordered case. In $d = 3$ the singularities of the disorder case resemble the ones of the clean case.

To gain a better understanding of how increasing disorder impacts the system, we present a graphical representation of the effective mass of stable states and the lifetime of

Figure 5.5 – Effective mass (5.28) (a) and lifetime (5.29) at $\mathbf{k}=\mathbf{0}$ (b). Both plots include the cases of $d=1$, $d=2$ and $d=3$ which are represented respectively by the dotted, the dot-dashed and the continuous red and blue lines. The dashed-black line in (a) represents the effective mass in the clean case (5.27). The dashed-green line in (b) correspond to time scale associated with the inverse of the disorder strength $1/\Delta$. We use the same value of the tunneling energy as the one used in Fig. 5.4.

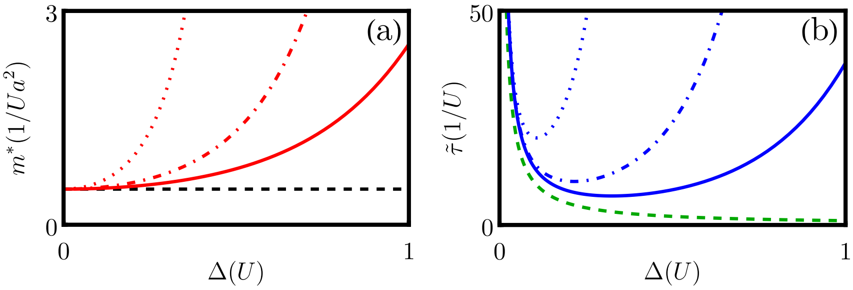

Source: Prepared by the author.

damped states in Fig. 5.5. In Fig. 5.5(a), the effects of disorder are clearly demonstrated by the increase in the effective mass of the stable states. This increase indicates that the dispersion of the states is becoming more flat as a result of the increased disorder strength. On the other hand, Fig. 5.5(b) shows the lifetime of the damped states. Our analysis of this plot reveals that the lifetime of these states (represented by the blue curve) increases as the disorder strength Δ increases. This means that the resonance becomes sharply peaked, making the damped states more stable. It is worth noticing that this effect occurs when the disorder strength Δ is of the same order as the interaction energy U. Hence, we conclude that disorder affects the energy dispersion of the stable states as well as the stability of the damped states.

By investigating how the gap for creating these excitations closes we can understand how the quantum phase transitions take place. The lower bound of the broad distribution in (5.32) defines the energy gap for the damped states

$$E_r = -\mu - \Delta/2. \tag{5.34}$$

For the stable states the gap can be obtained by expanding equation (5.24) as $\mathbf{k}\to\mathbf{0}$

$$E^+ = -\mu - \frac{\Delta}{2}\coth\left(\frac{\Delta}{4Jd}\right). \tag{5.35}$$

For sufficiently small tunneling energy, the difference between the energy gaps reads

$$E_r - E^+ \sim \Delta \mathrm{e}^{-\Delta/2Jd}. \tag{5.36}$$

Note that such an energy difference is always positive, thus, the gap for creating stable excitations closes before the gap for producing damped excitations when the disorder strength

Δ is increased. As it was discussed from Fig. 5.4 and Fig. 5.5, for strong disorder the damped states become stabler and dominate the energy spectrum while the stables states loose their dispersive nature. In this limit, when the gap closes, a phase transition from a Mott insulator to a Bose-glass state occurs. Therefore, we conclude that the damped excitations correspond to the low-energy excited states of the Bose-glass phase.

The existence of disorder prevents the occurrence of a direct Mott-superfluid transition [22, 164, 104, 43]. To fully comprehend the quantum phase diagram, it is necessary to take into account correlation between scattering processes at the same site [139]. To account for quantum and thermal fluctuations, an effective-action approach may be used [52, 53, 54]. A proposal has been made to define the disorder average of the mean particle density as an order parameter to distinguish the Bose-glass phase, similar to the Edwards-Anderson order parameter used in spin glass theory [165, 166, 1].

5.2.2 Mott lobe $n_0 = 1$

Considering frequencies over the real line, for $n_0 = 1$, equation (5.23) reduces to

$$\left(\omega+\mu-U-\frac{\Delta}{2}\right)^2\left(\omega+\mu+\frac{\Delta}{2}\right)+\alpha e^{\Delta/J(\mathbf{k})}\left(\omega+\mu-U+\frac{\Delta}{2}\right)^2\left(\omega+\mu-\frac{\Delta}{2}\right)=0, \tag{5.37}$$

where we have defined $\alpha=\pm1$. The bounds of the disorder distribution impose the following conditions to the frequencies

$$-\mu-\Delta/2 \quad < \quad \omega \quad < \quad -\mu+\Delta/2 \tag{5.38}$$

$$U-\mu-\Delta/2 \quad < \quad \omega \quad < \quad U-\mu+\Delta/2. \tag{5.39}$$

These intervals correspond to the regions of the energy spectrum where $\mathrm{Im}\overline{g_i(\omega)}$ is finite. As a consequence, solutions of (5.37) within the intervals (5.38) and (5.39) are associated with the dispersion of the damped excitations. Outside these intervals, $\mathrm{Im}\overline{g_i(\omega)}$ vanishes and the solutions (5.37) correspond to the energy dispersion of stable excitations.

The expanded form of (5.37) corresponds to a cubic equation given by

$$\omega^3+B_2\omega^2+B_1\omega+B_0=0. \tag{5.40}$$

For each value of α there exist three solutions for the above equation. By applying Cardano's method we can write the solutions in the following form

$$\omega_l=-\frac{B_2}{3}+\eta^l C-\frac{B_1-\frac{B_2^2}{3}}{\eta^l C}, \tag{5.41}$$

where we have defined the primitive cubic root of unity

$$\eta = \frac{-1+\mathrm{i}\sqrt{3}}{2}, \tag{5.42}$$

and the coefficients are given by

$$\begin{aligned}
C &= \left[\frac{1}{2}\left(\frac{B_1 B_2}{3} - B_0 - \frac{2B_2^3}{27}\right) + \sqrt{\frac{1}{4}\left(B_0 - \frac{B_1 B_2}{3} + \frac{2B_2^3}{27}\right)^2 + \frac{1}{27}\left(B_1 - \frac{B_2^2}{3}\right)^3}\,\right]^{\frac{1}{3}}, && (5.43)\\
B_2 &= 3\mu - 2U + \frac{\Delta}{2}\left(\frac{-1+\alpha \mathrm{e}^{\frac{\Delta}{J(\mathbf{k})}}}{1+\alpha \mathrm{e}^{\frac{\Delta}{J(\mathbf{k})}}}\right), && (5.44)\\
B_1 &= U^2 - \frac{\Delta^2}{4} - 4U\mu + 3\mu^2 + \Delta\mu\left(\frac{-1+\alpha \mathrm{e}^{\frac{\Delta}{J(\mathbf{k})}}}{1+\alpha \mathrm{e}^{\frac{\Delta}{J(\mathbf{k})}}}\right), && (5.45)\\
B_0 &= \mu U^2 - 2U\mu^2 + \mu^3 + \frac{U\Delta^2}{2} - \frac{\mu\Delta^2}{4} + \left(\frac{\Delta\mu^2}{2} - \frac{\Delta U^2}{2} - \frac{\Delta^3}{8}\right)\left(\frac{-1+\alpha \mathrm{e}^{\frac{\Delta}{J(\mathbf{k})}}}{1+\alpha \mathrm{e}^{\frac{\Delta}{J(\mathbf{k})}}}\right). && (5.46)
\end{aligned}$$

The exponent of the primitive cubic root in (5.41) is defined as $l \in \{0,1,2\}$. In the case of $\alpha = -1$, all three cases of l lead to real dispersion relations. On the other hand, for $\alpha = 1$ only the case $l = 1$ corresponds to a real dispersion. Consequently, these cases are the ones which represent real excitations of the Mott lobe $n_0 = 1$. We point out that in this case, equations (5.41) and (5.43)-(5.46) present an explicit dependence on the interaction energy U in contrast to the previous case of $n_0 = 0$.

We demonstrate in Fig. 5.6 the $d = 1$ band structure for the $n_0 = 1$ Mott lobe. One can observe that the energy spectrum resembles qualitatively the previous case of $n_0 = 0$ which was shown in Fig. 5.4. However, in the present case the energy spectrum presents both quasiparticles and quasiholes branches. The gap for stable excitations decreases and damped states emerge at the energy-band center. Furthermore, the dispersions have jumps at $k_x = \pi/2a$. These jumps appear as a result of the scattering against the random potential analogously to the previous $n_0 = 0$ case.

We plot the effective mass and lifetime for stable and damped states in the quasiparticle and quasihole branches in Fig. 5.7 using equations (5.16) and (5.20). Similar to what was seen in Fig. 5.5 for the case of $n_0 = 0$, we find that both the effective mass of stable states and the lifetime of damped states increase as the disorder strength is increased. Fig. 5.7 also shows that the dependence of the effective mass of the stable states and the lifetime of damped states in the quasihole branch (represented by dotted red line in (a) and dotted blue line in (b)) is more pronounced with increased disorder strength. We must make a comment on what happens when the gap for creating these excitations closes. Since in the present case the excitation spectrum has both the quasipaticle and the quasihole branches, in the generic phase transition the gap of one of these branches closes while the gap for the other one remains open. As discussed in Section 2.1, the closing of

Figure 5.6 – Band structure for the Mott lobe $n_0 = 1$ in the case of $d = 1$. The upper row depicts to the quasiparticle branch with $\mu = 0.8U$ and the lower row corresponds to the quasihole branch with $\mu = 0.2U$. (a) and (d) represent the spectral function (5.21). (b) and (e) follow from the dispersion relations (5.41). (c) and (f) result from the density of states (5.33). The shaded-lightblue region and the dotted-red lines in (b) and (e) correspond to the band of damped states of width Δ and the jumps of the dispersion relations, respectively. In all plots we have chosen $J = 0.025U$ and $\Delta = 0.2U$.

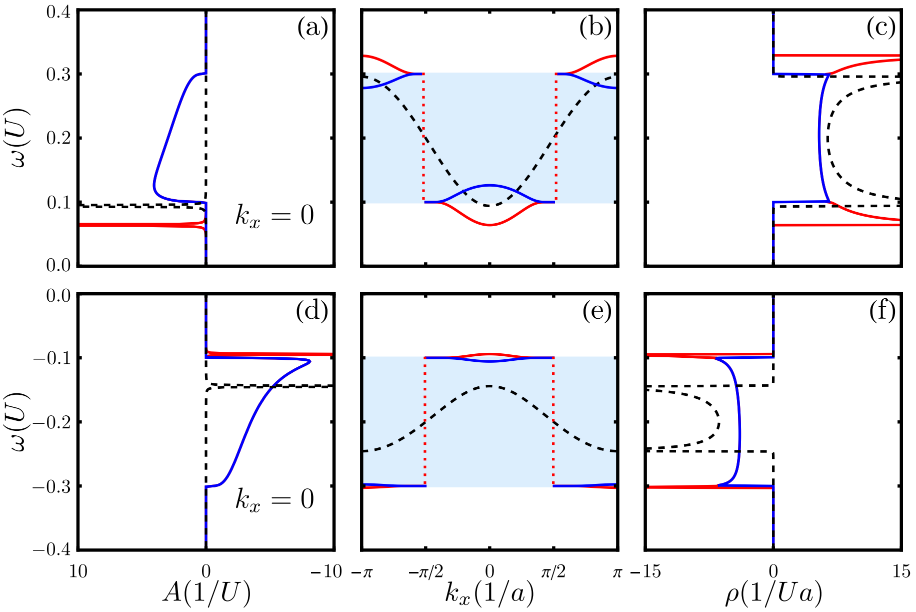

Source: Prepared by the author.

Figure 5.7 – (a) Effective mass (5.16). (b) Lifetime at $\mathbf{k} = \mathbf{0}$ (5.20). In both plots the dotted and continuous red and blue lines correspond to the quasihole and quasiparticle branches, respectively. The dashed and dot-dashed black lines in (a) correspond respectively clean-case quasiparticle and quasihole effective masses. The dashed-green line in (b) corresponds to the time scale associated with the inverse of the energy scale of disorder, i.e. $1/\Delta$. In both plots we chose $J = 0.025U$.

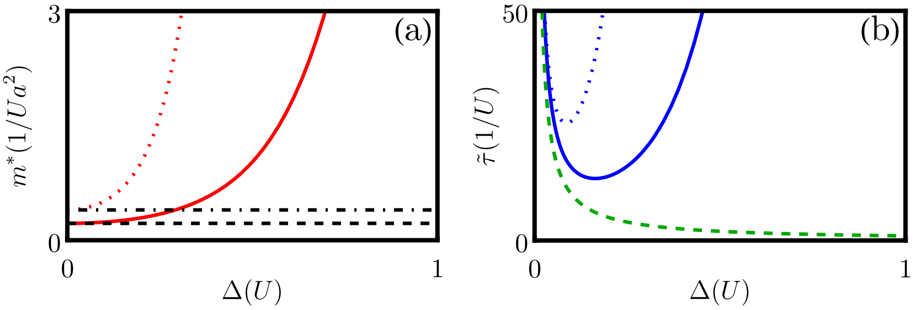

Source: Prepared by the author.

a gap indicates a quantum phase transition. In the clean case, for instance, it was demonstrated for first Mott lobe, that in the generic phase transition, when the quasiparticle gap closes it transforms continuously into a Nambu-Goldstone mode of superfluid phase, while the quasihole gap, which remains open during the transition, transforms continuously into a gapped Higgs amplitude mode [39]. Therefore, we expect that this scenario is maintained when disorder is present such that the stable and the damped excitations should transform continously into the excitations of the superfluid phase. However, a precise analysis on the effects of disorder on such superfluid excitations must be realized to draw further conclusions. In Chapters 7 and 8, we present some possible methods that could be applied in this regard. Our next focus is to study the propagation of the stable and damped excitations in space and time.

5.2.3 Green's function in space time

So far, we have analyzed the properties of excitation states in Fourier space. We now examine the real space and time effects of our previously demonstrated results. To do this, we investigate the complete retarded Green's function within the limits of our approximation.

One can extract important information concerning the propagation of excitations in space by analyzing the asymptotic behavior of the Green's function in the limit of large space separations. We use here the expression (4.20) for the Green's function which results from the partial summation method. The details of this calculation are demonstrated in Appendix C. In such a limit the Green's function is given by

$$\overline{G_{ij}(\omega)} \sim \frac{1}{|\mathbf{x}_i - \mathbf{x}_j|^{\frac{d-1}{2}}} \mathrm{e}^{-\frac{|\mathbf{x}_i - \mathbf{x}_j|}{\ell}} \quad \text{as} \quad |\mathbf{x}_i - \mathbf{x}_j| \to \infty, \tag{5.47}$$

where the exponential decay is characterized by the length scale

$$\ell = a \frac{\sqrt{J|\overline{G(\mathbf{0},\omega)}|}}{|\sin[\arg(\overline{G(\mathbf{0},\omega)})/2]|}. \tag{5.48}$$

Such a length scale corresponds to the mean free path which represents the average distance an excitation propagates before each scattering event against the disordered potential [119]. Note that the dependence of ℓ in ω results from the limit $\mathbf{k} \to \mathbf{0}$ of the Green's function defined in (4.20). For low energies, in the limit of vanishing $\mathrm{Im}\overline{g_i(\omega)}$ the mean free path of (5.48) diverges. As a consequence, the amplitude of the Green's function decays algebraically as $|\mathbf{x}_i - \mathbf{x}_j|^{-(d-1)/2}$. Such an algebraic decay characterizes the propagation of the stable excitations. On the other hand, in the energy range of the damped states, where $\mathrm{Im}\overline{g_i(\omega)}$ is finite, the amplitude of propagation of these excitations decays exponential with characteristic length ℓ denoted in (5.48).

To ivestigate the propagation in time, it is convenient to write the Green's function as an integral over the frequency domain of the spectral function (3.42) [73]. With this representation, the spatio-temporal profile of the Green's function can be obtained via

$$\overline{G_{ij}(t)} = -\mathrm{i}\Theta(t)\left(\frac{a}{2\pi}\right)^d \int_{\mathrm{BZ}} d^dk \int_{-\infty}^{\infty} d\omega \overline{A(\mathbf{k},\omega)}\mathrm{e}^{-\mathrm{i}\omega t+\mathrm{i}\mathbf{k}\cdot(\mathbf{x}_i-\mathbf{x}_j)}. \tag{5.49}$$

In the case of $t = 0$ the integral over the frequency domain is simplified by the sum rule. The integral over the first Brillouin zone then gives

$$\overline{G_{ij}(0)} = \prod_{p=1}^{d} \frac{\sin\left(\pi x_{ij}^{(p)}/a\right)}{\pi x_{ij}^{(p)}/a}, \tag{5.50}$$

where we have defined $x_{ij}^{(p)}$ is defined p-th component of the vector $\mathbf{x}_i - \mathbf{x}_j$. Thus, the amplitude of the Green's function is initially concentrated at small space separations, i.e. $|\mathbf{x}_i - \mathbf{x}_j| \to 0$. We remark that this result is true for both the clean and disordered cases.

Using the spectral function to represent the Green's function, we distinguish the contributions of the stables excitations from the ones of the damped excitations. For simplicity, we consider the case of $n_0 = 0$ where, for a uniform disorder distribution, the spectral function is given by (5.33). Thus, the contributions from the stable and damped states are respectively given by

$$\begin{aligned} \overline{G_{ij}^{+}(t)} &= -\mathrm{i}\Theta(t)\left(\frac{a}{2\pi}\right)^d \int_{\mathrm{BZ}} d^dk \frac{\Delta^2}{4J(\mathbf{k})^2}\operatorname{csch}^2\left(\frac{\Delta}{2J(\mathbf{k})}\right)\mathrm{e}^{-\mathrm{i}\omega^{+}(\mathbf{k})t}, && (5.51) \\ \overline{G_{ij}^{r}(t)} &= -\mathrm{i}\Theta(t)\left(\frac{a}{2\pi}\right)^d \int_{\mathrm{BZ}} d^dk \int_{-\mu-\frac{\Delta}{2}}^{-\mu+\frac{\Delta}{2}} d\omega \frac{\mathrm{e}^{-\mathrm{i}\omega t+\mathrm{i}\mathbf{k}\cdot(\mathbf{x}_i-\mathbf{x}_j)}}{\left[1-\frac{J(\mathbf{k})}{\Delta}\log\left|\frac{\omega+\mu-\Delta/2}{\omega+\mu+\Delta/2}\right|\right]^2+\pi^2 J(\mathbf{k})^2/\Delta^2}. && (5.52) \end{aligned}$$

By solving this integrals numerically for $d = 1$, we plot the absolute squared value of the Green's function in Fig. 5.8. Considering both contributions of (5.51) and (5.52), we observe in Fig. 5.8(a) a distinct behaviors of the total Green's function for short and long time scales. The amplitude of $|\overline{G_{ij}(t)}|^2$ is initially localized in the vicinity of $x_i - x_j = 0$. Around $t = 16/U$ the localized behavior fades away and the amplitude becomes extended. This extended behavior dominates the propagation at long time scales. We plot the contributions corresponding to stable excitations and damped excitations in Fig. 5.8(b) and (c) respectively. The amplitude of the stables states, in Fig. 5.8(b), spreads through space as time increases while the amplitude of the damped states remains localized and decays rapidly in time. From the asymptotic limit of the Green's function (5.47), we conclude that only the algebraic decay is not sufficient to localized the stable excitations, however the additional exponential decay leads to the localization of the damped states in space. Furthermore, we conclude that the amplitude of propagation of the full Green's function in Fig. 5.8(a) is dominated by the damped-localized states at short time scales whereas it is dominated by

Figure 5.8 – Time evolution of the absolute square value of the Green's function for $d = 1$ and $n_0 = 0$. (a) correspond to the total Green's function $\overline{|G_{ij}(t)|^2}$, where we have used feature scaling to better illustrate the behavior of the amplitude at long time scales. (b) Contribution $\overline{|G^+_{ij}(t)|^2}$ of the stable states. (c) Contribution $\overline{|G^r_{ij}(t)|^2}$ of the damped states. In all plots we chose $J = 0.035U$, $\Delta = 0.2U$ and $\mu = -0.3U$.

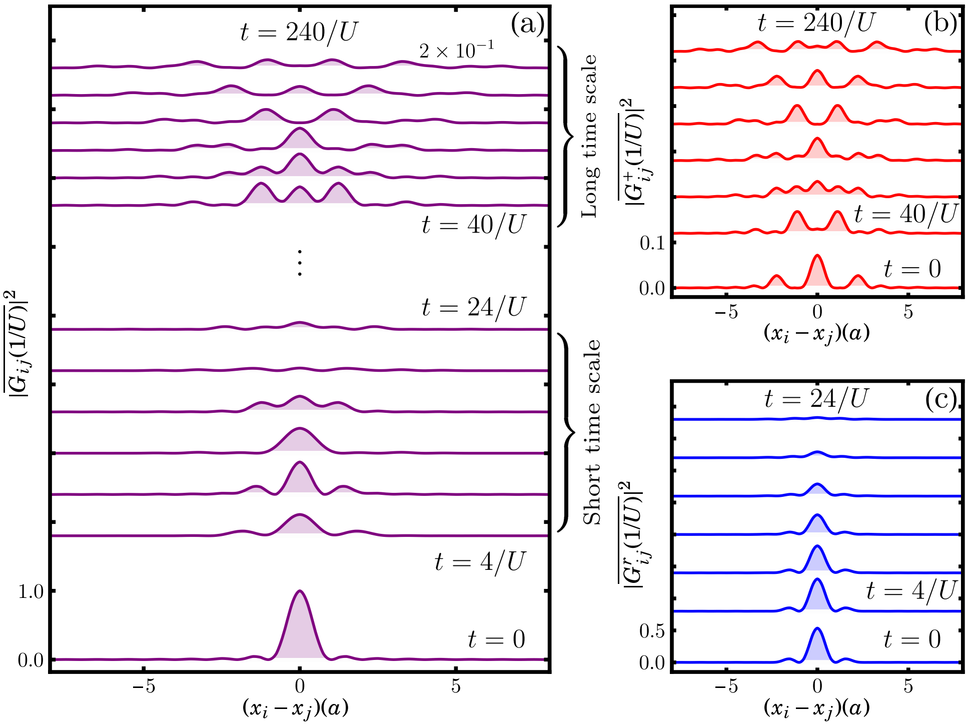

Source: Prepared by the author.

the stable-delocalized states for long time scales.

5.3 Summary of results

As we have demonstrated, disorder changes the energy spectrum of the Bose-Hubbard Hamiltonian in the strongly interacting limit by decreasing the gap for stable excitations, increasing their effective mass and producing in the center of the band damped-localized states which become stabler when disorder becomes of the order of the interactions. Such damped-localized states dominate the spectrum in the strong disorder limit. In this limit a phase transition from a Mott insulator to a Bose glass occurs. In order to get more information on the complete phase diagram, we propose in the next section the use of the local density of state to distinguish both insulating phases. It turns out that out approach works even when thermal fluctuations are included.

Chapter 6

Phase diagram at finite temperatures

So far we have been concerned with the nature of the elementary excitations of the disordered Bose-Hubbard model. We now turn our attention to the phase diagram of such a model. Many results in this direction have been obtained with numerical methods such as local [1] and stochastic mean field techniques [2, 3] or even Monte-Carlo calculations [40, 41, 42, 43, 44, 45, 46, 47, 48, 49]. However, in most cases the analytical results were restricted to mean field theory [38, 50, 51]. In the present chapter, we demonstrated how one can investigate the phase diagram of the Bose-Hubbard model by applying the result of local density of states obtained in Section 4.3 by means of the Poincaré-Lindstedt method. In particular, we use such a quantity to distinguish the Mott from the Bose glass ground state. In contrast to the superfluid state, both insulating phases are characterized by the absence of long-range order. Nevertheless, it turns out that difference in the spectral information of each insulating ground state is encoded into the local density of states. Such a quantity vanishes for zero energy excitations above the Mott state due to the finite gap, while it becomes finite for the Bose-glass phase as a consequence of its gapless spectrum. The results presented in this chapter were summarized and published in Ref. [139]. In what follows, we shall discuss them in detail.

6.1 Superfluid phase boundary

The microscopic origin of the superfluid phase in the Bose-Hubbard model lies on the emergence of phase coherence in the single-site macroscopic wave function. From the symmetry point of view, the existence of such macroscopic wave function implies the spontaneous breakdown of the global U(1) symmetry. We have discussed in Section 2.2 that the relevant fluctuations of the effective potential near the phase transition can be described by an order parameter field. In the normal phase, the effective potential is symmetric under transformation of the U(1)-symmetry group in the space of the order parameter. However, it peaks up a preferred direction at the transition point. The order parameter in the lattice case can be defined as the site dependent expectation value of $\psi_i = \langle \hat{a}_i \rangle$. The symmetry breaking is then characterized by the change in sign of the coefficient that multiplies the term of second order in the order parameter expansion the effective potential. This coefficient is found to be proportional to the inverse of the single-particle Green's function, as it is shown, for instance, in Refs. [141, 114]. In Chapter 7, we shall demonstrate such a relation within our partial summation approximation. Therefore, the change in sign of the second order coeffincient in the expansion of the effective potential in terms of the order parameter is equivalent to the divergence of the single-particle Green's function. Moreover, the breaking of a continuous U(1) symmetry is associated with the emergence of excitations which cost vanishing little energy to create at low momentum [167]. Hence, we conclude that the transition to the superfluid phase is marked by the divergence of long-wavelength correlations at low energies and the phase boundary is given by

$$G(\mathbf{0},0)^{-1} = 0. \tag{6.1}$$

This condition is the same used in [99] for studying the clean case phase diagram.

In the disordered case, considering the result of partial summation (4.20) obtained in Section 4.2, the superfluid phase boundary simplifies to

$$J(\mathbf{0}) = \left[\overline{g_i(0)}\right]^{-1}, \tag{6.2}$$

which explicitly can be written as

$$\frac{Jz}{U} = \left[\int_{-\infty}^{\infty} d\epsilon_i \mathscr{P}(\epsilon_i) \sum_{n=0}^{\infty} \frac{\mathrm{e}^{-\beta E_n(\epsilon_i)}}{Z_0(\epsilon_i)} \left(\frac{n+1}{\mu - \epsilon_i - Un} - \frac{n}{\mu - \epsilon_i - U(n-1)}\right)\right]^{-1}. \tag{6.3}$$

This expression for the phase boundary is a generalization of the results obtained in [52, 53, 54, 99] to the case where disorder is present. It is worth mentioning that expression (6.3) is exactly the same as the result obtained in [38] to the phase boundary of the disordered Bose-Hubbard model within the mean-field method.

Considering the uniform disorder distributions defined in (3.101), the equation for the phase boundary simplifies to

$$\frac{Jz}{U} = \left[\int_{-\Delta/2}^{\Delta/2} d\epsilon_i \mathscr{P}(\epsilon_i) \sum_{n=0}^{\infty} \frac{\mathrm{e}^{-\beta E_n(\epsilon_i)}}{Z_0(\epsilon_i)} \left(\frac{n+1}{\mu - \epsilon_i - Un} - \frac{n}{\mu - \epsilon_i - U(n-1)}\right)\right]^{-1}. \tag{6.4}$$

We plot such a phase boundary in Fig. 6.1. The red line marks the divergence of the single-particle Green's function. For values of the tunneling energy above that line, the equilibrium state of the system is found to be a superfluid state. The region enclosed below such a red line corresponds to the non-superfluid states. Note that for finite temperature, the superfluid state do not extends down to the vanishing-hopping line. One can observe

Figure 6.1 – Superfluid phase boundary obtained from (6.4) for the finite temperature $k_B T/U = 0.01$, with $z = 6$, and for different values of the disorder parameter. The disorder energy scales is set at $\Delta/U = 0.5$ in (a) and at $\Delta/U = 1$ in (b).

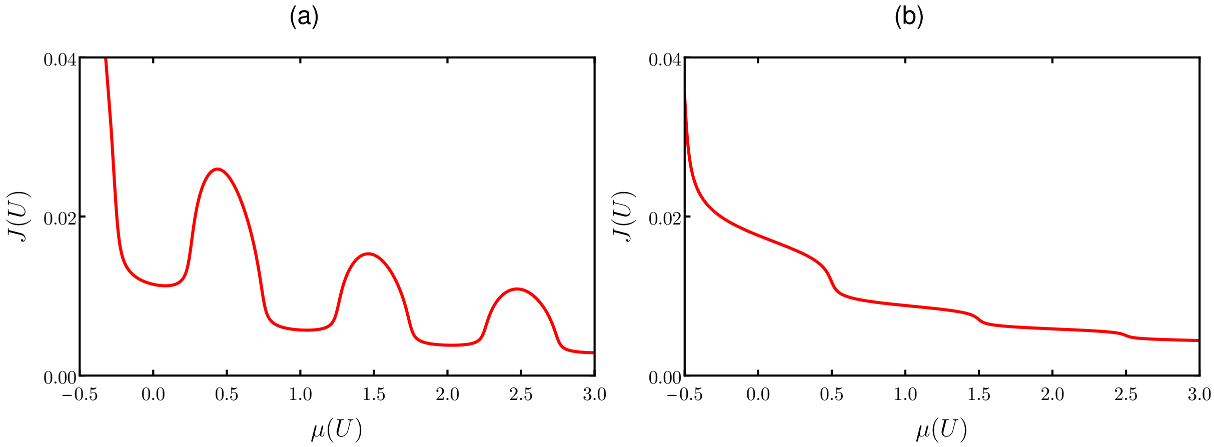

Source: Prepared by the author and published in Ref. [139].

in Fig. 6.1(a) that if disorder is not of the same order of the interaction energy, the curve of the phase boundary has local maxima which resemble the Mott-lobe tips of the clean case. We the disorder energy scale becomes of the same order of the interactions, in Fig. 6.1(b), the curve becomes smoother. Even though equation (6.4) provides a clear distinction from the superfluid to the non-superfluid ground states, it gives no discrimination between Mott insulator and Bose glass. As we shall discuss in the next section, one must consider a different parameter in order to study the phase transition between these insulating phases.

6.2 Local density of states

One essential property that distinguishes the insulating phases of the Bose-Hubbard model in the presence of disorder comes from their energy spectrum. While the Mott-insulator ground state is characterized by its gap for quasiparticle and quasihole excitations, the Bose-glass state corresponds to a gapless insulating phase. It was argued in Ref. [22], where this quantum phase transition was first investigated, that the low-energy excitations of the Bose-glass phase correspond essentially to localized quasiparticles and quasiholes. We have demonstrated in the last chapter that this is indeed the case, and that, in addition to being localized, such excitations are also damped. It was further stated in Ref. [22] that one could therefore study the Mott-Bose glass phase boundary by means of the local density of states at zero energy, which is supposed to vanish in the Mott phase due to presence of the gap acquiring finite values only in the Bose-glass state where the gap is closed. Here, we explore the validity of such argument for finite temperatures and slightly positive values of the tunneling energy.

Figure 6.2 – Density plot of the local density of states obtained from (6.5) for a uniform disorder distribution with $k_B T/U = 0.01$ and $z = 6$. The black regions correspond to the Mott-insulator phase, where $\overline{\rho_i(0)} = 0$, and the grey region corresponds to the Bose-glass phase, where $\overline{\rho_i(0)} \neq 0$. The red line indicates the result (6.4) for the phase boundary to the superfluid phase as shown in Fig. 6.1, which corresponds to the white region of the figures. The disorder strength is fixed with $\Delta/U = 0.5$ in (a) and $\Delta/U = 1$ in (b).

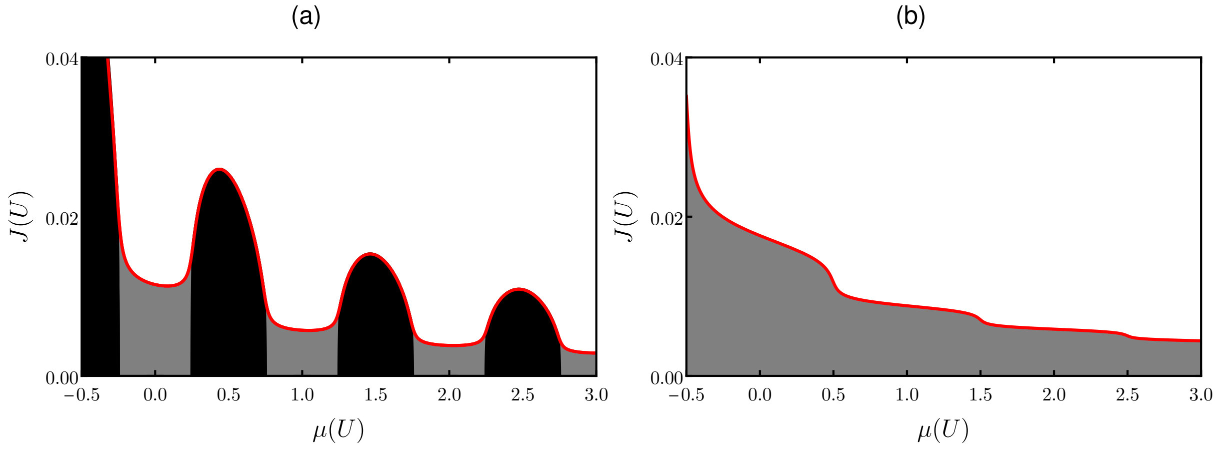

Source: Prepared by the author and published in Ref. [139].

These arguments were tested in Ref. [38], where it was shown that the local density of states serves as a parameter to characterize the insulating phases of the Bose-Hubbard model even for finite temperatures. However, the full phase diagram could not be investigated in such paper as their result is only valid in the zero-tunneling line. In Section 4.3, we have demonstrated that a correction in the hopping expansion can be included in the disorder-ensemble average of the local density of states by means of the Poincaré-Lindstedt method. To simplify the discussion of this section, we repeat here the result of equation (4.31) in its explicit form

$$\begin{aligned}\overline{\rho_i(\omega)} = {} & \sum_{n=0}^{\infty}(n+1)\frac{\mathrm{e}^{-\beta E_n(Un-\omega)}}{Z_0(Un-\omega)}\mathscr{P}\left[\omega+\mu-U(n-1)+zJ^2 n\frac{\mathrm{e}^{-\beta E_n(U(n-1)-\omega)}}{Z_0(U(n-1)-\omega)}\overline{g_j(\omega)}\right] \\ & -\sum_{n=0}^{\infty} n\frac{\mathrm{e}^{-\beta E_n(U(n-1)-\omega)}}{Z_0(U(n-1)-\omega)}\mathscr{P}\left[\omega+\mu-Un-zJ^2(n+1)\frac{\mathrm{e}^{-\beta E_n(Un-\omega)}}{Z_0(Un-\omega)}\overline{g_j(\omega)}\right]+\cdots.\end{aligned} \tag{6.5}$$

Note that, in this approximation, the hopping contributions appear in the argument of the disorder distribution. We have demonstrated in Section 3.1 that such distribution controls the size of the energy range where the damped-localized excitations appear. Therefore, the result of (6.5) implies that, within our perturbation method, increasing the tunneling energy leads to an alteration on the size of the region occupied by the damped-localized states the energy spectrum. To see how such a result affects the phase diagram, we plot $\overline{\rho_i(\omega)}$ for a uniform disorder distribution (3.101) in Fig. 6.2.

For vanishing tunneling energy, if the disorder energy scale is not of the order of the interaction energy, i.e. $\Delta < U$, there is always an interval, namely $\mu \in [U(n-1)+\Delta/2, Un-\Delta/2]$, where the chemical potential minimizes the local eigenenergies (3.79) of the unperturbed Hamiltonian (3.74) by fixing the single-site average particle density at integer values and the system reaches equilibrium in Mott-insulating ground state. For finite hopping, one expects a Mott lobe structure to appear. This is indeed what we verify in Fig. 6.2(a), where the region where the local density of states for zero energy excitations, i.e. $\overline{\rho_i(0)}$, vanishes is represented in black. However, we can now distinguish the grey regions where $\overline{\rho_i(0)}$ is finite, which correspond to the Bose-glass state. For finite temperatures, we observe that the Bose-glass emerges in between the Mott lobes. When the disorder strength becomes of the order of interactions, i.e. $\Delta \sim U$, the Bose glass dominates the insulating part of the phase diagram and the system can no longer reach equilibrium in a Mott insulating state. This is depicted in Fig. 6.2(b). From the analysis presented in Chapter 5, in this limit of strong disorder, the low-energy excitations of the system corresponds to gapless damped-localized states. We have calculated the local density of states only bellow the red line, which represents the result (6.4), where the phase transition to the superfluid phase takes place. To compute the analytical expression for the phase boundary between both insulating phases, we must further analyze the arguments of the distributions in (6.5). We shall do so in the next section.

6.3 Mott insulator to Bose glass phase boundary

Assuming that the probability distribution of the random potential $\mathscr{P}(\epsilon_i)$ is bounded on the interval $\epsilon_i \in [-\Delta/2, \Delta/2]$, implies that the region where the local density of states for zero energy excitations is finite, i.e. $\overline{\rho_i(0)} \neq 0$, is controlled by the following intervals

$$-\frac{\Delta}{2} \leq \gamma_n^- + z\Lambda_n^- J^2 \leq \frac{\Delta}{2}, \tag{6.6}$$

$$-\frac{\Delta}{2} \leq \gamma_n^+ - z\Lambda_n^+ J^2 \leq \frac{\Delta}{2}, \tag{6.7}$$

where have applied the definitions

$$\gamma_n^- = \mu - U(n-1), \tag{6.8}$$

$$\gamma_n^+ = \mu - Un, \tag{6.9}$$

$$\Lambda_n^- = n\frac{\mathrm{e}^{-\beta E_n(U(n-1))}}{Z_0(U(n-1))}\overline{g_j(0)}, \tag{6.10}$$

$$\Lambda_n^+ = (n+1)\frac{\mathrm{e}^{-\beta E_n(Un)}}{Z_0(Un)}\overline{g_j(0)}. \tag{6.11}$$

The intervals of (6.6) and (6.7) define the region occupied by the Bose-glass phase in the phase diagram in the case of $\Delta < U$. As a consequence, the Mott lobes would be enclosed

Figure 6.3 – Phase boundaries for the case of $k_B T/U = 0.01$, $z = 6$, and $\Delta/U = 0.5$. The continuous red line corresponds to (6.4), while the dashed-black lines indicate (6.12) for $n = 1,2,3$, i.e., the phase boundary between Mott insulator and Bose glass obtained from the result for the local density of states. The green dots represent the critical points where the three phases coexist.

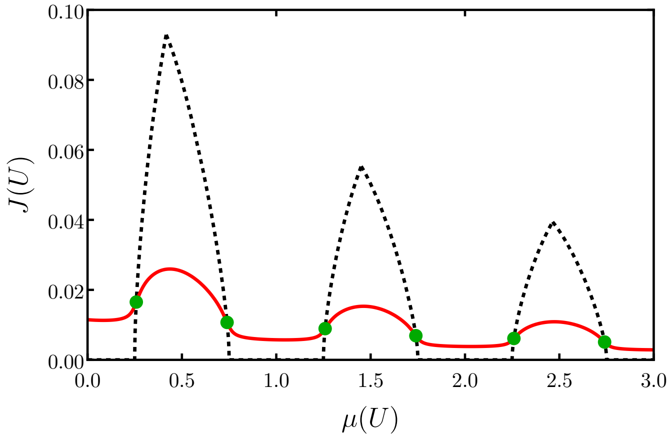

Source: Prepared by the author and published in Ref. [139].

by the values of the tunneling energy outside these intervals which obey the condition

$$\left(\frac{-\frac{\Delta}{2}-\gamma_n^-}{z\Lambda_n^-}\right)^{1/2} \quad \leq \quad J \quad \leq \quad \left(\frac{-\frac{\Delta}{2}+\gamma_n^+}{z\Lambda_n^+}\right)^{1/2}. \tag{6.12}$$

This result corresponds to the analytical expression of the phase boundary between Mott insulator and Bose glass. Note that, for each Mott lobe, one can obtain the phase boundary by just setting the corresponding integer values of the average particle density n which minimize the local eigenenergies (3.79). Such a result can be observed in Fig. 6.3.

It is important to mention that our result for the hopping corrections of the local density of states computed with the Poincaré-Lindstedt method goes beyond mean-field theory in the prediction of the Mott-Bose glass phase boundary. According to such a result, the regions enclosed by the black dashed lines in Fig. 6.3 represents the Mott lobes. Note that such region trespass the red line, which represents the phase transition to the superfluid phase. This would correspond to a direct phase transition from Mott to the superfluid ground states even in the presence of disorder. As we have mentioned in Chapter 2, it was argued in Ref. [22], that the most likely scenario is that, in presence of disorder, the Bose glass always intervenes and the Mott-superfluid transition is not allowed. These arguments were further sustained by quantum Monte Carlo simulations [40, 43, 44, 46]. Furthermore, with the use of the theorem of inclusions, it was proved in Ref. [104] that in the presence of any bounded disorder distribution no direct transition between Mott insulator and superfluid should occur. We can understand this disagreement between our results and predictions available in the literature, by remembering that we have considered only the first non-vanishing contribution in the hopping expansion of the local density o states. Thus, we expect that by including higher order corrections within our approximation to $\overline{\rho_i(\omega)}$, the critical points where the three phases coexist, represented by the green dots at each side of the Mott lobes in Fig. 6.3, would become closer together until eventually meet below the phase boundary to the superfluid phase. In this situation, the Bose-glass would emerge between the Mott and superfluid phases, forbidding a direct phase transition between them. We remark, however, that the calculations to include higher-order corrections in the hopping expansion to the renormalized local density of states are extremely involved. In order to achieve a better understanding about the complete phase diagram, one could observe how the energy functional behaves in each region of the phase diagram. We have mentioned in the last chapter that an effective-action approach should lead to progress in this regard [52, 53, 54].

Even though our result is not accurate in the prediction of the Mott-superfluid phase transition, it might be worthwhile to test it against some beyond mean-field numerical simulations. Such comparison is made in the next section.

6.4 Comparison with numerical results

In this section, we compare our result for the phase boundary of the first Mott lobe to numerical calculations from the literature. One comparison is made against the results of Ref. [1] for the zero-temperature limit in two dimensions. Those results were obtained by the introduction of an Edwards-Anderson like order parameter to identify the Bose glass, as it was proposed in [165, 166, 168, 169, 170]. In this case, such a parameter is defined as the variance of the local particle density after the disorder average is taken. The numerical calculations are then executed by applying a local mean-field method to calculate the energy functional which is minimized with a conjugate gradient algorithm. The other comparison is made against the results of Ref. [2, 3] for the three dimensional case at zero and finite temperatures. These references made use of a stochastic mean-field theory. Such a method is constructed as a single site theory and allows for the calculation of the probability density function which describes fluctuations of the local mean-field parameters in the thermodynamic limit. All three references have made use of a uniform disorder distribution.

First, we take the result of (6.12) to be valid only below the superfluid phase boundary of (6.4). In the zero-temperature limit and for a uniform disorder distribution, the unperturbed Green's function assumes the form of (5.22). In the case of $\omega = 0$, we define $\overline{g_i(0)} \equiv \overline{g}_{n_0}$, where

$$\overline{g}_{n_0} = \frac{n_0+1}{\Delta}\log\left|\frac{\mu - Un_0 - \Delta/2}{\mu - Un_0 + \Delta/2}\right| + \frac{n_0}{\Delta}\log\left|\frac{\mu - U(n_0-1) + \Delta/2}{\mu - U(n_0-1) - \Delta/2}\right|. \tag{6.13}$$

Figure 6.4 – Comparison between theoretical and numerical results for the first Mott lobe in the disordered case for two and three dimensions at both zero and finite temperatures. The continuous-red line corresponds to (6.4) and (6.12), i.e., the results of our Green's function approach, while the blue dots indicate the numerical predictions of [1] for the $d = 2$ case and [2, 3] for the $d = 3$ cases. Figures (a) and (b) show the $d = 2$ and $d = 3$ zero-temperature phase boundary with $\Delta/U = 0.6$ and $z = 4$ and $z = 6$, respectively. Figure (c) presents the finite temperature $3d$ phase boundary with $\Delta/U = 0.5$, $z = 6$, and $k_B T/U = 0.03$.

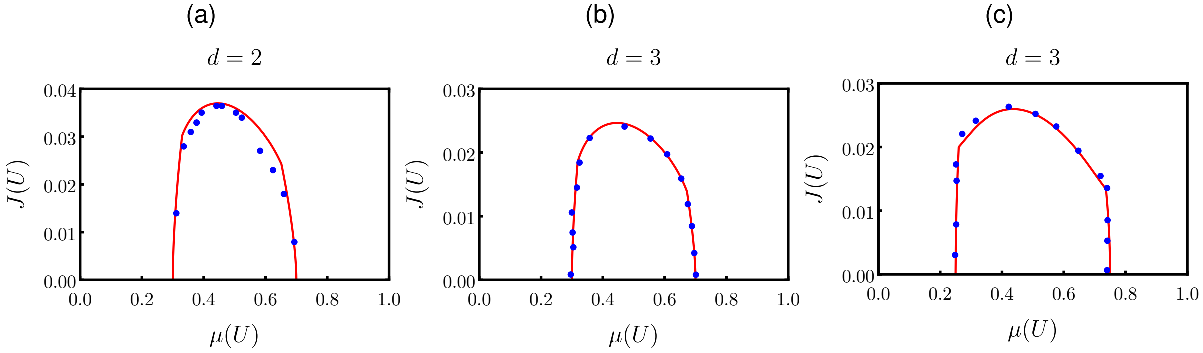

Source: Prepared by the author and published in Ref. [139].

Thus, equation (6.4) simplifies to

$$\frac{Jz}{U} = [\bar{g}_{n_0}]^{-1}, \tag{6.14}$$

while equation (6.12) becomes

$$\left(\frac{-\frac{\Delta}{2} - \gamma^-_{n_0}}{z n_0 \bar{g}_{n_0}}\right)^{1/2} \quad \leq \quad J \quad \leq \quad \left(\frac{-\frac{\Delta}{2} + \gamma^+_{n_0}}{z(n_0+1)\bar{g}_{n_0}}\right)^{1/2}. \tag{6.15}$$

With the above expressions, together with results of (6.4) and (6.12) for finite temperatures, we compare in Fig. 6.4 our results with the numerical calculations from the literature.

The results of our analysis are found to be in excelent agreement with the numerical data reported in the literature. In Fig. 6.4(a), although our prediction tends to overestimate the size of the first Mott lobe in the $d = 2$ case, the majority of the numerical points fall within the range of the red continuous line. However, our prediction for the $d = 3$ phase boundary shows remarkable agreement with the numerical data at both zero and finite temperatures, as demonstrated in Fig. 6.4(b) and (c), respectively. As temperature is introduced, the phase boundary to the superfluid phase, characterized by (6.4), becomes smoother, resulting in kinks at the tri-critical points where the three phases coexist, as shown at the intersection of this solution with the Mott insulator to Bose glass phase boundary of (6.12). We can therefore conclude that our analytical method to the phase boundary is equivalent to the numerical method of stochastic mean-field theory developed in Refs. [2, 3].

6.5 Summary of results

We developed an analytic approach to compute the finite-temperature phase diagram of the disordered Bose-Hubbard model and distinguish between the three possible ground states of the system. Our approach reproduced the results of mean-field theory and allowed us to construct a phase diagram that accurately differentiated between Mott insulator and Bose-glass phases. Our results compared significantly well to numerical results for both $d = 2$ and $d = 3$ cases. However, our phase diagram predicts a direct transition between Mott-insulator and superfluid phases, which conflicts with the proven absence of such a transition in the presence of bounded disorder. This approach has potential to go beyond mean-field theory and improve the prediction of the superfluid to Bose-glass phase transition with the inclusion higher-order corrections.

Part IV

Preliminary calculations

Chapter 7

Superfluid elementary excitations

In this chapter we introduce a powerful method that allows not only to recover the results we have shown in Chapter 5 for the excitations above the Mott insulator ground state, but also to investigate the elementary excitations of the superfluid phase. The key element of such a method is the effective-action functional, which generalizes the concept of a classical action including quantum fluctuations. The effective action is the generator of the one-particle irreducible correlation functions and therefore is composed only of the connected parts in the hopping expansion. By studying fluctuations on its equilibrium value, one can obtain the energy spectrum of the system. In addition, it is also possible to define an effective potential in order to apply Landau theory of phase transitions introduced in Section 2.1. The calculations of this chapter are inspired by the derivations of Refs. [52, 53, 54, 55].

7.1 Effective-action approach

In order to obtain the effective-action functional, we must first consider the next term in the cumulant expansion of the unperturbed free energy (4.12). Thus, the free energy becomes

$$\begin{aligned} W_0[\mathrm{j}^*,\mathrm{j}] = & \int_0^\beta d\tau_1 \int_0^\beta d\tau_1' \sum_i \mathrm{j}_i^*(\tau_1) g_i(\tau_1,\tau_1') \mathrm{j}_i(\tau_1') \\ & + \frac{1}{2!^2} \int_0^\beta d\tau_1 \int_0^\beta d\tau_2 \int_0^\beta d\tau_1' \int_0^\beta d\tau_2' \sum_i \mathrm{j}_i^*(\tau_1) \mathrm{j}_i^*(\tau_2) W_{0i}^{(4)}(\tau_1,\tau_2;\tau_1',\tau_2') \mathrm{j}_i(\tau_1') \mathrm{j}_i(\tau_2') + \cdots . \end{aligned} \tag{7.1}$$

By including the first correction in the hopping perturbation developed in Section 4.1, the free energy becomes

$$\begin{aligned}
W[\mathrm{j}^*,\mathrm{j}] = &\int_0^\beta d\tau_1 \int_0^\beta d\tau_1' \sum_i \mathrm{j}_i^*(\tau_1) g_i(\tau_1,\tau_1')\mathrm{j}_i(\tau_1') \\
&+ \sum_{ij} J_{ij} \int_0^\beta d\tau_1 \int_0^\beta d\tau \int_0^\beta d\tau_1' \mathrm{j}_i^*(\tau_1) g_i(\tau_1,\tau) g_j(\tau,\tau_1')\mathrm{j}_j(\tau_1') \\
&+ \frac{1}{2!^2} \int_0^\beta d\tau_1 \int_0^\beta d\tau_2 \int_0^\beta d\tau_1' \int_0^\beta d\tau_2' \sum_i \mathrm{j}_i^*(\tau_1)\mathrm{j}_i^*(\tau_2) W_{0i}^{(4)}(\tau_1,\tau_2;\tau_1',\tau_2')\mathrm{j}_i(\tau_1')\mathrm{j}_i(\tau_2') + \cdots .
\end{aligned} \tag{7.2}$$

The correlation function $W_{0i}^{(4)}$ can be obtained from its decomposition in terms of the connected parts [141]

$$W_{0i}^{(4)}(\tau_1,\tau_2;\tau_1',\tau_2') = \langle \mathscr{T}_\tau \hat{a}_i(\tau_1)\hat{a}_i(\tau_2)\hat{a}_i^\dagger(\tau_1')\hat{a}_i^\dagger(\tau_2')\rangle_0 - g_i(\tau_1,\tau_1')g_i(\tau_2,\tau_2') - g_i(\tau_1,\tau_2')g_i(\tau_2,\tau_1'). \tag{7.3}$$

The calculation of such a correlation function is extensive and we choose not to show it here. Instead, we just show its expression in the Matsubara space representation

$$
\begin{aligned}
&W_{0i}^{(4)}(\mathrm{i}\omega_{l_1},\mathrm{i}\omega_{l_2};\mathrm{i}\omega'_{l_1},\mathrm{i}\omega'_{l_2}) = \\
&\frac{\beta^2}{Z_0(\mu_i)}\left(\delta_{\omega_{l_1}\omega'_{l_1}}\delta_{\omega_{l_2}\omega'_{l_2}} + \delta_{\omega_{l_1}\omega'_{l_2}}\delta_{\omega_{l_2}\omega'_{l_1}}\right) \\
&\times\Bigg[\sum_{n=0}^{\infty} e^{-\beta E_n(\mu_i)}\left(\frac{n+1}{E_{n+1}(\mu_i)-E_n(\mu_i)-\mathrm{i}\omega_{l_2}} + \frac{n}{E_i(n-1)-E_i(n)+\mathrm{i}\omega_{l_2}}\right) \\
&\qquad\times\left(\frac{n+1}{E_{n+1}(\mu_i)-E_n(\mu_i)-\mathrm{i}\omega_{l_1}} + \frac{n}{E_{n-1}(\mu_i)-E_n(\mu_i)+\mathrm{i}\omega_{l_1}}\right) \\
&\qquad-\frac{1}{Z_0(\mu_i)}\sum_{n,m=0}^{\infty} e^{-\beta[E_n(\mu_i)+E_m(\mu_i)]}\left(\frac{n+1}{E_{n+1}(\mu_i)-E_n(\mu_i)-\mathrm{i}\omega_{l_2}} + \frac{n}{E_{n-1}(\mu_i)-E_n(\mu_i)+\mathrm{i}\omega_{l_2}}\right) \\
&\qquad\quad\times\left(\frac{m+1}{E_{m+1}(\mu_i)-E_m(\mu_i)-\mathrm{i}\omega_{l_1}} + \frac{m}{E_{m-1}(\mu_i)-E_m(\mu_i)+\mathrm{i}\omega_{l_1}}\right)\Bigg] \\
&+\frac{\beta}{Z_0(\mu_i)}\delta_{\omega'_{l_1}+\omega'_{l_2},\omega_{l_1}+\omega_{l_2}}\sum_{n=0}^{\infty} e^{-\beta E_n(\mu_i)} \\
&\quad\times\Bigg[\frac{(n+2)(n+1)}{[E_{n+1}(\mu_i)-E_n(\mu_i)-\mathrm{i}\omega'_{l_2}][E_{n+2}(\mu_i)-E_n(\mu_i)-\mathrm{i}\omega'_{l_1}-\mathrm{i}\omega'_{l_2}][E_{n+1}(\mu_i)-E_n(\mu_i)-\mathrm{i}\omega_{l_1}]} \\
&\qquad+\frac{n(n-1)}{[E_{n-1}(\mu_i)-E_n(\mu_i)+\mathrm{i}\omega_{l_2}][E_{n-2}(\mu_i)-E_n(\mu_i)+\mathrm{i}\omega_{l_1}+\mathrm{i}\omega_{l_2}][E_{n-1}(\mu_i)-E_n(\mu_i)-\mathrm{i}\omega'_{l_1}]} \\
&\qquad-\Bigg(\frac{n+1}{[E_{n+1}(\mu_i)-E_n(\mu_i)-i\omega_{l_1}][E_{n+1}(\mu_i)-E_n(\mu_i)-\mathrm{i}\omega'_{l_1}]} \\
&\qquad\qquad\qquad+\frac{n}{[E_{n+1}(\mu_i)-E_n(\mu_i)+\mathrm{i}\omega_{l_1}][E_{n+1}(\mu_i)-E_n(\mu_i)+\mathrm{i}\omega'_{l_1}]}\Bigg) \\
&\qquad\times\left(\frac{n+1}{E_{n+1}(\mu_i)-E_n(\mu_i)-\mathrm{i}\omega'_{l_2}} + \frac{n}{E_{n-1}(\mu_i)-E_n(\mu_i)+\mathrm{i}\omega_{l_2}}\right) + \begin{matrix}\omega_{l_1}\leftrightarrow\omega'_{l_1}\\ \omega_{l_2}\leftrightarrow\omega'_{l_2}\end{matrix}\Bigg],
\end{aligned}
\tag{7.4}
$$

where we indicate in the last line the extra terms generated by permutations of the Matsubara frequency variables. We remark that the explicit form of $W_{0i}^{(4)}$ was calculated in Refs. [53, 54, 55, 55]. Taking transformation to the Matsubara frequency domain as well as the disorder ensemble average of (7.2), we can define the order-parameter fields as functional derivatives of the averaged free energy with respect to the sources

$$
\overline{\psi_i(\mathrm{i}\omega_l)} = \overline{\langle\hat{a}_i(\mathrm{i}\omega_l)\rangle} = \frac{\delta\overline{W}}{\delta \mathrm{j}_i^*(\mathrm{i}\omega_l)}, \tag{7.5}
$$

$$
\overline{\psi_i^*(\mathrm{i}\omega_l)} = \overline{\langle\hat{a}_i^\dagger(\mathrm{i}\omega_l)\rangle} = \frac{\delta\overline{W}}{\delta \mathrm{j}_i(\mathrm{i}\omega_l)}. \tag{7.6}
$$

This definition motivates a Legendre transformation of the free energy, which gives the effective action

$$-\beta\mathscr{F}[\overline{\psi}^*,\overline{\psi}] = \overline{W} + \sum_i \sum_l \Big(\overline{\psi_i(\mathrm{i}\omega_l)}\mathrm{j}_i^*(\mathrm{i}\omega_l) + \overline{\psi_i^*(\mathrm{i}\omega_l)}\mathrm{j}_i(\mathrm{i}\omega_l) \Big). \tag{7.7}$$

As j^* and $\overline{\psi}$ are conjugate variables, in general we have

$$\mathrm{j}_i(\mathrm{i}\omega_l) = -\beta \frac{\delta\mathscr{F}}{\delta\overline{\psi_i^*(\mathrm{i}\omega_l)}} \quad , \quad \mathrm{j}_i^*(\mathrm{i}\omega_l) = -\beta \frac{\delta\mathscr{F}}{\delta\overline{\psi_i(\mathrm{i}\omega_l)}}. \tag{7.8}$$

We observe that the physical situation of interest corresponds to the case where the sources vanish, i.e. $\mathrm{j}(\mathrm{i}\omega_l) = \mathrm{j}^*(\mathrm{i}\omega_l) = 0$, thus the above equation becomes

$$\left.\frac{\delta\mathscr{F}}{\delta\overline{\psi}}\right|_{\psi=\psi_{eq}} = \left.\frac{\delta\mathscr{F}}{\delta\overline{\psi}^*}\right|_{\psi=\psi_{eq}} = 0. \tag{7.9}$$

Furthermore, when evaluated at the equilibrium value of the order parameter the effective action equals the free energy

$$-\beta\mathscr{F}|_{\psi=\psi_{eq}} = \lim_{\mathrm{j}\to 0} \overline{W}. \tag{7.10}$$

As a result of the Legendre transformation, the effective action can be expressed as an expansion in the order-parameter field given by

$$\begin{aligned} -\beta\mathscr{F}[\overline{\psi}^*,\overline{\psi}] &= \mathscr{F}^{(0)} + \frac{1}{\beta^2}\sum_{ij}\sum_{ll'} \overline{\psi_i^*(\mathrm{i}\omega_l)}\mathscr{F}_{ij}^{(2)}(\mathrm{i}\omega_l,\mathrm{i}\omega_l')\overline{\psi_j(\mathrm{i}\omega_l')} \\ &+ \frac{1}{2!^2\beta^4} \sum_{i_1 i_2 i_1' i_2'} \sum_{l_1 l_2 l_1' l_2'} \overline{\psi_{i_i}^*(\mathrm{i}\omega_{l_1})}\ \overline{\psi_{i_2}^*(\mathrm{i}\omega_{l_2})}\mathscr{F}^{(4)}_{i_1 i_2, i_1' i_2'}(\mathrm{i}\omega_{l_1},\mathrm{i}\omega_{l_2},\mathrm{i}\omega_{l_1}',\mathrm{i}\omega_{l_2}')\overline{\psi_{i_1'}(\mathrm{i}\omega_{l_1}')}\ \overline{\psi_{i_2'}(\mathrm{i}\omega_{l_2}')} \\ &+ \cdots, \end{aligned} \tag{7.11}$$

where

$$\begin{aligned} \mathscr{F}^{(0)} &= \prod_i \int_{-\infty}^{\infty} d\epsilon_i \mathscr{P}(\epsilon_i) \left[\sum_i \ln\left(\sum_{n=0}^{\infty} \mathrm{e}^{-\beta E_n(\epsilon_i)} \right) \right], & (7.12) \\ \mathscr{F}_{ij}^{(2)}(\mathrm{i}\omega_l,\mathrm{i}\omega_l') &= \beta\delta_{\omega_l\omega_l'}\Big(J_{ij} - \delta_{ij}[\overline{g_i(\mathrm{i}\omega_l)}]^{-1} \Big), & (7.13) \\ \mathscr{F}^{(4)}_{i_1 i_2, i_1' i_2'}(\mathrm{i}\omega_{l_1},\mathrm{i}\omega_{l_2},\mathrm{i}\omega_{l_1}',\mathrm{i}\omega_{l_2}') &= \delta_{i_1 i_2}\delta_{i_2 i_1'}\delta_{i_2' i_1} \frac{\overline{W_{0i_1}^{(4)}(\mathrm{i}\omega_{l_1},\mathrm{i}\omega_{l_2},\mathrm{i}\omega_{l_1}',\mathrm{i}\omega_{l_2}')}}{\overline{g_{i_1}(\mathrm{i}\omega_{l_1})}\ \overline{g_{i_1}(\mathrm{i}\omega_{l_2})}\ \overline{g_{i_1}(\mathrm{i}\omega_{l_1}')}\ \overline{g_{i_1}(\mathrm{i}\omega_{l_2}')}}. & (7.14) \end{aligned}$$

Note that only the term $\mathscr{F}_{ij}^{(2)}$ gains a contribution up to first order in the hopping expansion.

Using the transformation to reciprocal space, we write

$$\overline{\psi(\mathbf{k},\mathrm{i}\omega_l)} = \sum_i \overline{\psi_i(\mathrm{i}\omega_l)}\mathrm{e}^{-\mathrm{i}\mathbf{k}\cdot\mathbf{x}_i}, \tag{7.15}$$

therefore, the effective action becomes

$$\begin{aligned}
-\beta\mathscr{F}[\overline{\psi}^*,\overline{\psi}] = {} & \mathscr{F}^{(0)} + \frac{1}{\beta^2}\left(\frac{a}{2\pi}\right)^{2d}\sum_{ll'}\int d^dk\int d^dk'\overline{\psi^*(\mathbf{k},\mathrm{i}\omega_l)}\mathscr{F}^{(2)}(\mathbf{k},\mathrm{i}\omega_l,\mathbf{k}',\mathrm{i}\omega_l')\overline{\psi(\mathbf{k}',\mathrm{i}\omega_l')} \\
& + \frac{1}{2!^2\beta^4}\left(\frac{a}{2\pi}\right)^{4d}\sum_{l_1l_2l_1'l_2'}\int d^dk_1\int d^dk_2\int d^dk_1'\int d^dk_2' \\
& \times \overline{\psi^*(\mathbf{k}_1,\mathrm{i}\omega_{l_1})}\;\overline{\psi^*(\mathbf{k}_2,\mathrm{i}\omega_{l_2})}\mathscr{F}^{(4)}(\mathbf{k}_1,\mathrm{i}\omega_{l_1},\mathbf{k}_2,\mathrm{i}\omega_{l_2};\mathbf{k}_1',\mathrm{i}\omega_{l_1}',\mathbf{k}_2',\mathrm{i}\omega_{l_2}')\overline{\psi(\mathbf{k}_1',\mathrm{i}\omega_{l_1}')}\;\overline{\psi(\mathbf{k}_2',\mathrm{i}\omega_{l_2}')} \\
& + \cdots,
\end{aligned} \tag{7.16}$$

where the Fourier transform of each term reads

$$\mathscr{F}^{(2)}(\mathbf{k},\mathrm{i}\omega_l;\mathbf{k}',\mathrm{i}\omega_l') = \beta\left(\frac{2\pi}{a}\right)^d\delta(\mathbf{k}-\mathbf{k}')\delta_{\omega_l\omega_l'}\left[J(\mathbf{k}) - [\overline{g_i(\mathrm{i}\omega_l)}]^{-1}\right], \tag{7.17}$$

$$\begin{aligned}
\mathscr{F}^{(4)}(\mathbf{k}_1,\mathrm{i}\omega_{l_1},\mathbf{k}_2,\mathrm{i}\omega_{l_2};\mathbf{k}_1',\mathrm{i}\omega_{l_1}',\mathbf{k}_2',\mathrm{i}\omega_{l_2}') = {} & \left(\frac{2\pi}{a}\right)^d\delta(\mathbf{k}_1+\mathbf{k}_2-\mathbf{k}_1'-\mathbf{k}_2') \\
& \times \frac{\overline{W_{0i_1}^{(4)}(\mathrm{i}\omega_{l_1},\mathrm{i}\omega_{l_2};\mathrm{i}\omega_{l_1}',\mathrm{i}\omega_{l_2}')}}{\overline{g_{i_1}(\mathrm{i}\omega_{l_1})}\;\overline{g_{i_1}(\mathrm{i}\omega_{l_2})}\;\overline{g_{i_1}(\mathrm{i}\omega_{l_1}')}\;\overline{g_{i_1}(\mathrm{i}\omega_{l_2}')}}.
\end{aligned} \tag{7.18}$$

Note on the right hand side of (7.17) that the term in brackets corresponds to minus the inverse of the Green's function (4.20) obtained in Section 4.2 with the partial summation method,

$$[\overline{\mathscr{G}(\mathbf{k},\mathrm{i}\omega_l)}]^{-1} = [\overline{g_i(\mathrm{i}\omega_l)}]^{-1} - J(\mathbf{k}). \tag{7.19}$$

It is a general result that the two-point Green's function corresponds to the inverse of $\mathscr{F}^{(2)}$ [141]. Thus, we can see that the Legendre transformation is equivalent to the partial summation method.

We have already discussed that, after taking the disorder average, translational invariance is recovered. Considering that the temporal as well as the average translation symmetries are preserved in the equilibrium state of the Bose-Hubbard Hamiltonian, we define the equilibrium value of the order-parameter field in Fourier-Matsubara space to be given by

$$\psi_{\mathrm{eq}}(\mathbf{k},\mathrm{i}\omega_l) = \beta\left(\frac{2\pi}{a}\right)^D\delta_{\omega_l,0}\delta(\mathbf{k})\psi_{\mathrm{eq}}. \tag{7.20}$$

By plugging such an equilibrium value in equation (7.16), we can define the effective potential, which corresponds to the effective action divided by the number of lattice sites

$\mathscr{F}_{\text{pot}} = \mathscr{F}/L$. The Landau expansion of such an effective potential reads

$$\mathscr{F}_{\text{pot}} = \frac{\mathscr{F}^{(0)}}{\beta L} + \frac{\mathscr{F}^{(2)}(\mathbf{0},0,\mathbf{0},0)}{\beta L}|\psi_{\text{eq}}|^2 + \frac{1}{2!^2}\frac{\mathscr{F}^{(4)}(\mathbf{0},0,\mathbf{0},0;\mathbf{0},0,\mathbf{0},0)}{\beta L}|\psi_{\text{eq}}|^4 + \cdots . \tag{7.21}$$

In Section 2.2, we demonstrated that the spontaneous breaking of U(1)-global symmetry that occurs during a continuous phase transition can be mapped on the change of sign of the coefficient of second order in the order-parameter expansion of the effective potential. Hence, the phase boundary correspond exactly to the point where such a coefficient vanishes. From equation (7.19) and (7.21), one can observe that the condition $\mathscr{F}^{(2)} = 0$ leads to equation (6.1) from which we have extracted the phase boundary to the superfluid phase in Chapter 6. Therefore, this calculation justifies the use of the divergences of the Green's function to investigate such a phase transition.

To get analytical information on the excitation spectrum, we can study fluctuations of the effective action around the equilibrium value of the order parameter. Thus, considering the expansion

$$\overline{\psi(\mathbf{k},\mathrm{i}\omega_l)} = \psi_{\text{eq}}(\mathbf{k},\mathrm{i}\omega_l) + \delta\psi(\mathbf{k},\mathrm{i}\omega_l), \tag{7.22}$$

the expansion of the effective action (7.16) up to second order in $\delta\psi(\mathbf{k},\omega_l)$ becomes

$$\begin{aligned}
&-\beta\mathscr{F}\left[\delta\psi^*,\delta\psi\right] = \mathscr{F}^{(0)} + \mathscr{F}^{(2)}(\mathbf{0},0,\mathbf{0},0)|\psi_{\text{eq}}|^2 + \frac{1}{2!^2}\mathscr{F}^{(4)}(\mathbf{0},0,\mathbf{0},0,\mathbf{0},0,\mathbf{0},0)|\psi_{\text{eq}}|^4 \\
&+ \frac{1}{\beta^2}\left(\frac{a}{2\pi}\right)^{2d}\sum_{ll'}\int d^dk\int d^dk'\delta\psi^*(\mathbf{k},\mathrm{i}\omega_l) \\
&\times\left[\mathscr{F}^{(2)}(\mathbf{k},\omega_l,\mathbf{k}',\omega_l') + \mathscr{F}^{(4)}(\mathbf{k},\omega_l,\mathbf{0},0,\mathbf{k}',\omega_l',\mathbf{0},0)|\psi_{\text{eq}}|^2\right]\delta\psi(\mathbf{k}',\mathrm{i}\omega_l') \\
&+ \frac{1}{2!^2\beta^2}\left(\frac{a}{2\pi}\right)^{2d}\sum_{ll'}\int d^dk\int d^dk'\mathscr{F}^{(4)}(\mathbf{k},\omega_l,\mathbf{k}',\omega_l',\mathbf{0},0,\mathbf{0},0)|\psi_{\text{eq}}|^2 \\
&\times[\delta\psi(\mathbf{k},\mathrm{i}\omega_l)\delta\psi(\mathbf{k}',\mathrm{i}\omega_l') + \delta\psi^*(\mathbf{k},\mathrm{i}\omega_l)\delta\psi^*(\mathbf{k}',\mathrm{i}\omega_l')] + \cdots .
\end{aligned} \tag{7.23}$$

The properties of the excitations are related to the real-time dynamics of the system, and thus we must take the analytic continuation from Matsubara space to the real frequency domain. For the Matsubara frequencies the transformation related to the retarded response reads

$$\mathrm{i}\omega_l \to \omega + \mathrm{i}0^+, \tag{7.24}$$

as we have already shown in the previous chapters. For the Matsubara sums, such a transformation has the following form

$$\frac{1}{\beta}\sum_l \to \frac{1}{2\pi}\int_{\infty}^{\infty} d\omega. \tag{7.25}$$

With this expression we are now able to analyze the spectra in the disordered case of both in the Mott insulator and superfluid phases. By applying such an analytic continuation, the effective action of (7.23) can be written as

$$\begin{aligned}
&-\beta\mathscr{F}[\delta\psi^*,\delta\psi] = \mathscr{F}^{(0)} + \mathscr{F}^{(2)}(\mathbf{0},0;\mathbf{0},0)|\psi_{\text{eq}}|^2 + \frac{1}{2!^2}\mathscr{F}^{(4)}(\mathbf{0},0,\mathbf{0},0;\mathbf{0},0,\mathbf{0},0)|\psi_{\text{eq}}|^4 \\
&+\frac{1}{2\pi}\left(\frac{a}{2\pi}\right)^{2d}\int d\omega\int d^d k\,\delta\psi^*(\mathbf{k},\omega)\zeta_1(\mathbf{k},\omega)\delta\psi(\mathbf{k},\omega) \\
&+\frac{1}{4\pi}\left(\frac{a}{2\pi}\right)^{2d}\int d\omega\int d^d k\,\zeta_2(\mathbf{k},\omega)[\delta\psi(\mathbf{k},\omega)\delta\psi(-\mathbf{k},-\omega)+\delta\psi^*(\mathbf{k},\omega)\delta\psi^*(-\mathbf{k},-\omega)] \\
&+\cdots,
\end{aligned} \tag{7.26}$$

where we have defined the functions

$$\zeta_1(\mathbf{k},\omega) = \mathscr{F}^{(2)}(\mathbf{k},\omega+\mathrm{i}0^+;\mathbf{k},\omega+\mathrm{i}0^+) + \mathscr{F}^{(4)}(\mathbf{k},\omega+\mathrm{i}0^+,\mathbf{0},0;\mathbf{k},\omega+\mathrm{i}0^+,\mathbf{0},0)|\psi_{\text{eq}}|^2, \tag{7.27}$$

$$\zeta_2(\mathbf{k},\omega) = \frac{1}{2}\mathscr{F}^{(4)}(\mathbf{k},\omega+\mathrm{i}0^+,-\mathbf{k},-\omega-\mathrm{i}0^+;\mathbf{0},0,\mathbf{0},0)|\psi_{\text{eq}}|^2. \tag{7.28}$$

Considering the different cases of the equilibrium order parameter in each ground state, we can obtain the dispersion relation for the low-energy excitations from (7.26). Such calculation is presented in what follows.

7.2 Excitation spectra in the Mott-insulator phase

Inside the Mott-insulating state, since there is no long-range order, the equilibrium value of the order parameter vanishes, i.e. $\psi_{\text{eq}} = 0$. In this case, equation (7.26) reduces to

$$\mathscr{F}[\delta\psi^*,\delta\psi] = -\frac{\mathscr{F}^{(0)}}{\beta} + \frac{1}{2\pi}\left(\frac{a}{2\pi}\right)^{2d}\int d\omega\int d^d k\,\delta\psi^*(\mathbf{k},\omega)\zeta_0(\mathbf{k},\omega)\delta\psi(\mathbf{k},\omega), \tag{7.29}$$

where from equations (7.17) and (7.27), we obtain

$$\begin{aligned}
\zeta_0(\mathbf{k},\omega) &= \frac{1}{\beta}\zeta_1(\mathbf{k},\omega)|_{\psi_{\text{eq}}=0} \\
&= \frac{1}{\beta}\mathscr{F}^{(2)}(\mathbf{k},\omega+\mathrm{i}0^+;\mathbf{k},\omega+\mathrm{i}0^+) \\
&= \left(\frac{2\pi}{a}\right)^d\left[J(\mathbf{k}) - [\overline{g_i(\omega+\mathrm{i}0^+)}]^{-1}\right].
\end{aligned} \tag{7.30}$$

The stationary condition for the effective action (7.29) with respect to the fluctuations is given by

$$\zeta_0(\mathbf{k},\omega)\delta\psi(\mathbf{k},\omega) = 0, \tag{7.31}$$

which only admits non-trivial solutions in the case of

$$\zeta_0(\mathbf{k},\omega) = 0. \tag{7.32}$$

The above equations gives the dispersion relations of the excitations above the Mott-insulator ground state. In fact, the excitation spectrum which follows from this result is equivalent to the one obtained in Section 5.1. We now show how such an equivalence takes place.

Considering the separation of real and imaginary parts of the unperturbed Green's function after the analytic continuation (3.95), the condition (7.32) can be written as

$$\mathrm{Re}\,\overline{g_i(\omega)} + \mathrm{i}\,\mathrm{Im}\,\overline{g_i(\omega)} - \frac{1}{J(\mathbf{k})} = 0. \tag{7.33}$$

Since the imaginary part $\mathrm{Im}\,\overline{g_i(\omega)}$, given in the zero-temperature limit by (3.97), is controlled by the disorder distribution, in the energy range where it vanishes equation (7.33) becomes equivalent to (5.14) for the peaks of the spectral function. Such an imaginary part is only finite, for each fixed average particle density n_0, inside the intervals

$$\begin{aligned} U(n_0-1)-\mu-\frac{\Delta}{2} \quad &\leq \quad \omega \quad \leq \quad U(n_0-1)-\mu-\frac{\Delta}{2}, && (7.34)\\ Un_0-\mu-\frac{\Delta}{2} \quad &\leq \quad \omega \quad \leq \quad Un_0-\mu-\frac{\Delta}{2}. && (7.35) \end{aligned}$$

In the limit of zero temperature, for a uniform disorder distribution, the real part $\mathrm{Re}\,\overline{g_i(\omega)}$ simplifies to a logarithm form written in (5.22). In such a limit, (7.33) can be rewritten in following form

$$\begin{aligned} &\left|\omega+\mu-Un_0-\frac{\Delta}{2}\right|^{n_0+1}\left|\omega+\mu-U(n_0-1)+\frac{\Delta}{2}\right|^{n_0}\\ &-\mathrm{e}^{\Delta/J(\mathbf{k})-\mathrm{i}\Delta\,\mathrm{Im}\,\overline{g_i(\omega)}}\left|\omega+\mu-Un_0+\frac{\Delta}{2}\right|^{n_0+1}\left|\omega+\mu-U(n_0-1)-\frac{\Delta}{2}\right|^{n_0}=0. \end{aligned} \tag{7.36}$$

For energies outside the intervals (7.34) and (7.35), we recover from equation (7.36) the expression of (5.23) shown in Section 5.2. Inside the regions, where $\mathrm{Im}\,\overline{g_i(\omega)}$ is finite, where have

$$\Delta\,\mathrm{Im}\,\overline{g_i(\omega)} = \begin{cases} n_0\pi & \text{for } \omega \text{ in the interval (7.34)},\\ -(n_0+1)\pi & \text{for } \omega \text{ in the interval (7.35)}. \end{cases} \tag{7.37}$$

Therefore, for both $n_0 = 0$ and $n_0 = 1$ Mott lobes, we recover the equations that originated the dispersion relations found in Section 5.2.

We have therefore proven that the result of first order in the hopping approximation of the effective-action method is equivalent to the one obtained with the spectral function for the analyses of the elementary excitations of the Mott phase in Chapter 5. However, the present effective-action approach provides a venue to investigate the excitation spectrum of the superfluid phase. We describe such analysis in the subsequent section.

7.3 Excitation spectra in the superfluid phase

In order to obtain the energy spectrum for the excitations in the superfluid phase, we must consider equation (7.26) in its full content, since the equilibrium value of the order parameter is finite inside such a phase, i.e. $\psi_{\text{eq}} \neq 0$. Such equilibrium values is defined by the following relation

$$|\psi_{\text{eq}}|^2 = -2\frac{\mathscr{F}^{(2)}(\mathbf{0},0;\mathbf{0},0)}{\mathscr{F}^{(4)}(\mathbf{0},0,\mathbf{0},0;\mathbf{0},0,\mathbf{0},0)}. \tag{7.38}$$

In this case, the stationary condition to the effective action (7.26) with respect to the fluctuations $\delta\psi$ and $\delta\psi^*$ leads to the following coupled equations

$$\zeta_1(\mathbf{k},\omega)\delta\psi(\mathbf{k},\omega) + \zeta_2(\mathbf{k},\omega)\delta\psi^*(-\mathbf{k},-\omega) = 0, \tag{7.39}$$

$$\zeta_1(\mathbf{k},\omega)\delta\psi^*(\mathbf{k},\omega) + \zeta_2(\mathbf{k},\omega)\delta\psi(-\mathbf{k},-\omega) = 0. \tag{7.40}$$

One can observe that any fluctuation $\delta\psi$ which is purely imaginary and stationary with respect to its arguments is trivial solution of the above equations [54]. This is a consequence of global phase symmetry of the effective action (7.16). Non-trivial solutions of (7.39) and (7.40) correspond to gapless Nambu-Goldstone modes associated with long-wavelength fluctuations of the order parameter during the spontaneous breaking of the continuous global phase invariance.

By using the internal symmetries of the functions ζ_1 and ζ_2 defined in (7.27) and (7.28), we can rewrite equation (7.40) as

$$\delta\psi^*(\mathbf{k},\omega) = -\frac{\zeta_2(\mathbf{k},\omega)}{\zeta_1(\mathbf{k},-\omega)}\delta\psi(\mathbf{k},\omega), \tag{7.41}$$

and substitute it back into (7.39) to obtain

$$\left[\zeta_1(\mathbf{k},\omega) - \frac{\zeta_2(\mathbf{k},\omega)^2}{\zeta_1(\mathbf{k},-\omega)}\right]\delta\psi(\mathbf{k},\omega) = 0, \tag{7.42}$$

which leads to the following equation

$$\zeta_1(\mathbf{k},\omega)\zeta_1(\mathbf{k},-\omega) - \zeta_2(\mathbf{k},\omega)^2 = 0. \tag{7.43}$$

Solutions to the above equation correspond to the dispersion relations of the excitations of the superfluid phase. Thus, the effective action-approach presented here provides access to the energy spectrum of elementary excitations of both Mott insular and superfluid phases in the same formalism.

The analytical calculation of the solutions of (7.43) in the disorder case is not straightforward due to the fact that we must consider the average of the four-point correlation function (7.4) over all realizations of the random potential. Another complication comes from

Figure 7.1 – Dispersion relation of the excitations in the superfluid phase for a cubic lattice with $k_B T/U = 0.033$, $\mu = 0.4$ and different values of the tunneling energy. For the left, middle, and right images the values are $Jz = 0.18U$, $Jz = 0.20$, and $Jz = 0.22U$, respectively.

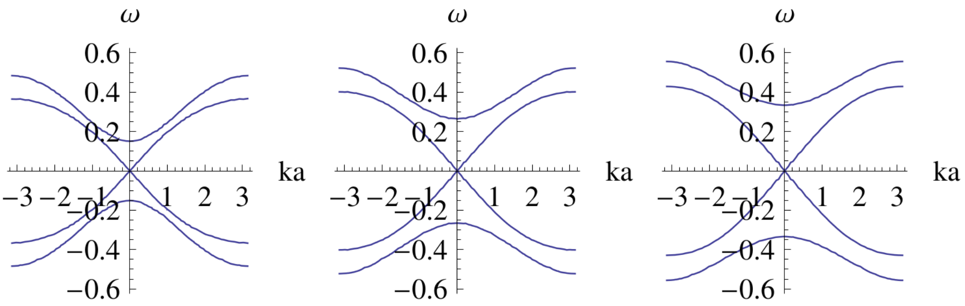

Source: Figure from Ref. [54].

the analytic continuation to the real frequency domain, which one must take care to guarantee convergence of the asymptotic behavior of the correlation functions. Considering first the limit of zero temperature and finding the solutions numerically might be a natural progression of the present work.

When the disorder distribution is given by (3.99), we recover the clean case. In such a case, (7.43) can be solved numerically, which yields the dispersion relations shown in Fig. 7.1. Such a figure shows a gapless Nambu-Goldstone mode together with a gaped mode whose gap decreases for smaller values of the tunneling energy, i.e. near the phase Mott-superfluid phase boundary. One characteristics of the Nambu-Goldstone excitations is the liniear dispersion for small values of the $\mathbf{k}$ vector. The massive gaped mode is often referred to as the Higgs amplitude mode. The excitation spectra of the Bose-Hubbard model in the clean case has been experimentaly investigated by exciting the system via non-destructive techniques such as lattice modulation [17, 171] or Bragg spectroscopy [172, 173, 174]. An important characteristics of these excitations of the superfluid state is that they transform continuously into the quasiparticle and quasihole excitations of the Mott phase when the clean-case phase boundary is crossed. This can be understood from the present calculation by noticing that equations (7.39) and (7.40) reduce to (7.31) at the phase boundary, where the equilibrium value of the order parameter vanishes, i.e. $\psi_{\text{eq}} = 0$.

Since the Bose glass, similarly to the Mott insulator, is characterized by the absence of long-range order, the present order parameter used to calculate the expansion of the effective action cannot be applied to study the excitation spectrum in this phase. Thus, a different order parameter is needed. In the next section, we introduce an alternative for such an order parameter.

7.4 Bose-glass spectra

In 1975, S. F. Edwards and P. W. Anderson propose a new order parameter to study the theory of spin glasses [175, 176]. In the spin glass problem, the exchange interactions between the spins are random. Thus, it was suggested in the above referred papers, that the time persistent part of local spin correlations could serve as an order parameter for such a phase. It turns out, that one can propose a similar definition to study the Bose-glass ground state.

Since the Bose-glass phase is characterized by the formation of rare disconnected condensate domains, such a ground state is not completely described by the usual superfluid order parameters of (7.5) and (7.6). However, by remembering that for sufficiently small tunneling energy, the Bose glass is distinguished by local fluctuations in average particle density per site, one may propose, in analogy to the Edwards-Anderson order parameter, the following quantity to identify such a ground state

$$q = \lim_{|\tau-\tau'|\to\infty} \overline{\langle \hat{a}_i(\tau)\hat{a}_i^\dagger(\tau')\rangle} - N_{\mathbf{0}}, \tag{7.44}$$

where $N_{\mathbf{0}}$ corresponds to the condensate density. Such order parameter was first proposed in the context of the Bose-glass physics in [165, 166] and has since been applied in a number of different investigations [168, 169, 1, 170]. The main idea of applying an effective-action approach would be to include both superfluid and Bose-glass order parameters such that one could describe each phase of the system within the same formalism. This would be a fruitful area for future work.

Chapter 8

Free lattice bosons with weak disorder

Another form to treat the problem of disorder in the Bose-Hubbard model would be to consider it as a perturbation. In this chapter, we present a disorder expansion for free bosons on a lattice with weak disorder. Such a theory is constructed in a similar manner as the one presented in Chapter 4. We argue that the two methods could be applied together in order to develop a theory where the fluctuations in the hopping expansion can be treated separately from the fluctuations in the disorder expansion. Furthermore, we show a single-site approximation to account for the effects of weak disorder.

8.1 Disorder expansion

We begin by considering the functional-integral formulation of the Bose-Hubbard model with an action given by (4.1). Furthermore, we introduce to this action the source term expressed in (4.4). We are interested in the case where the hopping energy is much larger then the other energy scales in the system. Assuming that $U/J \to 0$ and $\Delta/J \ll 1$, we can treat the system as composed of non-interacting particles and consider the local potential as a perturbation. Thus, in this limit, we define the unperturbed partition function to have the following form

$$\mathcal{Z}_0[\mathrm{j}^*,\mathrm{j}] \equiv \frac{\oint \mathcal{D}\psi^* \oint \mathcal{D}\psi \mathrm{e}^{(\psi|\mathcal{G}_0{}^{-1}\psi)+(\mathrm{j}|\psi)+(\psi|\mathrm{j})}}{\oint \mathcal{D}\psi^* \oint \mathcal{D}\psi \mathrm{e}^{(\psi|\mathcal{G}_0{}^{-1}\psi)}}, \tag{8.1}$$

such that $\mathcal{Z}_0[0,0] = 1$. Moreover, we use the definition

$$(\psi|\mathcal{G}_0{}^{-1}\psi) = \int_0^\beta \mathrm{d}\tau \sum_{ij} \psi_i^*(\tau)\left[J_{ij} - \delta_{ij}\left(\frac{\partial}{\partial\tau} - \mu\right)\right]\psi_j(\tau). \tag{8.2}$$

By completing the square in the argument of the exponential function in the numerator of (8.1), we obtain

$$
\begin{aligned}
\mathscr{Z}_0[\mathrm{j}^*,\mathrm{j}] &= \mathrm{e}^{-(\mathrm{j}|\mathscr{G}_0\mathrm{j})} \frac{\oint \mathscr{D}\psi^* \oint \mathscr{D}\psi \mathrm{e}^{(\psi+\mathrm{j}\mathscr{G}_0|{\mathscr{G}_0}^{-1}[\psi+\mathscr{G}_0\mathrm{j}])}}{\oint \mathscr{D}\psi^* \oint \mathscr{D}\psi \mathrm{e}^{(\psi|{\mathscr{G}_0}^{-1}\psi)}} \\
&= \mathrm{e}^{-(\mathrm{j}|\mathscr{G}_0\mathrm{j})},
\end{aligned}
\tag{8.3}
$$

where the second line is obtained by realizing that the integral in the numerator of the first line is equivalent to the integral in the denominator up to a change o variables.

Introducing the Matsubara-Fourier transform

$$
\psi_i(\tau) = \frac{1}{\beta}\left(\frac{a}{2\pi}\right)^d \sum_l \int_{\mathrm{BZ}} dk \mathrm{e}^{\mathrm{i}\mathbf{k}\cdot\mathbf{x}_i - \mathrm{i}\omega_l\tau} \psi(\mathbf{k}, \mathrm{i}\omega_l), \tag{8.4}
$$

we can write the unperturbed Green's function as

$$
\mathscr{G}_0(\mathbf{k}, \mathrm{i}\omega_l) = \frac{1}{\mathrm{i}\omega_l + \mu + J(\mathbf{k})}, \tag{8.5}
$$

where $J(\mathbf{k})$ is the lattice dispersion for a d-dimensional hypercubic lattice defined in (4.19). Note that the above unperturbed Green's function has the same form as the zero-temperature limit shown in equation (5.2) for the case of $n_0 = 0$. Similarly to what we have done in Section 4.1 to find the hopping expansion to the partition function (4.10), we can consider the local potential as a perturbation, and calculate corrections with respect to it via

$$
\mathscr{Z}[\mathrm{j}^*,\mathrm{j}] = \exp\left(-\sum_l \int_{\mathrm{BZ}} d^d k \int_{\mathrm{BZ}} d^d k' \epsilon(\mathbf{k},\mathbf{k}') \frac{\delta^2}{\delta \mathrm{j}^*(\mathbf{k}, \mathrm{i}\omega_l) \delta \mathrm{j}(\mathbf{k}', \mathrm{i}\omega_l)}\right) \mathrm{e}^{-(\mathrm{j}|\mathscr{G}_0\mathrm{j})}, \tag{8.6}
$$

where $\epsilon(\mathbf{k},\mathbf{k}')$ has the same form of (3.65). Therefore the full Green's function can be written as

$$
\mathscr{G}(\mathbf{k},\mathbf{k}';\mathrm{i}\omega) = -\left.\frac{\delta^2 \mathscr{Z}[\mathrm{j}^*,\mathrm{j}]}{\delta \mathrm{j}^*(\mathbf{k}, \mathrm{i}\omega_l) \delta \mathrm{j}(\mathbf{k}', \mathrm{i}\omega_l)}\right|_{\mathrm{j}^*,\mathrm{j}=0}. \tag{8.7}
$$

We point out that analogously to the hopping expansion of (4.10), where for each term the tunneling matrix coupled different local Green's functions (3.82) between different neighboring sites, in the present case of (8.6), the local energy shift couples free propagators (8.5) of states with different wavevectors.

Considering order by order in the perturbative expansion, it is possible to show that the terms which contribute to the full Green's function have the following form

$$
\begin{aligned}
\mathscr{G}(\mathbf{k},\mathbf{k}';\mathrm{i}\omega_l) &= \delta(\mathbf{k}-\mathbf{k}')\mathscr{G}_0(\mathbf{k},\mathrm{i}\omega_l) + \mathscr{G}_0(\mathbf{k},\mathrm{i}\omega_l)\epsilon(\mathbf{k},\mathbf{k}')\mathscr{G}_0(\mathbf{k}',\mathrm{i}\omega_l) \\
&+ \int_{\mathrm{BZ}} d^d k_1 \mathscr{G}_0(\mathbf{k},\mathrm{i}\omega_l)\epsilon(\mathbf{k},\mathbf{k}_1)\mathscr{G}_0(\mathbf{k}_1,\mathrm{i}\omega_l)\epsilon(\mathbf{k}_1,\mathbf{k})\mathscr{G}_0(\mathbf{k}',\mathrm{i}\omega_l) + \cdots .
\end{aligned}
\tag{8.8}
$$

To study the global properties of disorder, we must take the average over all realizations of the random potential

$$\begin{aligned}\overline{\mathscr{G}(\mathbf{k},\mathbf{k}';\mathrm{i}\omega_l)} &= \delta(\mathbf{k}-\mathbf{k}')\mathscr{G}_0(\mathbf{k},\mathrm{i}\omega_l)+\mathscr{G}_0(\mathbf{k},\mathrm{i}\omega_l)\overline{\epsilon(\mathbf{k},\mathbf{k}')}\mathscr{G}_0(\mathbf{k}',\mathrm{i}\omega_l)\\ &+\int_{\mathrm{BZ}} d^d k_1 \mathscr{G}_0(\mathbf{k},\mathrm{i}\omega_l)\overline{\epsilon(\mathbf{k},\mathbf{k}_1)\mathscr{G}_0(\mathbf{k}_1,\mathrm{i}\omega_l)\epsilon(\mathbf{k}_1,\mathbf{k})}\mathscr{G}_0(\mathbf{k}',\mathrm{i}\omega_l)+\cdots.\end{aligned} \tag{8.9}$$

We can understand the physical interpretation of the expansion, by treating each term separately. The first term on the right-hand side of (8.9) is not affected by the disorder and thus represents the free propagation of an excitation with wavevector $\mathbf{k}$ and energy $\mathrm{i}\omega_l$. The second term has a correction of first order in the disorder expansion. The averaging process turns out to be given by

$$\begin{aligned}\mathscr{G}_0(\mathbf{k},\mathrm{i}\omega_l)\overline{\epsilon(\mathbf{k},\mathbf{k}')}\mathscr{G}_0(\mathbf{k}',\mathrm{i}\omega_l) &= \left(\frac{a}{2\pi}\right)^d\sum_i \mathrm{e}^{-\mathrm{i}\mathbf{x}_i\cdot(\mathbf{k}-\mathbf{k}')}\mathscr{G}_0(\mathbf{k},\mathrm{i}\omega_l)\overline{\epsilon_i}\mathscr{G}_0(\mathbf{k}',\mathrm{i}\omega_l)\\ &= \delta(\mathbf{k}-\mathbf{k}')\mathscr{G}_0(\mathbf{k},\mathrm{i}\omega_l)\overline{\epsilon_i}\mathscr{G}_0(\mathbf{k},\mathrm{i}\omega_l),\end{aligned} \tag{8.10}$$

where we have used the explicit form of the random potential (3.65) and the representation of the sum over all sites of the exponential in the first line as a Dirac-delta distribution (3.88). This term can therefore be interpreted as a free propagation followed by one scattering event at site i and another free propagation. The averaging of the second-order term is given by

$$\int_{\mathrm{BZ}} d^d k_1 \overline{\epsilon(\mathbf{k},\mathbf{k}_1)\mathscr{G}_0(\mathbf{k}_1,\mathrm{i}\omega_l)\epsilon(\mathbf{k}_1,\mathbf{k})} = \left(\frac{a}{2\pi}\right)^{2d}\sum_{ij}\overline{\epsilon_i\epsilon_j}\int_{\mathrm{BZ}} d^d k_1 \mathrm{e}^{-\mathrm{i}\mathbf{x}_i\cdot(\mathbf{k}-\mathbf{k}_1)-\mathrm{i}\mathbf{x}_j\cdot(\mathbf{k}_1-\mathbf{k}')}\mathscr{G}_0(\mathbf{k}_1,\mathrm{i}\omega_l). \tag{8.11}$$

The correlation function of the random potential can be decomposed as

$$\overline{\epsilon_i\epsilon_j} = \delta_{ij}\overline{\epsilon_i^2}+\overline{\epsilon_i}\;\overline{\epsilon_j}. \tag{8.12}$$

For the first term on the right hand side of (8.12), equation (8.11) reduces to

$$\begin{aligned}\int_{\mathrm{BZ}} d^d k_1 \overline{\epsilon(\mathbf{k},\mathbf{k}_1)\mathscr{G}_0(\mathbf{k}_1,\mathrm{i}\omega_l)\epsilon(\mathbf{k}_1,\mathbf{k})} &= \overline{\epsilon_i^2}\left(\frac{a}{2\pi}\right)^{2d}\sum_i \mathrm{e}^{-\mathrm{i}\mathbf{x}_i\cdot(\mathbf{k}-\mathbf{k}')}\int_{\mathrm{BZ}} d^d k_1 \mathscr{G}_0(\mathbf{k}_1,\mathrm{i}\omega_l)\\ &= \delta(\mathbf{k}-\mathbf{k}')\overline{\epsilon_i^2}\mathscr{G}_{0ii}(\mathrm{i}\omega_l),\end{aligned} \tag{8.13}$$

where we have defined $\mathscr{G}_{0ii}$ as the local form of the inverse Fourier of (8.5) from reciprocal space to real space

$$\mathscr{G}_{0ij}(\mathrm{i}\omega_l) = \left(\frac{a}{2\pi}\right)^d\int_{\mathrm{BZ}} d^d k \mathrm{e}^{\mathrm{i}\mathbf{k}\cdot(\mathbf{x}_i-\mathbf{x}_j)}\mathscr{G}_0(\mathbf{k},\mathrm{i}\omega_l), \tag{8.14}$$

that is, $\mathscr{G}_{0ii}$ corresponds to the above equation when $i=j$,

$$\mathscr{G}_{0ii}(\mathrm{i}\omega_l) = \left(\frac{a}{2\pi}\right)^d\int_{\mathrm{BZ}} d^d k \mathscr{G}_0(\mathbf{k},\mathrm{i}\omega_l). \tag{8.15}$$

The expression (8.13) can be understood as representing a double scattering process at site i followed by a coherent superposition all values of the wavevector over the first Brillouin zone defined by (8.15). For the second term on the right hand side of (8.12), equation (8.11) simplifies to

$$\begin{aligned}\int_{\mathrm{BZ}} d^d k_1 \overline{\epsilon(\mathbf{k},\mathbf{k}_1)\mathscr{G}_0(\mathbf{k}_1,\mathrm{i}\omega_l)\epsilon(\mathbf{k}_1,\mathbf{k})} =& \left(\frac{a}{2\pi}\right)^{2d}\int_{\mathrm{BZ}} d^d k_1 \sum_{ij} \mathrm{e}^{-\mathrm{i}\mathbf{x}_i\cdot(\mathbf{k}-\mathbf{k}_1)-\mathrm{i}\mathbf{x}_j\cdot(\mathbf{k}_1-\mathbf{k}')}\overline{\epsilon_i}\mathscr{G}_0(\mathbf{k}_1,\mathrm{i}\omega_l)\overline{\epsilon_j} \\ =&\delta(\mathbf{k}-\mathbf{k}')\overline{\epsilon_i}\mathscr{G}_0(\mathbf{k}_1,\mathrm{i}\omega_l)\overline{\epsilon_j},\end{aligned} \tag{8.16}$$

which can be interpreted as a single scattering event at site i followed by a free propagation and then by another single scattering event at a different site j.

With this interpretation, we introduce a diagrammatic representation to describe all the possible terms of the perturbation expansion (8.9). Free propagation can be represented by

$$\mathscr{G}_0(\mathbf{k},\mathrm{i}\omega_l) \quad = \tag{8.17}$$

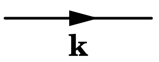

We define the diagram for a single scattering at one site between two free propagations (8.10) as

$$\mathscr{G}_0(\mathbf{k},\mathrm{i}\omega_l)\overline{\epsilon_i}\mathscr{G}_0(\mathbf{k},\mathrm{i}\omega_l) \quad = \tag{8.18}$$

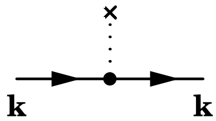

while the diagram representing (8.13) is defined as

$$\overline{\epsilon_i^2}\mathscr{G}_{0ii}(\mathrm{i}\omega_l) \quad = \tag{8.19}$$

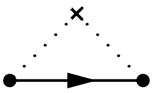

Note that arrow between the two dots in this case has no wavevector index, meaning that it represents the sum of the amplitude over all values of the wavevector in the first Brilloin zone. With this notation equation (8.9) of the average Green's function can be rewritten as

$$\overline{\mathscr{G}(\mathbf{k},\mathbf{k}';\mathrm{i}\omega_l)} = \delta(\mathbf{k}-\mathbf{k}')\Big[\;\cdots\;+\cdots\Big]. \tag{8.20}$$

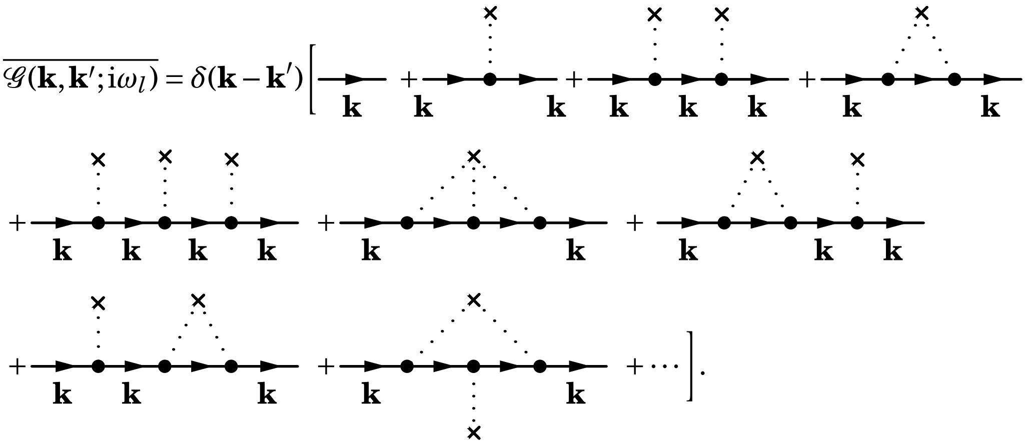

Note that all diagrams consist of free propagation followed by scattering once to infinitely many times at the same site and then by another another free propagation. Therefore, we can choose the sum of all internal diagrams representing the process of scattering once to infinitely many times with the disordered potential as the self-energy

$$\Sigma(\mathbf{k},\mathrm{i}\omega_l)=$$

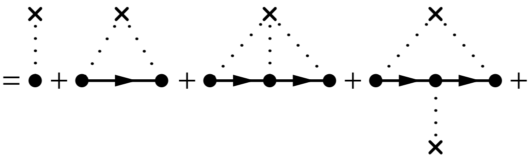

$$+\cdots. \tag{8.21}$$

Therefore, the sum of the full disorder-averaged Green's function can be reorganized in terms of the self-energy and represented diagrammatically as

$$\overline{\mathscr{G}(\mathbf{k},\mathbf{k}';\mathrm{i}\omega_l)}=\delta(\mathbf{k}-\mathbf{k}')\Bigg[$$

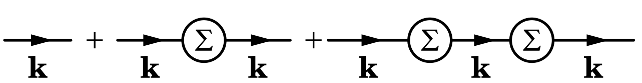

$$+\cdots\Bigg]. \tag{8.22}$$

Summing up an infinite amount of such diagrams we obtain

$$\overline{\mathscr{G}(\mathbf{k},\mathbf{k}';\mathrm{i}\omega_l)}=\delta(\mathbf{k}-\mathbf{k}')\frac{1}{\mathscr{G}_0(\mathbf{k},\mathrm{i}\omega_l)^{-1}-\Sigma(\mathbf{k},\mathrm{i}\omega_l)}, \tag{8.23}$$

which can be rewritten as

$$\overline{\mathscr{G}(\mathbf{k},\mathbf{k}';\mathrm{i}\omega_l)}=\delta(\mathbf{k}-\mathbf{k}')\frac{1}{\mathrm{i}\omega_m+\mu+J(\mathbf{k})-\Sigma(\mathbf{k},\mathrm{i}\omega_l)}. \tag{8.24}$$

Note that, as discussed in previous chapters, the averaged Green's function recovers translational invariance and represents the propagation of excitations which conserve crystal momentum. However, as a result of the scattering against the random potential, such states acquire a finite lifetime.

In the case of (8.24), applying the definition (3.60) leads to the following averaged spectral function

$$\overline{A(\mathbf{k},\omega)}=-\frac{1}{\pi}\frac{\mathrm{Im}\,\Sigma(\mathbf{k},\omega)}{[\omega+\mu+J(\mathbf{k})-\mathrm{Re}\,\Sigma(\mathbf{k},\omega)]^2+[\mathrm{Im}\,\Sigma(\mathbf{k},\omega)]^2}, \tag{8.25}$$

which has a form similar to equation (5.13). However, in the present case, we can see that the real part of the self-energy shifts the dispersion relation of the excitations

$$\omega(\mathbf{k})=-\mu-J(\mathbf{k})+\mathrm{Re}\,\Sigma(\mathbf{k},\omega), \tag{8.26}$$

while its imaginary part is related to their lifetime. Considering that the peaks of the spectral function are still close to the unperturbed dispersion, $\omega_0(\mathbf{k})=-\mu-J(\mathbf{k})$, we can estimate such a lifetime as

$$\bar{\tau}(\mathbf{k})\approx\frac{1}{|\,\mathrm{Im}\,\Sigma(\mathbf{k},\omega_0(\mathbf{k}))|}. \tag{8.27}$$

Thus, in this calculation, the self-energy incorporates the effects of disorder in the propagation of the elementary excitations.

In the hopping expansion, developed in Section 4.1, the unperturbed Green's functions corresponded to localized excitations calculated in the strongly interacting limit. This perturbation method is usually referred to as strong-coupling expansion, or even locator expansion in the case of free particles. Unlike the previous hopping expansion, the unperturbed Green's function in the present calculation corresponds to delocalized excitations. One can see this, by noticing that the inverse Fourier transform of (8.5) to real time and space represents a Bloch state. For this reason the present method is usualy called propagator expansion. From this point of view, the two methods are different. However, it was shown in Refs. [137, 138] that there is an equivalence relation between this two kinds of expansions in the non-interacting limit. The theory developed in this section with the disorder expansion could be applied together with the hopping expansion in chapter 4.1. For the results of the present work, this would amount to the substitution of (8.5) by the clean-case limit of the result (4.20) obtained by partial summation, which amounts to (5.1). In this way, fluctuations in the hoppping expansion could be treated separately from fluctuations in the disorder expansion. Hence, the present calculations provide an insight for future work.

What follows is an account of how to obtain the explicit form of the self energy via the single-site approximation.

8.2 Single-site approximation

Formally, the self-energy shown in (8.21) represents a complex quantity describing the average effects of the random potential on the free propagation of elementary excitations. Thus, its emergence implies that the presence of the disordered medium modifies the dynamical properties of the excitations. If the disorder is small, one can assume that the system can be represented as a collection of small regions which resemble a perfect lattice locally, except for a few sites where the energy shifts of the random potential would be finite. One can understand this local shifts as impurities on a system which is invariant under translations. In the limit that the concentration of this impurities is low, the correlation between scattering events of an excitation at different lattice sites could be neglected and repeated scatterings from one impurity becomes more important. An approximation in this limit is commonly referred to as a single-site approximation, which decouples multiple scattering events at different impurities [177].

One way to take these assumptions under consideration in the perturbation theory derived in the previous section, would be to consider only the diagrams which represent scattering once to infinitely many times at the same lattice site in the sum for the self-energy defined by (8.21). These consist of all diagrams which contain a single cross

$\Sigma(\mathbf{k},\mathrm{i}\omega_l) =$

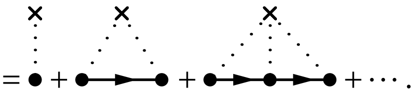

(8.28)

The physical interpretation of the above summation is that within each subsequent scattering event there occurs a coherent superposition of the amplitudes of propagation over all possible values of the wavevector in the first Brillouin zone. In its explicit representation, the above summation reads

$$\Sigma(\mathbf{k},\mathrm{i}\omega_l) = \sum_{m=0}^{\infty} \overline{\epsilon^{m+1}} \mathscr{G}_{0ii}(\mathrm{i}\omega_l)^m. \tag{8.29}$$

By noticing that the sum commutes with the disorder ensemble average, the summation can be directly evaluated to

$$\Sigma(\mathbf{k},\mathrm{i}\omega_l) = \int_{-\infty}^{\infty} d\epsilon \left[\frac{\epsilon}{1-\epsilon\mathscr{G}_{0ii}(\mathrm{i}\omega_l)} \right] \mathscr{P}(\epsilon), \tag{8.30}$$

where we show the explicit form of the disorder average (3.61). Note that the resulting expression for the self-energy has no dependency on the wavevector, i.e. $\Sigma(\mathbf{k},\mathrm{i}\omega_l) = \Sigma(\mathrm{i}\omega_l)$. This is a characteristics of such single-site approximations. One can thus understand the approximation presented here analogously to the coherent-potential approximation, initially developed in [178, 179] in the problem of disordered alloys and commonly applied to disordered lattice systems [118, 119, 107]. A further argument to justify the use of such an approximation is that it can be proved that the $\mathbf{k}$-dependence of the self-energy appears in (8.21) only for double cross diagrams of forth order in local potential. Therefore, we can conclude that at first approximation, disorder couples only to time-dependent degrees of freedom of the system.

For the uniform disorder distribution (3.101), the self-energy (8.30) becomes

$$\Sigma(\mathrm{i}\omega_l) = \frac{1}{\Delta\mathscr{G}_{0ii}(\mathrm{i}\omega_l)^2} \log\left[\frac{2+\Delta\mathscr{G}_{0ii}(\mathrm{i}\omega_l)}{2-\Delta\mathscr{G}_{0ii}(\mathrm{i}\omega_l)}\right] - \frac{1}{\mathscr{G}_{0ii}(\mathrm{i}\omega_l)}. \tag{8.31}$$

Note the analytic continuation of this self-energy to the real frequency domain, i.e. $\mathrm{i}\omega_l \to \omega + \mathrm{i}0^+$, would lead to a logarithmic branch cut on the disorder-averaged Green's function (8.24). In the previous analysis carried in Chapter 5 the logarithmic branch cut constituted the mathematical signature of the damped-localized excitations. Thus, the presence of such a branch cut in the present calculation can interpreted as a sign of the emergence of these damped-localized excitations.

Part V

Final remarks

Chapter 9

Summary and conclusions

Since the seminal work of Fisher et al. [22] in 1989, a substantial amount of research has been devoted to the problem of the disordered Bose-Hubbard model. The experimental realization of this model in ultracold atomic systems loaded in random optical lattices has contributed to the problem gaining more attention. Many methods have been used to address this problem, such as Monte Carlo simulations, mean-field theories, strong-coupling expansions, and renormalization group techniques. As a result, a great deal of information regarding important aspects of this model has been discovered. However, a precise analytical description was still lacking. The work developed in this thesis was constructed as an attempt to fill this void.

One important idea carried throughout the whole thesis was the possibility of characterizing and distinguishing each ground state of the Bose-Hubbard model in the presence of disorder by means of their low-energy excited states. These excited energy levels of the system were interpreted in the context of elementary excitations: the quasiparticles and quasiholes. These entities represent the emergent phenomena that originate from the interactions of the particles that constitute the system among themselves and with the external random lattice. As we have demonstrated, there is a crucial change in the energy spectrum of the elementary excitations in the strongly interacting limit of the system due to the presence of disorder. Furthermore, we have shown that this spectral information remains a reliable and trustworthy property to unambiguously distinguish both the Mott and Bose glass ground states, even at finite temperatures and slightly positive values of the tunneling energy.

The key quantity we have used to analyze these spectral properties, as well as the phase transitions, is the single-particle Green's function and its imaginary part in the Källén-Lehmann representation, i.e., the spectral function. As we have discussed, the singularities in the Green's function in such a representation reveal important information about the microscopic properties of the elementary excitations. These singularities are encoded in the spectral function. In the clean case, such singularities represent stable states for creating extended quasiparticle and quasihole excitations. In the vicinity of the Mott-insulator phase boundary, any finite amount of such excitations immediately produces superfluidity.

In the presence of diagonal disorder, the global properties were investigated by considering the ensemble average over many realizations of the random potential over a bounded uniform distribution. We have demonstrated that the terms of the random potential coupling to states that do not conserve momentum, average over to zero, such that translational invariance is restored on average. In the strongly interacting limit, in the absence of tunneling energy, the spectral function changes from a sharp Dirac-delta peak into a broad peak determined by the disorder distribution. For a continuous disorder distribution, this change originates from the transformation of the simple poles of the Green's function in the clean case into a branch cut singularity in the disordered case. Physically, this implies a change in the nature of the excitations. Disorder makes the excitations unstable, meaning that they only resemble eigenstates of the Bose-Hubbard Hamiltonian for a finite lifetime after which they decay.

In order to analyze the influences of slightly positive values of the tunneling energy, we constructed a strong coupling hopping expansion. This perturbation method was derived by means of the functional integral formulation based on Refs. [52, 53, 54, 39, 99, 139, 140]. By calculating hopping corrections to the cumulant expansion of the free-energy functional, we were able to obtain a perturbation expansion for the Matsubara Green's function. Using a partial summation method, we obtained an expression for the disorder-averaged Green's function in the Källén-Lehmann representation. This expression results from considering infinitely many contributions for the path of an excitation that is created in the system with a well-defined wavevector $\mathbf{k}$ and corresponding frequency $\omega(\mathbf{k})$, which hops through the lattice by scattering infinitely many times against the disordered potential at each site. In this approximation, scattering events at different lattice sites were considered to be uncorrelated.

Within the partial summation approximation, we have demonstrated that in the presence of disorder and for small values of the hopping energy, the spectral function features both a sharp peak for low energies and a broad peak for slightly higher energies. By calculating the frequencies associated with such peaks, we obtained the dispersion relations for the excitations. The sharp peaks are associated with stable states that still exist even in the presence of disorder, while the broad peaks are associated with damped states that emerge due to disorder. By integrating the spectral function over the first Brillouin zone, we computed the total density of states. With all this information, we constructed the band structure for one, two, and three dimensions. The damped states emerge in the center of such band structure, and the dispersion relations of both stable and damped excitations present jumps that correspond to the scattering against the random potential. Furthermore, the effective mass of the stable states increases with disorder, meaning that the excitations in that energy range become less dispersive in the limit of strong disorder. Additionally, the lifetime of the damped states increases with disorder, meaning that the excitations in that energy range become more stable. Moreover, by analyzing the propagation of these excitations in space, we have demonstrated that the stable states are extended at long time scales, and the damped states are localized at short time scales. In the limit of vanishing tunneling, as disorder is increased, the states for stable excitations become dispersionless, and the damped-localized states dominate the whole band. Since such damped-localized states are the ones that remain when the gap closes, we conclude that they correspond to the low-energy states available for single-particle excitations of the Bose-glass phase.

Considering the first non-vanishing contribution in the hopping expansion, we have constructed a renormalized expression for the local density of states based on the local Green's function. To achieve this, we employed the Poincaré-Lindsted method to renormalize the double-pole singularities that arose in the local density of states as derivatives of the disorder distribution. As a result, we obtained a hopping-dependent local density of states that generalizes the result found in [38] for the case of finite hopping. This approximation is equivalent to considering the first correction to the correlations between scattering events against the disordered potential that occur at different times on the same lattice site.

Using this result, we have confirmed that the local density of states is a reliable quantity for unambiguously distinguishing the Bose-glass from the Mott insulator phase, even at finite temperatures and for small values of the tunneling energy. We have obtained an analytical expression for the Mott-Bose glass phase boundary, which compares significantly well with numerical calculations from the literature. In the case of $d = 2$ and for finite temperatures, our result overestimates the sides of the first Mott lobe when compared to the local mean-field theory, but it agrees well around its tip. However, in the case of $d = 3$, our result shows remarkable agreement for both zero and finite temperatures when compared to the stochastic mean-field theory. This indicates that our method is equivalent to that method from the phase boundary point of view.

We remark that, although our results are best suited for high dimensions, they clearly go beyond simple mean-field theories. Additionally, we point out that for sufficiently small tunneling energy, we expect the qualitative aspects of these results to hold even for $d = 1$.

We have proposed an analytical effective-action method that allows us to recover the results obtained for the spectra using the Green's function. Furthermore, we have shown that this method can be applied to obtain the superfluid excitation spectrum in the presence of disorder. In the clean case, it was demonstrated in [39] that the quasiparticles and quasihole excitations transform continuously into the Nambu-Goldstone and Higgs amplitude modes when the Mott-superfluid phase boundary is crossed. In the presence of disorder, an interesting question would be to investigate how the damped-localized excitations of the Bose-glass phase play a role in such a transition. The effective-action method would certainly lead to a deeper understanding in this regard. In addition, we also suggest including an Edwards-Anderson-like order parameter to study the spectra in the Bose-glass state. A theory with both the superfluid and the Bose-glass order parameters would provide a concrete analytical picture of the complete phase diagram of the disordered Bose-Hubbard model. This would be a fruitful area for further work.

We have constructed a disorder expansion that could be used to obtain new results for the effects of disorder, and which could be applied in conjunction with the hopping expansion. One of the strengths of this disorder expansion is that it provides a clear physical interpretation concerning how disorder affects the path of an excitation. Each term in the expansion of the disorder-averaged Green's function can be understood by the number of scattering events against the random potential. By applying a single-site approximation to the self-energy, where only diagrams representing scattering once to infinitely many times at the same lattice site were considered, we demonstrated that it is possible to obtain a result for the branch cut singularity of the Green's function that is similar to the one found using the hopping expansion. This suggests an equivalence relation between such expansions, similar to the one found in [137, 138]. Both these perturbation methods could be applied together to investigate the regime where interactions are important. An advantage of using this approach would be that the loop correction of the hopping expansion, which represents internal interactions between the excitations, could be treated separately from the loop corrections of the disorder expansion, which represent correlations between scattering events at different lattice sites. Future research might explore the combined use of these expansions for further investigation of the effects of disorder on the excitations of the Bose-Hubbard model, as well as on the scaling behavior of the system near criticality.

In conclusion, this thesis has made significant contributions to our understanding of the disordered Bose-Hubbard model in the limit of strong interactions. The use of the hopping expansion has allowed us to construct analytical expressions for various properties of the system, including the spectral function, local density of states, and the Mott-Bose glass phase boundary. Our findings shed new light on the microscopic characterization of the effect of disorder on Mott-insulating phase excitations, giving further insight into the low-energy excitations of the Bose-glass state. By using the different nature of these elementary excitations, we have demonstrated that spectral information serves as a reliable property to distinguish these insulating phases even at finite temperatures. We have suggested additional analytical techniques that could be applied to extend our results and construct further investigations. The theoretical approaches proposed in this work have further expanded the applicability of analytical methods in studying the system of cold bosonic particles with short-range interactions in a random lattice potential. Our analysis is based on the single-particle Green's and spectral functions, which can be probed experimentally with Bragg spectroscopy or with the rf-transfer method. These findings provide a more precise and concrete characterization of the Bose-glass ground state, paving the way for further developments in the field.

References

[1] S. J. Thomson, L. S. Walker, T. L. Harte, and G. D. Bruce, “Measuring the Edwards-Anderson order parameter of the Bose glass: A quantum gas microscope approach,” *Physical Review A*, vol. 94, no. 5, p. 051601, 2016.

[2] U. Bissbort and W. Hofstetter, “Stochastic mean-field theory for the disordered Bose-Hubbard model,” *Europhysics Letters*, vol. 86, no. 5, p. 50007, 2009.

[3] U. Bissbort, R. Thomale, and W. Hofstetter, “Stochastic mean-field theory: Method and application to the disordered Bose-Hubbard model at finite temperature and speckle disorder,” *Physical Review A*, vol. 81, no. 6, p. 063643, 2010.

[4] P. W. Anderson, “More is different: broken symmetry and the nature of the hierarchical structure of science,” *Science*, vol. 177, no. 4047, pp. 393–396, 1972.

[5] H. T. Stoof, K. B. Gubbels, and D. Dickerscheid, *Ultracold quantum fields*. Springer, 2009.

[6] A. A. Abrikosov, L. P. Gorkov, and I. E. Dzyaloshinski, *Methods of quantum field theory in statistical physics*. Dover Publications, 1963.

[7] R. D. Mattuck, *A guide to Feynman diagrams in the many-body problem*. Courier Corporation, 1992.

[8] A. Einstein, “Quantentheorie des einatomigen idealen gases. akademie der wissenshaften,” *Kommission bei W. de Gruyter*, p. 2, 1924.

[9] A. Einstein, “Quantentheorie des einatomigen idealen gases. zweite ab- handlung, sitzungsberichte der preußischen akademie der wissenschaf ten (berlin).,” *Physikalisch-mathematische Klasse*, pp. 3–14, 1925.

[10] S. N. Bose, “Plancks gesetz und lichtquantenhypothese,” *Z. Physik*, 1924.

[11] M. H. Anderson, J. R. Ensher, M. R. Matthews, C. E. Wieman, and E. A. Cornell, “Observation of Bose-Einstein condensation in a dilute atomic vapor,” *Science*, vol. 269, no. 5221, pp. 198–201, 1995.

[12] K. B. Davis, M.-O. Mewes, M. R. Andrews, N. Van Druten, D. Durfee, D. Kurn, and W. Ketterle, “Bose-Einstein condensation in a gas of sodium atoms,” *Physical Review Letters*, vol. 75, no. 22, p. 3969, 1995.

[13] W. D. Phillips, “Nobel lecture: Laser cooling and trapping of neutral atoms,” *Reviews of Modern Physics*, vol. 70, no. 3, p. 721, 1998.

[14] R. P. Feynman, “Simulating physics with computers,” *Int. J. Theor. Phys.*, vol. 21, pp. 467 – 488, 1982.

[15] I. Bloch, “Ultracold quantum gases in optical lattices,” *Nature Physics*, vol. 1, no. 1, pp. 23–30, 2005.

[16] H. Moritz, T. Stöferle, M. Köhl, and T. Esslinger, “Exciting collective oscillations in a trapped 1d gas,” *Physical Review Letters*, vol. 91, no. 25, p. 250402, 2003.

[17] T. Stöferle, H. Moritz, C. Schori, M. Köhl, and T. Esslinger, “Transition from a strongly interacting 1d superfluid to a Mott insulator,” *Physical Review Letters*, vol. 92, no. 13, p. 130403, 2004.

[18] A. Hemmerich and T. Hänsch, “Two-dimesional atomic crystal bound by light,” *Physical Review Letters*, vol. 70, no. 4, p. 410, 1993.

[19] G. Grynberg, B. Lounis, P. Verkerk, J.-Y. Courtois, and C. Salomon, “Quantized motion of cold cesium atoms in two-and three-dimensional optical potentials,” *Physical Review Letters*, vol. 70, no. 15, p. 2249, 1993.

[20] S. B. Roy, *Mott Insulators: Physics and applications*. IOP publishing, 2019.

[21] S. Sachdev, *Quantum phase transitions*. Cambridge University Press, 2011.

[22] M. P. Fisher, P. B. Weichman, G. Grinstein, and D. S. Fisher, “Boson localization and the superfluid-insulator transition,” *Physical Review B*, vol. 40, no. 1, p. 546, 1989.

[23] M. Greiner, O. Mandel, T. Esslinger, T. W. Hänsch, and I. Bloch, “Quantum phase transition from a superfluid to a Mott insulator in a gas of ultracold atoms,” *Nature*, vol. 415, no. 6867, pp. 39–44, 2002.

[24] D. Jaksch, C. Bruder, J. I. Cirac, C. W. Gardiner, and P. Zoller, “Cold bosonic atoms in optical lattices,” *Physical Review Letters*, vol. 81, no. 15, p. 3108, 1998.

[25] M. Chan, K. Blum, S. Murphy, G. Wong, and J. Reppy, “Disorder and the superfluid transition in liquid he 4,” *Physical Review Letters*, vol. 61, no. 17, p. 1950, 1988.

[26] B. Nagler, M. Radonjić, S. Barbosa, J. Koch, A. Pelster, and A. Widera, "Cloud shape of a molecular Bose-Einstein condensate in a disordered trap: a case study of the dirty boson problem," *New Journal of Physics*, vol. 22, no. 3, p. 033021, 2020.

[27] D. Clément, A. F. Varón, J. A. Retter, L. Sanchez-Palencia, A. Aspect, and P. Bouyer, "Experimental study of the transport of coherent interacting matter-waves in a 1d random potential induced by laser speckle," *New Journal of Physics*, vol. 8, no. 8, p. 165, 2006.

[28] J. W. Goodman, *Speckle phenomena in optics: theory and applications*. Roberts and Company Publishers, 2007.

[29] Y.-X. Ren, R.-D. Lu, and L. Gong, "Tailoring light with a digital micromirror device," *Annalen der Physik*, vol. 527, no. 7-8, pp. 447–470, 2015.

[30] U. Gavish and Y. Castin, "Matter-wave localization in disordered cold atom lattices," *Physical Review Letters*, vol. 95, no. 2, p. 020401, 2005.

[31] B. Gadway, D. Pertot, J. Reeves, M. Vogt, and D. Schneble, "Glassy behavior in a binary atomic mixture," *Physical Review Letters*, vol. 107, no. 14, p. 145306, 2011.

[32] P. W. Anderson, "Absence of diffusion in certain random lattices," *Physical Review*, vol. 109, no. 5, p. 1492, 1958.

[33] J.-P. Fouque, *Diffuse waves in complex media*. Springer Science & Business Media, 2012.

[34] J. Billy, V. Josse, Z. Zuo, A. Bernard, B. Hambrecht, P. Lugan, D. Clément, L. Sanchez-Palencia, P. Bouyer, and A. Aspect, "Direct observation of Anderson localization of matter waves in a controlled disorder," *Nature*, vol. 453, no. 7197, pp. 891–894, 2008.

[35] G. Roati, C. D'Errico, L. Fallani, M. Fattori, C. Fort, M. Zaccanti, G. Modugno, M. Modugno, and M. Inguscio, "Anderson localization of a non-interacting bose–einstein condensate," *Nature*, vol. 453, no. 7197, pp. 895–898, 2008.

[36] T. Giamarchi, *Quantum physics in one dimension*, vol. 121. Clarendon Press, 2003.

[37] C. Meldgin, U. Ray, P. Russ, D. Chen, D. M. Ceperley, and B. DeMarco, "Probing the Bose glass-superfluid transition using quantum quenches of disorder," *Nature Physics*, vol. 12, no. 7, pp. 646–649, 2016.

[38] K. Krutitsky, A. Pelster, and R. Graham, "Mean-field phase diagram of disordered bosons in a lattice at nonzero temperature," *New Journal of Physics*, vol. 8, no. 9, p. 187, 2006.

[39] T. Graß, F. E. A. dos Santos, and A. Pelster, “Excitation spectra of bosons in optical lattices from the Schwinger-Keldysh calculation,” *Physical Review A*, vol. 84, no. 1, p. 013613, 2011.

[40] N. Prokof’Ev and B. Svistunov, “Comment on “one-dimensional disordered bosonic Hubbard model: A density-matrix renormalization group study”,” *Physical Review Letters*, vol. 80, no. 19, p. 4355, 1998.

[41] G. Astrakharchik, J. Boronat, J. Casulleras, and S. Giorgini, “Superfluidity versus Bose-Einstein condensation in a Bose gas with disorder,” *Physical Review A*, vol. 66, no. 2, p. 023603, 2002.

[42] B. Capogrosso-Sansone, N. Prokof’Ev, and B. Svistunov, “Phase diagram and thermodynamics of the three-dimensional Bose-Hubbard model,” *Physical Review B*, vol. 75, no. 13, p. 134302, 2007.

[43] V. Gurarie, L. Pollet, N. Prokof’Ev, B. Svistunov, and M. Troyer, “Phase diagram of the disordered Bose-Hubbard model,” *Physical Review B*, vol. 80, no. 21, p. 214519, 2009.

[44] Ş. G. Söyler, M. Kiselev, N. V. Prokof’ev, and B. V. Svistunov, “Phase diagram of the commensurate two-dimensional disordered Bose-Hubbard model,” *Physical Review Letters*, vol. 107, no. 18, p. 185301, 2011.

[45] H. Meier and M. Wallin, “Quantum critical dynamics simulation of dirty boson systems,” *Physical Review Letters*, vol. 108, no. 5, p. 055701, 2012.

[46] L. Pollet, “A review of monte carlo simulations for the Bose-Hubbard model with diagonal disorder,” *Comptes Rendus Physique*, vol. 14, no. 8, pp. 712–724, 2013.

[47] C. Zhang, A. Safavi-Naini, and B. Capogrosso-Sansone, “Equilibrium phases of two-dimensional bosons in quasiperiodic lattices,” *Physical Review A*, vol. 91, no. 3, p. 031604, 2015.

[48] R. Ng and E. S. Sørensen, “Quantum critical scaling of dirty bosons in two dimensions,” *Physical Review Letters*, vol. 114, no. 25, p. 255701, 2015.

[49] B. R. de Abreu, U. Ray, S. A. Vitiello, and D. M. Ceperley, “Properties of the superfluid in the disordered Bose-Hubbard model,” *Physical Review A*, vol. 98, no. 2, p. 023628, 2018.

[50] P. Buonsante, V. Penna, A. Vezzani, and P. Blakie, “Mean-field phase diagram of cold lattice bosons in disordered potentials,” *Physical Review A*, vol. 76, no. 1, p. 011602, 2007.

[51] P. Pisarski, R. Jones, and R. Gooding, “Application of a multisite mean-field theory to the disordered Bose-Hubbard model,” *Physical Review A*, vol. 83, no. 5, p. 053608, 2011.

[52] F. E. A. dos Santos and A. Pelster, “Quantum phase diagram of bosons in optical lattices,” *Physical Review A*, vol. 79, no. 1, p. 013614, 2009.

[53] B. Bradlyn, F. E. A. dos Santos, and A. Pelster, “Effective-action approach for quantum phase transitions in bosonic lattices,” *Physical Review A*, vol. 79, no. 1, p. 013615, 2009.

[54] F. E. A. dos Santos, *Ginzburg-Landau theory for bosonic gases in optical lattices*. PhD thesis, Freie Universität Berlin, 2011.

[55] R. S. Souza, “Effective-action approach to dirty bosons in optical lattices,” Master’s thesis, Universidade Federal de São Carlos, 2019.

[56] B. H. Bransden and C. J. Joachain, *Physics of atoms and molecules*. Pearson Education India, 2003.

[57] C. J. Pethick and H. Smith, *Bose–Einstein condensation in dilute gases*. Cambridge University Press, 2008.

[58] L. Pitaevskii and S. Stringari, *Bose-Einstein condensation and superfluidity*, vol. 164. Oxford University Press, 2016.

[59] R. Grimm, M. Weidemüller, and Y. B. Ovchinnikov, “Optical dipole traps for neutral atoms,” in *Advances in atomic, molecular, and optical physics*, vol. 42, pp. 95–170, Elsevier, 2000.

[60] C. J. Foot, *Atomic physics*, vol. 7. OUP Oxford, 2004.

[61] U. Bissbort, *Dynamical effects and disorder in ultracold bosonic matter*. PhD thesis, Johann Wolfgang Goethe-Universität Frankfurt, 2013.

[62] C. Becker, P. Soltan-Panahi, J. Kronjaeger, S. Dörscher, K. Bongs, and K. Sengstock, “Ultracold quantum gases in triangular optical lattices,” *New Journal of Physics*, vol. 12, no. 6, p. 065025, 2010.

[63] G.-B. Jo, J. Guzman, C. K. Thomas, P. Hosur, A. Vishwanath, and D. M. Stamper-Kurn, “Ultracold atoms in a tunable optical kagome lattice,” *Physical review letters*, vol. 108, no. 4, p. 045305, 2012.

[64] L. Fallani, C. Fort, and M. Inguscio, “Bose-Einstein condensates in disordered potentials,” *Advances in atomic, molecular, and optical physics*, vol. 56, pp. 119–160, 2008.

[65] N. Bender, H. Yılmaz, Y. Bromberg, and H. Cao, “Customizing speckle intensity statistics,” *Optica*, vol. 5, no. 5, pp. 595–600, 2018.

[66] B. Abdullaev and A. Pelster, “Bose-Einstein condensate in weak 3d isotropic speckle disorder,” *The European Physical Journal D*, vol. 66, pp. 1–11, 2012.

[67] K. Hueck, A. Mazurenko, N. Luick, T. Lompe, and H. Moritz, “Note: Suppression of khz-frequency switching noise in digital micro-mirror devices,” *Review of Scientific Instruments*, vol. 88, no. 1, p. 016103, 2017.

[68] J. M. Ziman, *Principles of the Theory of Solids*. Cambridge University Press, 1972.

[69] C. Kittel, *Introduction to solid state physics, Eighth edition*. Wiley, 2005.

[70] N. W. Ashcroft and N. D. Mermin, *Solid state physics*. Cengage Learning, 2022.

[71] A. M. Rey, *Ultracold bosonic atoms in optical lattices*. PhD thesis, University of Maryland, College Park, 2004.

[72] G. D. Mahan, *Many-particle physics*. Springer Science & Business Media, 2000.

[73] A. L. Fetter and J. D. Walecka, *Quantum theory of many-particle systems*. Courier Corporation, 2012.

[74] H. Bruus and K. Flensberg, *Many-body quantum theory in condensed matter physics: an introduction*. OUP Oxford, 2004.

[75] D. Jaksch and P. Zoller, “The cold atom Hubbard toolbox,” *Annals of physics*, vol. 315, no. 1, pp. 52–79, 2005.

[76] K. V. Krutitsky, “Ultracold bosons with short-range interaction in regular optical lattices,” *Physics Reports*, vol. 607, pp. 1–101, 2016.

[77] A. Albus, F. Illuminati, and J. Eisert, “Mixtures of bosonic and fermionic atoms in optical lattices,” *Physical Review A*, vol. 68, no. 2, p. 023606, 2003.

[78] W. Zwerger, “Mott-Hubbard transition of cold atoms in optical lattices,” *Journal of Optics B: Quantum and Semiclassical Optics*, vol. 5, no. 2, p. S9, 2003.

[79] A. Hoffmann and A. Pelster, “Visibility of cold atomic gases in optical lattices for finite temperatures,” *Physical Review A*, vol. 79, no. 5, p. 053623, 2009.

[80] M. Greiner, *Ultracold quantum gases in three-dimensional optical lattice potentials*. PhD thesis, Ludwig-Maximilians-Universität München, 2003.

[81] C. Foot and M. Shotter, “Double well potentials and quantum gates,” *American Journal of Physics*, vol. 79, no. 7, pp. 762–768, 2011.

[82] S. Fölling, S. Trotzky, P. Cheinet, M. Feld, R. Saers, A. Widera, T. Müller, and I. Bloch, “Direct observation of second-order atom tunnelling,” *Nature*, vol. 448, no. 7157, pp. 1029–1032, 2007.

[83] V. Jelic and F. Marsiglio, “The double-well potential in quantum mechanics: a simple, numerically exact formulation,” *European Journal of Physics*, vol. 33, no. 6, p. 1651, 2012.

[84] G.-H. Sun, Q. Dong, V. Bezerra, and S.-H. Dong, “Exact solutions of an asymmetric double well potential,” *Journal of Mathematical Chemistry*, vol. 60, no. 4, pp. 605–612, 2022.

[85] P. B. Weichman, “Dirty bosons: twenty years later,” *Modern Physics Letters B*, vol. 22, no. 27, pp. 2623–2647, 2008.

[86] P. D. Lett, R. N. Watts, C. I. Westbrook, W. D. Phillips, P. L. Gould, and H. J. Metcalf, “Observation of atoms laser cooled below the doppler limit,” *Physical Review Letters*, vol. 61, no. 2, p. 169, 1988.

[87] I. Yavin, M. Weel, A. Andreyuk, and A. Kumarakrishnan, “A calculation of the time-of-flight distribution of trapped atoms,” *American Journal of Physics*, vol. 70, no. 2, pp. 149–152, 2002.

[88] T. M. Brzozowski, M. Maczynska, M. Zawada, J. Zachorowski, and W. Gawlik, “Time-of-flight measurement of the temperature of cold atoms for short trap-probe beam distances,” *Journal of Optics B: Quantum and Semiclassical Optics*, vol. 4, no. 1, p. 62, 2002.

[89] K. Hardman, P. Wigley, P. Everitt, P. Manju, C. C. Kuhn, and N. Robins, “Time-of-flight detection of ultra-cold atoms using resonant frequency modulation imaging,” *Optics Letters*, vol. 41, no. 11, pp. 2505–2508, 2016.

[90] J. Lye, L. Fallani, M. Modugno, D. Wiersma, C. Fort, and M. Inguscio, “Bose-Einstein condensate in a random potential,” *Physical Review Letters*, vol. 95, no. 7, p. 070401, 2005.

[91] L. Fallani, J. Lye, V. Guarrera, C. Fort, and M. Inguscio, “Ultracold atoms in a disordered crystal of light: Towards a Bose glass,” *Physical Review Letters*, vol. 98, no. 13, p. 130404, 2007.

[92] C. D’Errico, E. Lucioni, L. Tanzi, L. Gori, G. Roux, I. P. McCulloch, T. Giamarchi, M. Inguscio, and G. Modugno, “Observation of a disordered bosonic insulator from weak to strong interactions,” *Physical Review Letters*, vol. 113, no. 9, p. 095301, 2014.

[93] M. Pasienski, D. McKay, M. White, and B. DeMarco, “A disordered insulator in an optical lattice,” *Nature Physics*, vol. 6, no. 9, pp. 677–680, 2010.

[94] R. K. Pathria, *Statistical mechanics*. Elsevier, 2016.

[95] M. Continentino, *Quantum scaling in many-body systems*. Cambridge University Press, 2017.

[96] L. Landau, “The theory of phase transitions,” *Nature*, vol. 138, no. 3498, pp. 840–841, 1936.

[97] L. Landau, “On the theory of phase transitions,” *Ukr. J. Phys.*, vol. 11, pp. 19–32, 1937.

[98] J. Y. Fu, “On the landau theory of phase transitions: a hierarchical dynamic model,” *Journal of Physics: Condensed Matter*, vol. 25, no. 7, p. 075903, 2013.

[99] M. Ohliger and A. Pelster, “Green’s function approach to the Bose-Hubbard model,” *World Journal of Condensed Matter Phyisics*, vol. 3, no. 2, pp. 125–130, 2013.

[100] T. Vojta, “Phases and phase transitions in disordered quantum systems,” in *AIP Conference Proceedings*, vol. 1550, pp. 188–247, American Institute of Physics, 2013.

[101] U. Ray, *Properties of dirty bosons in disordered optical lattices*. PhD thesis, University of Illinois at Urbana-Champaign, 2015.

[102] C. Meldgin, *Dynamics of ultracold bosons in a disordered optical lattice*. PhD thesis, University of Illinois at Urbana-Champaign, 2016.

[103] J. Chayes, L. Chayes, D. S. Fisher, and T. Spencer, “Finite-size scaling and correlation lengths for disordered systems,” *Physical Review Letters*, vol. 57, no. 24, p. 2999, 1986.

[104] L. Pollet, N. Prokof’ev, B. Svistunov, and M. Troyer, “Absence of a direct superfluid to Mott insulator transition in disordered Bose systems,” *Physical Review Letters*, vol. 103, no. 14, p. 140402, 2009.

[105] R. B. Griffiths, “Nonanalytic behavior above the critical point in a random Ising ferromagnet,” *Physical Review Letters*, vol. 23, no. 1, p. 17, 1969.

[106] Z. Yao, K. P. da Costa, M. Kiselev, and N. Prokof’ev, “Critical exponents of the superfluid-Bose-glass transition in three dimensions,” *Physical Review Letters*, vol. 112, no. 22, p. 225301, 2014.

[107] G. Rickayzen, *Green’s functions and condensed matter*. Academic Press, London, 1980.

[108] R. Kubo, M. Toda, N. Hashitsume, R. Kubo, M. Toda, and N. Hashitsume, "Statistical mechanics of linear response," *Statistical Physics II: Nonequilibrium Statistical Mechanics*, pp. 146–202, 1991.

[109] R. Kubo, "Statistical-mechanical theory of irreversible processes. i. general theory and simple applications to magnetic and conduction problems," *Journal of the Physical Society of Japan*, vol. 12, no. 6, pp. 570–586, 1957.

[110] L. P. Kadanoff, G. Baym, and J. D. Trimmer, "Quantum statistical mechanics," *American Journal of Physics*, vol. 31, no. 4, pp. 309–309, 1963.

[111] S. Weinberg, *The quantum theory of fields*, vol. 1. Cambridge University Press, 1995.

[112] H. Lehmann, "Über eigenschaften von ausbreitungsfunktionen und renormierungskonstanten quantisierter felder," *Il Nuovo Cimento (1943-1954)*, vol. 11, pp. 342–357, 1954.

[113] C. Jarlskog, "Paper [1952a]: On the definition of the renormalization constants in quantum electrodynamics: Helv. phys. acta 25 (1952) 417," 2014.

[114] J. Zinn-Justin, *Quantum field theory and critical phenomena*, vol. 171. Oxford University Press, 2021.

[115] R. A. Jishi, *Feynman diagram techniques in condensed matter physics*. Cambridge University Press, 2013.

[116] J. Schwinger, "On the Euclidean structure of relativistic field theory," *Proceedings of the National Academy of Sciences*, vol. 44, no. 9, pp. 956–965, 1958.

[117] T. Matsubara, "A new approach to quantum-statistical mechanics," *Progress of Theoretical Physics*, vol. 14, no. 4, pp. 351–378, 1955.

[118] J. M. Ziman, *Models of disorder: the theoretical physics of homogeneously disordered systems*. Cambridge University Press, 1979.

[119] E. N. Economou, *Green's functions in quantum physics*, vol. 7. Springer Science & Business Media, 2006.

[120] K. Krutitsky, M. Thorwart, R. Egger, and R. Graham, "Ultracold bosons in lattices with binary disorder," *Physical Review A*, vol. 77, no. 5, p. 053609, 2008.

[121] P. J. Martin, B. G. Oldaker, A. H. Miklich, and D. E. Pritchard, "Bragg scattering of atoms from a standing light wave," *Physical Review Letters*, vol. 60, no. 6, p. 515, 1988.

[122] P. Berman and B. Bian, "Pump-probe spectroscopy approach to Bragg scattering," *Physical Review A*, vol. 55, no. 6, p. 4382, 1997.

[123] J. Stenger, S. Inouye, A. P. Chikkatur, D. Stamper-Kurn, D. Pritchard, and W. Ketterle, "Bragg spectroscopy of a Bose-Einstein condensate," *Physical Review Letters*, vol. 82, no. 23, p. 4569, 1999.

[124] A. Brunello, F. Dalfovo, L. Pitaevskii, S. Stringari, and F. Zambelli, "Momentum transferred to a trapped Bose-Einstein condensate by stimulated light scattering," *Physical Review A*, vol. 64, no. 6, p. 063614, 2001.

[125] A. M. Rey, P. B. Blakie, G. Pupillo, C. J. Williams, and C. W. Clark, "Bragg spectroscopy of ultracold atoms loaded in an optical lattice," *Physical Review A*, vol. 72, no. 2, p. 023407, 2005.

[126] R. Wild, S. Papp, J. Pino, S. Ronen, J. Bohn, D. Jin, C. Wieman, and E. Cornell, "Bragg spectroscopy of a strongly interacting ^{85}Rb Bose-Einstein condensate," in *APS Division of Atomic, Molecular and Optical Physics Meeting Abstracts*, vol. 39, pp. OPL–21, 2008.

[127] N. Fabbri, S. D. Huber, D. Clément, L. Fallani, C. Fort, M. Inguscio, and E. Altman, "Quasiparticle dynamics in a Bose insulator probed by interband Bragg spectroscopy," *Physical Review Letters*, vol. 109, no. 5, p. 055301, 2012.

[128] M. Lingham, K. Fenech, T. Peppler, S. Hoinka, P. Dyke, P. Hannaford, and C. Vale, "Bragg spectroscopy of strongly interacting fermi gases," *Journal of Modern Optics*, vol. 63, no. 18, pp. 1783–1794, 2016.

[129] H. Biss, L. Sobirey, N. Luick, M. Bohlen, J. J. Kinnunen, G. M. Bruun, T. Lompe, and H. Moritz, "Excitation spectrum and superfluid gap of an ultracold fermi gas," *Physical Review Letters*, vol. 128, no. 10, p. 100401, 2022.

[130] R. Kubo, "The fluctuation-dissipation theorem," *Reports on Progress in Physics*, vol. 29, no. 1, p. 255, 1966.

[131] K. Sturm, "Dynamic structure factor: An introduction," *Zeitschrift für Naturforschung A*, vol. 48, no. 1-2, pp. 233–242, 1993.

[132] M. Greiner, I. Bloch, O. Mandel, T. W. Hänsch, and T. Esslinger, "Exploring phase coherence in a 2d lattice of Bose-Einstein condensates," *Physical Review Letters*, vol. 87, no. 16, p. 160405, 2001.

[133] W. Ketterle, D. S. Durfee, and D. Stamper-Kurn, "Making, probing and understanding Bose-Einstein condensates," *arXiv preprint cond-mat/9904034*, 1999.

[134] T. L. Harte, E. Bentine, K. Luksch, A. J. Barker, D. Trypogeorgos, B. Yuen, and C. J. Foot, “Ultracold atoms in multiple radio-frequency dressed adiabatic potentials,” *Physical Review A*, vol. 97, no. 1, p. 013616, 2018.

[135] V. V. Volchkov, M. Pasek, V. Denechaud, M. Mukhtar, A. Aspect, D. Delande, and V. Josse, “Measurement of spectral functions of ultracold atoms in disordered potentials,” *Physical Review Letters*, vol. 120, no. 6, p. 060404, 2018.

[136] J. J. Sakurai and E. D. Commins, “Modern quantum mechanics, revised edition,” 1995.

[137] J. Kroha, T. Kopp, and P. Wölfle, “Self-consistent theory of Anderson localization for the tight-binding model with site-diagonal disorder,” *Physical Review B*, vol. 41, no. 1, p. 888, 1990.

[138] J. Kroha, “Diagrammatic self-consistent theory of Anderson localization for the tight-binding model,” *Physica A: Statistical Mechanics and its Applications*, vol. 167, no. 1, pp. 231–252, 1990.

[139] R. S. Souza, A. Pelster, and F. E. A. dos Santos, “Green’s function approach to the Bose-Hubbard model with disorder,” *New Journal of Physics*, vol. 23, no. 8, p. 083007, 2021.

[140] R. S. Souza, A. Pelster, and F. E. A. dos Santos, “Emergence of damped-localized excitations of the Mott state due to disorder,” *arXiv:2209.02435*, 2022.

[141] H. Kleinert and V. Schulte-Frohlinde, *Critical Properties of ϕ^4-theories*. World Scientific, 2001.

[142] A. Irving and C. Hamer, “Methods in hamiltonian lattice field theory (ii). linked-cluster expansions,” *Nuclear Physics B*, vol. 230, no. 3, pp. 361–384, 1984.

[143] M. P. Gelfand, R. R. Singh, and D. A. Huse, “Perturbation expansions for quantum many-body systems,” *Journal of Statistical Physics*, vol. 59, pp. 1093–1142, 1990.

[144] J. Freericks, H. Krishnamurthy, Y. Kato, N. Kawashima, and N. Trivedi, “Strong-coupling expansion for the momentum distribution of the Bose-Hubbard model with benchmarking against exact numerical results,” *Physical Review A*, vol. 79, no. 5, p. 053631, 2009.

[145] E. Fradkin, *Quantum field theory: an integrated approach*. Princeton University Press, 2021.

[146] M. I. Trappe, D. Delande, and C. A. Müller, “Semiclassical spectral function for matter waves in random potentials,” *Journal of Physics A: Mathematical and Theoretical*, vol. 48, no. 24, p. 245102, 2015.

[147] A. Signoles, B. Lecoutre, J. Richard, L.-K. Lim, V. Denechaud, V. V. Volchkov, V. Angelopoulou, F. Jendrzejewski, A. Aspect, L. Sanchez-Palencia, *et al.*, “Ultracold atoms in disordered potentials: elastic scattering time in the strong scattering regime,” *New Journal of Physics*, vol. 21, no. 10, p. 105002, 2019.

[148] R. E. Mickens, *An introduction to nonlinear oscillations.* CUP Archive, 1981.

[149] C. M. Bender, S. Orszag, and S. A. Orszag, *Advanced mathematical methods for scientists and engineers I: Asymptotic methods and perturbation theory*, vol. 1. Springer Science & Business Media, 1999.

[150] A. Pelster, H. Kleinert, and M. Schanz, “High-order variational calculation for the frequency of time-periodic solutions,” *Physical Review E*, vol. 67, no. 1, p. 016604, 2003.

[151] I. Vidanović, A. Balaž, H. Al-Jibbouri, and A. Pelster, “Nonlinear Bose-Einstein-condensate dynamics induced by a harmonic modulation of the s-wave scattering length,” *Physical Review A*, vol. 84, no. 1, p. 013618, 2011.

[152] H. Al-Jibbouri, I. Vidanović, A. Balaž, and A. Pelster, “Geometric resonances in Bose-Einstein condensates with two-and three-body interactions,” *Journal of Physics B: Atomic, Molecular and Optical Physics*, vol. 46, no. 6, p. 065303, 2013.

[153] O. E. Alon, A. I. Streltsov, and L. S. Cederbaum, “Zoo of quantum phases and excitations of cold bosonic atoms in optical lattices,” *Physical Review Letters*, vol. 95, no. 3, p. 030405, 2005.

[154] K. Sengupta and N. Dupuis, “Mott-insulator–to–superfluid transition in the Bose-Hubbard model: A strong-coupling approach,” *Physical Review A*, vol. 71, no. 3, p. 033629, 2005.

[155] M. Knap, E. Arrigoni, and W. von der Linden, “Spectral properties of strongly correlated bosons in two-dimensional optical lattices,” *Physical Review B*, vol. 81, no. 2, p. 024301, 2010.

[156] S. Ejima, H. Fehske, and F. Gebhard, “Dynamic properties of the one-dimensional Bose-Hubbard model,” *Europhysics Letters*, vol. 93, no. 3, p. 30002, 2011.

[157] T. Zaleski, “Momentum-resolved spectral function of ultracold bosons in two-dimensional optical lattices,” *Physical Review A*, vol. 85, no. 4, p. 043611, 2012.

[158] J. Panas, A. Kauch, J. Kuneš, D. Vollhardt, and K. Byczuk, “Numerical calculation of spectral functions of the Bose-Hubbard model using bosonic dynamical mean-field theory,” *Physical Review B*, vol. 92, no. 4, p. 045102, 2015.

[159] B. Grémaud and G. G. Batrouni, “Excitation and dynamics in the extended Bose-Hubbard model,” *Physical Review B*, vol. 93, no. 3, p. 035108, 2016.

[160] L. Van Hove, “The occurrence of singularities in the elastic frequency distribution of a crystal,” *Physical Review*, vol. 89, no. 6, p. 1189, 1953.

[161] P. Nozieres, *Theory of interacting Fermi systems*. Westview Press, 1997.

[162] A. Aspect and M. Inguscio, “Anderson localization of ultracold atoms,” *Physics Today*, vol. 62, no. 8, p. 30, 2009.

[163] G. Roux, A. Minguzzi, and T. Roscilde, “Dynamic structure factor of one-dimensional lattice bosons in a disordered potential: a spectral fingerprint of the Bose-glass phase,” *New Journal of Physics*, vol. 15, no. 5, p. 055003, 2013.

[164] S. Rapsch, U. Schollwöck, and W. Zwerger, “Density matrix renormalization group for disordered bosons in one dimension,” *Europhysics Letters*, vol. 46, no. 5, p. 559, 1999.

[165] S. Morrison, A. Kantian, A. J. Daley, H. G. Katzgraber, M. Lewenstein, H. P. Büchler, and P. Zoller, “Physical replicas and the Bose glass in cold atomic gases,” *New Journal of Physics*, vol. 10, no. 7, p. 073032, 2008.

[166] R. Graham and A. Pelster, “Order via nonlinearity in randomly confined Bose gases,” *International Journal of Bifurcation and Chaos*, vol. 19, no. 08, pp. 2745–2753, 2009.

[167] T. Lancaster and S. J. Blundell, *Quantum field theory for the gifted amateur*. OUP Oxford, 2014.

[168] T. Khellil and A. Pelster, “Hartree-Fock mean-field theory for trapped dirty bosons,” *Journal of Statistical Mechanics: Theory and Experiment*, vol. 2016, no. 6, p. 063301, 2016.

[169] T. Khellil, A. Balaž, and A. Pelster, “Analytical and numerical study of dirty bosons in a quasi-one-dimensional harmonic trap,” *New Journal of Physics*, vol. 18, no. 6, p. 063003, 2016.

[170] T. Khellil and A. Pelster, “Dirty bosons in a three-dimensional harmonic trap,” *Journal of Statistical Mechanics: Theory and Experiment*, vol. 2017, no. 9, p. 093108, 2017.

[171] M. Endres, T. Fukuhara, D. Pekker, M. Cheneau, P. Schauβ, C. Gross, E. Demler, S. Kuhr, and I. Bloch, “The ‘Higgs’ amplitude mode at the two-dimensional superfluid-Mott insulator transition,” *Nature*, vol. 487, no. 7408, pp. 454–458, 2012.

[172] D. Clément, N. Fabbri, L. Fallani, C. Fort, and M. Inguscio, “Exploring correlated 1d Bose gases from the superfluid to the Mott-insulator state by inelastic light scattering,” *Physical Review Letters*, vol. 102, no. 15, p. 155301, 2009.

[173] P. T. Ernst, S. Götze, J. S. Krauser, K. Pyka, D.-S. Lühmann, D. Pfannkuche, and K. Sengstock, “Probing superfluids in optical lattices by momentum-resolved Bragg spectroscopy,” *Nature Physics*, vol. 6, no. 1, pp. 56–61, 2010.

[174] U. Bissbort, S. Götze, Y. Li, J. Heinze, J. S. Krauser, M. Weinberg, C. Becker, K. Sengstock, and W. Hofstetter, “Detecting the amplitude mode of strongly interacting lattice bosons by Bragg scattering,” *Physical Review Letters*, vol. 106, no. 20, p. 205303, 2011.

[175] S. F. Edwards and P. W. Anderson, “Theory of spin glasses,” *Journal of Physics F: Metal Physics*, vol. 5, no. 5, p. 965, 1975.

[176] S. Edwards and P. Anderson, “Theory of spin glasses. ii,” *Journal of Physics F: Metal Physics*, vol. 6, no. 10, p. 1927, 1976.

[177] J. A. e Castro, “Multiple-scattering theory of binary alloys in single-site approximation,” *Physica B+ C*, vol. 113, no. 3, pp. 317–335, 1982.

[178] P. Soven, “Coherent-potential model of substitutional disordered alloys,” *Physical Review*, vol. 156, no. 3, p. 809, 1967.

[179] D. Taylor, “Vibrational properties of imperfect crystals with large defect concentrations,” *Physical Review*, vol. 156, no. 3, p. 1017, 1967.

[180] J. W. Negele and H. Orland, *Quantum many-particle systems*. Westview Press, 1998.

[181] I. S. Gradshteyn and I. M. Ryzhik, *Table of integrals, series, and products*. Academic press, 2014.

Appendices

Appendix A

Functional-integral formalism

In this appendix, we derive the path integral formulation for the Bose-Hubbard model. This derivation follows from Ref. [180].

A.1 Lattice occupation number representation and Fock space

When investigating the quantum aspects of many-particle systems on a lattice it is convenient to use the occupation number representation. For bosonic particles a general many-body state $|\Psi\rangle$ can be expressed by the superposition

$$|\Psi\rangle = c \sum_{n_1 \dots n_L} \psi_{n_1 \dots n_L} |n_1 \dots n_L\rangle, \tag{A.1}$$

where c is some normalization constant, $\psi_{n_1,\dots,n_L}$ represents a set of expansion coefficients, L is the total number of lattice sites, and n_i is the number of particles in the site i. This state with an arbitrary number of particles is accommodated in the Fock space given by

$$\mathscr{F} = \bigoplus_{N=0}^{\infty} \mathscr{F}^N, \tag{A.2}$$

where $\mathscr{F}^0$ is the one dimensional Hilbert space whose element is the state with no particles present, the so-called vacuum state, and so on. The normalization condition together with the completeness relation of the basis states are respectively given by

$$\langle n_1 \dots n_L | m_1 \dots n_L \rangle = \delta_{n_1 m_1} \cdots \delta_{n_L m_L}, \tag{A.3}$$

$$\sum_{n_1 \dots n_L} |n_1 \dots n_L\rangle \langle n_1 \dots n_L| = \hat{1}. \tag{A.4}$$

In order to construct a path integral formulation for the time evolution of a state given in (A.1), we must choose a set of suitable eigenstates of the many-body Hamiltonian which absorbs as much as possible the quantum dynamical phase accumulated during short-time propagations. Given that such Hamiltonians are conveniently expressed in terms of the creation and annihilation operators, the idea would be to search for the eigenstates of such operators. These are the so-called coherent states.

A.2 Coherent states

With the propose of developing the coherent-state representation, we introduce the creation and annihilation operators which satisfy the following commutation relations

$$\left[\hat{a}_i, \hat{a}_j^\dagger\right] = \delta_{ij}, \quad [\hat{a}_i, \hat{a}_j] = 0, \quad \text{and} \quad \left[\hat{a}_i^\dagger, \hat{a}_j^\dagger\right] = 0, \tag{A.5}$$

where $\hat{a}_i$ ($\hat{a}_i^\dagger$) annihilates (creates) a particles in site i. Using (A.1) to represent the many-particle state, we can see that if the minimum of particles in $|\Psi\rangle$ is n_0 the minimum of particles in $\hat{a}_i^\dagger |\Psi\rangle$ must be $n_0 + 1$. Thus, the creation operators cannot posses eigenstates.

Assuming that $|\Psi\rangle$ is an eigenstate of the annihilation operator, the condition

$$\hat{a}_i |\Psi\rangle = \psi_i |\Psi\rangle \tag{A.6}$$

must be satisfied. This implies the following condition for the coefficients

$$\psi_i \psi_{n_1 \dots n_i - 1 \dots n_L} = \sqrt{n_i}\psi_{n_1 \dots n_L}, \tag{A.7}$$

for all $\{n_i\}$. Setting the vacuum coefficient equal to 1 and considering its relation by induction to the other coefficients, we obtain

$$\psi_{n_1 \dots n_L} = \frac{\psi_1^{n_1}}{\sqrt{n_1!}} \cdots \frac{\psi_L^{n_L}}{\sqrt{n_L!}}. \tag{A.8}$$

Therefore, we can rewrite (A.1) as

$$|\Psi\rangle = c \sum_{n_1 \dots n_L} \frac{\psi_1^{n_1}}{\sqrt{n_1!}} \cdots \frac{\psi_L^{n_L}}{\sqrt{n_L!}} |n_1 \dots n_L\rangle. \tag{A.9}$$

Assuming that $\langle\Psi|\Psi\rangle = 1$, we find

$$\begin{aligned}
\langle\Psi|\Psi\rangle &= c^*c \sum_{m_1\ldots m_L}\sum_{n_1\ldots n_L} \frac{(\psi_1^*)^{m_1}}{\sqrt{m_1!}}\ldots\frac{(\psi_L^*)^{m_L}}{\sqrt{m_L!}}\frac{\psi_1^{n_1}}{\sqrt{n_1!}}\ldots\frac{\psi_L^{n_L}}{\sqrt{n_L!}}\langle m_1\ldots m_L|n_1\ldots n_L\rangle \\
&= c^*c \sum_{n_1,\ldots,n_L}\frac{(\psi_1^*\psi_1)^{n_1}}{n_1!}\ldots\frac{(\psi_L^*\psi_L)^{n_L}}{n_L!} = c^*c \quad e^{\psi_1^*\psi_1}\ldots e^{\psi_L^*\psi_L} \qquad (A.10)\\
&= c^*c \quad \exp\left(\sum_{i=1}^{L}\psi_i^*\psi_i\right) = 1 \implies c = \exp\left(-\frac{1}{2}\sum_{i=1}^{L}\psi_i^*\psi_i\right).
\end{aligned}$$

Hence, we can write the normalized coherent state as

$$|\Psi\rangle = \exp\left(-\frac{1}{2}\sum_{i=1}^{L}\psi_i^*\psi_i\right)\sum_{n_1\ldots n_L}\frac{\psi_1^{n_1}}{\sqrt{n_1!}}\ldots\frac{\psi_L^{n_L}}{\sqrt{n_L!}}|n_1\ldots n_L\rangle\,. \qquad (A.11)$$

We now have a normalized basis of the Fock space in terms of the coherent states.

In order to derive the over completeness relation, we define the following operator

$$\hat{I} = \int\prod_{i=1}^{L}\frac{d\psi_i^* d\psi_i}{2\pi i}|\Psi\rangle\langle\Psi|, \qquad (A.12)$$

where the integration runs over the whole complex plane. A general matrix element of this operator can be written as

$$\begin{aligned}
\langle n_1\ldots n_L|\hat{I}|m_1\ldots n_L\rangle &= \int\prod_{i=1}^{L}\frac{d\psi_i^* d\psi_i}{2\pi i}\langle n_1\ldots n_L|\Psi\rangle\langle\Psi|m_1\ldots n_L\rangle \\
&= \prod_{i=1}^{L}\int\frac{d\psi_i^* d\psi_i}{2\pi i}e^{-\psi_i^*\psi_i}\frac{(\psi_i^*)^{m_i}}{\sqrt{m_i!}}\frac{(\psi_i)^{n_i}}{\sqrt{n_i!}},
\end{aligned} \qquad (A.13)$$

using the polar coordinates $\psi_i = re^{i\phi}$ and $\psi_i^* = re^{-i\phi}$ the integration becomes

$$\int\frac{d\psi_i^* d\psi_i}{2\pi i}e^{-\psi_i^*\psi_i}\frac{(\psi_i^*)^{m_i}}{\sqrt{m_i!}}\frac{(\psi_i)^{n_i}}{\sqrt{n_i!}} = \frac{1}{\pi\sqrt{n_i!}\sqrt{m_i!}}\int_0^\infty dr r^{m_i+n_i+1}e^{-r^2}\int_0^{2\pi}d\phi e^{i\phi(n_i-m_i)}. \qquad (A.14)$$

For the integration over the angular coordinate, we have

$$\int_0^{2\pi}d\phi e^{i\phi(n_i-m_i)} = \frac{e^{i2\pi(n_i-m_i)}-1}{i(n_i-m_i)} = \begin{cases} 2\pi & \text{for} \quad n_i = m_i, \\ 0 & \text{for} \quad n_i \neq m_i. \end{cases} \qquad (A.15)$$

Thus, we can rewrite (A.14) as

$$\int\frac{d\psi_i^* d\psi_i}{2\pi i}e^{-\psi_i^*\psi_i}\frac{(\psi_i^*)^{m_i}}{\sqrt{m_i!}}\frac{(\psi_i)^{n_i}}{\sqrt{n_i!}} = \frac{2\delta_{n_i m_i}}{n_i!}\int_0^\infty dr r^{2n_i+1}e^{-r^2}, \qquad (A.16)$$

the transformation $r^2 \to x$ gives

$$\int \frac{\mathrm{d}\psi_i^* \mathrm{d}\psi_i}{2\pi \mathrm{i}} \mathrm{e}^{-\psi_i^*\psi_i} \frac{(\psi_i^*)^{m_i}}{\sqrt{m_i!}} \frac{(\psi_i)^{n_i}}{\sqrt{n_i!}} = \frac{\delta_{n_i m_i}}{n_i!} \int_0^\infty \mathrm{d}x x^{n_i} \mathrm{e}^{-x}, \tag{A.17}$$

if we notice that

$$\frac{\mathrm{d}\mathrm{e}^{-\alpha x}}{\mathrm{d}\alpha} = -x\mathrm{e}^{-\alpha x}, \quad \frac{\mathrm{d}^2\mathrm{e}^{-\alpha x}}{\mathrm{d}\alpha^2} = x^2\mathrm{e}^{-\alpha x}, \quad \ldots \quad , \quad \frac{\mathrm{d}^{n_i}\mathrm{e}^{-\alpha x}}{\mathrm{d}\alpha^{n_i}} = (-1)^{n_i} x^{n_i} \mathrm{e}^{-\alpha x} \tag{A.18}$$

we can write

$$\begin{aligned} \int \frac{\mathrm{d}\psi_i^* \mathrm{d}\psi_i}{2\pi \mathrm{i}} \mathrm{e}^{-\psi_i^*\psi_i} \frac{(\psi_i^*)^{m_i}}{\sqrt{m_i!}} \frac{(\psi_i)^{n_i}}{\sqrt{n_i!}} &= \frac{\delta_{n_i m_i}}{(-1)^{n_i} n_i!} \int_0^\infty \mathrm{d}x \left. \frac{\mathrm{d}^{n_i}\mathrm{e}^{-\alpha x}}{\mathrm{d}\alpha^{n_i}} \right|_{\alpha=1} \\ &= \frac{\delta_{n_i m_i}}{(-1)^{n_i} n_i!} \frac{\mathrm{d}^{n_i}}{\mathrm{d}\alpha^{n_i}} \int_0^\infty \mathrm{d}x \left. \mathrm{e}^{-\alpha x} \right|_{\alpha=1} \\ &= \frac{\delta_{n_i m_i}}{(-1)^{n_i} n_i!} \frac{\mathrm{d}^{n_i}}{\mathrm{d}\alpha^{n_i}} \left. \left(\frac{1}{\alpha} \right) \right|_{\alpha=1} \\ &= \frac{\delta_{n_i m_i}}{(-1)^{n_i} n_i!} \left. \frac{(-1)^{n_i} n_i!}{\alpha^{n_i+1}} \right|_{\alpha=1} \\ &= \delta_{n_i m_i}. \end{aligned} \tag{A.19}$$

Therefore,

$$\langle n_1 \ldots n_L | \hat{I} | m_1 \ldots n_L \rangle = \langle n_1 \ldots n_L | m_1 \ldots n_L \rangle = \delta_{n_1 m_1} \cdots \delta_{n_L m_L}, \tag{A.20}$$

and $\hat{I}$ is the unity operator in Fock space

$$\hat{I} = \int \prod_{i=1}^{L} \frac{\mathrm{d}\psi_i^* \mathrm{d}\psi_i}{2\pi \mathrm{i}} |\Psi\rangle \langle\Psi| = \hat{1}. \tag{A.21}$$

We are now in position to develop the coherent-state functional integral representation for the Bose-Hubbard model.

A.3 Imaginary-time path integral and the partition function

The partition function of the system in the occupation number representation can be written as

$$\begin{aligned} \mathcal{Z} &= \mathrm{tr}\left(\mathrm{e}^{-\beta \hat{H}} \right) \\ &= \sum_{n_1 \ldots n_L} \langle n_1 \ldots n_L | \mathrm{e}^{-\beta \hat{H}} | n_1 \ldots n_L \rangle \end{aligned} \tag{A.22}$$

Using the completeness relations of (A.4) and (A.21) this expression becomes

$$\begin{aligned}\mathcal{Z} &= \int\prod_{i=1}^{L}\frac{\mathrm{d}\psi_i^*\mathrm{d}\psi_i}{2\pi\mathrm{i}}\sum_{n_1\ldots n_L}\langle n_1\ldots n_L|\Psi\rangle\,\langle\Psi|\mathrm{e}^{-\beta\hat{H}}|n_1\ldots n_L\rangle\\ &= \int\prod_{i=1}^{L}\frac{\mathrm{d}\psi_i^*\mathrm{d}\psi_i}{2\pi\mathrm{i}}\langle\Psi|\mathrm{e}^{-\beta\hat{H}}\sum_{n_1\ldots n_L}|n_1\ldots n_L\rangle\,\langle n_1\ldots n_L|\Psi\rangle\\ &= \int\prod_{i=1}^{L}\frac{\mathrm{d}\psi_i^*\mathrm{d}\psi_i}{2\pi\mathrm{i}}\langle\Psi|\mathrm{e}^{-\beta\hat{H}}|\Psi\rangle\,.\end{aligned}\tag{A.23}$$

Hence, the partition function may be thought of as the sum over the diagonal matrix elements of the imaginary-time evolution operator $\hat{\mathcal{U}}(\tau,\tau')=\mathrm{e}^{-(\tau'-\tau)\frac{\hat{H}}{\hbar}}$ evaluated over the interval $\tau'-\tau=\hbar\beta$. By breaking the time interval into M steps of size $\Delta\tau=\frac{\tau'-\tau}{M}$, we can rewrite the matrix elements considering the periodic condition to the coherent states $|\Psi_0\rangle=|\Psi\rangle$ and $\langle\Psi_M|=\langle\Psi|$ as

$$\begin{aligned}\langle\Psi_M|\mathrm{e}^{-(\tau'-\tau)\frac{\hat{H}}{\hbar}}|\Psi_0\rangle &= \langle\Psi_M|\mathrm{e}^{-M\frac{\Delta\tau}{\hbar}\hat{H}}|\Psi_0\rangle\\ &= \langle\Psi_M|\underbrace{\mathrm{e}^{-\frac{\Delta\tau}{\hbar}\hat{H}}\cdots\mathrm{e}^{-\frac{\Delta\tau}{\hbar}\hat{H}}}_{M\ \text{times}}|\Psi_0\rangle\,.\end{aligned}\tag{A.24}$$

Using the completeness relation (A.21) between each step of the interval we get

$$\langle\Psi_M|\mathrm{e}^{-(\tau'-\tau)\frac{\hat{H}}{\hbar}}|\Psi_0\rangle=\lim_{M\to\infty}\int\prod_{l=1}^{M-1}\prod_{i=1}^{L}\frac{\mathrm{d}\psi_{i,l}^*\mathrm{d}\psi_{i,l}}{2\pi\mathrm{i}}\prod_{l=1}^{M}\langle\Psi_l|\mathrm{e}^{-\frac{\Delta\tau}{\hbar}\hat{H}}|\Psi_{l-1}\rangle\,,\tag{A.25}$$

where each matrix element is given by

$$\begin{aligned}\langle\Psi_l|\mathrm{e}^{-\frac{\Delta\tau}{\hbar}\hat{H}}|\Psi_{l-1}\rangle &= \langle\Psi_l|\hat{1}-\frac{\Delta\tau}{\hbar}\hat{H}+\mathcal{O}(\Delta\tau^2)|\Psi_{l-1}\rangle\\ &= \langle\Psi_l|\Psi_{l-1}\rangle\left(1-\frac{\Delta\tau}{\hbar}\frac{\langle\Psi_l|\hat{H}|\Psi_{l-1}\rangle}{\langle\Psi_l|\Psi_{l-1}\rangle}+\mathcal{O}(\Delta\tau^2)\right).\end{aligned}\tag{A.26}$$

Considering the Bose-Hubbard Hamiltonian

$$\hat{H}_{BH}(\hat{a}^\dagger,\hat{a})=\frac{U}{2}\sum_i\hat{a}_i^\dagger\hat{a}_i^\dagger\hat{a}_i\hat{a}_i-\sum_i\mu_i\hat{a}_i^\dagger\hat{a}_i-\sum_{ij}J_{ij}\hat{a}_i^\dagger\hat{a}_j,\tag{A.27}$$

we have

$$\begin{aligned}\langle\Psi_l|\hat{H}_{BH}(\hat{a}^\dagger,\hat{a})|\Psi_{l-1}\rangle &= \left(\frac{U}{2}\sum_i\psi_{i,l}^*\psi_{i,l}^*\psi_{i,l-1}\psi_{i,l-1}-\sum_i\mu_i\psi_{i,l}^*\psi_{i,l-1}\right.\\ &\qquad\left.-\sum_{ij}J_{ij}\psi_{i,l}^*\psi_{j,l-1}\right)\langle\Psi_l|\Psi_{l-1}\rangle\\ &= H_{BH}(\psi_l^*,\psi_{l-1})\,\langle\Psi_l|\Psi_{l-1}\rangle\,.\end{aligned}\tag{A.28}$$

Thus, the matrix elements can be written as

$$
\begin{aligned}
\langle\Psi_l|\mathrm{e}^{-\frac{\Delta\tau}{\hbar}\hat{H}}|\Psi_{l-1}\rangle &= \mathrm{e}^{-\frac{1}{2}\sum_{i=1}^{L}\left(\psi^*_{i,l}(\psi_{i,l}-\psi_{i,l-1})-\psi_{i,l-1}(\psi^*_{i,l}-\psi^*_{i,l-1})\right)} \\
&\qquad \times\left(1-\frac{\Delta\tau}{\hbar}H_{BH}(\psi^*_l,\psi_{l-1})+\mathcal{O}(\Delta\tau^2)\right) \\
&= \mathrm{e}^{-\frac{\Delta\tau}{\hbar}\left[\frac{1}{2}\sum_{i=1}^{L}\left(\hbar\psi^*_{i,l}\frac{\psi_{i,l}-\psi_{i,l-1}}{\Delta\tau}-\hbar\psi_{i,l-1}\frac{\psi^*_{i,l}-\psi^*_{i,l-1}}{\Delta\tau}\right)+H_{BH}(\psi^*_l,\psi_{l-1})\right]}.
\end{aligned} \tag{A.29}
$$

Inserting this relation in (A.25) we get

$$
\begin{aligned}
\langle\Psi_M|\mathrm{e}^{-(\tau'-\tau)\frac{\hat{H}}{\hbar}}|\Psi_0\rangle &= \lim_{M\to\infty}\int\prod_{l=1}^{M-1}\prod_{i=1}^{L}\frac{\mathrm{d}\psi^*_{i,l}\mathrm{d}\psi_{i,l}}{2\pi\mathrm{i}} \\
&\qquad\times\prod_{l=1}^{M}\mathrm{e}^{-\frac{\Delta\tau}{\hbar}\left[\frac{1}{2}\sum_{i=1}^{L}\left(\hbar\psi^*_{i,l}\frac{\psi_{i,l}-\psi_{i,l-1}}{\Delta\tau}-\hbar\psi_{i,l-1}\frac{\psi^*_{i,l}-\psi^*_{i,l-1}}{\Delta\tau}\right)+H_{BH}(\psi^*_l,\psi_{l-1})\right]} \\
&= \lim_{M\to\infty}\int\prod_{l=1}^{M-1}\prod_{i=1}^{L}\frac{\mathrm{d}\psi^*_{i,l}\mathrm{d}\psi_{i,l}}{2\pi\mathrm{i}} \\
&\qquad\times\mathrm{e}^{-\frac{\Delta\tau}{\hbar}\sum_{l=1}^{M}\left[\frac{1}{2}\sum_{i=1}^{L}\left(\hbar\psi^*_{i,l}\frac{\psi_{i,l}-\psi_{i,l-1}}{\Delta\tau}-\hbar\psi_{i,l-1}\frac{\psi^*_{i,l}-\psi^*_{i,l-1}}{\Delta\tau}\right)+H_{BH}(\psi^*_l,\psi_{l-1})\right]}
\end{aligned} \tag{A.30}
$$

It is convenient to introduce the trajectory representation $\psi_i(\tau)$ to represent the set $\{\psi_{i,1},\cdots,\psi_{i,M}\}$, where in the limit $M\to\infty$ we can write

$$
\begin{aligned}
\psi^*_{i,l}\frac{\psi_{i,l}-\psi_{i,l-1}}{\Delta\tau} &\to \psi^*_i(\tau)\frac{\partial\psi_i(\tau)}{\partial\tau}, \\
\psi_{i,l-1}\frac{\psi^*_{i,l}-\psi^*_{i,l-1}}{\Delta\tau} &\to \psi_i(\tau)\frac{\partial\psi^*_i(\tau)}{\partial\tau}, \\
H_{BH}(\psi^*_l,\psi_{l-1}) &\to H_{BH}(\psi^*(\tau),\psi(\tau)),
\end{aligned} \tag{A.31}
$$

where the exponent in (A.30) becomes

$$
\begin{aligned}
-\frac{\Delta\tau}{\hbar}\sum_{l=1}^{M}&\left[\frac{1}{2}\sum_{i=1}^{L}\left(\hbar\psi^*_{i,l}\frac{\psi_{i,l}-\psi_{i,l-1}}{\Delta\tau}-\hbar\psi_{i,l-1}\frac{\psi^*_{i,l}-\psi^*_{i,l-1}}{\Delta\tau}\right)+H_{BH}(\psi^*_l,\psi_{l-1})\right] \\
&= -\frac{1}{\hbar}\int_0^{\hbar\beta}\mathrm{d}\tau\left[\frac{1}{2}\sum_{i=1}^{L}\left(\hbar\psi^*_i(\tau)\frac{\partial\psi_i(\tau)}{\partial\tau}-\hbar\psi_i(\tau)\frac{\partial\psi^*_i(\tau)}{\partial\tau}\right)+H_{BH}(\psi^*(\tau),\psi(\tau))\right],
\end{aligned} \tag{A.32}
$$

therefore we can write the partition function in the trajectory representation as

$$
\mathcal{Z}=\oint\mathcal{D}\psi^*\oint\mathcal{D}\psi\,\mathrm{e}^{-\frac{1}{\hbar}\int_0^{\hbar\beta}\mathrm{d}\tau\left[\frac{1}{2}\sum_{i=1}^{L}\left(\hbar\psi^*_i(\tau)\frac{\partial\psi_i(\tau)}{\partial\tau}-\hbar\psi_i(\tau)\frac{\partial\psi^*_i(\tau)}{\partial\tau}\right)+H_{BH}(\psi^*(\tau),\psi(\tau))\right]} \tag{A.33}
$$

where

$$
\oint\mathcal{D}\psi^*\oint\mathcal{D}\psi=\lim_{M\to\infty}\int\prod_{l=1}^{M}\prod_{i=1}^{L}\frac{\mathrm{d}\psi^*_{i,l}\mathrm{d}\psi_{i,l}}{2\pi\mathrm{i}}, \tag{A.34}
$$

and we have the periodic condition in imaginary time $\psi(\beta) = \psi(0)$. Integrating by parts the imaginary-time derivative, we can write the partition function

$$\mathcal{Z} = \oint \mathcal{D}\psi^* \oint \mathcal{D}\psi \exp\left(-\frac{1}{\hbar} S[\psi^*, \psi]\right), \tag{A.35}$$

where the action is given by

$$S[\psi^*, \psi] = \int_0^{\hbar\beta} \mathrm{d}\tau \left[\sum_{i=1}^{L} \hbar \psi_i^*(\tau) \frac{\partial \psi_i(\tau)}{\partial \tau} + H_{BH}(\psi^*(\tau), \psi(\tau))\right]. \tag{A.36}$$

We can now use this formulation to study the correlations of the system.

Appendix B

Sum rule for the case of $n_0 = 0$

We want to show that equation (5.32) satisfies the sum rule, namely that

$$\int_{-\infty}^{\infty} d\omega \overline{A(\mathbf{k},\omega)} = 1. \tag{B.1}$$

The integral separates into two terms. The first term, corresponding to the stable states, consists on the integration of a Dirac delta distribution resulting in the following expression

$$\int_{-\infty}^{\infty} d\omega \overline{A^{+}(\mathbf{k},\omega)} = \frac{\Delta^2}{4J^2(\mathbf{k})} \operatorname{csch}^2\left(\frac{\Delta}{2J(\mathbf{k})}\right). \tag{B.2}$$

The integration of the second term, which corresponds to the damped states, is more involved. As a consequence of the uniform disorder distribution the integration reduces to

$$\int\limits_{-\mu-\Delta/2}^{-\mu+\Delta/2} d\omega \overline{A^{r}(\mathbf{k},\omega)} = \int\limits_{-\mu-\Delta/2}^{-\mu+\Delta/2} d\omega \frac{1/\Delta}{\left[1 - \frac{J(\mathbf{k})}{\Delta}\log\left|\frac{\omega+\mu-\Delta/2}{\omega+\mu+\Delta/2}\right|\right]^2 + \pi^2 J(\mathbf{k})^2/\Delta^2}. \tag{B.3}$$

One can simplify such an integration by applying the change of variables

$$\omega = -\mu - \frac{\Delta}{2}\tanh(u). \tag{B.4}$$

The integral can thus be written as

$$\int\limits_{-\mu-\Delta/2}^{-\mu+\Delta/2} d\omega \overline{A^{r}(\mathbf{k},\omega)} = \frac{\Delta^2}{2}\int_{-\infty}^{\infty} du \frac{\operatorname{sech}^2(u)}{\Delta^2(2J(\mathbf{k})u+1)^2 + \pi^2 J^2(\mathbf{k})}. \tag{B.5}$$

One can solve the above integral by going into the complex plane and applying the residue theorem. This leads to

$$\int\limits_{-\mu-\Delta/2}^{-\mu+\Delta/2} d\omega\overline{A^r(\mathbf{k},\omega)} = -\frac{\Delta^2}{4J^2(\mathbf{k})}\operatorname{csch}^2\left(\frac{\Delta}{2J(\mathbf{k})}\right)+\sum_{l=0}^{\infty}\frac{4\mathrm{i}\pi\Delta^2 J(\mathbf{k})(\Delta+\mathrm{i}J(\mathbf{k})\pi(1+2l))}{\left[\Delta^2-4J(\mathbf{k})^2\pi^2 l(1+l)+2\mathrm{i}\pi\Delta J(\mathbf{k})(1+2l)\right]^2}, \tag{B.6}$$

where the first term stands for the residue of the simple pole in the upper half of the complex plane on the denominator of the right-hand side of (B.5), while the second term consists of the sum of infinitely many residues in the upper half of the complex plane coming from the hyperbolic secant function in the numerator. Choosing

$$f(l) = \sum_{l=0}^{\infty}\frac{4\mathrm{i}\pi\Delta^2 J(\mathbf{k})(\Delta+\mathrm{i}J(\mathbf{k})\pi(1+2l))}{\left[\Delta^2-4J(\mathbf{k})^2\pi^2 l(1+l)+2\mathrm{i}\pi\Delta J(\mathbf{k})(1+2l)\right]^2}, \tag{B.7}$$

such a summation can be directly evaluated by applying the Poison summation formula

$$\begin{aligned}\sum_{l=0}^{\infty} f(l) &= \sum_{l=0}^{\infty}\int_{-\infty}^{\infty} dx\delta(x-l)f(x) \\ &= \sum_{m=-\infty}^{\infty}\int_{-\infty}^{\infty} dx f(x)\mathrm{e}^{2\mathrm{i}\pi m x}.\end{aligned} \tag{B.8}$$

Applying once more the residue theorem, it is possible to show that

$$\sum_{l=0}^{\infty}\frac{4\mathrm{i}\pi\Delta^2 J(\mathbf{k})(\Delta+\mathrm{i}J(\mathbf{k})\pi(1+2l))}{\left[\Delta^2-4J(\mathbf{k})^2\pi^2 l(1+l)+2\mathrm{i}\pi\Delta J(\mathbf{k})(1+2l)\right]^2} = 1. \tag{B.9}$$

Therefore, considering all the parts the sum rule reads

$$\int_{-\infty}^{\infty} d\omega\overline{A(\mathbf{k},\omega)} = \frac{\Delta^2}{4J^2(\mathbf{k})}\operatorname{csch}^2\left(\frac{\Delta}{2J(\mathbf{k})}\right) - \frac{\Delta^2}{4J^2(\mathbf{k})}\operatorname{csch}^2\left(\frac{\Delta}{2J(\mathbf{k})}\right)+1, \tag{B.10}$$

which clearly equals to unity.

Appendix C

Limit of large space separations

The inverse Fourier transform of the partial summation result for the Green's function (4.20) reads

$$\begin{aligned} \overline{G_{ij}(\omega)} &= \left(\frac{a}{2\pi}\right)^{2d} \int_{\mathrm{BZ}} d^d k \int_{\mathrm{BZ}} d^d k' \overline{G(\mathbf{k},\mathbf{k}';\omega)} \mathrm{e}^{\mathrm{i}(\mathbf{k}\cdot\mathbf{x}_i - \mathbf{k}'\cdot\mathbf{x}_j)} \\ &= \left(\frac{a}{2\pi}\right)^{d} \int_{\mathrm{BZ}} d^d k \frac{\mathrm{e}^{\mathrm{i}\mathbf{k}\cdot(\mathbf{x}_i - \mathbf{x}_j)}}{[\overline{g_i(\omega)}]^{-1} - J(\mathbf{k})}, \end{aligned} \tag{C.1}$$

where we have already considered the analytic continuation $\mathrm{i}\omega_l \to \omega + \mathrm{i}0^+$ from Matsubara to real frequencies.

In order to simplify the integration, one can apply the identity

$$\frac{1}{\mathscr{A}} = \int_0^\infty d\nu \mathrm{e}^{-\mathscr{A}\nu}, \tag{C.2}$$

where the variable ν is usually called the Feynman-Schwinger parameter. We choose $\mathscr{A} = [\overline{g_i(\omega)}]^{-1} - J(\mathbf{k})$ an substitute this back in (C.1), which takes the form

$$\overline{G_{ij}(\omega)} = \left(\frac{a}{2\pi}\right)^{d} \int_0^\infty d\nu \mathrm{e}^{-\nu\left[\overline{g_i(\omega)}\right]^{-1}} \int_{\mathrm{BZ}} d^d k \mathrm{e}^{\mathrm{i}\mathbf{k}\cdot(\mathbf{x}_i - \mathbf{x}_j) + \nu J(\mathbf{k})}. \tag{C.3}$$

In the limit of large separations in space, i.e. $|\mathbf{x}_i - \mathbf{x}_j| \to \infty$, one can interpret that only the low momentum modes would contribute and lattice spacing a becomes negligible such that the dispersion (4.19) can be expanded as

$$J(\mathbf{k}) \approx 2Jd - Ja^2|\mathbf{k}|^2. \tag{C.4}$$

Including the above expansion in (C.3) and considering the limit of $a \to 0$, we obtain that the integrals in k become Gaussian. Such integration results in the following expression

$$\overline{G_{ij}(\omega)} \sim \int_0^\infty d\nu \frac{\mathrm{e}^{-\nu[\overline{G(\mathbf{0},\omega)}]^{-1} - |\mathbf{x}_i - \mathbf{x}_j|^2/4Ja^2\nu}}{\nu^{d/2}} \quad \text{as} \quad |\mathbf{x}_i - \mathbf{x}_j| \to \infty. \tag{C.5}$$

Since, we are only interested in the overall asymptotic behavior, we do not show the proportionality constants. We now define the rescaling of v as

$$v = \sqrt{\frac{\overline{G(\mathbf{0},\omega)}}{4Ja^2}}\,|\mathbf{x}_i - \mathbf{x}_j|\,u, \tag{C.6}$$

which allows us to write the exponents in (C.5) in following form

$$\frac{v}{\overline{G(\mathbf{0},\omega)}} + \frac{|\mathbf{x}_i - \mathbf{x}_j|^2}{4Ja^2 v} = \frac{|\mathbf{x}_i - \mathbf{x}_j|}{\sqrt{4Ja^2\overline{G(\mathbf{0},\omega)}}}\left(u + \frac{1}{u}\right). \tag{C.7}$$

After this change of variables, the equation (C.5) becomes

$$\overline{G_{ij}(\omega)} \sim \frac{1}{|\mathbf{x}_i - \mathbf{x}_j|^{\frac{d}{2}-1}} K_{\frac{d}{2}-1}\left(\frac{|\mathbf{x}_i - \mathbf{x}_j|}{a\sqrt{J\overline{G(\mathbf{0},\omega)}}}\right) \quad \text{as} \quad |\mathbf{x}_i - \mathbf{x}_j| \to \infty, \tag{C.8}$$

where we have introduced the modified Bessel function of second kind

$$K_m(y) = \frac{1}{2}\int_0^\infty du\; u^{m-1} \mathrm{e}^{-\frac{y}{2}\left(u + \frac{1}{u}\right)}, \tag{C.9}$$

with

$$m = \frac{d}{2} - 1 \quad \text{and} \quad y = \frac{|\mathbf{x}_i - \mathbf{x}_j|}{a\sqrt{J\overline{G(\mathbf{0},\omega)}}}. \tag{C.10}$$

In the long distance limit, i.e. for $y \gg 1$, a calculation with the saddle-point method [181, 145] shows that the following asymptotic behavior for the Bessel function

$$K_m(y) = \sqrt{\frac{\pi}{2y}}\,\mathrm{e}^{-y}\left[1 + \mathcal{O}\left(\frac{1}{y}\right)\right]. \tag{C.11}$$

Therefore, the asymptotic behavior of the Green's function becomes

$$\overline{G_{ij}(\omega)} \sim \frac{1}{|\mathbf{x}_i - \mathbf{x}_j|^{\frac{d-1}{2}}}\,\mathrm{e}^{-\frac{|\mathbf{x}_i - \mathbf{x}_j|}{\ell}}\left[1 + \mathcal{O}\left(\frac{1}{|\mathbf{x}_i - \mathbf{x}_j|}\right)\right] \quad \text{as} \quad |\mathbf{x}_i - \mathbf{x}_j| \to \infty, \tag{C.12}$$

where

$$\ell = a\frac{\sqrt{J|\overline{G(\mathbf{0},\omega)}|}}{|\sin[\arg(\overline{G(\mathbf{0},\omega)})/2]|}. \tag{C.13}$$